AD NUMBER
AD811679
LIMITATION CHANGES

TO:

Approved for public release; distribution is unlimited.

FROM:

Distribution authorized to U.S. Gov't. agencies and their contractors; Administrative/Operational Use; APR 1967. Other requests shall be referred to Arnold Engineering Development Center, Arnold AFB, TN.

AUTHORITY

AEDC ltr, 2 Oct 1972

UNCLASSIFIED

STUDY OF HIGH-DENSITY
HYPERVELOCITY FLOWS AND SIMILITUDES

DO NOT RETURN

C. E. Wittliff, T. R. Sundaram, W. J. Rae, and J. A. Lordi

Cornell Aeronautical Laboratory, Inc.

Buffalo, New York

April 1967

This document has been approved for public release its distribution is unlimited.

ARNOLD ENGINEERING DEVELOPMENT CENTER
AIR FORCE SYSTEMS COMMAND
ARNOLD AIR FORCE STATION, TENNESSEE

FORCE

000/1200

NOTICES

STUDY OF HIGH-DENSITY
HYPERVELOCITY FLOWS AND SIMILITUDES

C. E. Wittliff, T. R. Sundaram, W. J. Rae, and J. A. Lordi

Cornell Aeronautical Laboratory, Inc.
Buffalo, New York

FOREWORD

The work reported herein was sponsored by Arnold Engineering Development Center (AEDC), Air Force Systems Command (AFSC), Arnold Air Force Station, Tennessee, under Program Element 62410034, Project 5950.

The research study presented in this report was performed by the Aerodynamic Research Department of Cornell Aeronautical Laboratory, Inc., Buffalo, New York, under Contract AF 40(600)-1131. The research was performed during the period May 1965 to May 1966, and the manuscript was submitted for publication on March 28, 1967.

The reproducibles used in the reproduction of this report were supplied by the author.

Information in this report is embargoed under the Department of State International Traffic in Arms Regulations. This report may be released to foreign governments by departments or agencies of the U. S. Government subject to approval of the Arnold Engineering Development Center (AETS), or higher authority within the Department of the Air Force. Private individuals or firms require a Department of State export license.

This technical report has been reviewed and is approved.

Harold L. Rogler   Edward R. Feicht
Captain, USAF   Colonel, USAF
Advanced Plans Division   Director of Plans and
Directorate of Plans and Technology   Technology

ABSTRACT

This report presents the results of a study of hypervelocity flows, with particular emphasis on the similitude requirements. A primary objective has been to delineate the similitude parameters for certain typical flows and, where possible, to evaluate the effects of not duplicating all of the similitude parameters in wind-tunnel tests. As a part of this study, a comprehensive review of inviscid and viscous similitude is given, as well as a state-of-the-art survey of flow solutions. It is shown that in many instances there do not exist, at present, sufficient experimental data or theoretical solutions to evaluate the sensitivity of various flow quantities to variations in the similitude parameters nor to determine whether some similitude parameters are less important than others. Such an evaluation has been accomplished for certain simple flows, such as wedges, cones, blunt-nosed flat plates and stagnation-region flows. For these flows it is found that in the flight regime of interest (velocities from 10,000 to 36,000 fps and altitudes from 50,000 ft. to 250,000 ft.) duplication of density-altitude and free-stream velocity are more important than duplication of free-stream Mach number (i.e., temperature). However, lack of duplication of Mach number can introduce significant errors in the case of slender bodies. Other topics that have been investigated are the effects of alkali-metal seed on hypervelocity flows, the importance of simulating ablation phenomena in wind-tunnel tests, and the testing time requirements for hypervelocity wind tunnels.

TABLE OF CONTENTS

LIST OF FIGURES

LIST OF TABLES

LIST OF SYMBOLS

a	speed of sound
A/A^*	nozzle area ratio
C_H	$q/\rho_\infty U_\infty (H_s - H_w)$, heat-transfer coefficient
C_*	Chapman-Rubesin constant
C_L , C_D	lift, drag coefficients
C_p	pressure coefficient, $(p - p_\infty)/\frac{1}{2}\rho_\infty U_\infty^2$; also used for specific heat at constant pressure
C_{D_N}	nose-drag coefficient
d_N	thickness or diameter of blunt nose, Sec. III
h_{eff} , h_a	heats of ablation, Sec. X
H	enthalpy
L	reference length
Le	Lewis number
M	Mach number
m	molecular weight
$\dot{m}$	mass addition rate, mass per unit time, area
n	number density
Nu	Nusselt number
p	pressure
p_o'	pitot pressure
Pr	Prandtl number
q	heat transfer rate, energy per unit time and area
R	gas constant for undissociated air
R_N	nose radius

LIST OF SYMBOLS (CONT.)

Re	Reynolds number
S	entropy
s, n	coordinates along and normal to body surface
T	temperature
u, v	velocity components s, n directions
U	tunnel or flight velocity
$\bar{V}$	hypersonic viscous parameter
x	distance behind a normal shock wave
$\bar{x}_R$	reaction coordinate, Eq. (VI-4)
X_j	mole fraction of species j
Y	mass fraction of contaminant species, Sec. IV
α	degree of dissociation
γ	specific heat ratio
θ_c	cone half-angle
θ_w	wedge angle
μ	dynamic viscosity
ν	0, 1 for two-dimensional or axisymmetric flow
ξ	cone nose-to-base radius ratio, R_N / R_B
ρ	mass density
σ	shock angle
τ	thickness ratio; also used for characteristic time
τ_w	surface shear stress
$\chi, \bar{\chi}$	viscous interaction parameter, $M^3/\sqrt{Re}$, $M^3\sqrt{C/Re}$

LIST OF SYMBOLS (Cont.)

Subscripts

$(\ )_e$	boundary-layer edge
$(\ )_{eq, neq}$	equilibrium, nonequilibrium
$(\ )_f$	frozen
$(\ )_{F,T}$	flight, tunnel
$(\ )_{inj}$	injectant
$(\ )_o$	total or reservoir conditions
$(\ )_s$	behind shock
$(\ )_{s,e}$	stagnation conditions at boundary-layer edge
$(\ )_w$	wall
$(\ )_\infty$	free-stream
$(\ )_*$	evaluated at reference temperature

I. INTRODUCTION

Traditionally the wind tunnel has been a tool for simulating rather than duplicating the flight conditions of a vehicle. As velocities have increased from subsonic to hypersonic, the problems associated with aerodynamic testing have grown both in number and complexity. This has resulted in such a proliferation of similitude parameters that for some flight conditions one is led to the conclusion that no simulation is possible and the ambient flow conditions, vehicle velocity and size must all be reproduced in the wind tunnel; i.e., the flight condition must be completely duplicated. This is particularly true in the case of high-density, hypervelocity flight where the flow contains viscous and inviscid regions, both containing equilibrium and nonequilibrium real-gas effects. However, the reservoir temperature and, more particularly, the pressure requirements for a wind tunnel are so severe as to make full duplication of low-altitude, hypervelocity flight conditions presently impossible.

On the other hand, experience has shown that flight testing is not only extremely expensive, but also impractical as far as providing detailed investigations of fundamental flow phenomena. In view of this state of affairs, it is necessary that the similitude requirements in the high-density, hypervelocity flight regions be carefully examined from the standpoint of delineating the more important similarity parameters and determining the degree to which the less important similitude requirements can be relaxed. This report presents the result of a study directed at this question.

The flight regime of interest here is the altitude range from 50,000 ft to 250,000 ft for velocities from 10,000 fps to 36,000 fps. The primary objectives of this investigation have been: to determine the similarity and scaling laws required to correlate model test data with full-scale flight vehicles, to quantitatively evaluate the effect of relaxing the duplication requirements of the less sensitive similitude parameters, to assess the maximum permissible degree of relaxation of the individual similitude variables without loss of meaningful test results, and to determine the

minimum test times required to produce valid data for hypervelocity vehicles. Consideration has also been given to: delineating the frozen, nonequilibrium and equilibrium boundaries for both inviscid and viscous flows; assessing the influence of nonequilibrium nozzle flow on test results; determining the effect of seeding the air stream with alkali-metal vapor; and assessing the significance of ablation on aerodynamic phenomena.

It must be emphasized that the specific objectives outlined above are exceedingly broad and complex in relation to the current state of knowledge in this problem area. At the outset it was realized that complete answers to the problem were presently unattainable. Hence, while all aspects of the problem area have been considered to the degree of assessing current knowledge, significant accomplishment of the specific objectives has necessarily been limited to judiciously selected flows. Thus, normal shock waves, blunt-body stagnation regions, wedge flows, cone flows and the blunt-nosed flat plate have been studied in depth since they typify the flow phenomena encountered on more complex vehicle shapes.

In this report, the altitude-velocity map for the high-density, hypervelocity flight regime is discussed first in conjunction with the flight paths of typical vehicles. In order to quantitatively assess the effects of not duplicating all the flight conditions, it was necessary to hypothesize a performance map for a hypervelocity wind tunnel. This is presented in relation to the flight regime in the second section. Following this, the hypersonic similitudes for inviscid and viscous flows about slender and blunt bodies are reviewed in some detail (Sec. III, IV). That review, as a necessary first stage of the investigation, serves to delineate the numerous similitude parameters as well as establish the current state of knowledge of such flows. The remainder of the report presents the results of specific studies of normal shock waves (Sec. V), slender and blunt body flows (Sec. VI-VIII), effects of seeding the air stream (Sec. IX), ablation phenomena (Sec. X) and test-time requirements (Sec. XI). Finally, the important results of the investigation are summarized, the degree to which the initial objectives have been accomplished is discussed, and suggestions for further research are outlined (Sec. XII).

2

II.   FLIGHT REGIME OF INTEREST

A.   INTRODUCTION

Before investigating the similitude requirements for high-density, hypervelocity flight, it is important to define the flight regime under consideration.   Furthermore, it is necessary to establish some reference level of wind-tunnel performance in order to show the areas in which full duplication cannot be achieved.   Also, since hypervelocity nozzle flows are not always in thermodynamic equilibrium, nonequilibrium effects must be taken into consideration.   These matters are treated in this section.

B.   HIGH-DENSITY HYPERVELOCITY FLIGHT REGIME

As stated, the high-density, hypervelocity flight regime of interest in this study is the altitude range from 50,000 ft to 250,000 ft for velocities from 10,000 fps to 36,000 fps, Fig. 1.   This regime encompasses all of the continuous flight corridor[1] lying above 10,000 fps velocity and below 250,000 ft altitude, all of the reentry corridor for manned satellites and lunar vehicles (except portions of skip trajectories), and the critical flight regime for reentering missiles.   These flight regions are also shown in Fig. 1 where it can be seen that the flight regime being considered is one of real concern for hypervelocity vehicles.   This altitude-velocity map further serves to define the range of values for various similarity parameters and will be referred to frequently in subsequent sections.

The severe requirements that duplication of ambient altitude conditions at hypersonic speeds imposes on a wind tunnel are illustrated in Fig. 2.   This altitude-velocity map shows the nozzle reservoir pressures and temperatures necessary for duplicating flight conditions assuming an isentropic expansion of real air in thermodynamic equilibrium.   It should be noted that there are no facilities presently operating at reservoir pressures greater than 2000 atm.   The nozzle reservoir conditions are not specified beyond the 4000 atm curve for the simple reason that the thermo-

dynamic state of air is uncertain at these extreme pressures and temperatures. Velocities greater than 20,000 fps can be obtained, but pressure, temperature and density for altitudes below 250,000 ft cannot be duplicated simultaneously at such velocities in existing facilities.

The extreme reservoir pressure requirements can be circumvented to some extent by not stagnating the air prior to expansion, e.g., a non-reflected shock tunnel. The performance improvement resulting from that mode of operation is typified by the dashed curve in Fig. 2 which represents the duplication capability of a nonreflected shock tunnel operating at 4000 atm behind the incident shock. (The curves labelled T_∞ will be discussed subsequently.) This improvement is substantial; still it does not permit altitude duplication below 250,000 ft at velocities above 27,000 fps. Clearly, the attainment of flight conditions for altitudes below 250,000 ft at velocities above 25,000 fps requires new concepts in hypervelocity facilities. Three new approaches that are under current study are MHD-augmented shock tunnels,[2,3] the expansion tube[4,5,6] and the isentropic compression tube.[7]

C.   HYPOTHESIZED WIND-TUNNEL PERFORMANCE

It is not the purpose of the present study to investigate the possible capabilities of future hypervelocity facilities; however, the quantitative assessment of not duplicating simultaneously all the similitude parameters requires specification of a wind tunnel capability; consequently, a hypothetical performance has been assumed. This is shown in Fig. 2 also. Above the full duplication boundary of Fig. 2, both flight velocity and ambient conditions can be duplicated in the test section if the nozzle expansion remains in equilibrium. Below this boundary line the flight velocity and only one of the ambient altitude conditions (e.g., density-altitude or free-stream temperature) can be duplicated. It should be mentioned that it is tacitly assumed that the facility will be of an intermittent nature and, consequently, will have relatively short test times.

4

Before investigating the flight simulation region of Fig. 2, it is pertinent to consider the problem of nozzle flow nonequilibrium. A considerable simplification is afforded if the region of significant test flow nonequilibrium lies within the region where full duplication of velocity and altitude conditions is possible. If this is the case, the nonequilibrium effects on test-flow conditions may be obtained knowing the effective reservoir enthalpy and entropy corresponding to full duplication of flight conditions. On the other hand, in the region where altitude-velocity conditions cannot be fully duplicated, the lack of duplication of free-stream properties results solely from facility limitations. Moreover, there is then no effect on free-stream composition in the flight simulation region.

D.   NOZZLE FLOW NONEQUILIBRIUM

Nonequilibrium effects on expansions of air to high velocities have been examined at CAL[8,9] and elsewhere [10-12] utilizing numerical solutions of inviscid, one-dimensional nozzle flows with coupled chemical reactions. Solutions have been reported for reservoir temperatures up to 15,000° K and densities up to 100 times sea level density. Lordi and Mates[9] have noted that the nozzle flow nonequilibrium effects on the composition and thermodynamic state of the gas could be correlated with the reservoir entropy. Although the solutions reported in Ref. 9 were for a hyperbolic, axisymmetric nozzle, the dependence of the results on nozzle geometry is weak. Hence, the correlation presented in Ref. 9 has been used here. Some of these results are shown in Fig. 3 which presents the frozen enthalpy (i.e., enthalpy lost in the nonequilibrium expansion) as a function of reservoir entropy. The straight line drawn through the calculated points has been used in the present analysis to obtain the frozen enthalpy H_f for a given reservoir entropy. The nonequilibrium effect on velocity at large nozzle area ratios is given by

$$\frac{U_{neq}}{U_{eq}} = \sqrt{1 - \frac{H_f}{H_o}}$$

(II-I)

where H_o is the total or reservoir enthalpy. Equation (II-I) and the results of Fig. 3 may be used to determine the nonequilibrium effect on test flow velocity. The correlation of frozen species concentrations with reservoir entropy is shown in Fig. 4. These results are applicable for nozzle area ratios $A/A^* \geq 10^3$.

Assuming an equilibrium nozzle expansion, the reservoir conditions corresponding to given flight conditions are found from the entropy corresponding to the thermodynamic state of the atmosphere at a given altitude and the relation $H_o = \frac{1}{2} U_\infty^2$. Knowing S_o, and hence H_f from Fig. 3, H_f/H_o can be calculated. Then the reduction in test flow velocity due to nonequilibrium effects can be calculated from Eq. (II-I). Since the frozen species concentrations also correlate with reservoir entropy [9, 13], the free-stream composition can be determined from Fig. 4.

In order to define the region of the altitude-velocity map where nonequilibrium effects are important, a slightly different procedure has been used. From the entropy corresponding to a given altitude, a value of H_f is obtained from Fig. 3. Then the reservoir enthalpies corresponding to various values of H_f/H_o are found. The flight velocities equivalent to these values of H_o then permit lines to be drawn on the altitude-velocity map for given values of H_f/H_o in the corresponding test flow. The lines for $H_f/H_o = 0.02$ and 0.05 are shown in Fig. 5. It is significant to note that the line corresponding to $H_f/H_o = 0.02$ lies within the full duplication region of the postulated wind-tunnel performance map. Hence, below this line the nonequilibrium effect on velocity is less than 1%. At the end points of the $H_f/H_o = 0.02$ curve, the mass fractions of oxygen atoms and nitric oxide molecules are:

Free-stream Velocity	Mass Fractions	
U_∞	[O]	[NO]
10,000 fps	0.0075	0.096
36,000 fps	0.058	0.0066

The nitrogen atom concentrations are negligible.

The maximum frozen enthalpy occurs at 10,000 fps and 250,000 ft altitude where $H_f/H_o = 0.25$ and the frozen mass fractions of O and NO are 0.053 and 0.075, respectively.

While the above results indicate that the nonequilibrium effects on velocity and composition are negligible below the full-duplication boundary, the effect on static temperature and pressure may not be. In Ref. 9, the nonequilibrium effects on nozzle static pressure and temperature were also correlated with reservoir entropy. Again assuming that full duplication of flight conditions could be attained if nonequilibrium effects were absent, the effects of static pressure and temperature can be correlated with a given flight altitude. For the altitudes (reservoir entropy) corresponding to the higher velocity end of the full duplication line, the nonequilibrium static temperature may be as low as one-half the corresponding equilibrium flow value. As will be seen later, such a mismatch in free-stream temperature (or pressure) could be significant in test flows over slender body.

Another cautionary note on the above relation of nonequilibrium nozzle flow solutions to tunnel performance is in order. The correlation of nozzle flow solutions in terms of reservoir entropy[9] was accomplished for a range of reservoir conditions that did not encompass the entire flight regime being considered here. Consequently, a detailed study of nozzle nonequilibrium effects must be carried out before making definite conclusions on the magnitude of these effects in a given facility.

E.   FLIGHT SIMULATION CONDITIONS

1.   General Considerations

We now turn our attention to determining the mismatch in both the free-stream quantities and the various similitude parameters occurring in the flight simulation region. On the basis of the postulated wind-tunnel performance, it is assumed that the flight velocity can be duplicated throughout this region. However, there will be some cases where a mismatch in velocity is considered.

The various simulation techniques whereby certain similitude parameters are duplicated at the expense of others have been described by several authors (e.g., see Ref. 14). Basically, simulation is the technique of duplicating only the nondimensional parameters or flow conditions most intimately associated with the flow phenomenon being studied. For example, in boundary layer flows, Reynolds number is generally of prime importance; in force and pressure measurements on slender bodies, generally the hypersonic similarity parameter $M\tau$ (where τ is the thickness ratio or angle of attack) is the governing variable; and in viscous interactions, the important parameter is a combination of Mach number and Reynolds number, $\chi = M^3/\sqrt{Re}$. Thus, each experiment requires an analysis of the flow phenomenon to determine the important parameters or conditions requiring duplication. The particular parameters pertinent to the various flow situations are treated in following sections of the report. Here, we will consider only some of the more important parameters to illustrate the degree of mismatch that results in the nonduplicated quantities. Furthermore, our attention will be concentrated on the lower boundary of the flight regime since that is where the maximum deviations will occur.

2. Density-Altitude and Velocity Duplication

For certain flow phenomena, the important parameters to be duplicated are the density-altitude (i.e., the free-stream density) and the flight velocity. These two parameters then insure duplication of the flux of free-stream momentum ($\rho_\infty U_\infty^2$) and energy ($\frac{1}{2} \rho_\infty U_\infty^3$).

Duplication of density-altitude and free-stream velocity implies a higher free-stream static temperature than in flight and, hence, a lower Mach number and unit Reynolds number (i.e., Reynolds number per foot, $\rho_\infty U_\infty / \mu_\infty$). For inviscid flows that are Mach number independent (e.g., blunt bodies), the lower flow Mach number imposes no restriction provided it is hypersonic (i.e., about 5 or greater). Similarly, for slender bodies, the hypersonic similarity parameter $M_\infty \tau$ can be maintained constant if the test model is thicker than the flight vehicle. Several curves of constant free-stream static temperature are shown in Fig. 2 when density-altitude and

8

velocity are duplicated. These curves are for reservoir conditions corres-
ponding to the full-duplication boundary line. It is seen that the static
temperatures can exceed 1500°K whereas the ambient altitude temperatures
are in the range 200°K to 300°K.

The following procedure has been used to determine test-section
conditions along the lower boundary of the flight regime when the density-
altitude and flight velocity are duplicated. First, the reservoir enthalpy
($H_o = \frac{1}{2} U_\infty^2$) and entropy (given by the altitude) corresponding to the full-
duplication boundary line (Fig. 2) are used to define on a Mollier diagram
for air [15] the maximum reservoir enthalpy available for equilibrium
expansion at a given entropy. For reference purposes this is shown in Fig.
6 (also shown for reference are several constant pressure lines); the altitude
data are given in Ref. 16 for the 1962 U.S. Standard Atmosphere. Next, for
a given velocity, the thermodynamic state along the full duplication line defines
an entropy. For this entropy, the temperature corresponding to the desired
density is read from the Mollier diagram[15]. If the resulting ambient tem-
perature is high enough so that the static enthalpy is not negligible compared
to the flow kinetic energy, then the total enthalpy must be increased by this
static enthalpy to preserve velocity duplication. In the calculations, the
total enthalpy was increased by moving along the limiting $H_o - S_o$ line
(Fig. 6) to a new entropy. Then, allowing an isentropic expansion to the
desired density, a new test flow static temperature was obtained and the
flow velocity recalculated. This single iteration preserved velocity dupli-
cation to within 1%. In Table II-1, the results are shown for the mismatch
in static temperature, Mach number and unit Reynolds number resulting
from velocity and density duplication of flight conditions along the lower
boundary of the altitude-velocity map.

4.   Reynolds Number Duplication

If the test models are smaller than the flight vehicle by a scale factor $\lambda < 1$, Reynolds number duplication requires that the unit Reynolds number of the test flow be λ^{-1} times greater than the flight unit Reynolds number. This is a severe requirement since, if the free-stream temperature and velocity of the test flow are of the same order as the flight values, then the test flow density must be λ^{-1} times greater than the flight density. As indicated in Ref. 8, high Reynolds numbers can be obtained by testing at low reservoir temperatures with the maximum available reservoir pressure and at low test flow Mach numbers. There will result, of course, a mismatch in all of the other flow quantities and only Reynolds number will be duplicated. Until the scale factor λ is specified, the required test conditions cannot be determined; hence, no calculations are presented here.

F.   FLOW REGIMES

In most of the high-density, hypervelocity flight regime the flow over a typical vehicle will contain regions of frozen, nonequilibrium and equilibrium chemistry. Significant simplifications in the similitude requirements result if all regions of the flow are frozen or in equilibrium. Thus, it would be desirable to be able to delineate such flow regimes. Unfortunately, any such delineation is dependent on the vehicle geometry, i.e., on the type of flow. Harney[17] has studied the particular cases of blunt-nose flow and the flow downstream of a specific oblique shock wave. He has delineated regions where the chemical effects are negligible (frozen flow), where nonequilibrium chemistry predominates and where the chemistry is in equilibrium. His results for these two cases are shown in Fig. 8, where it is seen that their boundaries are not coincident.

In the present work, the results of a series of nonequilibrium normal shock-wave solutions (Sec. V) have been used to delineate the flow regimes. The criteria adopted here differ from that used by Harney and are both more precise and somewhat stricter. Whereas Harney defined the boundary between frozen and nonequilibrium flows on the basis of no more than 10%

dissociation of oxygen, inspection of the temperature profiles behind normal shock waves (Sec. V) indicates that a suitable definition of the frozen flow boundary is the point at which the temperature has dropped to 99% of the initial, frozen temperature. At this point the degree of dissociation is small for all the cases investigated. For the boundary between nonequilibrium and equilibrium flows, Harney adopted a criterion based on the distance for atomic nitrogen to reach 90% of its equilibrium value. In the present work, the criterion is that the temperature be within 1% of the final equilibrium value, a point where all of the species concentrations are nearly at their equilibrium values also. These results are shown in Fig. 9. The advantage of the present criteria over those used by Harney is that they apply for all flight conditions, whereas the atomic nitrogen criterion is inappropriate at low velocity ($\simeq$ 10,000 fps) where nitrogen atoms are insignificant. The 1% deviation of temperature could be relaxed, of course, to provide criteria somewhat closer to those of Harney.

A comparison of the flow regimes delineated by the two sets of criteria is given in Fig. 10 for the stagnation streamline of a hemispherical body with a radius of one foot. Following Harney, the shock standoff distance is taken as 0.0961 ft. The flow is considered to be frozen when according to the above criterion the extent of frozen flow is equal to or greater than this shock standoff distance. The boundary for equilibrium flow in the nose region is taken to be when the equilibrium criterion is met at a distance of 1/10 the shock standoff distance. Because the present calculations were made only for altitudes up to 250,000 ft., the frozen-flow boundary required extrapolations of the curves in Fig. 9. It is observed in Fig. 10, that the present frozen-flow boundary is considerably higher than that given by Harney. This difference is largely due to the different criteria and only slightly affected by the extrapolation. The equilibrium flow boundaries given by the two criteria are in reasonable agreement in the velocity range 15,000 fps to 25,000 fps, but exhibit significantly different trends outside this range.

Two important conclusions about the flow over the flight vehicle can be drawn from these results. First, the only region where the flow may be

considered as completely frozen is at low velocity and high altitude. Second, in the region below the full duplication boundary for the postulated wind-tunnel performance, the flow will be in equilibrium or nearly so. For small scale tunnel models, the curves in Fig. 10 would move to lower altitudes at a fixed velocity. Thus, the flow over a model might be frozen,whereas the flow over the flight vehicle would be in the nonequilibrium regime; or the model flow might be of a nonequilibrium nature, whereas the flight vehicle experienced a completely equilibrium flow. This clearly serves to indicate the importance of understanding the influence of chemical kinetics on hypervelocity flows.

G.   SUMMARY

The flight regime of interest here has been shown to include that portion of the flight path lying below 250,000 ft altitude and above 10,000 fps velocity for most hypervelocity vehicles. Present-day wind tunnels are capable of fully duplicating the altitude-velocity conditions for only a limited region of this flight regime. Consequently, a performance map for a future wind tunnel has been postulated and the resulting test conditions have been investigated. It was found that for this hypothetical wind tunnel nozzle-flow nonequilibrium effects on velocity and gas composition will be restricted to the region where the tunnel could, in their absence, fully duplicate the flight conditions. The various frozen, nonequilibrium and equilibrium flow regimes have been briefly considered and it was shown that the nonequilibrium flow regime is roughly coincident with the full-duplication region of the hypothesized wind tunnel,whereas equilibrium flow exists in the region where simulation must be employed.

Before investigating the consequences of this situation for various flows, the appropriate hypersonic similitudes for inviscid and viscous flows will be reviewed.

III. REVIEW OF HYPERSONIC INVISCID SIMILITUDES

A. GENERAL FEATURES

It is always necessary to keep in mind that a similitude is not a theory for predicting flow fields, i.e., it does not provide any solutions to the problem, but only a relation between solutions. The point here is that the effects of mismatches in the similitude parameters between tunnel test and flight can be evaluated only if there exist flow field solutions. In this respect, numerical solutions are useful for evaluating a few specific cases; on the other hand, analytical solutions have a broader application with regard to trends or the effects of more than one similitude parameter. With this thought in mind, the existing similitudes for inviscid hypersonic flows have been reviewed.

The problem of similitude at hypersonic speeds and, in addition, its relation to the capabilities of experimental facilities has received considerable attention in the past (e.g., see Refs. 14, 18-34). In view of the difficulties inherent in wind-tunnel duplication of extreme flight conditions, it is obviously very desirable to extend the traditional role of the wind tunnel as a device for simulation of flight situations. Certainly in the past, the great success of wind-tunnel testing has depended very heavily on certain powerfully broad similitude or scaling laws which permit data obtained from tunnel tests at other than flight conditions (i.e., model scaling) to be interpreted for the flight situation. For example, in the ideal-gas regime appropriate to lower hypersonic velocities than those of present interest, the basic similitude parameters for inviscid air flows are the (constant) specific heat ratio γ and the ambient flow Mach number M_∞. For a tunnel model which is geometrically similar to the flight vehicle, only these two parameters need to be duplicated for correct inviscid flow similarity. In particular, ambient density, velocity, and model scale are arbitrary within rather wide limits. The Mach number requirement per se may be further relaxed for slender pointed bodies characterized by a thickness ratio $\tau, (\tau^2 \ll 1)$. In that case, only γ and the hypersonic similarity parameter $M_\infty \tau$ need be duplicated[22, 23].

In viscous hypersonic flows most of the generality inherent in the above inviscid similitude is lost. Additional parameters introduced by the inclusion of viscosity are Reynolds number, Prandtl number, and wall-to-stagnation temperature ratio. Furthermore, when the boundary layer displacement thickness is large enough to alter the outer inviscid flow, an interaction parameter $\chi = M^3 / \sqrt{Re}$ must be introduced.

In the flight regime of present interest, the principal difficulty in the similitude question is, of course, the enormously complicated physical-chemical behavior of air at the high temperatures occurring behind strong shock waves. Rather than being characterized by the single parameter γ as in the ideal-gas regime, this aspect of the question now involves: at best, a complex system of nonlinear differential equations describing physical-chemical rate processes for energy transfer and species formation; at worst, the phenomenological description of the pertinent chemical and ionization rate processes may not even be known. For air, the dependence of the mathematical description of chemical kinetics on temperature is so complex that the possibility of relaxing the requirement for duplication of the temperature level in a general sense appears remote. This fact implies velocity duplication for geometrically similar bodies. In turn, scale duplication is therefore necessary in order that characteristic particle residence times L/U_∞ be preserved for geometrically similar bodies. There has been considerable effort devoted to studying a single-species diatomic gas (e.g., see Ref. 34-38) to investigate the important aspects of equilibrium and nonequilibrium phenomena. While such an approach has been successful in a qualitative manner, it has been less effectual when quantitative results pertinent to air flows are desired.

The fact that there appears little possibility of general similitudes for hypervelocity air flows over geometrically similar bodies does not mean that useful similitudes of a restrictive nature do not exist or cannot be found. Indeed, the results of the present work offer some contribution in this respect. One simplifying aspect of the current regime of interest is that because of the relatively high densities (Reynolds numbers) involved, the regime is one where separation of the flow field into an outer inviscid layer and a (relatively) thin inner boundary layer is a valid approximation in general (see, for example,

the estimates by Harney, in Ref. 17). Consequently, it is appropriate to review the present status of hypersonic similitudes under the headings of inviscid and viscous flows.

B. MACH NUMBER INDEPENDENCE PRINCIPLE

Although Oswatitsch[39] in his analysis of the hypersonic flow of an ideal gas gave Mach number independence as a similitude, Hayes and Probstein[25] (pp. 24-26) have pointed out that it is more properly a principle rather than a similitude and have generalized it to include real gas effects. Mach number independence results as a limiting process ($M_\infty \longrightarrow \infty$) when the free-stream density and velocity of the undisturbed flow are fixed. A requirement of the principle is that at any point on the bow shock wave about a body the density ratio be independent of M_∞, i.e., the shock wave must be everywhere strong. If σ is the shock angle relative to the free-stream velocity, then the requirement is that $M_\infty^2 \sin^2 \sigma$ be large compared to the density ratio across the shock. Thus, it is clear why blunt bodies exhibit Mach number independence at lower values of M_∞ than slender bodies do.

For a perfect gas, the Mach number independence principle states that the flow field behind the bow shock wave of a blunt body reaches a limiting configuration as the free-stream Mach number becomes very large. In particular, the pressure coefficient, the density ratio across the shock wave, and all the quantities which determine the geometry of the flow field behind the shock wave, such as streamline inclinations and Mach angles, tend to a constant limiting value. However, the temperature and pressure ratios across the shock wave increase unbounded as the square of the Mach number.

Hayes and Probstein[25] state the Mach number independence principle as follows: "The flow around a body and behind the bow shock depends only upon the density ρ_∞ and the uniform velocity U_∞ of the given gas in the free-stream, and is independent of the free-stream pressure p_∞, enthalpy H_∞, temperature T_∞, and speed of sound a_∞." Thus, two geometrically similar flows with the same ρ_∞ and U_∞ and large, but different,

M_∞ , are not merely similar, but are essentially identical behind the bow shock. Hence, the independence principle applies to all real fluid effects: viscosity, heat conduction, relaxation, diffusion, etc. As a consequence of this, the Mach number independence principle holds for boundary layers in hypersonic flows provided that the outer inviscid flow follows the principle.

Obviously, the Mach number independence principle is a powerful concept since it is more general than a similitude. However, the principle would be even more powerful if the limits of its application were clearly delineated. It is also worthwhile noting here that different flow quantities attain Mach number independence at different values of the free-stream Mach number. Thus, the pressure coefficient behind an oblique shock wave in a perfect gas reaches Mach number independence at a lower Mach number than the density ratio across the shock wave [40]. Also, experimental evidence has shown that the flow fields behind many blunt bodies reach Mach number independence at surprisingly low Mach numbers. For example, Hodges [41] has found that the drag coefficient on a sphere becomes Mach number independent at a free-stream Mach number of about four. This, of course, is also the justification for obtaining hypersonic stagnation point heat-transfer data in a shock tube where the free-stream Mach number is only about three[42,43].

C.   HYPERSONIC SMALL DISTURBANCE SIMILITUDE

The similarity laws of hypersonic, inviscid, irrotational flows of an ideal gas with constant specific heats over slender, pointed bodies were first given by Tsien[22]. Hayes [23] showed the equivalence of a steady hypersonic flow over a slender body with an unsteady flow in one less space dimension and thus extended Tsien's results to rotational flow. Subsequently, many investigators have looked into various aspects of this hypersonic similitude for slender bodies of revolution, planar bodies, and wing-body combinations at small angle of attack [26-32]. The studies confirm that similitude applies only among flow fields having the same specific heat ratio γ as well as the same value of the hypersonic similarity parameter $M_\infty \gamma$.

The classical similitude of Tsien and Hayes states that for a family of affinely related slender bodies of characteristic thickness ratio γ in a perfect gas of constant specific heat ratio γ , the dependence of the pressure

coefficient C_p on M_∞ and γ separately, may be reduced to a dependence of C_p/γ^2 on the single parameter $M_\infty \gamma$. Similarly, the lift and drag coefficients can be expressed as

$$C_L = \gamma^2 \; fcn \; (M_\infty \gamma, \; \gamma)$$

$$C_D = \gamma^3 \; fcn \; (M_\infty \gamma, \; \gamma)$$

if the lateral projected area is used as the reference for both coefficients.

Cheng[33] has made an important extension of this classical slender-body hypersonic similitude to include the effects of small nose bluntness and equilibrium real-gas phenomena. The equilibrium real-gas similitude obtained by Cheng requires duplication of the ambient flow thermodynamic and chemical state (i.e., pressure p_∞ , density ρ_∞ , temperature T_∞ , and species concentrations X_{i_∞}) in addition to $M_\infty \gamma$ and a nose bluntness parameter

$$K_N \equiv M_\infty^{\frac{3+\nu}{1+\nu}} \; C_{D_N}^{\frac{1}{1+\nu}} \; \frac{d_N}{L} \qquad\qquad (\text{III-I})$$

where ν = 0 and 1 for plane and axisymmetric flows, respectively, C_{D_N} is the nose drag coefficient, d_N is the thickness or diameter of the blunt nose, and L is the body length. When the ambient free-stream state is duplicated and the parameters $M_\infty \gamma$ and K_N are reproduced, correct similitude is obtained without the restriction of duplicating U_∞ and L , per se. They are arbitrary, provided the flow is everywhere in complete thermo-chemical equilibrium. It may be noted that the local flow-field temperature and density are duplicated in this similitude by virtue of the duplication of $M_\infty \gamma$.

The equilibrium real-gas similitude of Cheng is applicable only for slender bodies. For blunt geometries, the Mach number itself must be duplicated in addition to the free-stream state when flight and tunnel bodies are geometrically similar. When the Mach number independence principle applies, duplication of the free-stream state is not required. In either event, this means duplication of U_∞ . Therefore, the only remaining freedom,

in general, is in the model scale L . By virtue of the equilibrium assumption, this remains arbitrary for the inviscid problem. It should be noted, however, that for the viscous or boundary-layer problem even this freedom is lost as the Reynolds number $\rho_\infty U_\infty L/\mu_\infty$ must be duplicated.

Another point to note with regard to the present study is that the requirements of completely equilibrium flow and duplication of the ambient free-stream thermodynamic state are incompatible in terms of the present hypothetical wind-tunnel performance and the equilibrium flow regime for slender blunted bodies; that is, the flow is most likely to be in complete equilibrium in the altitude-velocity range where the tunnel cannot duplicate all of the free-stream conditions. Where the tunnel can duplicate the ambient altitude state, the flow will probably exhibit nonequilibrium regions. Cheng[33] briefly considered the question of extension of the hypersonic similitude to nonequilibrium flows. He suggested that for slender bodies, a nonequilibrium similitude should exist for a two-component reacting gas when $M_\infty \gamma \gg 1$. The nonequilibrium similitude requires that the particle transit time L/U_∞ be duplicated in addition to $M_\infty\gamma$, K_N , p_∞ , ρ_∞ , and X_{i_∞} . Then, the scale L is not arbitrary as for equilibrium, but is fixed by the choice of U_∞ .

The formal development of the nonequilibrium hypersonic similitude for a single-species diatomic gas has been carried out by Inger[34], who reached the same conclusion as Cheng.

Inger showed that the solution of the hypersonic small-disturbance equations is the same for all slender bodies of the form $y_{body}/\tau L = f(x/L)$ when each of the following parameters is held constant:

α_∞ the free-stream atom mass fraction

$\lambda_D = T_D/T_\infty$ where T_D is the characteristic dissociation temperature of the diatomic gas

$\lambda_v = T_v/T_\infty$ where T_v is the characteristic vibration temperature

$\lambda_\rho = \rho_D/\rho_\infty$ where ρ_D is the characteristic dissociation density

$\bar{e}_{v_\infty} = e_v / R_M T_\infty$ where e_v is the energy in molecular vibration and R_M is the undissociated gas constant

ω, β the recombination rate and vibrational relaxation rate temperature dependence exponents, respectively

$K_R = \dfrac{k_R L T_\infty^\omega \rho_\infty^2}{U_\infty \, m_M^2}$ the ratio of residence time to reaction time (k_R is the recombination rate constant and m_M is the molecular weight of the molecule)

$K_v = \dfrac{k_v L T_\infty^\beta \rho_\infty}{U_\infty \, m_M}$ the ratio of residence time to vibrational relaxation time (k_v is the vibrational relaxation rate constant)

K_N the nose bluntness parameter introduced by Cheng

$M_\infty \tau$ the hypersonic similitude parameter

Inger[34] then specialized this similitude to cones and wedges in a manner similar to that of Cheng for equilibrium flows. The essence of this similitude is that the ambient free-stream conditions must be duplicated, as well as the similitude parameters K_R, K_v, K_N and $M_\infty \tau$. The results are of rather limited value as far as correlating experimental data or numerical solutions because of these requirements. However, the required test conditions necessary to simulate a specific flight condition may be determined. It can be seen that duplication of K_R and K_v for a given gas reduces to duplicating L/U_∞ if the free-stream conditions are duplicated. These special similitudes will be discussed further in Section VI, Slender Bodies.

Inger[34] also considered alleviation of the duplication of ρ_∞, U_∞, and T_∞ for the case of a Lighthill gas[35]. His result is an example of binary scaling and will be discussed in that context next.

Just as in the case of Mach number independence, these theories do not and cannot give the lower limit of the Mach number or the upper limit of the slenderness ratio for which the theories would yield reasonable results. Often, the similarity parameters obtained from these theories are applicable over a wider range of Mach numbers and slenderness ratios than might be expected from the assumptions made in their derivation. For example,

Ehret, Rossow, and Stevens[26] have used exact numerical solutions obtained by the method of characteristics to check the range of applicability of the hypersonic similarity law for the flow of a perfect gas about bodies of revolution. They considered flow past conical and ogival nosed cylinders of nose length to diameter ratio varying between 3 and 12 in the Mach number range between 3 and 12. They found that even at the lowest Mach number and length-to-diameter ratio, the results correlated very well with the hypersonic similarity parameter, $M\gamma$. It is not clear whether such good correlations would be obtained when the body is two-dimensional or when real gas effects are included. Clearly, the practical usefulness of hypersonic similarity laws would be greatly enhanced if the range of their applicability could be determined.

D. BINARY SCALING

As described in Refs. 44-47, binary scaling offers relief from the requirement that the ambient density level be duplicated. The concept applies whenever the chemical kinetics of the nonequilibrium problem are governed by two-body collision processes only. This is the case whenever three-body atomic and/or ionic recombination are unimportant. Such a situation is favored by high altitude (low density), small scale, and low velocity U_∞. When the approximation is valid, the entire nonequilibrium flow fields about two geometrically-similar blunt bodies characterized by scale L are identical, provided that the ambient velocity U_∞ and the binary scaling parameter $\rho_\infty L$ are the same for both bodies. While this similitude does not relax the requirement for velocity duplication, it does relax the requirement on duplicating ρ_∞ and L individually. Either ρ_∞ or L may be chosen arbitrarily, within limits of the basic assumptions involved, and the remaining quantity is then determined. It may be noted that M_∞ need not be duplicated for the blunt nose region itself, provided $M_\infty >> 1$ and the strong shock assumption is locally satisfied along the bow shock wave (i.e., $M_\infty^2 \sin^2 \sigma >> 1$). Binary scaling is applied to blunt body flows by the shock-mapping technique described by Gibson and Marrone[48].

Correlations of numerical solutions of nonequilibrium airflows are given in Refs. 45 and 46. The detailed examples of nonequilibrium scaling described by Gibson and Marrone[46] demonstrate the applicability of binary scaling to flight conditions of practical interest. Reference 46 notes that binary scaling could also apply to vibrational and electronic relaxation processes. An important consequence is that shock-layer radiation may be scaled. Furthermore, Ref. 44 indicates that binary scaling is also expected to apply to viscous nonequilibrium flows.

Inger[34] has pointed out the further extension of Cheng's blunt slender-body similitude for inviscid nonequilibrium flow when the concept of binary scaling applies. In this case, duplication of ρ_∞, as well as U_∞, can be relaxed. For the same ambient gas composition in flight and tunnel, binary scaling for the slender, blunt-nosed body is governed by the parameters.

$$M_\infty \gamma \, , \qquad K_N = M_\infty^{\frac{3+\nu}{1+\nu}} C_{D_N}^{\frac{1}{1+\nu}} \frac{d_N}{L} \, , \qquad \frac{\rho_\infty L}{U_\infty} \, , \qquad T_\infty \, , \qquad \text{and} \quad X_{i_\infty}$$

Thus, additional freedom is obtained with binary scaling in this case: both U_∞ and ρ_∞ may be chosen arbitrarily, provided the above parameters are duplicated and all other pertinent assumptions are satisfied. The consequences of this are discussed in Sec. VI, Slender Bodies.

A basic question of importance is the determination of the limits of validity of binary scaling with respect to ρ_∞ (or altitude), U_∞ and L. This has been studied by Gibson and Marrone[46,47] on the basis of the shock-mapping technique which relates normal shock and blunt-body flows through a shock-mapping parameter. They define a limit of applicability of binary scaling as the condition where the ratio of reverse to forward reaction rates in the nitrogen dissociation process attains a value of 0.3 downstream of a normal shock wave. Further study of this question has been reported by Ellington[49] who used a mass fraction criterion for determining the limit of binary scaling. A comparison of the two criteria has been given by Ellington who finds a somewhat wider range of applicability than claimed by Gibson

and Marrone. As part of the present work, the solutions of nonequilibrium normal shocks have been studied from the standpoint of binary scaling, and even more general applicability than reported by Ellington has been found. These results are reported in Sec. V of this report.

E. FREE-STREAM DISSOCIATION

It has already been shown in Sec. II-D that free-stream dissociation caused by nonequilibrium effects occurring in hypervelocity nozzle airflows will be restricted to the region where the wind tunnel could otherwise completely duplicate the flight condition. Although there is no similitude for the problem of ambient dissociation in the free-stream, Gibson[50] has developed a promising approach to the problem for blunt-body shapes of arbitrary geometry on the basis of velocity duplication between tunnel and flight.

In Ref. 50, a subtraction rule correlation is developed for relating tunnel and flight nonequilibrium flows. For a pure diatomic gas, this relation is expressed by $\alpha_F = \alpha_T - \alpha_{\infty_T}$ where α is the local degree of dissociation in the body flow field, and α_{∞_T} is the ambient degree of dissociation in the tunnel ($\alpha_{\infty_F} = 0$), and the subscripts F and T refer to flight and tunnel, respectively. This relation applies to corresponding points in the tunnel and flight cases, the geometric relation between such points depending on a scale factor involving α_{∞_T} . At such corresponding points, the gas temperatures are also equal in tunnel and flight cases, and the densities are in a constant ratio. Model geometries in tunnel and flight are simply related by predetermined constant scale factors. The subtraction rule concept is further extended in Ref. 50 from a pure diatomic gas to a simplified (oxygen dissociation) model of air. Consideration is also given to wind tunnel gas mixtures other than normal undissociated air, and it is shown that the range of validity of the subtraction rule can thereby be widely extended in regard to the magnitude of α_{∞_T} .

IV. REVIEW OF HYPERSONIC VISCOUS SIMILITUDES

A. INTRODUCTION

This section presents a summary of the similitudes that apply to hypersonic flows for cases where transport effects due to viscosity, diffusion, thermal conduction, and the like all play a role. Generally speaking, the Reynolds number and wall-to-free-stream temperature ratio now enter the problem, in addition to the parameters that already have appeared in treatment of the inviscid portion of the flow. Furthermore, other parameters may be important, for example, the ratios of typical chemical reaction times to typical flow times. On the other hand, there are also cases when the separate effects of Mach number and Reynolds number can be combined in the form of some composite parameter.

In order to simplify the discussion, the ten categories of viscous flow that will be considered are identified in Table IV-1 according to the section letter in which they will be discussed. Here, the viscous flows are grouped as laminar, transitional or turbulent. The table is divided according to whether the particular quantity of interest is the pressure distribution or the heat transfer on the one hand, or the distribution of chemical species on the other hand. A further subdivision is made into flows with and without mass addition.

In this review, no attempt has been made to include all of the pertinent references. Instead, only a representative sample has been considered. It should also be pointed out that the results given below contain much less definitive numerical information about the effects of relaxation of similitude requirements than is given for inviscid flows in other sections. However, quantitative estimates of this sort are given for a number of cases.

TABLE IV-1

CATEGORIES FOR VISCOUS SIMILITUDES

	LAMINAR			TRANSITIONAL	TURBULENT	
PRESSURE DISTRIBUTION FORCES, MOMENTS HEAT TRANSFER	No Mass Addition	With Mass Addition			No Mass Addition	With Mass Addition
		steady	unsteady			
	Ⓑ	Ⓓ	Ⓔ	Ⓖ	Ⓗ	Ⓙ
SPECIES DISTRIBUTION CHEMICAL NONEQUILIBRIUM SURFACE-CATALYTIC EFFECTS	Ⓒ	Ⓕ			Ⓘ	Ⓚ

QUANTITIES OF INTEREST

Note: The viscous similitudes for each category are discussed in Sec. IV under the subsections indicated by the letter

B. LAMINAR BOUNDARY LAYERS WITHOUT CHEMICAL REACTIONS OR ABLATION

1. Blunt Body at High Reynolds Number

One of the simplest similitudes is that concerned with stagnation-point heat transfer at relatively high Reynolds number. For such problems, it has been shown by Vidal et al[42], Rose and Stark[43], and others that the Mach number dependence disappears at Mach numbers as low as three. Thus, it is only necessary to duplicate the Reynolds number and the enthalpy difference across the boundary layer. This conclusion can be seen by examining any of the correlation formulas giving the solution to the stagnation-point heat transfer problem. One of the best known of these formulas is that proposed by Fay and Riddell[51].

$$q = \frac{0.76}{(P_r)^{0.6}} \left(\frac{\rho_{s,e}\,\mu_{s,e}}{\rho_w\,\mu_w}\right)^{0.4} \left\{ 1 + \left(Le^{0.52} - 1\right)\frac{H_D}{H_{s,e}}\right\}(H_{s,e} - H_w)\sqrt{\rho_w\,\mu_w\left(\frac{du}{ds}\right)_{s,e}} \qquad (IV-1)$$

Further discussion regarding the effects of mismatches in the similitude parameters for this case is given in Sec. VIII-C.

2. Blunt Body at Low Reynolds Number

When the Reynolds number becomes sufficiently low, a variety of second-order effects enter the problem. One of the first papers to call attention to this fact is that of Ferri and Libby[52], who pointed out the influence of vorticity at the boundary-layer edge. Later Rott and Lenard[53] called attention to the fact that, in any consistent second-order treatment, all of the pertinent effects must be included. Subsequent papers on this general problem have considered the influence of external vorticity, viscous interaction, transverse curvature, surface slip effects, and of departures from the Rankine-Hugoniot relations behind the shock wave. The general form of these second-order corrections is usually expressed in terms of the ratio of stagnation-point heat transfer with the second-order

effects included to that in the so-called "boundary layer" regime where these effects are negligible. When expressed in this fashion, the second-order corrections are inversely proportional to the Reynolds number and have a coefficient that depends chiefly on the density ratio across the shock. Expressions of this general form have been given in several survey papers by Van Dyke [54, 55]. Generally speaking, the corrections to the boundary-layer results can be on the order of 10 to 40%, depending on the circumstances.

Some quantitative estimates of these effects, and also an indication of the minimum Reynolds number at which they can be neglected, can be found in the work of Ferri, Zakkay, and Ting[56], and also in the work of Howe and Sheaffer[57]. It appears from the work of Ferri, Zakkay, and Ting[56] that the increase in heat transfer over the value with vorticity excluded is less than 5% when $\omega < 0.03 \sqrt{2 A\, Re_{F\&T}}$

where

$$\omega = \frac{\partial(u/u_e)}{\partial(n/R_N)} \quad , \quad Re_{F\&T} = \frac{\rho_{s,e}\, R_N \sqrt{H_0}}{\mu_{s,e}} \quad , \quad A = \frac{\partial\left(u/\sqrt{H_0}\right)}{\partial(s/R_N)}$$

The shock-layer calculations of Howe and Sheaffer[57], which include effects of radiative transport, indicate that the heat-transfer increase is less than 5% provided $\dfrac{\rho_s\, R_N \sqrt{H_s}}{\mu_s} > 10^4$, for flight speeds up to 30,000 fps. The correction increases with increasing flight speed; for $U_\infty = 50,000$ fps, corrections are encountered for $\rho_s R_N \sqrt{H_s}/\mu_s < 10^5$. A similar comparison has been given by Cheng[58] who indicates that a 5% (or less) increase in heat transfer is experienced when $\rho_s R_N \sqrt{H_s}/\mu_s > 3 \times 10^4$.

It must be pointed out that quantitative estimates of the second-order effects, as given by Ferri et al[56], have been criticized by Van Dyke[55] and also by Cheng[58], in that consistent account of all the second-order effects was not taken. Partly for this reason, an accurate estimate of the influence of the second-order effects is not easy to make, and the point at which a 5% increase is met is somewhat uncertain.

3. Slender Body at High Reynolds Number

Recently, a great deal of attention has been centered on the use of slender shapes for reentry vehicles. In order to make predictions of the

heat transfer and pressure distribution around such a body, it is necessary to extend the stagnation-point theory referred to above. The most appropriate theory appears to be that of local similarity, first introduced by Lees[59] and subsequently refined by Kemp, Rose, and Detra[60], among others. Of course, as one moves around the spherical nose toward the conical afterbody, the Mach number at the boundary-layer edge begins to increase and, for that reason, the neglect of Mach number as an external-flow parameter begins to introduce serious errors. However, since one is primarily interested in the stagnation-point heat transfer, very little attention has been given to the question of how far around the body one can extend the local-similarity analysis without including the effect of external Mach number variations.

A thorough study of laminar heat transfer to blunted slender cones has been given by Griffith and Lewis[61]. These authors have succeeded in presenting a correlation of cone surface pressures in the form

$$\frac{C_p}{2\theta_c^2} = fcn\left(\frac{\theta_c^2}{\gamma \epsilon C_{D_N}}, \frac{x}{d_N}\right) \tag{IV-2}$$

where $C_p = (p_w - p_\infty)/\frac{1}{2}\rho_\infty U_\infty^2$, x is axial distance, θ_c is the cone half-angle, $\epsilon = \frac{\gamma - 1}{\gamma + 1}$, d_N is the nose diameter $(2R_N)$, and C_{D_N} is the nose-drag coefficient. They were also successful in correlating heat transfer in the form

$$\left(\epsilon C_{D_N}\right)^{1/4} C_H \sqrt{\frac{Re_{\infty,d}}{C_*}} \Bigg/ M_\infty^2 \theta_c^2 \left(1 + \frac{2}{\gamma M_\infty^2 C_p}\right) = fcn\left(\frac{\theta_c^2}{\gamma \epsilon C_{D_N}}, \frac{x}{d}\right) \tag{IV-3}$$

where

$$C_H = \frac{q}{\rho_\infty U_\infty (H_o - H_w)}, \qquad Re_{\infty,d} = \frac{\rho_\infty U_\infty d_N}{\mu_\infty}$$

and the Chapman-Rubesin viscosity constant, evaluated at the reference temperature $T_* = \frac{T_o}{6}\left(1 + 3\frac{T_w}{T_o}\right)$, is

$$C_* = \frac{\mu_*}{\mu_\infty} \frac{T_\infty}{T_*}$$

This work has also led to a proportionality between the ratio of local heat-transfer rate to the stagnation-point heat-transfer rate and the quantity $C_p + \frac{2}{\gamma M_\infty^2}$ which is a measure of the surface pressure. For γ equal to 1.4, the correlation takes the form

$$\frac{q_w}{q_{s,w}} = 0.8 \left(C_p + \frac{2}{\gamma M_\infty^2} \right) \tag{IV-4}$$

This correlation is valid for

$$0.05 < \frac{\theta_c^2}{\gamma \epsilon C_{D_N}} \frac{x}{d_N} < 0.60$$

4. Slender Body at Low Reynolds Number

The literature describing the effects encountered at low Reynolds number on a slender body includes many parameters which are composites of the Mach number and Reynolds number. An interesting discussion of these composite parameters has been given by Charwat[21], who points out that the Mach number effect arises from the scale of the flow distortion due to wave effects, whereas the Reynolds number enters because of the scale of flow distortion due to diffusive effects. Typical of parameters of this type is the quantity $\bar{\gamma}$ (see Hayes and Probstein[25], p. 338) and also the parameter $\overline{V}_\infty$, whose derivation is discussed by Lewis and Whitfield[62].

At sufficiently low Reynolds number, the principal contribution to the drag of a slender vehicle is due to viscous effects. Several authors, among them Whitfield and Griffith[63], Crawford[64], and Dayman[65] have presented calculations of the drag-coefficient increase due to viscous effects. The various authors usually find a linear dependence of viscous drag on $\overline{V}_\infty$, with the influence of shape, i.e., of cone angle, playing a relatively minor role for values of $\overline{V}_\infty$ greater than 0.3. The effect of wall temperature has been studied, among others, by Dayman[65] and Crawford[64]. The latter author found the slope of the total drag versus temperature curves to be linear. The slope increases for increasing bluntness and also depends on the hypersonic viscous parameter $\overline{V}_\infty$.

Some measurements of heat transfer and pressure on pointed cones at low Reynolds number have been given recently by Waldron[66]. He reported good agreement with Cheng's viscous-layer analysis[58] for non-slender cones. For sufficiently small cone angle and sufficiently high Reynolds number, his results merged with those of a conventional boundary-layer analysis, including transverse-curvature effects. Waldron was led to the conclusion that transport processes behind the shock constitute the largest effect and that this effect is correctly predicted by Cheng's theory[58], even for slender cones where transverse-curvature effects are present.

C. LAMINAR BOUNDARY LAYERS WITH CHEMICAL REACTIONS, NO ABLATION

In the discussion above of similitudes for heat transfer, it was as-sumed that the gas was chemically inert. In many cases of interest, however, the chemical reactions occurring in the gas must be considered. When these considerations enter, they bring with them new similitude parameters which must be duplicated. These generally take the form of the ratio of a chemical relaxation time to a typical flow time. In addition, the presence of chemical reaction in the flow raises the question whether chemical reactions may also occur at the surface. For many cases it is possible to achieve substantial reductions in heat-transfer rate by the use of a noncatalytic surface. Con-siderations of this effect can be found, for example, in papers by Fay and Riddell[51], Inger[67,68], Hartunian and Thompson[69], Carden[70], and Rosner[71]. The general conclusion from these papers is that there is little influence of chemical reactions on heat transfer if the surfaces are catalytic or if the reactions maintain a nearly equilibrium condition. On the other hand, if the reactions produce a nonequilibrium condition, a noncatalytic wall may exper-ience heat-transfer rates as much as 50% below those for a catalytic wall.

Most of the effective similitudes for hypersonic flows in which chemical reaction must be considered are based on simplification of the chemical reaction rate, either by neglect of recombination or dissociation rates. One of the earliest similitudes of this type is that dealing with stagnation-point flows at relatively high Reynolds number. For this type of

problem most of the chemical production occurs immediately behind the shock and, for that reason, the boundary layer on a highly cooled stagnation point experiences mainly recombination as the dominant chemical reaction[67]. Rose and Stark[43] point out that flows of this type can be simulated by duplicating the parameter $\rho_s^2 R_N$ where ρ_s denotes the stagnation-region density and R_N denotes the body nose radius. A similar conclusion is reached in the work of Chung and Liu[72].

The combined effect of recombination-dominated gas-phase chemistry and the consequences of surface-catalytic reaction are considered by Inger[60]. The result of his analysis is a prediction of the quantity $P - P_f / P_{\eta} - P_f$ where P may represent either the surface value of the atom concentration, its gradient, the temperature, or the heat transfer. This ratio is predicted to depend chiefly on the parameter Γ^*, which is a composite Damköhler number that accounts for the combined effects of homogeneous and heterogeneous reactions.

This method has been extended, via a local-similarity analysis, to flows around blunt-nosed bodies in Ref. 73. This generalization introduces the new parameter $u_e^2 / 2 \bar{C}_{p_e} T_e$, which is a measure of the temperature rise due to viscous dissipation. For sufficiently large values of this parameter, the temperature rise is so large that dissociation reactions predominate over those of recombination. Inger points out that for highly cooled surfaces, the flow remains controlled by the recombination rate, even in the presence of viscous dissipation, provided that $u_e^2 / 2 \bar{C}_{p_e} T_e \lesssim 1$.

For cases when the Reynolds number is sufficiently low, Inger[68] has presented a generalization of Cheng's solution[74] to include nonequilibrium reaction, diffusion, and surface catalysis. Finally, the effect of free-stream dissociation on such flows has been considered by Buckmaster[75].

The opposite extreme for the chemical reaction is to consider the case where the chemistry is dominated by production reactions, that is to say by two-body reactions. For this type of flow, Gibson and Marrone[47] have pointed out that similitude can be achieved by matching the product of ambient density with the characteristic length in the problem. This binary-

scaling similitude was applied to the case of a flat-plate laminar boundary layer by Rae[76]. The general type of similitude implied in such an analysis has been discussed briefly by Chung[77].

The most useful application of binary similitude in chemically reacting boundary layers is that discussed by Levinsky and Fernadez[78]. The principal contribution made by these authors was to simplify the coupled chemical kinetic reactions for air near the tip of a sharp slender cone, where viscous heating causes dissociation of oxygen, followed by the rapid "shuffle" reactions, and production of electrons. Based upon their simplification, these authors derived a scaling law in which the maximum electron density in the boundary layer on a sharp cone displays a cubic-power dependence on distance from the apex of the cone in the following manner

$$\frac{n_{e^-}}{p} = 1.48 \times 10^{+8} \left(\frac{1000}{T}\right)^{6.5} \left(\frac{p\,s}{U_\infty}\right)^{3} exp \left\{-\frac{185,000}{T}\right\} \qquad \text{(IV-5)}$$

Here, n_{e^-} denotes the maximum electron number density in the boundary layer, in cm^{-3}, p the cone-surface pressure in atm, and T the maximum temperature in the boundary layer, in degrees Kelvin. This correlation appears to work successfully up to values of $p s/U_\infty$ on the order of 10^{-5} atm-sec for cone half-angles on the order of 10°, which correspond to maximum boundary-layer temperatures on the order of 4500°K. It is interesting to note that in addition to the results correlated in Ref. 78, some more recent calculations presented by Mondrzyk[79] also yield to a cubic scaling law. Fig. 11 shows the results found from Ref. 79.

The correlations of electron densities on sharp cones show an approach to the equilibrium concentration when the parameter $p s/U_\infty$ approaches 10^{-4} atm-sec. It is of interest to relate this parameter to a value of the local Reynolds number in order to see whether the approach to equilibrium appears before or after the onset of turbulent flow. Using the correlation of Griffith and Lewis[61], neglecting the ambient pressure and taking the pressure coefficient to be unity for a sharp cone on the order of 8° half-angle, the surface pressure can be written $p_w \approx \rho_\infty U_\infty \theta_c^2$.

33

Using this relation, the Reynolds number based upon free-stream conditions and on distance s from the vertex can be related to the binary scaling parameter of Levinsky and Fernandez[78] as

$$\frac{\not p s}{U_\infty} = \frac{\rho_\infty U_\infty^2 \theta_c^2 s}{U_\infty} \quad , \quad \frac{\rho_\infty U_\infty s}{\mu_\infty} = \frac{\not p s / U_\infty}{\mu_\infty \theta_c^2} \qquad (IV-6)$$

For altitudes between 100 and 250 Kft, the viscosity in the ambient stream has a value of approximately 1.7×10^{-10} atm-sec, and thus for a cone half-angle of 8°, the Reynolds number at which gas-phase reaction approaches equilibrium is on the order of 2×10^7. The conclusion is that the boundary layer is probably close to transition (see the discussion below concerning transition Reynolds number) if not already turbulent at the point where the gas-phase reactions are approaching equilibrium.

The similitude requirements that are imposed when one is interested not only in the distribution of electrons, but also in their interaction with an impressed electromagnetic wave, have been discussed by Flax[80] and by Glick[81]. The latter author concludes that full duplication of the flight condition is required in cases where chemical nonequilibrium occurs.

D. LAMINAR BOUNDARY LAYERS WITH STEADY ABLATION, NO CHEMICAL REACTIONS

1. General Considerations

The use of either ablation or mass injection in order to limit heat-transfer rates to re-entry vehicles has led to an extensive literature concerning viscous flows with mass addition at the surface. Generally speaking, the effect of introducing mass at the surface requires that two parameters be duplicated. One of these is the Reynolds number, while the new parameter is a measure of the rate of injection.

Usually the effects of mass injection on heat transfer are much more significant than its effects on pressure distribution or shock shape. There does exist an upper limit, however, after which the rate of mass injection becomes severe enough to exert an influence on the pressure and shock shape as well.

The similitude requirements and potential similitude methods for flows with mass injection are treated in Section X.

2.   Blunt Body at High Reynolds Number

The central question that surrounds the problem of mass injection at a blunt stagnation point has to do with the percentage reduction in heat transfer rate as a function of the mass-injection rate. There exists a substantial number of formulas for correlating the ratio of heat transfer with mass addition to heat transfer without mass addition. For fairly moderate values of the mass-injection rate, many authors employ a reduction that is linear in the mass-injection rate. For example, Lees[82], Adams[83], and Georgiev, Hidalgo, and Adams[84] use the following formula which is based largely on work by Baron[85] and by Reshotko and Cohen[86]

$$\frac{q_{\dot{m} \neq 0}}{q_{\dot{m} = 0}} = 1 - \frac{2}{3} \left(\frac{m_{air}}{m_{inj}} \right)^{1/4} \frac{\dot{m} \left(H_s - H_w \right)}{q_{\dot{m} = 0}} \qquad (IV-7)$$

One of the notable features of this equation is its relatively weak dependence on the molecular-weight ratio of the injectant to the ambient air.

At larger values of the injection rate a linear reduction obviously ceases to apply since it would predict a negative heat-transfer rate. Various authors have sought an improvement of the linear reduction law, some by choosing a quadratic variation. More recently, Howe and Sheaffer[57] have recommended an exponential decay, in the following form

$$\frac{q_{\dot{m} \neq 0}}{q_{\dot{m} = 0}} = exp \left\{ -b \left(-f_w \right)^{3/2} \right\} \qquad (IV-8)$$

35

In this expression, the quantity f_w is the value of the dimensionless stream function at the wall. It is proportional to the product of the mass injection rate times the Reynolds number in the following fashion

$$-f_w = \sqrt{\frac{\rho_s U_\infty R_N}{(\nu+1)\mu_s}} \; \frac{\rho_\infty}{\rho_s} \; \frac{\rho_w v_w}{\rho_\infty U_\infty} \; ; \; \nu = \begin{cases} 0, & \text{two-dimensional} \\ 1, & \text{axisymmetric} \end{cases} \qquad \text{(IV-9)}$$

The quantity b depends upon the flight velocity and takes on the following values

$$b = \begin{cases} 0.706 + 1.6\,\overline{U} - 0.28\,\overline{U}^2 \;, & \overline{U} < 3 \\[2ex] \dfrac{45}{\overline{U}^2}\left(1 - \dfrac{300}{\overline{U}^6}\right) \;, & \overline{U} > 3 \end{cases} \; ; \; \overline{U} = \frac{U_\infty\,[fps]}{10^4} \qquad \text{IIV-10)}$$

It would appear from the above results that, no matter what the specific form is for the heat transfer reduction, duplication of the mass injection rate and the Reynolds number is essential. Howe and Sheaffer give a physical interpretation of the requirement that $\dot{m}$ and R_e be duplicated by pointing out that f_w is the quantity controlling the injectant species concentration at the wall, whereas the Reynolds number determines its penetration into the flow field.

It should be pointed out that the analysis presented by Howe and Sheaffer is a shock-layer analysis and includes a coupled accounting for the radiation field. The heat-transfer correlation formula presented above is described by Howe and Sheaffer as applying for "convection only". The title does not mean that radiation has been neglected, but only that their correlation pertains to the convective part of the heat transfer from a gas in which radiative transport occurs.

It would appear that the formula proposed by Howe and Sheaffer is not entirely successful in correlating solutions from other authors. In particular, an attempt was made to apply the Howe-Sheaffer correlation formula to the results recently presented by DeRienzo and Pallone[87]. These authors considered heat transfer from a stagnation-point flow of an ionized,

equilibrium, nonradiating gas and made use of the most recent calculations of transport properties of high-temperature nitrogen. The results obtained by attempting to apply the Howe-Sheaffer correlation formula to the results of DeRienzo and Pallone are shown in Fig. 12. It is clear that the correlation is relatively unsuccessful, although it should be pointed out that the values . of the blowing parameter f_w used by DeRienzo and Pallone, when cast into the notation of Howe and Sheaffer, exceed those for which the correlation was presented. It is also possible that the failure to correlate these results stems in part from the absence of radiative transport in the calculations of DeRienzo and Pallone. In any event, it appears to be a reasonable conclusion that the correlation formula proposed by Howe and Sheaffer does not correlate all of the existing high-speed, high-temperature, stagnation-point heat-transfer calculations.

The similitude requirements imposed by mass addition have been discussed by Cresci and Libby[88]. These authors point out that the standard heat-transfer parameter $Nu/\sqrt{Re}$ can be expressed as a function of the parameter N_1 defined as

$$N_1 \equiv \frac{\int \dot{m}\, dA}{R_N\, \mu_{s,e}\, \sqrt{\tilde{N}_R}} \qquad , \qquad \tilde{N}_R \equiv \frac{\rho_{s,e}\, \sqrt{H_{s,e}}\, R_N}{\mu_{s,e}} \sqrt{\frac{p_{s,e}}{\rho_{s,e}\, H_{s,e}}}$$

In addition, the heat transfer will depend on properties of the coolant and on the distribution of wall temperature and body shape.

This paper also presents a parameter which can be used as an indication of the blowing rate at which the stand-off distance of the shock (and hence, the aerodynamic effects, such as pressure distribution as well) is affected. The parameter is defined as

$$N_3 \equiv \frac{\int \dot{m}\, dA \left(\dfrac{T_w}{T_{s,e}}\, \mathfrak{M}_{s,e} \right)^{1/2}}{R_N^2 \left(\mathfrak{M}_{inj}\, p_{s,e}\, \rho_{s,e} \right)^{1/2}}$$

Cresci and Libby, on the basis of experiments performed on a spherically blunted, 8° half-angle cone, concluded that aerodynamic features, such as the shock stand-off distance, were altered when this parameter exceeded a value between 1/4 and 1/3. Their parameter N_s makes use of the total mass injection rate (pounds per second) and their figure of 1/4 to 1/3 is based on injection through a porous plug of 30° included half-angle as shown in the sketch below
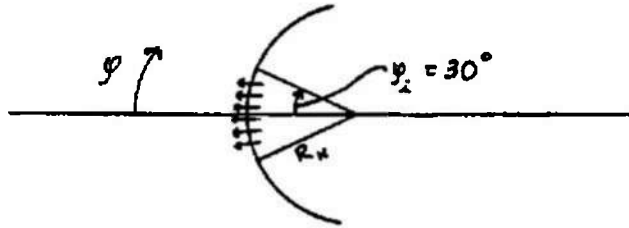
In order to recast their parameter so as to introduce the mass addition rate per unit area, it is only necessary to note that the area of their spherical sector had the value

$$A = 2 \pi R_N^2 \left(1 - \cos \varphi_i\right)$$

(IV-11)

Thus, their parameter can be rewritten in the form

$$\frac{\int \dot{m} \, dA}{2 \pi R_N^2 \left(1 - \cos \varphi_i\right)} \left[\frac{T_w \, \mathfrak{M}_{s,e}}{T_{s,e} \, \mathfrak{M}_{inj} \, P_{s,e} \, \rho_{s,e}}\right]^{1/2} = \frac{k}{2 \pi \left(1 - \cos \varphi_i\right)}$$

(IV-12)

where k stands for the transition value, reported to be either 1/4 or 1/3. If Cresci and Libby had chosen to express their result in terms of the mass addition rate per unit area, they would have employed the expression

$$\dot{m} \left[\frac{T_w}{T_{s,e}} \frac{\mathfrak{M}_{s,e}}{\mathfrak{M}_{inj}} \frac{1}{P_{s,e} \, \rho_{s,e}}\right]^{1/2} = \frac{k}{2 \pi \left(1 - \frac{\sqrt{3}}{2}\right)}$$

(IV-13)

Using the results that

$$p_{s,e} \approx \rho_\infty U_\infty^2 \quad , \qquad \frac{T_w}{T_{s,e}} \frac{m_{s,e}}{m_{inj}} = \frac{\rho_{s,e}}{\rho_{inj}} \quad , \qquad \dot{m} = \rho_{inj} \, v_w \qquad \text{(IV-14)}$$

it can be shown that the Cresci-Libby criterion takes the form

$$\frac{\rho_{inj} \, v_w}{\rho_\infty U_\infty} \sqrt{\frac{\rho_\infty}{\rho_{inj}}} = \frac{k}{0.840} \cong 0.3 \; to \; 0.4 \qquad \text{(IV-15)}$$

It should be pointed out that in the regime where major modifications of the flow field occur, the ordinary boundary-layer-plus-inviscid-flow-field model is no longer appropriate. Instead, one has a region of essentially constant shear and relatively constant temperature, supporting the outer inviscid flow. These two regions are joined by a relatively thin vortical layer. This general structure of the flow field at large blowing rates was first described by Libby[89].

Certain conclusions analogous to those drawn by Cresci and Libby have also been advanced by Kaattari[90]. Kaattari presents the similitude parameter $\sqrt{\dfrac{m_{s,e}}{m_{inj}}} \dfrac{\rho_{inj} \, v_w}{\rho_\infty U_\infty}$, which he states is adapted from the considerations of Katzen and Kaattari[91], and also of Cresci and Libby[88]. It can be seen that the parameter used by Kaattari differs slightly from that employed by Cresci and Libby. Kaattari applied this parameter to correlations of shock stand-off distance obtained in measurements at Mach number of 3 with air injection and a Mach number of 5 with air, freon and helium injection. Two models were used, one of which had a spherical-segment face and the other of which was flat-faced. These results demonstrated a linear dependence, of the ratio of shock stand-off distance with blowing to that without blowing, on the similitude parameter introduced by Kaattari.

There were some cases in which unsteady flows developed at relatively high blowing rates. Kaattari suggests that blowing does not provide a good simulation of ablation at high rates of injection.

Some of the effects encountered at relatively high rates of injection are discussed in a recent paper by Barber[92]. He performed experiments at Mach numbers from 6 to 8 in an arc-jet facility with injection of helium, hydrogen and nitrogen in the form of a thin jet at the stagnation point. From his experimental observations, he was led to identify three regions. The first region, in which no alteration of the boundary-layer structure is experienced, is said to occur for values of $\dfrac{\rho_w\, v_w}{\rho_\infty\, U_\infty}$ less than about 3. At somewhat higher injection rates, the jet essentially pierces the normal shock and leads to an extremely large stand-off distance. At still higher values of the blowing rate, the structure of the blown jet collapses, with the result that the shock stand-off distance reduces again.

S.H. Lam[93] has shown that injection at relatively high rates is controlled by the parameter $\dfrac{\rho_w\, v_w}{\rho_\infty\, U_\infty}\sqrt{\dfrac{m_{inj}}{m_\infty}}$. It can be seen that this parameter resembles that used by Cresci and Libby[88] and Kaattari[90].

3.   Blunt Body at Low Reynolds Number

The low Reynolds number stagnation-point flows that are described in Sec. IV-B-2 are further complicated when mass addition at the surface is allowed. Hoshizaki[94] was among the first to present a theoretical description of such flows. He presented solutions of the incompressible Navier-Stokes equations and succeeded in showing that the ratio of heat transfer, with vorticity considered, to that without vorticity increases with increasing mass addition. Another way of putting this conclusion is to say that external vorticity decreases the effectiveness of mass addition in decreasing heat-transfer rates. The effect is noticeable at Reynolds numbers less than about 10^5 for a sphere and about 10^4 for a cylinder, where the Reynolds number is defined as $\dfrac{\rho_s\, U_\infty\, R_N}{\mu_s}$.

In a recent paper, Martin[95] has called attention to the possible existence of another second-order effect that may be present when mass addition at the surface is considered. Martin uses the expression "boundary shock wave" to describe the phenomena involved. The proposed effect can be thought of as arising from the fact that, whenever mass transfer occurs at the wall, the vertical velocity component in the boundary layer does not

vanish at the surface, whereas the streamwise component does. For this
reason, the conventional boundary-layer assumption, which states that the
vertical component is of order δ compared to the streamwise component
(which is of order unity), must break down at some point near the surface.
The injection rate at which a significant failure of the boundary-layer
structure occurs is not yet clear. Presumably, the departure from the
condition of constant pressure across the boundary layer, noted by Scala
and Gilbert[96] in studies of extremely large sublimation rates, is a mani-
festation of the phenomenon described by Martin.

A fairly representative appraisal of the state of both theory and
experiment for low-density stagnation-point flows with mass addition can
be taken from a recent paper by Vojvodich and Pope[97]. These authors
made measurements of the heat-transfer rates to nonablating, spherically-
blunted cylinders by means of a calorimeter, and they also made measure-
ments of the mass-loss rate of ablating Teflon models in several arc-heated
wind tunnels. They then attempted to interpret their measurements in terms
of the existing heat-transfer literature. For example, they employed the
empirical correlation of Hickman and Giedt[98]

$$\frac{q_{vorticity}}{q_{no\ vorticity}} = 1 + \frac{0.735}{\sqrt{Re}} \quad ; \qquad Re \equiv \frac{\sqrt{H_{s,e}}\ \rho_{s,e}\ R_N}{\mu_{s,e}} \qquad \text{(IV-16)}$$

in order to account for the heat transfer increase due to external vorticity.
In addition, they gave consideration to the possibility of surface catalytic
effects and to the coupling between heat and mass transfer. They were led
to the conclusion that the heat-transfer reduction with blowing reaches an
asymptotic condition at large blowing rates and proposed a heat-transfer
reduction formula of the form

$$\frac{q_{\dot{m} \neq 0}}{q_{\dot{m} = 0}} = A + B \ \exp\left\{ -C \ \frac{\dot{m}(H_{s,e} - H_w)}{q_{\dot{m} = 0}} \right\}$$

The existence of such an asymptotic condition at large blowing rates at present remains unresolved.

4.   Slender Body at High Reynolds Number

Just as in Sec. IV-B-3, a slender body requires that one consider the distribution of Mach number at the boundary-layer edge, and this new parameter presents new problems of similitude. The problem is further compounded when mass addition at the surface is permitted. Partly for this reason, the literature dealing with mass transfer along the surface of a slender body at high Reynolds number is relatively sparse.

An approximate analysis leading to the identification of a similitude parameter has been given by Whitfield and Griffith[63] for the case of film cooling. These authors considered theoretically, and performed experiments on, a model in which the mass is injected tangentially to the surface near the vertex of a slender pointed cone. Their analysis is based on an approximate treatment given by Swenson[99] and leads to the conclusion that the ratio of the integrated heat transfer over the body with mass injection to that without mass injection, Q_F/Q_A , and the ratio of the total frictional drag coefficient with blowing to that without blowing, $\dfrac{(C_{Df})_F}{(C_{Df})_A}$ are dependent only on the parameter $\dfrac{m_F}{\rho_\infty U_\infty S_B \overline{V}_H}$ where $\overline{V}_H = M_\infty \sqrt{C_H/Re_{\infty,L}}$. Here C_H is the Chapman-Rubesin constant defined previously (p. 29), m_F is the injection rate (mass per unit time), S_B the base area, and L the model length. Comparison of this theoretical prediction with experiment shows relatively poor agreement. Whitfield and Griffith list several possible reasons for this behavior.

5.   Slender Body at Low Reynolds Number

The problems encountered in theory and experiment when mass addition is permitted are made more difficult at low Reynolds number. A typical example is to be found in the work of King and Talbot[100]. These authors performed a number of tests at very low Reynolds numbers on a sharp, partly porous, 5° half-angle cone. They found that blowing increased the induced surface pressure, but reduced the total drag, and that air was more

effective than helium at the same mass flow. They made several theoretical attempts to solve the problem with the inclusion of viscous-interaction effects, transverse-curvature effects, and so on, but on the whole their theories were not very successful in correlating the experimental results. Part of the difficulty which they faced and which affects all attempts to perform realistic analyses was that the distribution of mass addition rate was considerably different from that embraced by their theoretical analysis.

Some more refined tests and more extensive theoretical considerations have been reported in a recent paper by Lewis, Marchand, and Little[101]. Their tests were carried out on a 9° half-angle cone at Mach numbers between 9 and 10, Reynolds numbers per inch from around 400 to around 40,000, and with wall-to-stagnation-temperature ratios in the range from 0.02 to 0.075. The results of their experiments, some of which had relatively uniform injection downstream of a nonporous leading edge, are compared with a rather complete set of boundary-layer calculations in which inviscid-viscous flow-field matching, transverse curvature, wall slip and temperature jump were all included in an iterated solution.

They achieved fairly good agreement between their calculations and the experiments, and also with the experiments of King and Talbot[100], at least for viscous-induced pressure without mass transfer, and for zero-lift drag with and without mass transfer. Some of the comparisons between their theory and the experiments were found to be rather poor, partly because of the nonuniformity of injection.

Their paper does not present any general conclusions as to the identification of similitude parameters nor of the range of their applicability. It is probably representative of the fact that the theoretical considerations are so extensive that they call for a great deal of numerical calculation. There is not yet enough evidence at hand on which to base a reasonable correlation formula.

E.   LAMINAR BOUNDARY LAYERS WITH UNSTEADY ABLATION,
     NO CHEMICAL REACTIONS

The phenomena encountered when mass addition occurs in an un-
steady flow are very closely associated with certain current problems in
ablation-induced instability. For that reason, this category is discussed
in a later section entitled Ablation Phenomena (Sec. X).

F.   LAMINAR BOUNDARY LAYERS WITH COMBINED EFFECTS OF
     ABLATION AND CHEMICAL REACTIONS

Interest in the distribution of chemical species in hypersonic
boundary layers stems mainly from the desire to make detailed studies
of the kinetics and of the radiative properties of ablating materials. As
always, the introduction of chemical kinetic considerations adds, to the
list of similitude parameters that must be duplicated, the ratio of chemical
times to flow times.

An analysis of the similitude requirements based on essentially this
concept has been set forth in recent papers by Wray, Rose, and Koritz[102],
and Wray and Kemp[103]. In the first of these papers, it is suggested that
ablation chemical kinetics can be simulated by duplicating the ratio of the
time that an ablated particle spends in the boundary layer to the average
time between its collisions with other particles. Based on some relatively
simple statistical-mechanical considerations, these authors derive an
expression for the ratio in the following form

$$\frac{\tau_{FLOW}}{\tau_{COLLISIONS}} = \left\{ a\sqrt{2}\, X_j \; \frac{Re_j}{M_j^2} \left(\frac{E^*}{kT} + 1 \right) exp\left(-\frac{E^*}{kT} \right) \right\}_{avg} \qquad (IV-18)$$

where

$a \approx \frac{1}{2}$, X_j denotes the mole fraction of species

$$Re_j = \frac{\rho_j\, u_j\, L}{\mu_j} \;, \qquad M_j = \frac{u_j}{\bar{c}_j} \quad .$$

Here, L denotes the characteristic length, $\bar{C}_i$ the mean thermal speed, and $\not{k}$ is Boltzmann's constant. E^* represents an activation energy, and the average is to be taken across the boundary layer. Because of the exponential dependence on E^*, and in view of the difficulty of estimating it, Wray, Rose, and Koritz recommend duplication of the collision partners and of the maximum boundary-layer temperature.

These papers report radiative measurements of an ablating Teflon model composed of a flat plate that is inserted into the sidewall of an arc-heated wind tunnel. By appealing to the similitude discussed above, it is argued that the boundary layer on the arc-tunnel sidewall provides a partial duplication of the flight condition that might be experienced on a slender hypersonic body. The portion of the boundary layer that appears to be simulated is that occurring near to the surface of the hypersonic body, since the boundary-layer temperature profiles for the two cases have qualitatively the appearance sketched below
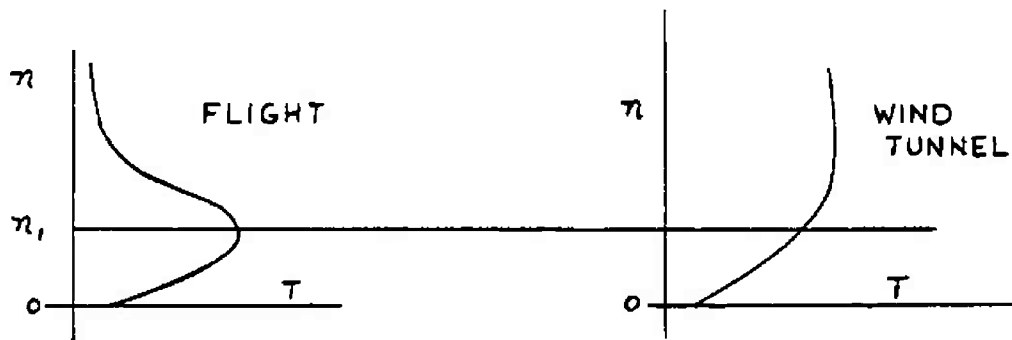
The argument set forth is that the zone from O to n_1 may be simulated in the arc facility. It must be stressed that the simulation suggested here is in the nature of a tentative proposal that is not well substantiated as yet.

For cases when certain of the ablating species are present only in very small concentrations so that they can be considered as small corrections to a basic flow, Williams[104] has pointed out that an approximate solution can be expressed in relatively simple form. The similitude implications of Williams' solution have been discussed in a report by Eschenroeder[105], as part of a more general survey of similitude principles.

The solution set forth by Williams assumes that the basic flow is of a similar nature so that, for example, the mass fractions of the constituents of the basic flow depend only on the usual boundary-layer similarity parameter η . For cases in which this approximation can be satisfied, Williams shows that the mass fraction of a small contaminant species takes the form

$$Y = \xi \, z(\zeta)$$

<div align="right">(IV-19)</div>

where

$$\xi = \int_0^s \rho \mu \, ds$$

$$\zeta = \int_0^\eta Sc \, d\eta \; , \qquad \eta = \sqrt{\frac{u_e}{2\xi}} \int_0^n \rho \, dn$$

and where z is a solution of

$$z'' + f \, z' - 2 f' z = -2\omega$$

<div align="right">(IV-20)</div>

In this equation, $\quad f' = \dfrac{df}{d\zeta} = \dfrac{\partial f}{\partial \eta} \dfrac{d\eta}{d\zeta} = \dfrac{1}{Sc} \dfrac{u}{u_e}$

$$\omega = \frac{W}{u_e \rho^2 \mu} = \frac{W}{\rho \mu \cdot \rho u_e}$$

The factor W is the mass rate of production of the contaminant species per unit volume, and is assumed to occur from reactions of the type

$$\sum_{i=1}^{N} \nu_i' A_i \longrightarrow \sum_{i=1}^{N} \nu_i'' A_i + \sum_{i=1}^{L} \nu_i P_i$$

<div align="right">(IV-21)</div>
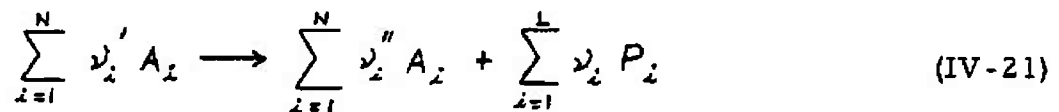
where the symbol A_i denotes the so-called active (or basic-flow) components, and the symbol P_i denotes the so-called passive (or trace) components.

Williams goes on to calculate the average value of the contaminant species, defined as follows

$$\langle Y_j \rangle \equiv \frac{\text{total mass flux of contaminant in boundary layer}}{\text{total mass flux of all species in boundary layer}}$$

and succeeds in showing that this average value is given by the expression

$$\langle Y_j \rangle = \frac{s}{\rho_e u_e} \int_0^\infty \frac{\rho_e}{\rho} W d\eta \qquad (IV-22)$$

The expression that Williams uses for the chemical kinetics is of the following form

$$W_i = m_i \nu_i B e^{-E/R_o T} \prod_{j=1}^N \left(\frac{X_j \, p}{R_o T} \right)^{\nu'_j} \qquad (IV-23)$$

where the product is taken over all the active components, B is a frequency factor (possibly temperature-dependent), E represents the activation energy, R_o is the universal gas constant, T the temperature, p the pressure, and X_j the mole fraction of j. Thus, apart from temperature-dependent factors, the chemical production rate has the following proportionality

$$W_i \propto p^{\Sigma \nu'_j} \prod (X_j)^{\nu'_j} \qquad (IV-24)$$

Eschenroeder[105] pointed out that for trace species which obey binary kinetics, $\sum \nu'_j = 2$, with the result that

$$\langle Y_j \rangle \propto \frac{s}{\rho_e u_e} p^2 \propto \frac{\rho_\infty s}{u_\infty} \qquad (IV-25)$$

provided that the pressure in the boundary layer is proportional to ρ_∞.

Eschenroeder further indicates that the details of the kinetics by which the injected species react chemically are not yet well enough determined to permit an appraisal of whether binary kinetics are appropriate for such a description. On the one hand, the slow velocity and relatively low temperature of the injected species near the wall tend to promote three-body reactions, but, on the other hand, the presence of large radicals in the ablation species promotes two-body catalytic paths.

An approximate expression for the species mass fraction, analogous to that derived by Williams, can be obtained by proceeding in the manner that was followed by Levinsky and Fernandez[78]. The essential item in their method of approximation was to assume a proportionality between the mass fraction of the trace species and the product of the chemical reaction rate (evaluated at typical conditions within the boundary layer) multiplied by a typical flow time in the following fashion:

$$ Y \hookrightarrow \frac{\omega}{\rho} \frac{s}{u_e} \tag{IV-26} $$

The basis for an expression of this type can be found in the work of Rae[76] where it was found that the concentration of atoms in a dissociating, diatomic-gas boundary layer could be approximated by an equation of this type. The only factors that are omitted are those which account for diffusion of the produced species, which is a relatively small correction. If one now introduces into this expression the production rate given by Williams, one finds the following relation for the mass fraction of the trace species

$$ Y_j \hookrightarrow \frac{s}{u_e} \rho^{\Sigma \nu_i' - 1} \nu_j \, \mathfrak{M}_j \, k_F(T) \prod_{\alpha=1}^{N} (X_j)^{\nu_\alpha'} \tag{IV-27} $$

$$ k_F \equiv B e^{-E/R_o T} $$

The relation between the mole and mass fractions is

$$Y_j = \frac{X_j \, m_j}{m_{MIXTURE}}$$

(IV-28)

Thus, an approximate relation for the trace-species concentrations can be written in the following form

$$Y_j \hookrightarrow \frac{s}{u_e} \, \rho^{\Sigma \nu_i' - 1} \, \nu_j \, m_j \, m_{MIXT.}^{\Sigma \nu_i'} \, k_F(T) \, \pi \left(\frac{Y_\alpha}{m_\alpha}\right)^{\nu_\alpha'}$$

(IV-29)

In this expression, the product is taken over the active species only. Thus, in the case considered by Levinsky and Fernadez[78], the mass fractions of atomic oxygen and atomic nitrogen would be calculated as being proportional to the product of the mass fraction of molecular oxygen times that of molecular nitrogen.

For the problem considered by Williams[104], the same general conclusion as reached by Eschenroeder[105] can be seen in the equation above. For species which obey binary kinetics, the maximum mass fraction is proportional to $\rho_\infty s / u_\infty$. It should be repeated that the concentration given by this equation is essentially a measure of the maximum concentration within the boundary layer. On the other hand, the average mass fraction derived more rigorously by Williams pertains to the value of the species concentration averaged over the entire boundary-layer thickness.

G. TRANSITION

1. General Considerations

The conditions of hypersonic flight at altitudes on the order of 50 to 100 Kft raise the possibility that boundary layers may be turbulent rather than laminar. In order to provide proper simulation, then, it is necessary that the test conditions should   turbulent flows whenever they might be expected on the flight vehicle. The heart of the problem is

to simulate the important parameters affecting transition (e.g., Mach number, unit Reynolds number, wall-to-recovery temperature ratio and surface roughness so that transition occurs at the same relative position on the model as on the flight vehicle.

Unfortunately, the present state of information regarding the location of transition is relatively incomplete, particularly in cases when mass addition is encountered and when walls are highly cooled. It is, for practical purposes, impossible with the present state of information to make anything more than order-of-magnitude estimates for the location of the transition point. Partly for these reasons, the information that follows is by no means an exhaustive review of the literature of boundary-layer transition. Rather, what has been done is to make a representative sampling of recent literature that serves to indicate the general magnitude of transition Reynolds numbers for hypersonic flows and which hopefully gives a picture of the amount of information that is presently available.

2. Flows Without Mass Addition

The shock tube was used to investigate the occurrence of boundary-layer transition on highly cooled blunt bodies by Stetson[106]. His experiments were conducted at wall-to-free-stream stagnation enthalpy ratios of 0.03 to 0.25 and transition was inferred from measurements of the heat transfer rate.

Transition was found to occur for $Re_\theta = \dfrac{\rho_e u_e \theta}{\mu_e}$ (where θ denotes the momentum thickness) from approximately 225 to 400. These values correspond to Reynolds numbers based on distance from the stagnation point on the order of 3×10^5 and they are appropriate to unit Reynolds numbers of approximately 0.6×10^6 per inch.

Some measurements of transition taken from spark shadowgraph pictures are presented in Part 3 of Ref. 107. These measurements were taken on sharp, 5° half-angle cones in a ballistic range at a Mach number of 8. These data as well as some data taken at Mach numbers of 3 and 5, show a decrease in transition Reynolds number as the wall-to-recovery temperature ratio decreases, i.e., the greater the heat transfer, the

less stable is the boundary layer. Some of these data (at $M_\infty = 5$) indicate a return to the normal behavior (transition Reynolds number increasing with decreasing wall temperature) at sufficiently low wall temperatures. These results are apparently in accord with the predictions of a stability analysis by Reshotko[108].

The transition Reynolds numbers for this entire series of tests varied from approximately 2×10^6 up to approximately 12×10^6, depending on the ratio of wall-to-recovery temperature.

A more thorough probing of a hypersonic turbulent boundary layer was carried out by Potter and Whitfield[109]. These authors made measurements of the boundary layer on a blunted hollow cylinder. They found transition Reynolds numbers generally on the order of 0.5×10^6 up to about 5×10^6. The transition Reynolds number was found to increase generally with increasing unit Reynolds number $\rho_\infty U_\infty / \mu_\infty$.

They found that the transition Reynolds numbers at Mach numbers up to about 8 show a dependence on the bluntness Reynolds number, on the flow inclination angle, on the free-stream Mach number and on the unit Reynolds number, among other factors. Generally speaking, the transition Reynolds number was found to increase with increasing Mach number.

These measurements make it clear that the question of transition in a hypersonic, highly cooled boundary layer is an extremely complex problem. It cannot be said that the present state of the literature clarifies what the separate influences of various factors are.

3. Flows with Mass Addition

The complexity of boundary-layer transition is increased when mass addition is present. It is extremely difficult to make controlled measurements in any experimental facility with such a complicated factor present.

Some measurements which illustrate the problems involved are reported in Ref. 110 by Wilkins and Tauber. These authors conducted ballistic-range measurements on 30° half-angle cones constructed of polycarbonate and of acetal polyformaldehyde. The basic measurements made

consisted of mass-loss data on models recovered from the end of the range, and measurements of the fraction of the surface covered by turbulence wedges. It was found rather difficult to correlate the inferred transition Reynolds numbers because of the extreme deceleration which the model experienced and the associated rapid decrease in heat-transfer rate. However, the experiments generally indicate that laminar boundary layers can be maintained at Reynolds numbers up to approximately 3 to 4 times 10^6 on an ablating cone of this size.

On the theoretical side, it is only recently that studies have begun of the stability analysis of laminar boundary layers with mass injection. A very recent paper has been presented by Powers and Albacete[111]. These authors considered Mach numbers between 0 to 1.3 and injection of helium, air and carbon tetrachloride into an air stream. They found that stability was generally increased by the use of a heavier injectant. In view of the species likely to be introduced by the ablation of relatively high molecular-weight materials, these results would seem to indicate that ablating boundary layers may be found to be relatively stable.

The entire question of location of transition in the hypersonic boundary layer can probably be set in perspective by examining a recent paper by Seiff and Tauber[112] in which analyses of hyperbolic entry vehicles were made. It was necessary, in making estimates of heating loads for this purpose, to estimate the Reynolds number at which transition would occur. These authors state, "the appropriate number for the Reynolds number limit ... [corresponding to transition] ... is not now known for the case of very high total enthalpy flow over an ablating surface". The paper goes on to make use of transition Reynolds numbers which lie between 1 and 20 x 10^6.

H.   TURBULENT BOUNDARY LAYERS WITHOUT CHEMICAL REACTIONS
      OR ABLATION

When the viscous flow is fully turbulent, the similitude requirements, in general, consist of duplicating at least the Mach number and Reynolds number of the flow and the wall-to-free-stream enthalpy ratio as well. For

certain cases, however, there are indications that some of these parameters can be relaxed. For example, the blunt body in turbulent flow affords the same simplification that is encountered in laminar flow in that it is not necessary to duplicate the Mach number even for Mach numbers as low as three. This has been pointed out, for example, by Rose, Probstein, and Adams[113], who derived a composite formula based on a modified Reynolds analogy as follows

$$Nu \equiv \frac{q \; Pr \; s}{\mu_e (H_e - H_w)} = 0.029 \, (Re_s)^{0.8} \left\{ 1 + \left(Le^\beta - 1 \right) \frac{H_{De}}{H_e} \right\} Pr^{1/3} \qquad \text{(IV-30)}$$

where

$$Re_s = \frac{\rho_e \, u_e \, s}{\mu_e}$$

The same conclusions essentially are reached by Hayes and Probstein[25] (pp. 325-332). The quantity β lies between 0.5 and 1.0.

An extension to cover cases in which there is a pressure variation is given by Probstein, Adams, and Rose[114]. These authors made use of a momentum integral method to derive the following formula for heat transfer

$$\frac{q \; Pr \; s}{\mu_e (H_e - H_w)} = 0.029 \, (Re_s)^{0.8} \left[F(s) \right]^{1/5} \left\{ 1 + \left(Le^\beta - 1 \right) \frac{H_{De}}{H_e} \right\} Pr^{1/3} \qquad \text{(IV-31)}$$

where

$$\left[F(s) \right]^{-1} \equiv \frac{\left(\rho_\infty u_e / \mu_e \right)^{1/4}}{u_e^{5/4} \, r^{5/4} \, \rho_e^{5/4}} \; \frac{1}{s} \int_0^s \left(\frac{\mu_e}{u_e} \right)^{1/4} u_e^{5/4} \, r^{5/4} \, \rho_e^{5/4} \; ds$$

A summary of several heat-transfer expressions of this type is given in a recent paper by Murphy and Rubesin[115]. These authors point out that turbulent heat transfer can generally be written in the form

$$\frac{q}{H_s - H_w} = \frac{A}{(Pr)_r^e} \frac{z^a \mu_r^a \rho_r^d u_e^e \, r^{1/4}}{\left\{ \int_0^s z^b \, \mu_r^c \, \rho_r^d \, u_e^q \, r^{5/4} \, ds \right\}^{1/5}} \left(1 + B \, \frac{H_D}{H_s} \right) \qquad \text{(IV-32)}$$

where the constants are given according to the following table.

	A	B	a	b	c	d	e	g	z	$( )_r$
Rose et al[116]	0.0301	0.4	2/3	0	1/4	1	5/4	9/4	1	boundary-layer edge
Bromberg[117]	0.0288	0	0	0	1/4	1	1	1	1	boundary-layer edge
Rubesin[118]	0.0296	0	2/3	5/4	1/4	1	1	1	$\dfrac{H_{rec}-H_w}{H_s-H_w}$	$h_r = 0.28 h_e + 0.22 h_{rec} + 0.5 h_w$

The subscript $( )_r$ denotes evaluation at the reference-enthalpy conditions shown in the last column, and at the local pressure. Subscript $( )_{rec}$ denotes the recovery value, usually taken as

$$H_{rec} = H_e + \sqrt{Pr} \, \frac{u_e^2}{2} \tag{IV-33}$$

The symbol H_s denotes the enthalpy in dissociation.

There appears to be some hope of deriving a more general correlation of turbulent-flow heat-transfer data. This approach is initiated in a paper by Spalding and Chi[119], for flows without mass transfer and has been extended in a more recent paper by Spalding, Auslander, and Sundaram[120] to flows in which mass transfer occurs. Both of these papers are discussed below in Sec. IV-J.

I. TURBULENT BOUNDARY LAYERS WITH CHEMICAL REACTIONS NO ABLATION

The problem of predicting species distributions in turbulent, chemically reacting boundary layers is still in an extremely primitive state. Many authors employ a simple approximation in which the diffusivities of momentum, energy, and of all species are the same, so that a similarity between the enthalpy and concentration profiles can be established.

At a more fundamental level of investigation, the major problem awaiting solution is the effect of turbulence on chemical reactions, and the corresponding influence of the heat release in the reactions on the turbulence. Recent contributions to this growing field of literature have been made in papers by Lin [121] and by Eschenroeder[122]. This general topic, in fact, has been the subject of a recent AIAA conference[123].

J.   TURBULENT BOUNDARY LAYERS WITH ABLATION, NO CHEMICAL REACTIONS

The addition of mass injection to the list of factors to be simulated requires that a dimensionless function characterizing the mass injection be duplicated, in addition to the usual requirements that the Reynolds number, Mach number and wall-to-free-stream temperature ratio be duplicated.

A recent approach, mentioned briefly above in Sec. IV-H, is that undertaken by Spalding and various co-workers[119, 120]. In these papers, a correlation of the general form

$$\frac{C_f}{2} F_c = fcn\left(Re_{\delta_2}, F_{R\delta}\right)$$

(IV-34)

is suggested as a means for bringing together the results of experiments at various Mach numbers, Reynolds numbers, wall-to-free-stream temperature ratios and blowing rates. In Equation (IV-34), the function indicated is the classical skin-friction law, e.g., the 1/5th power law.

$$C_f \equiv \frac{\tau_w}{\frac{1}{2}\rho_e u_e^2} \quad , \quad Re_{\delta_2} \equiv \frac{\rho_e u_e \delta_2}{\mu_e} \quad , \quad \delta_2 \equiv \int_o^\delta \frac{\rho u}{\rho_e u_e}\left(1 - \frac{u}{u_e}\right) dn$$

The correlation is to be achieved by proper choice of the functions F_c and $F_{R\delta}$, each of which depend on the two parameters Mach number and temperature ratio, but which exhibit no dependence on the Reynolds number. For flows in which mass transfer occurs, the suggested forms for these equations are as follows

55

$$F_c = \left[\int_o^1 \left(\frac{\rho/\rho_e}{1 + B_u \frac{u}{u_e}} \right)^{1/2} d\left(\frac{u}{u_e} \right) \right]^{-2} \tag{IV-35}$$

$$F_{R\delta} = \frac{\mu_e}{\mu_w} \left(1 + B_u \right)^{-3/2}, \qquad B_u \equiv \frac{\dot{m} \, u_e}{\tau_w}$$

Application of these correlation formulas to a relatively large amount of data shows a good, but not entirely satisfactory, correlation. However, the method holds promise and indicates one means by which turbulent flows with mass addition may possibly yield to a similitude in which changes in Mach number or Reynolds number may partially be offset by compensating changes in the mass addition rate.

A recent thesis by Meroney[124] (which contains an extensive list of references) is representative of a more traditional way of attempting to correlate turbulent heat transfer data in the presence of mass addition. The type of correlation used has the form

$$\frac{C_H^*}{C_{H_o}^*} = fcn \left(\frac{F^*}{C_{H_o}^*} \right); \qquad fcn(s) = \frac{s}{\left(1 + \frac{s}{3}\right)^3 - 1} \tag{IV-36}$$

where

$$C_H^* = \frac{q_w}{\rho^* \bar{C}_p^* u_e (T_{AW} - T_w)}, \qquad F^* = \frac{\rho_w v_w}{\rho^* u_e}$$

$(\ )_{AW} \sim$ adiabatic wall, $(\ )^* \sim$ reference-temperature state,

$(\ )_o \sim$ no blowing, $\bar{C}_p \sim$ specific heat.

Again the correlation appears to be reasonable, but there is still a large amount of scatter present.

Another recent paper which exemplifies the type of correlation that can be achieved is that presented by Danberg, Winkler, and Chang[125]. In this work, measurements of both temperature and pitot-pressure profiles were made on a flat plate at a Mach number of 6.7. Air was injected into the boundary layer with a mass flux between 0.04 and 0.25% of the free-

stream mass flux and with wall-to-free-stream temperature ratios between, roughly, 4 and 8. The Reynolds number for these tests was between 3 and 11×10^6. The data were found to support the Reynolds analogy in either of the forms $St = \dfrac{C_f}{2}$, or $St = \dfrac{C_f}{2}(Pr)^{-2/3}$. Also, a linear decrease in both skin friction and heat transfer rate with increased mass injection rate was found in the range of injection rates studied.

All of these studies can be summarized by stating the general conclusion that one must duplicate Reynolds number, Mach number, wall-to-free-stream temperature ratio and the quantity $\dfrac{\rho_w v_w}{\rho_e u_e}$ which duplicates the mass injection rate.

K. TURBULENT BOUNDARY LAYERS WITH COMBINED EFFECTS OF ABLATION AND CHEMICAL REACTIONS

The approximation used most frequently to determine the distribution of species in turbulent, chemically reacting boundary-layers, is that in which momentum, energy, and all species are assumed to have equal diffusivities (see, for example, Refs. 103, 126). Under these conditions, a similarity between the species mass fractions and the enthalpy distribution through the boundary layer can be established.

Calculations of the species distributions in turbulent boundary layers are usually done under the approximation of chemical equilibrium. It should be pointed out that the calculations (referred to above in Sec. IV-C) by Levinsky and Fernandez[78] and also by Mondrzyk[79] suggest that chemical equilibrium on a sharp, slender cone is approached at approximately the point where transition might be expected to occur.

A somewhat more elaborate application of approximations of this type has been presented in a recent report by Brant and Burke[127]. These authors present calculations of chemical-equilibrium, turbulent flow, on an 8° half-angle graphite cone at velocities on the order of 20,000 fps and altitudes ranging from 40 to 100 Kft. The approximation used for calculating the mass addition rate is that of diffusion-controlled sublimation (which is discussed in the later section on Ablation Phenomena, Sec. X). In these calculations, a relatively simplified boundary-layer analysis is coupled

with an equilibrium program for calculating chemical species; the result is a prediction of the distribution through the boundary layer of a variety of carbon, carbon-nitrogen, and carbon-oxygen products.

It is interesting to note in these results that the concentration of electrons is contributed to very heavily by the air products present and relatively little effect is felt due to the presence of the subliming ablation material. This phenomenon is attributed to the low ionization potential of NO . It is a relatively common practice in ablation calculations to assume that the injected species behave like air (see, for example, Howe and Sheaffer[57]). Apparently in some cases this approximation is satisfactory, at least for the electron concentrations.

For species distributions in turbulent reacting boundary layers, there appear to be no simple similitude criteria which relate calculations for one set of conditions to any other set.

V. NORMAL SHOCK WAVES

A.   INTRODUCTION

The work of Gibson and Marrone[46,48] on the shock-mapping technique has established a correspondence between normal shock-wave flows and blunt-body flows. In addition, there exists the direct correspondence of normal shock flows to wedge flows whenever the gas is ideal, the flow chemistry is frozen, or thermodynamic equilibrium exists everywhere behind the shock. Thus, there are very practical reasons for a detailed investigation of normal shock-wave flows over and above the obvious one of their simplicity. As part of the present study, a systematic set of solutions for the nonequilibrium flow behind a normal shock were calculated on an IBM 7044 computer. The primary purposes of these solutions were to investigate the applicability of binary scaling for shock-wave flows over the flight regime of interest, to delineate frozen and equilibrium flow regimes, and to investigate the correspondence of normal shock flows and the nonequilibrium flow about a sharp wedge.

Before discussing these solutions, consideration is first given to ideal gas and equilibrium normal shocks, followed by a brief description of the nonequilibrium computer program and calculations. Then the results of the nonequilibrium shock waves are discussed as they pertain to the specific purposes listed above.

B. NORMAL SHOCK WAVE SOLUTIONS

1. General Considerations

The three conservation equations for mass, momentum and energy when applied across a normal shock wave can be manipulated to yield the Hugoniot relation

$$H_s - H_\infty = \frac{1}{2}\left(p_s - p_\infty\right)\left(\frac{1}{\rho_\infty} + \frac{1}{\rho_s}\right) \tag{V-1}$$

where the subscripts ∞ and s refer to conditions ahead of and behind the shock, respectively. The importance of the Hugoniot relation lies in the fact that it provides a relation connecting the thermodynamic state variables on the two sides of the shock and does not involve the flow velocities. Furthermore, it holds for both real and ideal gases since it does not involve the equation of state.

2. Gas with Constant Specific Heat Ratio

For an ideal gas with constant specific heat ratio γ, explicit expressions for the ratios across the shock of all physical quantities can be obtained. These are listed and tabulated, for example, in Ref. 128. The results for an ideal gas with constant γ are applicable in the present study only for the region where the chemistry is completely frozen. In this region it is only necessary to match the flight values of γ and M_∞. Any effects of not duplicating these quantities in the frozen-flow regimes can be evaluated from the equations given in Ref. 128.

AEDC-TR-67-72

3. Equilibrium Normal Shock Waves

Where the flow is not chemically frozen, the first concern is knowing at what free-stream velocity or Mach number the real gas effects become significant. This is readily determined for flight conditions by comparing the results contained in Ref. 128 with equilibrium real gas solutions, such as are reported in Refs. 129 and 130. One finds that in the altitude range 0-250,000 ft the real gas effect on density ratio across the shock ρ_s/ρ_∞ exceeds 10% for free-stream velocities above 5500 fps. A 10% effect on temperature ratio occurs at velocities above 6300 fps, whereas the same effect on pressure does not occur until the free-stream velocity exceeds 11,000 fps.

It is also significant that for all quantities altitude effects are unimportant below 6500 fps. These delineations also apply to wind-tunnel test flows when the free-stream static temperature is 300°K or less.

The next point to be considered i· the sensitivity of flow conditions behind the equilibrium normal shock to mismatch in free-stream quantities. For the flight case, these sensitivities can be estimated from the results presented in Ref. 129. Considering first the effect of mismatch in free-stream density (i.e., $\rho_{\infty T} \neq \rho_{\infty F}$) when T_∞ is constant (e.g., between 35,000 ft and 85,000 ft altitude), it is seen from Graph 1 of Ref. 129 that an order of magnitude difference in ρ_∞ (roughly 50,000 ft in altitude) produces at most an 11% difference in ρ_s/ρ_∞ . From Graph 2 of Ref. 129 it is seen that an order of magnitude mismatch in p_∞ when T_∞ is constant (again between 35,000 and 85,000 ft altitude) produces no change in the pressure ratio p_s/p_∞ ; hence, p_s varies directly with p_∞ . The effect of mismatch in free-stream temperature is most readily obtained by comparing the normal shock solutions reported in Refs. 129, 130 or 131 with those of Ref. 132. References 129-131 report normal shock results for flight conditions (i.e., at various velocities and altitudes) whereas Ref. 132 reports solutions for laboratory conditions (i.e., a constant free-stream temperature of 300°K). A comparison of Refs. 129 and 132 for $p_\infty = 1\,atm$ indicates that a 1% increase in T_∞ produces about a 1% decrease in T_s/T_∞ for velocities from 10,000 to 26,000 fps. The effect

60

of the much larger differences in T_∞ that result from density-altitude and velocity duplication along the lower boundary of the flight regime of interest are shown in the following table. These results were obtained from equilibrium normal shock solutions computed for the density-altitude and velocity duplication conditions listed in Table II-1.

TABLE V-1

EFFECT OF FREE-STREAM TEMPERATURE ON TEMPERATURE
BEHIND A NORMAL SHOCK WAVE

U_∞ , fps	Altitude, Ft.	$T_{\infty_T}/T_{\infty_F}$	T_{s_T}/T_{s_F}
10,000	50,000	3.57	1.063
15,000	50,000	5.19	1.062
20,000	50,000	7.10	1.030
25,000	87,000	4.89	1.017
30,000	125,000	3.02	1.008
35,000	160,000	1.88	1.014

Here, it is seen that even a large mismatch in T_∞ has only a small effect on T_s for equilibrium flows.

Although it has been presumed that velocity duplication can be achieved throughout the flight regime, it is interesting to note the effect of small mismatches in U_∞ on the equilibrium state behind a normal shock. Figure 13, which shows the sensitivity of T_s (i.e., $\Delta T_s/T_s$) to changes in U_∞ (i.e., $\Delta U_\infty/U_\infty$) was obtained by taking tabular differences of the results of Refs. 129 and 130. The notable features here are the two peaks at about 13,000 fps and 30,000 fps and the wide variation with U_∞ . The first peak is a result of the completion of oxygen dissociation before the onset of significant nitrogen dissociation, and the second is due to the completion of nitrogen dissociation before significant ionization occurs. Thus, even though small errors in U_∞ do not produce large errors in T_s , the errors are of the same order of magnitude and one should be aware that the effect is

strongly velocity and altitude dependent. For an ideal gas with constant specific heat ratio we note that $(dT_s/T_s)/(dU_\infty/U_\infty) = 2$ for $M_\infty \gg 1$. Hence, for real gas in equilibrium the sensitivity is generally less than for an ideal gas. In this regard, it should be noted that the magnitudes of the peaks in Figure 13 must be taken cautiously because the finite-difference method used in obtaining the curves can introduce large errors when T_s is varying rapidly with U_∞. This is particularly noticable between 28,000 fps and 32,000 fps where the peaks exceed the ideal-gas value of 2, a physically impossible situation.

The case of equilibrium normal shocks may be generally summed up as follows: if the free-stream velocity is large, the effect of mismatches in the free-stream thermodynamic state on conditions behind the shock is strongly attenuated. This is a direct result of the fact that as long as the free-stream enthalpy is small compared to U_∞^2, the flow behind the shock is primarily dependent only on U_∞ in the hypervelocity flight regime. On the other hand, mismatches in U_∞ result in errors of the same magnitude in the flow conditions behind the shock.

4.   Nonequilibrium Normal Shock Waves

Nonequilibrium normal shock waves have been studied both theoretically and experimentally. The experiments, mostly in shock tubes, have been primarily concerned with obtaining rate data for various chemical reactions. The calculations which used these rate-constant data serve to illustrate the relaxation phenomena for a wide range of conditions. Bond[133] calculated normal shocks in argon studying ionization nonequilibrium. Duff and Davidson[134] reported calculations in air for T_∞ = 300°K and Mach numbers from 8 to 15 in a study of the dissociation relaxation. Batchelder[135] calculated nonequilibrium normal shock waves for six velocity-altitude conditions neglecting ionization; however, his calculations did not extend to the equilibrium state. Lin and Teare[136] have reported calculations in air for studying specifically the ionization nonequilibrium.

Burke, Curtis, and Boyer[137] have also reported nonequilibrium normal shock solutions for air. They have correlated these solutions in

terms of binary scaling, delineated the extent of the nonequilibrium zone, related the normal shock solutions to blunt nose flows, and presented results for a particular case with free-stream dissociation. Their approach is similar to that used in the present study although their computations did not cover as extensive a range of velocity or altitude as the calculations made during the present work.

The computer program used here to calculate the flow behind a normal shock wave with coupled, finite-rate chemical reactions is a modification of that reported by Marrone[132]. For most of the calculations an 8-species (N_2, O_2, Ar, N, O, NO, NO^+, e^-) air model involving 10 reactions was used. The reactions and rate constants are given in Table II of Ref. 138[*]. The calculations were made for free-stream velocities of 10,000, 15,000, 20,000, 25,000, and 30,000 fps at altitudes of 100,000, 170,000, and 250,000 ft. In addition, several solutions at velocities of 30,000 and 36,000 fps were computed with a 12-species, 64-reaction air model in order to study the influence of the additional ions (N_2^+, N^+, O_2^+ and O^+) which occur at the higher velocities. In all cases, the solutions were computed until thermodynamic equilibrium was attained or for a distance behind the translational shock of 10 ft, whichever came first. At 100,000 ft, altitude the computations went to equilibrium at all velocities; at 170,000 ft, equilibrium conditions were reached in less than 10 ft except at 10,000 fps; at 250,000 ft, only the 25,000 fps and 30,000 fps shocks attained equilibrium within 10 ft.

The computations included both vibrational and dissociative relaxation processes. However, a coupled vibration-dissociation model was not used because it was felt that the empirical rate constants which were used included the effect of such a coupling[139, 140].

---

[*] Table II of Ref. 138 lists 11 reactions of which the first 10 are used in 8-10 air model. The eleventh reaction $N_2 + O_2 \rightleftharpoons 2NO$ was dropped because it is unimportant except in the immediate vicinity of the translational shock. Its exclusion does not affect the results presented here.

C.   NONEQUILIBRIUM NORMAL SHOCK WAVES AND BINARY SCALING

Because the first purpose of the nonequilibrium normal shock cal-
culations was a more systematic investigation of the applicability of binary
scaling to normal shock flows, the results are presented in terms of the
binary scaling parameter $\rho_\infty x$ where x is the distance from the trans-
lational shock front. It has been found that at each velocity U_∞ the results
for all three altitudes correlate in terms of $\rho_\infty x$ nearly up to the point
where thermodynamic equilibrium is attained. This is illustrated in detail
in Fig. 14 which shows the temperature in the relaxation region for the
three altitudes when U_∞ is 30,000 fps. The symbols represent selected
points from the computer results and are not indicative of the step size.
The correlation is seen to be excellent throughout most of the region. The
species concentrations exhibit a similar behavior as is shown in Fig. 15
which presents the NO concentrations for the same conditions as Fig. 14.
The three cases correlate perfectly as regards the magnitude and location
of the NO peak and deviate only as final equilibrium is attained.

The correlation for all velocities and the two extreme altitudes
(100,000 ft. and 250,000 ft.) is shown in Fig. 16 (temperature), Fig. 17
(pressure), Fig. 18 (density), Fig. 19 (NO concentrations) and Fig. 20
(oxygen concentrations). In these figures, solid lines are used rather than
individual points. Where the solution was not computed to equilibrium, a
dashed line represents the extrapolation to the equilibrium value. All of
these results are for the 8-10 air model only. A significant feature of the
results is that at all velocities, binary scaling holds nearly to the point where
the temperatures behind the lower altitude shock waves reach their equilib-
rium values. Indeed, the breakoff of the lower-altitude curve is so sharp
that very little error is introduced if the high-altitude curves are used up
to the point where the lower-altitude equilibrium temperature is attained.
Thus, a single high-altitude solution can be used to give the temperatures,
pressure and density history for all lower altitudes (at least down to 100,000
ft) within the accuracy shown in Figs. 16-18. It is also noted that the overall
change in pressure behind a nonequilibrium normal shock wave (Fig. 17) is

less than ten percent. By conservation of mass, the velocity profile is the inverse of the density profile, Fig. 18, and hence, has not been shown.

The behavior of the various gas species concentrations is essentially the same as that shown for the thermodynamic variables. The nitric oxide concentrations in moles of NO per original mole of air (Fig. 19) exhibit excellent correlation until the lower altitude equilibrium value is reached for all velocities except 10,000 fps. This exception appears to be related to the fact that the NO concentration displays a peak at the higher velocities, but not at 10,000 fps. This peak is a result of the fast two-body exchange reactions which are more important at the higher velocities[138]. In any event, for the 10,000 fps shock wave, the high-altitude solution is not sufficient to predict the NO concentration at lower altitude although it is satisfactory for predicting temperature, pressure, density, and the other species. The situation appears to be unique for nitric oxide because in one case its behavior is monotonic whereas in the other cases a peak occurs; on the other hand, the other species (N_2, N, O_2, O) always exhibit a monotonic variation. This is illustrated in Fig. 20 which shows the oxygen atom concentrations. Here we note essentially no difference between the two different altitudes for velocities of 15,000 fps and higher. At 10,000 fps there is a noticeable deviation as the lower-altitude case breaks off to its lower equilibrium concentration. Again, the breakoff is quite sudden so that, to a good approximation, the high-altitude solution is sufficient to determine the concentrations for all lower altitudes. The NO^+ and e^- distributions exhibit a behavior similar to NO in that there is an overshoot at all velocities except 10,000 fps. The peak of this overshoot occurs shortly downstream of the NO peak.

If the present results for U_∞ = 20,000 fps are compared with those of Burke et al[137] at this same velocity, it is observed that small differences occur. These differences result from the fact that in the present work the vibrational nonequilibrium is not coupled to the dissociation, whereas in Ref. 137 a coupling was used. The effect of the coupling is to delay dissociation and, hence, shift the curves in Figs. 15-20 to higher values of $\rho_\infty x$. As we mentioned previously, this coupling was not included in the present calculations because it is felt that the empirical rate constants implicitly account for it.

The simplified 8-10 air model used in these calculations contained only NO^+ as an ionized species and clearly is inaccurate for the ionized species at high temperatures. An indication of the importance of other ionized species and reactions is contained in the estimates of nonequilibrium ionization phenomena for a blunt body reported by Dunn et al[141]. On the basis of their findings, additional normal shock calculations were made using the more complex 12-species, 64-reaction air model[141]. Here the ionized species are NO^+, N^+, N_2^+, O^+, and O_2^+. A comparison of the two models showed significant differences in the NO^+ concentrations and much smaller differences in the neutral species concentrations. However, the important result is that binary scaling still held nearly up to the point where the lower-altitude concentrations reached their equilibrium values.

This study of nonequilibrium normal shock waves has shown that binary scaling can be a powerful tool throughout the flight regime of present interest whenever the nonequilibrium flow over a body can be related to a corresponding normal shock-wave flow. This includes blunt bodies, as already mentioned, and nonslender wedges, as will be shown later. Its practical significance as far as tunnel testing is concerned lies not so much in the similitude it provides as in the correlation and interpretation it permits of tunnel-test data. That is, if $\rho_\infty L$ is to be constant and the tunnel model is of smaller scale than the flight vehicle, then binary scaling requires the tunnel test be performed at a higher free-stream density. At the lower altitudes, this is increasingly difficult to achieve. Even with moderate increases in density, binary scaling still permits model flows to be related to similar flight flows though over a restricted length.

D.   FLOW REGIMES BEHIND NORMAL SHOCK WAVES

The use of the nonequilibrium normal shock solutions to delineate the frozen, nonequilibrium, and equilibrium flow regimes has been briefly described and an example application has been given in Sec. II. Here, we present additional detail . Delineation of the boundaries of the various flow regimes requires the selection of suitable criteria. Examination of the normal shock solutions has indicated that the temper-

ature profiles (Figs. 14 and 16) offer a logical basis for this selection. The temperature starts at the frozen value, decreases rapidly through the dissociation region, and quickly flares out to the final equilibrium value. Consequently, the following criteria have been adopted:

1. The boundary between frozen flow and nonequilibrium flow is taken as the point where the temperature deviates from the frozen temperature immediately behind the shock by 1%.

2. The boundary between nonequilibrium and equilibrium flow is the point where the temperature is within 1% of the final equilibrium value.

Inspection of the species concentrations shows that these criteria are reasonable. When the temperature is 99% of the frozen temperature, the degree of dissociation is small. This is shown in the following table which presents the ratios of the O, N, and NO concentrations at $T = 0.99T_{frozen}$ to the final equilibrium concentrations for the highest and lowest altitudes.

TABLE V-2

RATIO OF CONCENTRATIONS AT FROZEN FLOW BOUNDARY
TO EQUILIBRIUM CONCENTRATION

Altitude, Ft.	Velocity, fps	(O)	(N)	(NO)
100,000	10,000	0.0177	0.0243	5.72×10^{-5}
	15,000	0.0239	0.0075	0.00093
	20,000	0.0201	0.0069	0.0026
	25,000	0.0174	0.0075	0.0061
	30,000	0.0210	0.0095	0.0386
250,000	10,000	0.0096	*	0.00019
	15,000	0.0219	0.0045	0.0025
	20,000	0.0243	0.0065	0.00048
	25,000	0.0210	0.0076	*
	30,000	0.0189	0.0077	*

$(O) = [O]_{T=0.99T_{fr}} \big/ [O]_{T_{eq}}$, etc. where $[O]$ = moles of O per original mole of air.

*The ratios omitted are misleadingly large since these species are relatively unimportant at these velocity-altitude conditions.

When the temperature is within 1% of the equilibrium temperature, the species concentrations are similarly very close to the final equilibrium values. This is shown in the following table as the ratio of concentrations at the equilibrium boundary ($T = 1.01 \, T_{eq}$) to the equilibrium values. Here, the fact that not all solutions were carried to equilibrium results in a less complete table than the previous one.

TABLE V-3

RATIO OF CONCENTRATIONS AT EQUILIBRIUM FLOW BOUNDARY
TO FINAL EQUILIBRIUM CONCENTRATIONS

Altitude, Ft.	Velocity, fps.	(O)	(O$_2$)	(N)	(N$_2$)	(NO)	(NO$^+$)
100,000	10,000	.975	1.057	.816	1.007	.755	*
100,000	15,000	.977	1.032	1.018	.999	1.031	1.039
100,000	20,000	.999	1.074	.987	1.003	1.056	1.026
100,000	25,000	.999	1.058	.992	1.010	1.045	1.025
100,000	30,000	1.000	1.050	.994	1.050	1.048	1.022
170,000	15,000	.996	1.228	.944	1.000	1.137	1.009
170,000	25,000	.995	1.081	.995	1.010	1.062	1.027
170,000	30,000	1.000	1.138	.993	1.108	1.131	1.024
250,000	30,000	1.000	*	.994	*	*	1.025

(O) = $[O]_{T = 1.01 T_{eq}}$ / $[O]_{eq}$ etc. where $[O]$ = moles of O per original mole of air.

These tables lend validity to the temperature criteria for the boundaries of the flow regimes. Application of these criteria produced the results already presented in Fig. 9. Burke et al [137] have also used their nonequilibrium normal shock results to define a distance to equilibrium (or a "relaxation length"). They defined three relaxation lengths (λ_o , λ_N , λ_e) as follows:

---

* The ratios omitted are misleadingly large since these species are relatively unimportant at these velocity-altitude conditions.

λ_{o} (or λ_{N}) is the distance behind the shock front at which the atomic oxygen (or atomic nitrogen) concentration has reached 80% of its theoretical equilibrium value; λ_{e} is the distance behind the shock front at which the maximum electron concentration occurs. From Table V-3, it is evident that these lengths are shorter than the distance based on our temperature criterion. In addition, the 80% criterion for λ_{N} is less stringent than the 90% criterion used by Harney[11]. They found, as would be expected, that λ_{N} was greater than λ_{o} or λ_{e} at all the velocities they calculated. Their λ_{N} is about 1/3 our x_{eq} for 160,000 ft and 20,000 fps and nearly an order of magnitude smaller at 200,000 ft and the same velocity.

With the aid of Fig. 9, the flow regimes for various bodies can be delineated whenever the flow can be related to a normal shock-wave flow. A specific example of this was given in Sec. II for comparison with Harney's results[17].

Some general conclusions that may be drawn from Fig. 9 are: (1) in the flight regime of interest, the extent of frozen flow over full-scale vehicles is negligible; (2) no similar conclusion can be made for tunnel models unless a model scale is specified; however, small scale models will experience more extensive regions of frozen flow than flight vehicles; (3) at the lower altitudes, flight vehicles can experience extensive regions of equilibrium flow; (4) small-scale tunnel models may not experience similar equilibrium flows; (5) throughout most of the flight regime, both flight vehicles and test models will experience large regions of nonequilibrium flow.

E. APPLICATION OF NORMAL-SHOCK SOLUTIONS TO WEDGE FLOWS

The relationship between a normal shock wave and the oblique shock wave generated by a sharp wedge is, of course, well known (e.g., Ref. 25, pg. 21). Once the shock angle σ is known, the flow over the wedge can be calculated in a straightforward manner. In general, however, it is the Mach number M_{∞} and the wedge angle γ that are given. Even for an ideal gas with constant specific heat ratio γ, however, there is only an

implicit relation between the shock angle σ and the wedge angle τ for a given M_∞ :

$$\tan \tau = 2 \cot \sigma \, \frac{M_\infty^2 \sin^2 \sigma - 1}{M_\infty^2 (\gamma + \cos 2\sigma) + 2} \tag{V-2}$$

Charts of this relationship and the flow quantities downstream of the oblique shock are given in Ref. 128, for example. Hammitt and Murthy[142] have shown that Eq. (V-2) can be written as a cubic in $\tan \sigma$ which can be solved explicitly for σ as a function of τ and M_∞ . They also show that for slender wedges at hypersonic Mach numbers, this reduces to the usual hypersonic small-disturbance relation

$$\sigma = \frac{\gamma+1}{4} \, \tau + \sqrt{\left(\frac{\gamma+1}{4}\right)^2 \tau^2 + M_\infty^{-2}} \tag{V-3}$$

In addition, they give an approximate solution valid for $M_\infty \gg 1$ and τ large also. Finally, they present an iterative scheme for explicit determination of σ that is valid for all τ if $M_\infty \gg 1$. In their comparison with the exact results of Ref. 128, they show that the iterative method gives excellent agreement for $M_\infty \tau \geq 2$.

Solutions for high free-stream Mach numbers or velocity where real gas effects become important are given in Refs. 143-145. In addition, a method of solution for an oblique shock wave attached to a surface at arbitrary angle of attack, sweep and dihedral has been given by Trimpi and Jones[146]. The extensive tabulation of the results presented by them are applicable to real air in thermodynamic equilibrium. To use their results, one requires a knowledge of the effective specific heat ratio γ_e as a function of Mach number for a normal shock in air. This effective specific heat ratio, which is defined as

$$\gamma_e \equiv 2 \, \frac{\left(1 - M_\infty^{-2}\right)}{\left(1 - \rho_\infty / \rho_s\right)} - 1 \tag{V-4}$$

70

has been calculated by Wittliff and Curtis[129], and Marrone[131] for all their normal shock-wave solutions. It can also be calculated for the solutions presented by Lewis and Burgess[130]. Thus, these results (Refs. 129-131) can be used in conjunction with Ref. 146 to determine conditions behind oblique shock waves for a wide range of velocities and wedge angles in flight. It should be mentioned, however, that each oblique shock case requires either iteration or cross-plotting to obtain a solution. Hence, it is of limited value if a large number of solutions are desired. An approximate, but simple, method for generating equilibrium oblique shock-wave parameters from normal shock-wave solutions is given later in Sec. VII-C.

The application of normal shock-wave solutions to oblique shock waves (i.e., wedge flows) results from the fact that the wedge flow is self-similar under certain conditions. In that case, the flow quantities behind the shock are constant along the streamlines and both the shock and streamlines are straight. However, in the flight regime, where there is an extensive relaxation zone behind the shock, the shock wave and streamlines are no longer straight and the flow is nonsimilar. Strictly speaking, normal shock waves can no longer be mapped into oblique shocks. In the present work, we have attempted to assess the inaccuracies involved when such a mapping is attempted. The general subject of wedge flows is treated in the following section on Slender Bodies (Sec. VI); hence, here attention is confined to two specific cases of nonslender wedges that have been studied.

Spurk, Gerber, and Sedney[147] have made characteristics calculations of the flow fields over wedges and cones including the effects of flow chemistry. They used an air model consisting of a mixture of N_2, O_2, NO, N, and O with vibrational equilibrium assumed and calculated wedge flows for Mach numbers of 15 and 20 with a wedge angle of about 41°. Their results showed monotonic variations of all quantities except NO. In their results, the pressure variation along the wedge is opposite to that for the normal shock, however, in that pressure decreases with distance from the wedge apex, whereas behind a normal shock wave the pressure

increases with distance. In both cases, though, the total change is small, being about 6% for a 41° wedge at M_∞ = 15 and 20 and less than 10% for all of the normal shock solutions. This small change led Spurk et al to make further calculations under the assumption that the pressure (or velocity) is constant. These approximate results yield a temperature distribution along the wedge that is in excellent agreement with the exact calculation and species concentrations that are in good agreement. Although these comparisons do not cover an extended range of Mach numbers, free-stream densities and wedge angles, the results obtained were considered sufficient justification for investigating the application of nonequilibrium normal shock solutions to nonslender wedge flows.

Closely related to the nonequilibrium flow over a wedge is the non-equilibrium flow behind a plane, oblique shock wave. Sedney,[148] Epstein,[149] Hsu and Anderson,[150] and Chu[151] have shown that the latter flow is associated with cusped bodies. Chu has pointed out that the "non-equilibrium flow behind an oblique shock wave with curved streamlines and apparently very nonuniform flow properties is equivalent to a nonequilibrium flow behind a normal shock wave". The direct equivalence observed by Chu for oblique shock waves does not exist for wedge flows where both the shock and the streamlines (except for the streamline wetting the body) are curved. However, if the streamline curvature is small, the nonequilibrium flow behind an oblique shock may closely approximate that over a wedge. As indicated above, Spurk et al[147] found that the pressure along the wedge changed only 6% for the two examples they calculated. In addition, all flow properties behind a straight oblique shock are constant along lines parallel to the shock[149-151]. Under these circumstances, the pressure gradient normal to the streamline will be small also, implying that the streamline curvature is small from the usual relation

$$\frac{\partial p}{\partial n} = -\frac{\rho w^2}{R} \qquad (V-5)$$

where n is direction normal to the streamline, w is the flow velocity in the streamline direction and R is the radius of curvature of the streamline.

The two wedge flows reported in Ref. 147 are for the following conditions:

M_∞	20	15
U_∞	21,780 fps	16,330 fps
τ	41.04°	40.68°

In both cases, the free-stream static pressure p_∞ is 0.01 atm, the initial value of the shock-wave angle σ at the wedge leading edge is 50° and the final equilibrium oblique shock angles are 46.8° and 46.9° for M_∞ = 20 and 15, respectively. The air model used 5 species, 10 reactions and assumed vibrational equilibrium. As part of the present work, two normal shock solutions have been computed to correspond to those of Ref. 147, using an identical air model and taking the free-stream velocity component normal to the shock as $U_\infty \sin 50°$. Since the change in shock angle due to relaxation is small, it is anticipated that the normal shock, calculated for such a fixed velocity, would be a reasonably good approximation.

The nonequilibrium flow along a wedge has been related to the flow behind a normal shock wave by neglecting the shock curvature effects and considering only the variation in quantities in the direction normal to the shock wave. Equating differential flow times in directions parallel to the wedge surface and normal to the shock wave yields

$$\frac{ds}{\sqrt{U_\infty^2 \cos^2\sigma + \left(\frac{\rho_\infty}{\rho}\right)^2 U_\infty^2 \sin^2\sigma}} = \frac{dx}{\left(\frac{\rho_\infty}{\rho}\right) U_\infty \sin\sigma} \tag{V-6}$$

where s is the distance along the wedge surface, x is the distance normal to the shock, and ρ is the density behind the shock at the distance x. This can be rearranged to give

$$s = \int_0^x \sqrt{\left(\frac{\rho}{\rho_\infty}\right)^2 \cot^2\sigma + 1}\; dx \tag{V-7}$$

When the shock wave and streamlines are straight (i.e., ideal gas or completely equilibrium real gas and no boundary-layer displacement effects), the density ratio ρ/ρ_∞ is constant and the integration is trivial. For the specific examples considered here, σ is taken as constant and equal to the frozen-flow value of 50°. Noting that $\left(\dfrac{\rho}{\rho_\infty}\right)^2 \cot^2 50° \gg 1$, the following approximation is adopted for mapping the normal shock solution to a wedge flow

$$s \simeq \cot 50° \int_0^x \left(\frac{\rho}{\rho_\infty}\right) dx \tag{V-8}$$

where ρ/ρ_∞ is a function of x given by the nonequilibrium normal shock solution. Although some average value of ρ/ρ_∞ could be used to obtain a simple algebraic relation between s and x, in the present work the integral has been evaluated numerically. This mapping is essentially the same as that used by Chu[151].

The results of the comparison are shown in Figs. 21 and 22[*]. Figs. 21a and 22a indicate that the temperature from the mapped normal shock solution agrees with that of the characteristics solution to within 1% throughout the nonequilibrium region. It is observed in Figs. 21b and 22b, however, that the two solutions yield opposite pressure trends. This is distinctly a result of the two-dimensional nature of the wedge flow which the normal shock solution cannot exhibit. Two comments are appropriate here: first, the discrepancy amounts to no more than 10% in either case; second, the initial, frozen pressure represents a good average of the two solutions. The density variations are compared in Figs. 21c and 22c where it is seen that the mapped normal shock solution yields a density that is about 8 to 10% higher than the wedge characteristics solution. This, of course, follows directly from the comparisons of temperature and pressure. In view of the reasonably good agreement for pressure and density and the very good agreement for temperature, it would be anticipated that the species concentrations would compare favorably. These results are shown in Figs. 21d and 22d where the overall agreement is seen to be exceptionally good. A few comments are appropriate here: in Fig. 21d, the differences between the two solutions for

N_2 and O are less than 1% throughout the flow; also, in Fig. 21d, the agreement of the other species, particularly the NO-peak, is remarkable; in Fig. 22d, the two solutions for N_2 are identical within the scale of the graph; no curve for N is given in Fig. 22d because the amount present was an order of magnitude less than that for any of the other species.

These results graphically indicate that normal shock-wave solutions have some degree of application to nonslender wedge flows even in the presence of nonequilibrium phenomena. The temperature and species concentrations are very well predicted by the mapped normal shock solutions, and the initial, frozen pressure represents a good approximation, for engineering purposes, to the pressure on the wedge. The range of applicability of normal shock solutions to nonequilibrium wedge flows has not been established here. To do so requires detailed consideration of the two basic restrictions that the shock and streamline curvatures be small. The shock curvature is primarily dependent on the free-stream velocity component normal to the shock and the free-stream density. The streamline curvature dependence is given by Eq. (V-5).

F.   MAPPING NORMAL SHOCK SOLUTIONS TO BLUNT BODY FLOWS

The correspondence between normal shock and blunt-body flows has been developed by Gibson and Marrone for both a Lighthill gas[46] and for air[46, 48]. This correspondence applies in general for Newtonian flows when two-body processes dominate. Along the stagnation streamline, it is not restricted to two-body processes. The basic analytic approach was developed for the Lighthill gas and then extended to nonequilibrium airflows. A simple freezing criterion was derived for predicting frozen species concentrations in the afterbody flow. This correspondence or shock-mapping was compared with exact numerical solutions for airflows[46, 137] and very good agreement was obtained for the blunt nose region at free-stream velocities of 15,000 fps and 23,000 fps.

Burke et al[137] have made a similar comparison at U_∞ = 14,000 fps for two altitudes (182,000 ft and 235,000 ft). They also found very good agreement between the mapped normal shock solutions and exact numerical solutions obtained by the inverse method.

This shock-mapping technique becomes an even more powerful tool for obtaining flow-field solutions in view of the results of the present work regarding nonequilibrium normal shocks and binary scaling. Since approximate normal shock solutions can be obtained for many altitudes from a single solution at high altitude, it is no longer necessary to calculate a separate normal shock for every flight condition of interest.

G. EFFECT OF FREE-STREAM DISSOCIATION ON FLOW BEHIND NORMAL SHOCK WAVES

The effect of free-stream dissociation on the nonequilibrium flow behind normal shock waves has been studied by several authors. Inger[152] has investigated the influence of free-stream dissociation for the two extremes of frozen flow and equilibrium flow behind normal and oblique shock waves of velocities from 15,000 fps to 30,000 fps. He found that significant changes in the post-shock density, temperature, dissociation and ionization can occur if 10% or more of the total energy is contained in preshock dissociation. We have already shown (Sec. II-D) that the frozen enthalpy can amount to as much as 25% of the total enthalpy; hence, this is a real effect for the flight regime of interest here. Yalamanchili[153] has also investigated the effects of free-stream dissociation for normal and oblique shock waves; however, he only treats a few extreme cases as regards the degree of free-stream dissociation. Neither of these authors has investigated the nonequilibrium relaxation zone behind a shock when free-stream dissociation exists. Completely equilibrium flow behind a normal shock exists only at the lower altitudes of the flight regime being considered and in this region no free-stream dissociation exists. Where free-stream dissociation occurs, the normal shock wave will have an extensive nonequilibrium zone. Therefore, Inger's results can only serve to bracket the magnitude of this effect. To study the detailed effect of $\alpha_\infty \neq 0$ on

nonequilibrium normal shocks would require extensive numerical calculations. Burke et al[137] have investigated this effect for one specific case. They calculated the nonequilibrium hypersonic nozzle flow for a reservoir temperature of 7600°K and pressure of 10,000 psi (U_∞ = 16,500 fps). A nonequilibrium normal shock was then calculated by using tunnel nonequilibrium test section conditions as the free-stream conditions. The results of this normal shock are compared with a flight case (α_∞ = 0) at the same free-stream velocity. The temperature profile was very little affected by the free-stream dissociation and the velocity (and density) profile only slightly more (less than 10%). As would be expected, the species concentrations were orders of magnitude different immediately behind the shock front and in good agreement as equilibrium was approached.

Gibson has applied his subtraction rule to several cases of nonequilibrium normal shocks in air[50]. He found very good correlation with exact numerical calculations confirming the validity of the subtraction rule for airflows with free-stream dissociation. This rule provides a means of correlating nonequilibrium normal shocks in wind tunnels, when O atoms and NO are present in the free stream, with flight conditions.

VI. SLENDER BODIES

A.   INTRODUCTION

The general similitudes for slender bodies have been discussed in Secs. III and IV. It is convenient in the present section to consider first the case of wedges and then the case of cones. Attention is restricted to simple flows because more is known about them and they serve to illustrate the effects being studied; namely, the sensitivity of the flows to the similitude parameters.

In the discussion of each of these flows, the ideal gas case will be considered first, not only because it is pertinent to many slender bodies even at high free-stream velocities, but also because, in many instances,

it is the only case for which sufficient solutions are available to permit the evaluation of the effects of mismatches in the similitude parameters. For the case of equilibrium real gas flows, some estimates of the sensitivity of the flows to the similitude parameters are presented. For nonequilibrium flows, the present paucity of solutions precludes any such estimates and we are restricted to presenting only a more detailed discussion of the similitudes reviewed in Sec. III.

B.   WEDGE FLOWS

1.   Inviscid Flow

Tsien's hypersonic similarity law[22] for the inviscid flow about a sharp slender wedge shows the governing parameter to be $M_\infty \tan \Theta_w$, where Θ_w is the wedge angle. For ideal gases, the similarity also depends upon the specific heat ratio γ , whereas for real gas flows, Cheng[33] has shown that similarity requires duplication of the free-stream pressure, temperature and species concentrations. In view of the highly restrictive nature of this last requirement, it is important to delineate where real gas effects become significant.

Because wedge flows support a plane oblique shock wave (except in the case of nonequilibrium phenomena), appeal can be made to normal shock flows to establish the onset of real gas effects. The question of when real gas effects become important is not a simple one. As regards pressures, and hence forces, one would establish a criterion based on when the pressure ratio across the shock differs by, say, 5% from the ideal gas ratio. This occurs when the temperature behind the shock is 2300°K or greater. On the other hand, the local heat-transfer rate is approximately proportional to the square root of the local density outside the boundary layer. Thus, a 5% effect on heat transfer would correspond to approximately a 10% deviation from ideal gas theory in density ratio across the shock. Furthermore, in terms of deviations from ideal gas theory, the density ratio is the most sensitive parameter (see Sec. V-B-3, for example). The density across the shock wave differs from the ideal gas ratio by 10% when the temperature

behind the shock is in the range 1400 to 1500°K. For the flight regime of interest here and for wind-tunnel test flows having a free-stream static temperature in the range 200 to 300°K, the 10% deviation in density ratio occurs at a normal shock Mach number of about 5. Investigation of the shock angle-wedge angle relationship for ideal gas flows indicates that M_{n_∞} = 5 occurs for a nearly constant value of M_∞ tan θ_w equal to about 4 for all $M_\infty \geq$ 10 and $\tan^2 \theta_w << 1$. Since for slender wedges tan $\theta_w \simeq \theta_w$, we find that the ideal gas regime is restricted to $M_\infty \theta_w \simeq M_\infty \tan \theta_w \leq 4$. This criterion, of course, is not applicable when the free-stream static temperature in the wind tunnel is high (e.g., Table II-1). In such cases, the temperature behind the oblique shock may be high enough to introduce real gas effects at much lower values of M_{n_∞} or $M_\infty \theta_w$.

In the ideal gas regime, the flow about slender wedges can be determined from hypersonic small-disturbance theory. Linnell[154] gives the solution for the pressure ratio as

$$\frac{p_w}{p_\infty} = 1 + \frac{\gamma}{2} \left(M_\infty \theta_w \right)^2 \left[\frac{\gamma+1}{2} + \sqrt{\left(\frac{\gamma+1}{2} \right)^2 + \frac{4}{\left(M_\infty \theta_w \right)^2}} \right] , \quad \theta_w \text{ in radians}$$

(VI-1)

where p_w is the pressure on the wedge surface. For $\theta_w \leq 30°$ and $M_\infty \geq 10$, this formula gives good agreement with ideal gas, oblique shock-wave theory. A comparison of pressure ratios given by Eq (VI-1) and pressure ratios computed for real air in thermodynamic equilibrium[144] is shown in Fig. 23. The real air solutions are for free-stream velocities from 15,000 fps to 26,000 fps and altitudes of 50,000 ft and 250,000 ft. It is noted that these real gas pressure ratios correlate very well in terms of $M_\infty \theta_w$ for both altitudes. This correlation can be used to study the sensitivity of the pressure on slender wedges to mismatches in the free-stream quantities.

From Fig. 23 it has been observed that for $5 \leq M_\infty \theta_w \leq 13$, the equilibrium real gas pressures may be represented to within 5% accuracy by

$$\frac{p_w}{p_\infty} = 2.20 \left(M_\infty \theta_w \right)^{1.84}$$

(VI-2)

If the density-altitude is duplicated, then the sensitivity of wedge pressure to mismatches in U_∞, T_∞ or θ_w is

$$\frac{\delta p_w}{p_w} = 1.84 \, \frac{\delta \theta_w}{\theta_w} + 1.84 \, \frac{\delta U_\infty}{U_\infty} + 0.08 \, \frac{\delta T_\infty}{T_\infty} \tag{VI-3}$$

The significant feature here is the weak dependence on a mismatch in T_∞ relative to a mismatch in U_∞. This results because a mismatch in free-stream static temperature introduces not only a mismatch in M_∞, but also in p_∞ if free-stream density is duplicated.

The sensitivities of density and temperature on the wedge to mismatches in U_∞ and T_∞ when ρ_∞ is duplicated are discussed in Sec. VII-C as part of a special study of wedge-nosed flat plates. The results given there also show a greater sensitivity to mismatches in U_∞ than in T_∞.

Cheng[33] has shown that in the equilibrium real gas regime the hypersonic similarity parameter also correlates the other flow parameters, such as density ratio, temperature ratio, and compressibility factor behind the shock. In this regime, however, the sensitivity of these various quantities to mismatches in the similitude parameter is altitude dependent. Inspection of his results shows a nearly linear variation with $M_\infty \theta_w$ in the range $6 \leq M_\infty \theta_w \leq 11$. Thus, the sensitivity of temperature or density can be readily determined from an empirical relation in the same manner as for the pressure. The sensitivity of the particular quantity of interest as a function of altitude requires more extensive correlations of the type made by Cheng.

Cheng's real gas similitude requires simulation of the free-stream thermodynamic state. However, for the postulated wind-tunnel performance, large mismatches in free-stream temperature occur along the lower boundary of the flight regime of interest when the density-altitude is duplicated. The effect of such mismatches can only be evaluated accurately by numerical solution.

Nonequilibrium wedge flows have been studied by several groups in recent years, e.g., Refs. 148, 155-161. All of these papers are concerned primarily with nonslender wedges ($\theta_w \gtrsim 20°$) and report numerical results for a few specific cases only. Also, the previously mentioned solutions of the nonequilibrium flow behind plane, oblique shock waves[148-151] are restricted to nonslender bodies (i.e., oblique shock angles of 40° or greater). The nonequilibrium flow over a slender wedge has been studied by Moore and Gibson[162] and Clarke[163] who obtained approximate and exact solutions, respectively, for the linearized problem. Sundaram[164] has shown, however, that even Clarke's exact linearized solution is applicable only to very slender wedges ($\theta_w \lesssim 1/2°$). Thus, although the nonequilibrium similitude for slender wedge flows has been established by Inger,[34] there are no solutions available for evaluating the effects of not duplicating the pertinent similitude parameters.

The case of a blunt-nosed slender wedge is somewhat similar. Cheng[33] developed the equilibrium similitude which Inger[34] later extended to nonequilibrium flows. Again, however, there are no solutions available to evaluate the similitude. The nonequilibrium similitude for sharp, slender wedges given by Inger requires complete duplication of free-stream thermodynamic state and species concentrations. When $M_\infty \gamma$ = constant, the nonequilibrium distributions of pressure, etc., and the shock shapes for a family of affinely related sharp slender wedges are functions only of a nondimensional "reaction coordinate" $\bar{x}_R$ (the ratio of the local distance to a characteristic relaxation length) defined by

$$\bar{x}_R = k_R \rho_\infty^2 T_\infty^\omega x \Big/ V_\infty m_M^2 \quad \propto \quad x/V_\infty \tag{VI-4}$$

where the quantities have been defined previously in Sec. III-B-2.

When the slender wedge has a blunt leading edge, then, in addition to duplication of the free-stream state, Inger's similitude requires duplication of

$$K_{R_N} = \left(k_R T_\infty^\omega \rho_\infty^2 \Big/ V_\infty m_M^2 \right) M_\infty^3 C_{D_N} d_N \tag{VI-5}$$

and

$$1/\bar{z}_N = M_\infty^3 \, C_{D_N} \, d_N / x$$

(VI-6)

Thus, when K_{R_N} is the same for two flows, the pressure distribution, etc., will be correlated by the nondimensional distance $\bar{z}_N$. At present, there exist no exact solutions for verification of this similitude.

In view of the restriction of this nonequilibrium similitude to a single species gas and the paucity of exact solutions for comparison, no attempt has been made to evaluate the effects of mismatches in the similitude parameters.

2. Viscous Phenomena in Wedge Flows

The general, aspects of viscous similitudes have been described in Sec. IV. The interaction between the boundary layer and the outer inviscid flow has been studied extensively, both theoretically and experimentally (e. g., see Ref. 25, Sec. IX). The governing parameter is $\bar{\chi} = M_\infty^3 \, \sqrt{C} / \sqrt{Re_x}$ where C is the Chapman-Rubesin viscosity factor. One of the most extensive combined theoretical and experimental investigations of this interaction is that of Cheng et al [165] who studied both leading-edge bluntness and boundary-layer displacement effects essentially in the ideal gas regime. They have shown that for the sharp leading-edge case, the interaction is governed by $\bar{\chi}$ and that for the blunt leading-edge case, the proper parameter is

$$\beta = \chi_\epsilon \, K_\epsilon^{-2/3}$$

(VI-7)

where

$$\chi_\epsilon = \epsilon \left(0.664 + 1.73 \, \frac{H_w}{H_o} \right) \frac{M^3 \sqrt{C}}{\sqrt{Re_x}}$$

$$K_\epsilon = M^3 \, \frac{\epsilon \, C_{D_N} \, t}{x}$$

with

$$\epsilon = \gamma - 1 / \gamma + 1$$

H_w, H_o = the total specific enthalpy at the wall and free stream, respectively

$C_{D_N} = D_N / \frac{1}{2} \rho_\infty V^2 t$ = the leading edge (nose) drag coefficient

t = the thickness of the blunt leading edge

A detailed assessment of the effects of mismatches in the similitude parameters for complex flows of this type is beyond the scope of the present work. We must content ourselves with indicating the differences in the interaction parameter $\bar{\chi}$ between the flight and tunnel case for the lower boundary of the flight regime when velocity and density-altitude are duplicated. Since $C \simeq 1$, this is readily computed from Table II-1, taking $x = 1$ ft.

TABLE VI-1

VISCOUS INTERACTION PARAMETER FOR VELOCITY AND
DENSITY-ALTITUDE DUPLICATION

Velocity, fps. U_{∞}, fps	Altitude, ft	$\bar{\chi}$ flight	$\bar{\chi}$ tunnel
10,000	50,000	0.317	0.0773
15,000	50,000	0.865	0.140
20,000	50,000	1.78	0.203
25,000	87,000	7.33	1.29
30,000	125,000	25.5	7.52
35,000	160,000	70.7	35.2

Thus, we see that to duplicate $\bar{\chi}$ requires test models that are from 2 to 9 times longer than the flight vehicle if velocity and density-altitude are duplicated. Inspection of Table II-2 indicates that if the velocity and free-stream Mach number are duplicated, then the mismatch in $\bar{\chi}$ between test and flight regime varies from 2 to 14. Hence, mismatches in other free-stream parameters must accompany duplication of the interaction parameter $\bar{\chi}$. The problem is very similar to that of duplicating Reynolds number (Sec. II).

C.   SHARP SLENDER CONES

1.   Inviscid Flow

The supersonic flow field for a cone is not as simple as that for a wedge since the flow downstream of the bow shock is not uniform. It is, however, constant along each ray from the cone vertex. Taylor and Macoll[166] obtained the solution for an ideal gas and Kopal[167] and Sims[168] have published

extensive tables of solutions. There are also many approximation formulas applicable for γ = constant[142, 169-172]. Romig has published solutions for the case of real air in thermal and chemical equilibrium[173]. These latter solutions cover semi-vertex angles, θ_c, from 20° to 50°, velocities from 10,000 to 32,000 fps and free-stream pressures from 10^{-1} to 10^{-4} atm (approximately 50,000 ft. to 215,000 ft. in altitude) for a free-stream temperature of 273.16° K. Use of the hypersonic similarity parameter, $M_\infty \sin \theta_c$, permitted correlation of the aerodynamic and thermodynamic flow properties with an error of less than 1% in all cases. Romig also has compared her numerical results with empirical formulas developed by Linnell and Bailey[172] for the Kopal tables[167]. The cone surface pressure correlates very well with the equation

$$\frac{C_p}{4 \sin^2 \theta_c} = \frac{2.5 + 8\sqrt{M_\infty^2 - 1} \, \sin \theta_c}{1 + 16 \sqrt{M_\infty^2 - 1} \, \sin \theta_c} \tag{VI-8}$$

Romig's results are at most 2% higher than predicted by this empirical equation. Since $\sqrt{M_\infty^2 - 1} \rightarrow M_\infty$ as M_∞ increases, the equation can be simplified and utilized to investigate the sensitivity of cone surface pressure to mismatches in free-stream velocity and static temperature. Replacing $\sqrt{M_\infty^2 - 1}$ with M_∞, Eq. (VI-8) can be written as

$$\frac{p_c}{p_\infty} = 1 + 2\gamma \left(M_\infty \sin \theta_c\right)^2 \frac{2.5 + 8 M_\infty \sin \theta_c}{1 + 16 M_\infty \sin \theta_c} \tag{VI-9}$$

For the range $\left(M_\infty \sin \theta_c\right) \geq 1$, we can neglect 1 in comparison with $16 M_\infty \sin \theta_c$. Assuming density-altitude duplication, we obtain for a given cone angle θ_c

$$\frac{\delta p_c}{p_c} = \left[\frac{32 \gamma (M_\infty \sin \theta_c)^2 + 5\gamma (M_\infty \sin \theta_c)}{16 \gamma (M_\infty \sin \theta_c)^2 + 5\gamma (M_\infty \sin \theta_c) + 16}\right] \frac{dU_\infty}{U_\infty} + \left[\frac{2.5 \gamma (M_\infty \sin \theta_c) + 16}{16 \gamma (M_\infty \sin \theta_c)^2 + 5\gamma (M_\infty \sin \theta_c) + 16}\right] \frac{dT_\infty}{T_\infty} \tag{VI-10}$$

Fig. 24 shows $\dfrac{\delta p_c / p_c}{\delta U_\infty / U_\infty}$ and $\dfrac{\delta p_c / p_c}{\delta T_\infty / T_\infty}$ as a function of $M_\infty \sin \theta_c$.

As in the case of the wedge, the sensitivity of the pressure to mismatches in U_∞ is appreciably greater than the sensitivity to changes in T_∞.

Of course, when the flow becomes Mach number independent, the sensitivity to δT_∞ is zero.

Romig[173] has pointed out that it is not possible to fit simple curves to the cone flow parameters other than pressure and shock-wave angle. Hence, the sensitivity of these parameters (e.g., density and temperature) to mismatches in free-stream quantities cannot be determined in a simple manner.

A comparison of Romig's solutions with the ideal gas solutions tabulated by Kopal indicate that real gas effects become significant at values of $M_\infty \sin \theta_c \geq 3$ when $T_\infty = 300°K$. This is only approximate, however, since Romig's real gas solutions do not extend below $M_\infty \sin \theta_c = 6$. Her solutions show a dependence on free-stream pressure (or density) as is expected and, hence, verify Cheng's conclusion that similitude of such real gas flows requires duplication of free-stream conditions[33].

It is worth noting here that although there are several approximate methods for calculating the conical shock angle θ_s as a function of M_∞ and θ_c for γ = constant[142, 169, 172], Romig has presented an empirical formula which agrees with her numerical results to within ± 1% for $M_\infty \sin \theta_c \geq 6$ and which includes the dependence on p_∞.

$$M_\infty \sin \theta_s = (0.39 - 0.01 \log p_\infty) + (1.03 + 0.005 \log p_\infty) M_\infty \sin \theta_c \qquad \text{(VI-11)}$$

where p_∞ is in atmospheres.

For flows where nonequilibrium effects are important, the similitude has been given by Inger[34], but too few solutions have been reported to evaluate effects of mismatches in the similitude parameters. The similitude found by Inger for a sharp cone is the same as for wedges, and similar flows correlate in terms of $\bar{x}_R$ for a dissociating diatomic gas when $M_\infty \sin \theta_c$ is constant. Spurk, Gerber, and Sedney[147] have reported two solutions by the method of characteristics for chemical relaxation of a 5 species air model (c.f., Sec. V). However, these two solutions were for different values of $M_\infty \sin \theta_c$ and, hence, cannot be compared in terms of Inger's similitude.

Sedney and Gerber[174] also calculated the vibrational relaxation for cones by the method of characteristics. Although they apparently have calculated flows ranging from $M_\infty = 6$, $\theta_c = 48°$ to $M_\infty = 15$, $\theta_c = 15°$, complete results were reported only for $M_\infty = 12$, $\theta_c = 46.39°$ in nitrogen, and partial results for $M_\infty = 15$, $\theta_c = 15.3°$. Lee[175] has analyzed vibrational nonequilibrium flows over slender bodies by applying a perturbation to the frozen flow behind the shock wave. He has compared his solution for a 20° cone at $M_\infty = 15$ in oxygen with an unpublished characteristics solution of Sedney and Gerber and obtained at least qualitative agreement.

2. Viscous Effects on Cones

At high Reynolds numbers where the boundary layer is thin compared to the distance between the cone and the bow shock, the boundary layer on the cone can be related to that on a wedge or flat plate by the Mangler transformation (Ref. 19, pg. 290) which accounts for the changing cross-sectional area of the cone. This introduces the factor of $\sqrt{3}$, so that the heat transfer, for example, is given by

$$St = \frac{q}{\rho_c U_c (H_{AW} - H_W)} = 0.332 \sqrt{3} \ Pr_W^{-2/3} \sqrt{(C/Re_x)_c} \qquad (VI-12)$$

where q is the heat transfer rate, Pr, the Prandtl Number, H the static enthalpy, the subscripts c, AW and W refer to the outer edge of the boundary layer on the cone, adiabatic wall and wall conditions, respectively. Since the variation of Prandtl number with temperature is small, Reynolds number remains as the primary similitude parameter.

When the boundary-layer thickness introduces appreciable displacement effects, perturbations of the outer inviscid flow must be considered. Probstein[176] has shown that for a slender cone the induced pressure changes are a function of the interaction parameter $\bar{\chi}_c = M_c^3 / \sqrt{(C/Re_x)_c}$ and the hypersonic similarity parameter $M_\infty \sin \theta_c$. Peter et al[177] have developed an empirical approach that gives very good agreement with the iterative scheme of Talbot et al[178] and with the experiments of King[179] at $M_\infty \simeq 4$. On the other hand, Waldron[66] has shown that Probstein's analysis gives good agreement with experiment at hypersonic Mach numbers.

However, the effect of boundary-layer displacement on heat-transfer rate is significantly less than that introduced by transverse curvature. This latter effect results from the circumferential spreading of the boundary layer due to the increasing cross section of the cone. Probstein and Elliot[180] have obtained solutions for this effect for an ideal gas and $Pr = 1$. The increase in heat transfer is a function of M_c, T_w/T_e, θ_c and $\sqrt{(C/Re_x)_c}$. Wittliff and Wilson[181] have shown that the heat transfer to a sharp, slender ($\theta_c = 5°$) cone at zero angle of attack is well predicted by theory when boundary-layer displacement and transverse curvature effects are taken into account for the range $11.3 \leq M_\infty \leq 13.0$ and $8.5 \times 10^4 \leq Re \leq 1.5 \times 10^6$. Waldron[66] has obtained comparable agreement at higher Mach numbers ($M_\infty \simeq 20$).

When the cone is nonslender and the Reynolds number is low, the analysis of Cheng[58] becomes applicable. In this regime, a rarefraction parameter

$$\bar{\mathcal{X}} = Re_{x_\infty} \Big/ \gamma M_\infty^2 \ C_* \ \cos\theta_c$$

$$\text{(VI-13)}$$

is introduced in addition to the interaction parameter $\bar{\chi}$. Waldron[66] has reported correlation of experimental heat-transfer measurements with Cheng's theory and found good agreement in the ideal gas regime.

Thus, it appears that for sharp cones in the ideal gas regime, the existing theories for both low and high Reynolds number flows are well substantiated and can be used to correlate tunnel and flight conditions. Some of the literature dealing with the more complex situation introduced by real gas and nonequilibrium phenomena has been discussed in Sec. IV.

D. BLUNTED SLENDER CONES

Because of the special interest in blunt-nosed slender cones as practical reentry vehicles, they have been the object of considerable study in recent years. As a result of facility limitations most of the experimental data for this configuration is restricted to the ideal gas regime. Theoretical analyses, on the other hand, have in some cases included real gas and nonequilibrium effects. Here, a full description of the ideal gas regime will be

given first and it will be shown that our knowledge of this flow is quite complete. In the real gas regime, the similitude is established, but there is a dearth of theoretical solutions or experimental results. Hence, the effects of mismatches in the similitude parameters cannot be evaluated.

As Flax[18] has pointed out, the blunt-nosed slender body is special in that it is neither very slender nor very blunt and, in addition, the part which is blunt is well separated from the part which is slender. On such bodies the local flow Mach number varies from subsonic in the nose region to supersonic along the slender body, making it difficult to formulate general similarity criteria. Blast-wave theory has been used to account for nose-bluntness effects on otherwise slender bodies. Lukasiewicz[182] has reviewed the basic theory and has presented an extensive correlation of exact flow-field calculations, as well as pertinent experimental data. He has shown that the important similitude parameter coming from blast-wave theory is $M_\infty^2 \sqrt{C_{D_N}}$ where C_{D_N} is the nose drag coefficient.* Cheng's analysis of hypersonic similitude for blunt-nosed slender bodies[33] in the case of a real gas in equilibrium also exhibits this parameter since he relied on blast-wave theory to account for nose bluntness. Cheng also has reported a comprehensive theoretical study of ideal gas hypersonic flow with combined leading-edge bluntness and boundary-layer displacement effects in which the slender blunted cone is treated for the special case of negligible boundary-layer displacement effect[183]. His analysis predicts a pressure distribution that is similar to that found by Chernyi (see Ref. 184, pg. 226).

Wittliff and Wilson[181] found qualitative agreement between heat transfer and shock-shape measurements and Cheng's theory. Lewis[185] compared pressure distributions and shock shapes with both Cheng's and Chernyi's theories and also found qualitative agreement. Burke and Curtis[186] have also compared pressure distributions with the theories of Cheng and Chernyi. There are a number of other papers correlating pressure distributions and shock shapes; however, the results reported in Refs. 181, 185, 186 are typical. Griffith and Lewis[61] have presented correlations of both

---

*During the present work it has been noted that if the blunt nose has a point (e. g., a large angle conical nose) the nose drag coefficient can be expressed as $C_{D_N} = \frac{0.5}{L/d}$, accurate to within 10%. This also gives similar accuracy for a hemispherical nose. For a flat nose, $C_{D_N} = 1.88$.

pressure and laminar heat-transfer distributions in terms of Cheng's param-
eters (see Sec. IV-B-3). They found that for the heat-transfer distribution,
a modification of Cheng's parameter to account for the fact that the cone
surface pressure is not always much larger than the free-stream static
pressure made a significant improvement. They found further that Lees'
local-similarity theory for heat transfer[59] was in good agreement with the
experimental data. On the basis of these comparisons, it is concluded that
for spherically blunted slender cones at $M_\infty \geq 10$ when real gas effects are
negligible, the pressure distribution correlates as $C_p / 2\theta_c^2 = fcn \left(\dfrac{\theta_c^2}{\gamma \epsilon C_{D_N}} \dfrac{x}{d_N} \right)$
where the θ_c is the cone half-angle in radians, $\epsilon = (\gamma-1)/(\gamma+1)$, C_{D_N}
is the nose drag coefficient, and d_N is the nose diameter. Thus, the C_p
distribution is independent of M_∞. Furthermore, the heat-transfer distri-
bution is given with about $\pm 10\%$ accuracy by

$$\frac{q_w}{q_0} = 0.80 \left(C_p + \frac{2}{\gamma M_\infty^2} \right)$$

(VI-14)

for $0.05 \leq (x/d_N) \theta_c^2 / \gamma \epsilon C_{D_N} \leq 0.60$ where q_w is the local heat-
transfer rate and q_0 is the stagnation-point heat-transfer rate (see Sec. IV
or VIII). Hence, at zero angle of attack the pressure and heat-transfer
distributions are well established in the ideal gas regime.

In this same regime there is also good agreement between Newtonian
theory and experimental data for normal-force and pitching-moment coef-
ficients (e.g., see Ref. 187). Whitfield and Wolny[188] correlated measure-
ments of these coefficients for a Mach number range from 8 to 21.7 and
Reynolds number range (based on model length) from 9.4×10^4 to 3.1×10^6.
The cone half-angles varied from 6.3° to 20° and the nose bluntness ratio
(R_N / R_B) varied from 0 to 0.30. The normal-force coefficients were
correlated in terms of a parameter ζ given by

$$\zeta = \alpha \left(2 + \frac{\alpha}{\theta_c} \right) \left(1 - \xi^2 \right)$$

(VI-15)

where α is the angle of attack (in radians), θ_c is the cone half-angle
(in radians) and $\xi = R_N/R_B$. Edenfield[189] correlated additional data

obtained from both hotshot and shock tunnels with this parameter, and was in agreement with the results of Whitfield and Wolny[188]. Trimmer[190] has correlated normal-force and pitching-moment coefficients calculated by Newtonian theory and also finds substantial agreement with experimental correlation of Ref. 188. As a part of the present study, an empirical equation has been fitted to these correlations. Thus, normal-force coefficient may be represented by

$$C_N = 0.754 \, \ln(1+\zeta) + 0.030 \, \zeta \, (\zeta - 1) \qquad \text{(VI-16)}$$

for values of $\zeta \leq 5$.

Whitfield and Wolny[188], Edenfield[189], and Trimmer[190] also correlated the pitching-moment coefficients, obtaining the result

$$C_m = -0.513 \, C_N \, (\bar{x}/R_b) \qquad \text{(VI-17)}$$

where

$$\frac{\bar{x}}{R_b} = \frac{2}{3\theta_c}\left(\frac{1-\xi^3}{1-\xi^2}\right) - \xi\left(\frac{1-\theta_c}{\theta_c}\right)$$

and C_m is about the nose.

It is observed here that these relations are independent of both Mach number and Reynolds number. It should be noted, however, that Wilkinson and Harrington[191] found a Reynolds number effect on both C_N and C_m. For their test conditions, where the Reynolds number was in the range covered by Whitfield and Wolny[188], Wilkinson and Harrington's data agree with the above correlations for C_N and C_m[189]. On the other hand, they obtained data at lower Reynolds number ($\simeq 2 \times 10^4$) which fell about 20% higher than the normal force predicted by Eq. (VI-16). Their pitching-moment coefficients at this Reynolds number were about 50% lower than the empirical relation (Eq. VI-13) would predict. Thus, these empirical correlations must not be used outside the range of parameters quoted.

Edenfield[189] has correlated axial-force coefficients in terms of the viscous parameter $\bar{V}_\infty = M_\infty \sqrt{(C/Re_L)_\infty}$, where $C_\infty = (\mu_w/\mu_\infty)(T_\infty/T_w)$, for a 9° half-angle cone with $R_N/R_b = 0.03$ and 0.3. As part of this

90

present study, these data have been cross-plotted as a function of angle of attack for $\overline{V}_\infty$ = constant. It has been found that for the case $\xi = R_N/R_B = 0.30$ the axial-force coefficients can be expressed (with ±5% accuracy) as

$$C_A = C_{A_{\alpha=0}}\, e^{1.39\alpha} \qquad \text{for} \qquad 0 \leq \overline{V}_\infty \leq 0.06 \qquad \text{(VI-18)}$$

where

$$C_{A_{\alpha=0}} = 0.130 + 1.12\,\overline{V}_\infty + 2.81\,\overline{V}_\infty^{\,2}$$

Hence, the angle of attack effect on axial force for this nose bluntness is primarily an inviscid phenomenon.

For the case ξ = 0.03, the angle of attack effects show a definite dependence on $\overline{V}_\infty$. Again, by cross-plotting, we have found that, to within ±5% accuracy, the results can be represented by

$$C_A = C_{A_{\alpha=0}}\, e^{0.350\alpha/\sqrt{\overline{V}_\infty}}$$

$$\text{(VI-19)}$$

Thus, for slightly blunted cones (ξ = 0.03) it is found that the angle of attack effect on axial force coefficient involves viscous phenomena whereas for blunter cones (ξ = 0.3) the effect is essentially inviscid. There does not exist sufficient data at present to delineate the dependence in terms of nose bluntness ratio.

The expression cited above for $C_{A_{\alpha=0}}$ results from Ref. 63 wherein Whitfield and Griffith investigated the contributions of inviscid-flow pressure, skin friction, boundary-layer displacement effect and transverse curvature effect on the drag of blunted slender cones. The constants in this expression hold only for a particular flow condition (ξ = 0.3, θ_c = 9°, M_∞ = 19, T_w/T_0 = 0.1, nitrogen test gas); hence, this equation must not be used indiscriminately.

Other papers on viscous effects on blunted slender cones have been cited in Section IV-B. Mention should be made here of the free-flight range experiments of Lyons et al[192], who found that for a slightly blunted

$(R_N / R_B = 0.035)$, slender $(\theta_c = 8°)$ cone, the drag coefficients are linear functions of the mean squared angle of attack for constant values of flight Mach number and Reynolds number. The slope of these lines remains constant for different flight conditions and the lines are simply translated to give different values of $C_{D_{\alpha=0}}$. Using the analysis of Wilson[193] to evaluate a mean viscous interaction parameter $\bar{\chi}_M$, Lyons, et al, also found that for a fixed flight Mach number, the values of $C_{D_{\alpha=0}}$ can be correlated in terms of $\bar{\chi}_M$. They found that $C_{D_{\alpha=0}}$ also correlates about as well with the viscous parameter $\bar{V}_\infty$.

A final comment with regard to the expressions reported here for C_N, C_m and C_A is worthwhile. Whitfield and Griffith[63] noted that their theory accurately predicted $(L/D)_{max}$ (the maximum lift-drag ratio) for $R_N / R_B = 0.03$ and $\theta_c = 9°$ as a function of $\bar{V}_\infty$ using the aforementioned empirical relation for C_N; however, their theory overpredicted $(L/D)_{max}$ for $R_N / R_B = 0.30$ and $\theta_c = 9°$. They have also plotted L/D as a function of angle of attack, comparing hotshot tunnel data at $M_\infty = 20$ and $R_N / R_B = 0.30$ with their simplified theory. They note that their theory overpredicts L/D at all angles of attack. If the relation $C_A = C_{A_{\alpha=0}} e^{1.39\alpha}$ and the cited empirical expression for $C_N = fcn(\zeta)$ (Eq. VI-16) are used to compute L/D for various angles of attack, the experimental points are reproduced accurately. This, of course, is to be expected since both expressions for C_N and C_A are known to be good empirical representations of the data.

Finally, we conclude from the brief résumé presented here that flow conditions, forces, etc. on blunted slender cones are well predicted by existing theoretical or empirical equations for the ideal-gas regime.

The question of when real gas effects become important is not a simple one to answer for the blunted slender cone. On the basis of our earlier comments one expects real gas effects in the nose region at $M_\infty > 4$ when $T_\infty \simeq 300°K$. On the other hand, the afterbody flow along the cone will not experience real gas effects until $M_\infty \sin\theta_c > 3$ (i.e., $M_\infty > 10$) when $T_\infty \simeq 300°K$.

Thus, it is necessary to have a detailed analysis of the flow field in order to determine when real gas effects become important and, further, to evaluate the effect of not duplicating the free-stream conditions. A comparison of ideal gas and real gas flows for blunted cones can be accomplished utilizing the calculations in Refs. 194 and 195 for an ideal gas and Ref. 196 for equilibrium real air. The only comparison that can be readily made from these results is pressure distribution which is a poor parameter for determining the importance of real gas effects. It would be more significant to compare temperature distributions; however, this involves considerable effort and has not been done. In addition, the solutions presented in Ref. 196 for real air are not sufficient for establishing the sensitivity of the various flow parameters to variations in free-stream conditions.

In spite of our inability to evaluate the effects of not duplicating free-stream conditions, Cheng's similitude can be utilized to qualitatively relate flight and wind-tunnel tests. As indicated in Sec. III, Cheng's similitude requires that the hypersonic similarity parameter $M_\infty \tau$ and the bluntness parameter $K_N = M_\infty^2 \sqrt{C_{D_N}} (d_N/L)$ be duplicated in addition to the free-stream conditions. If density-altitude and free-stream velocity are duplicated, but not T_∞ and p_∞, the tunnel and flight conditions are related as follows: if $\rho_{\infty_T} = \rho_{\infty_F}$ and $U_{\infty_T} = U_{\infty_F}$, then $M_\infty \tau = $ constant requires that $M_{\infty_T} = \beta M_{\infty_F}$ where $\beta \simeq \sqrt{T_{\infty_F}/T_{\infty_T}} < 1$ and, hence, $\tau_T = \frac{1}{\beta} \tau_F$ with the restriction $\tau_T << 1$. For a given β, this fixes the maximum value of τ_F that can be simulated. From $K_N = $ constant comes the requirement $(d_N/L)_T = \frac{1}{\beta^2}(d_N/L)_F$, and if $L_T = \lambda L_F$, we have $d_{N_T} = \frac{\lambda}{\beta^2} d_{N_F}$. Under these conditions neither flow transit times nor Reynolds number will be duplicated. Duplication of the flow transit time requires $L/U_\infty = $ constant and, hence, implies $L_T = L_F$ if $U_{\infty_T} = U_{\infty_F}$. The resulting differences in Reynolds number are given in Table I of Sec. II for the lower boundary of the flight regime being considered here. Nonduplication of T_∞, of course, violates one of the restrictions of Cheng's similitude and should be investigated. In Sec. VIII, the effect of $T_{\infty_T} > T_{\infty_F}$ on the blunt-nose flow is evaluated along the lower boundary of the flight envelope. It is shown that the effect can amount to as much as 15% on stagnation-point heat transfer although the

inviscid-flow quantities are affected by, at most, 10%. The effect of $T_{\infty_T} > T_{\infty_F}$ on the flow along the cone has not been evaluated.

In the nonequilibrium-flow regime, two possible situations exist because of the assumed tunnel performance. Above the full-duplication line (Fig. 2) the free-stream conditions could be duplicated except for the matter of nozzle flow nonequilibrium. Throughout most of this regime the frozen enthalpy is small compared to the total enthalpy (Fig. 5) and the major effect is on the free-stream pressure, temperature and composition. Assuming that the effects on pressure and temperature are not large and that the effect on composition can be accounted for by Gibson's subtraction rule[50] (Sec. III), Inger's similitude for nonequilibrium flow of a diatomic gas[34] can be extended to air flows if α_∞ and $\bar{e}_{v_\infty}$ are duplicated for each of the components of air. The similitude is then the same as Cheng's except for the additional parameter L/U_∞. Inger points out that because only two arbitrary geometrical scaling factors (r and L) appear in the three basic similitude parameters $M_\infty r$, K_N and K_R or K_v, the simulation of nonequilibrium flows over blunt-nosed slender bodies abolishes any freedom in choosing the scale of the tunnel models. Nonduplication of Reynolds number is unavoidable.

Below the full duplication line (Fig. 2) there is no free-stream dissociation; however, the flight free-stream conditions cannot be duplicated because of tunnel limitations. Thus, the basic restrictions of the non-equilibrium similitude are violated although the similarity parameters $M_\infty r$, K_N and L/U_∞ can be duplicated. It is important, therefore, to investigate the effect of mismatch in, say, ρ_∞ or T_∞ on this similitude. Again, this cannot be done at present because of the lack of theoretical solutions or experimental data.

field at low speeds where real gas effects are small, and at high altitudes where the chemistry is likely to be frozen. Similarly, the equilibrium-equilibrium model will yield a reasonable approximation at high speeds and low altitudes. The range of application of the equilibrium-frozen model has been discussed by Whalen[199].

With the above remarks in mind, the formulation of the problem studied and the assumptions made thereof are then as follows:

(a) Throughout the present study it will be assumed that the proposed facility is capable of correct density-altitude duplication over the entire flight envelope, and effects of nonduplication of free-stream velocity and temperature on the afterbody flow quantities will be studied.

(b) Effects of any ambient dissociation present in the facility will not be considered in detail. However, estimates of the effect of ambient dissociation will be made.

(c) Molecular transport properties like viscosity, diffusion, and heat conduction will not be considered.

(d) The three idealized models of flow chemistry outlined above will be studied in detail. For all of these three models, the flow field will be particle-isentropic behind the leading-edge shock wave; that is, the entropy will be constant along each streamline behind the shock wave.

(e) Throughout the present analysis, only small deviations from the free-stream conditions will be considered. That is, the analysis will be essentially of a linearized nature, and squares and products of the deviations will be neglected as small compared to the deviations themselves.

(f) The analysis of the afterbody will be confined to the region close to the corner. In particular, the "blast wave" effects that will be present some distance downstream of the corner will not be considered.

VII.   A SPECIAL STUDY OF BLUNT-NOSED FLAT PLATES AND CYLINDERS

A.   FORMULATION OF THE PROBLEM

As we have seen in the preceding section, the similitude for equilibrium and nonequilibrium real gas flows over slender bodies requires duplication of the ambient free-stream thermodynamic state. However, at the high velocities associated with these flows, wind tunnel limitations prohibit such duplication over much of the flight regime of interest.   The effect of not duplicating p_∞ , T_∞ , etc. cannot be evaluated from existing theoretical solutions or experimental data.   Therefore, a special study of the flat plate and cylinder having wedge and conical noses, respectively, was undertaken. These body shapes are representative of a class of blunted, slender bodies where possible effects of incorrect simulation on the afterbody flow are of particular interest.

The simplicity of the wedge leading edge permits a variety of limiting cases of flow chemistry to be analyzed, from which the general importance of nonequilibrium effects for this class of bodies can be established.   The analysis for the conical-nosed cylinder is considerably more difficult even under the simplifying assumptions made here.   Therefore, only a preliminary analysis of this case has been possible.   Another important advantage of the class of bodies chosen is that the results obtained for the wedge-nosed flat plate and the conical-nosed cylinder can be easily extended to other two- and three-dimensional bodies by using the tangent-wedge and tangent-cone approximations[25, 184] or the more accurate shock expansion methods[25, 197, 198].

Because of the complicated physical-chemical nature of the flows past even the above simplified geometries,only certain limiting cases of flow chemistry are considered; namely, the case when the flow is frozen everywhere, the case when the flow is in equilibrium behind the leading-edge shock wave but is frozen through the afterbody expansion, and the case when the flow is in equilibrium everywhere.   Henceforth, these three flow models will be referred to as the frozen-frozen (f-f), equilibrium-frozen (e-f), and equilibrium-equilibrium (e-e) models, respectively.   The frozen-frozen model can be expected to be a reasonable approximation to the actual flow

(g) To avoid the difficulty of submerged subsonic regions, only cases with attached shock waves will be considered. In particular, the analysis will be carried out in detail for wedge half-angles of 20°, 30°, and 40°.

(h) It will be assumed that the rotational and vibrational degrees of freedom are in equilibrium at the local translational temperature.

B. ANALYSIS OF THE FROZEN-FROZEN MODEL

In this section, the effect of nonduplication of free-stream velocity and temperature on the afterbody flow variables of a wedge-nosed flat plate will be calculated by assuming that the flow behaves like a perfect gas with a constant specific heat ratio. The problem logically subdivides into two parts, namely, the effect of changes in the free-stream quantities on the forebody quantities and the effect of changes of the forebody quantities on the afterbody flow quantities. Accordingly, these two parts will be analyzed separately. Also, since the flow is assumed to behave like a perfect gas, the flow can be analyzed in terms of Mach number alone.

We first find the changes in the quantities behind an oblique shock wave with small changes in free-stream Mach number for a fixed flow deflection angle. For this purpose, it will, of course, be most convenient to express the oblique shock relations in terms of the free-stream Mach number and the flow deflection angle. However, no such explicit relation exists, and the analysis is carried out as follows.

The density ratio across an oblique shock wave is given by (see, for example, Ref. 128).

$$\frac{\rho_2}{\rho_1} = \frac{(\gamma+1) M_1^2 \sin^2 \sigma}{(\gamma-1) M_1^2 \sin^2 \sigma + 2} \qquad \text{(VII-1)}$$

where the shock angle σ is related to the flow deflection angle θ by the relation

$$M_1^2 \sin^2 \sigma - 1 = \frac{\gamma+1}{2} \frac{\sin \sigma \sin \theta}{\cos(\sigma - \theta)} M_1^2 \qquad \text{(VII-2)}$$

Here, the subscripts 1 and 2 denote the free-stream and forebody flow quantities, respectively.

From Eq. (VII-1), a change in the density behind the shock wave due to a change in free-stream Mach number is given by

$$\frac{\delta \rho_2}{\rho_2} = \frac{2 \, \delta M_1 / M_1}{1 + \frac{\gamma-1}{2} M_1^2 \sin^2 \sigma} + \frac{2 \cot \sigma \, \delta \sigma}{1 + \frac{\gamma-1}{2} M_1^2 \sin^2 \sigma} \qquad (VII\text{-}3)$$

where $\delta \sigma$ represents the change in the shock angle due to the change in free-stream Mach number, and it can be obtained from Eq. (VII-2) as

$$\delta \sigma = - \left[\frac{2 \sin \sigma \cos(\sigma - \theta)}{M_1^2 \sin^2 \sigma \cos(2\sigma - \theta) + \cos \theta} \right] \frac{\delta M_1}{M_1} \qquad (VII\text{-}4)$$

It should be emphasized here again that it has been assumed that the proposed facility is capable of density-altitude duplication throughout the flight regime of interest.

Equations (VII-3) and (VII-4) can be combined to give

$$\frac{\delta \rho_2}{\rho_2} = \frac{2 K \dfrac{\delta M_1}{M_1}}{1 + \frac{\gamma-1}{2} M_1^2 \sin^2 \sigma} \qquad (VII\text{-}5a)$$

where

$$K = \frac{(M_1^2 \sin^2 \sigma - 1) \cos(2\sigma - \theta)}{M_1^2 \sin^2 \sigma \cos(2\sigma - \theta) + \cos \theta} \qquad (VII\text{-}5b)$$

The effect of a change in free-stream Mach number on the other flow variables can be obtained in a similar manner, and one obtains

$$\frac{\delta p_2}{p_2} - \frac{\delta p_1}{p_1} = \frac{\frac{4\gamma}{\gamma+1} K M_1^2 \sin^2 \sigma}{1 + \frac{2\gamma}{\gamma+1}(M_1^2 \sin^2 \sigma - 1)} \frac{\delta M_1}{M_1} \qquad (VII\text{-}6)$$

$$\frac{\delta T_2}{T_2} - \frac{\delta T_1}{T_1} = \frac{2 K \left[\frac{\gamma-1}{\gamma+1} \right] \left[1 + \gamma M_1^4 \sin^4 \sigma \right]}{\left[1 + \frac{\gamma-1}{2} M_1^2 \sin^2 \sigma \right] \left[1 + \frac{2\gamma}{\gamma+1}(M_1^2 \sin^2 \sigma - 1) \right]} \frac{\delta M_1}{M_1} \qquad (VII\text{-}7)$$

and

$$\frac{\delta M_2}{M_2} - \frac{\delta U_1}{U_1} = \frac{2 \tan \sigma \sin \theta \; \frac{\delta M_1}{M_1}}{M_1^2 \sin^2 \sigma \cos(2\sigma - \theta) + \cos \theta} - \frac{1}{2} \frac{\delta T_2}{T_2} \qquad \text{(VII-8)}$$

where the second terms on the left-hand sides of Eqs. (VII-6) and (VII-7) are meaningful only when change in free-stream Mach number is caused by a change in free-stream temperature. Similarly, the second term on the left hand side of Eq. (VII-8) is meaningful only when a change in free-stream Mach number is caused by a change in free-stream velocity. Equations (VII-5) to (VII-8) can be expressed in terms of changes in free-stream velocity or temperature by using the relation $M_1^2 = U_1^2 / \gamma R T_1$. Therefore,

$$\frac{\delta M_1}{M_1} = \frac{\delta U_1}{U_1} \qquad \text{with } T_1 \text{ held constant}$$

and

$$\frac{\delta M_1}{M_1} = \frac{1}{2} \frac{\delta T_1}{T_1} \qquad \text{with } U_1 \text{ held constant}$$

Also, the equation of state, $p_1 = \rho_1 R T_1$ gives (for constant ρ_1)

$$\frac{\delta p_1}{p_1} = \frac{\delta T_1}{T_1}$$

The above equations can be combined with Eqs. (VII-5) to (VII-8) to obtain the sensitivity of any quantity on the forebody to changes in either the free-stream velocity or temperature. Thus, for example,

$$\frac{(\delta p_2 / p_2)}{(\delta U_1 / U_1)} = \frac{\frac{4\gamma}{\gamma+1} K M_1^2 \sin^2 \sigma}{\left[1 + \frac{2\gamma}{\gamma+1} \left(M_1^2 \sin^2 \sigma - 1 \right) \right]} \qquad \text{(VII-9)}$$

while

$$\frac{(\delta p_2 / p_2)}{(\delta T_1 / T_1)} = 1 - \frac{\frac{2\gamma}{\gamma+1} K M_1^2 \sin^2 \sigma}{\left[1 + \frac{2\gamma}{\gamma+1} \left(M_1^2 \sin^2 \sigma - 1 \right) \right]} \qquad \text{(VII-10)}$$

Similar expressions can also be written down for the sensitivity of the other flow variables on the forebody.

When the Mach number is large and the corner angle is small, we can let

$$\cos \theta \approx 1 \quad \text{and} \quad \cos (2\sigma - \theta) \approx 1$$

Then, the above equations correlate in terms of the normal shock Mach number $M_1 \sin \sigma$ or, equivalently, the hypersonic similarity parameter $M_1 \sin \theta$. It will be seen below that this correlation is still valid even when the above approximations are not strictly satisfied.

Also, in the limit of very large Mach numbers the above relations yield

$$\frac{(\delta \rho_2/\rho_2)}{(\delta U_1/U_1)} \longrightarrow 0; \quad \frac{(\delta T_2/T_2)}{(\delta U_1/U_1)} \longrightarrow 2; \quad \frac{(\delta p_2/p_2)}{(\delta U_1/U_1)} \longrightarrow 2; \quad \frac{(\delta M_2/M_2)}{(\delta U_1/U_1)} \longrightarrow 0 \qquad \text{(VII-11)}$$

and

$$\frac{(\delta \rho_2/\rho_2)}{(\delta T_1/T_1)} \longrightarrow 0; \quad \frac{(\delta T_2/T_2)}{(\delta T_1/T_1)} \longrightarrow 0; \quad \frac{(\delta p_2/p_2)}{(\delta T_1/T_1)} \longrightarrow 0;$$

$$\frac{(\delta M_2/M_2)}{(\delta T_1/T_1)} \longrightarrow 0 \qquad \text{(VII-12)}$$

Equations (VII-11) and (VII-12) are merely statements of the Mach number independence principle. Equation (VII-11) states that the density and Mach number behind an oblique shock are independent of free-stream velocity in the limit of large free-stream Mach numbers while Eq. (VII-12) states that all quantities behind an oblique shock are independent of free-stream temperature in the limit of large free-stream Mach numbers.

To assess the range of applicability of the hypersonic similarity law and the Mach number independence principle to oblique shock waves, the sensitivity of the forebody quantities are shown in Figs. 25 and 26 for wedge half-angles of 20°, 30°, and 40°. It will be assumed that a forebody quantity becomes Mach number independent (with respect to changes in free-stream temperature) when its variation is less than ten per cent of the variation of the free-stream temperature.

In Fig. 25, the sensitivity of the forebody pressure and density to changes in free-stream velocity are correlated in terms of the parameter $M_1 \sin \theta$. The three curves for flow deflection angles of 20°, 30°, and 40° are indistinguishable from one another beyond a value of $M_1 \sin \theta$ of about five. The sensitivity of the temperature is not shown in Fig. 25 since it can be inferred from the sensitivities of the pressure and density. In Fig. 26, the sensitivity of the forebody temperature and density to changes in free-stream temperature are correlated in terms of $M_1 \sin \theta$. Again, it can be seen that the density and temperature on the forebody become independent of the free-stream temperature at values of $M_1 \sin \theta$ of about five and seven, respectively.

It is also interesting to note that the effects of changes in free-stream temperature on the forebody density are never large in the range of flow deflection angles under consideration. Moreover, since for a flow deflection angle of forty degrees a value of $M_1 \sin \theta$ of five corresponds to a value M_1 of only about eight, the hypersonic similarity principle applies over the entire range of free-stream Mach numbers of interest. Therefore, the sensitivity curves for the lowest flow deflection angle are sufficient to compute the sensitivities at any other flow deflection angle in the range of free-stream conditions that are of interest here.

As mentioned previously, it can be seen that the hypersonic similarity principle is valid over a wider range of conditions than is implied by the assumptions made in its derivation. However, it should be noted that the flow is not Mach number independent over the entire region of interest. For example, it can be seen, from Fig. 25, that for a flow deflection angle of twenty degrees, the forebody density does not become independent of free-stream velocity until a Mach number of about twenty-four is reached.

We next consider the changes in afterbody flow quantities due to changes in forebody flow quantities. Since the whole flow is assumed to behave like a perfect gas with constant specific heat ratio, the only relevant forebody parameter that need be considered is the Mach number, M_2. The Mach numbers on the forebody and afterbody are related by the Prandtl-Meyer relation given by (see Ref. 40, for example),

$$\sqrt{\frac{\gamma+1}{\gamma-1}} \left[\tan^{-1} \sqrt{\frac{\gamma-1}{\gamma+1}\left(M_3^2-1\right)} - \tan^{-1}\sqrt{\frac{\gamma-1}{\gamma+1}\left(M_2^2-1\right)} \right]$$

$$\text{(VII-13)}$$

$$+ \tan^{-1}\sqrt{M_3^2-1} - \tan^{-1}\sqrt{M_2^2-1} = \theta$$

where the subscript 3 is used to denote the afterbody flow quantities. From Eq. (VII-13), one obtains

$$\frac{\delta M_3}{M_3} = \left(\frac{M_2^2-1}{M_3^2-1}\right)^{1/2} \frac{1+\frac{\gamma-1}{2}M_3^2}{1+\frac{\gamma-1}{2}M_2^2} \frac{\delta M_2}{M_2} \qquad \text{(VII-14)}$$

The sensitivity of the afterbody Mach number due to changes in free-stream Mach number can be obtained by introducing Eq. (VII-8) into Eq. (VII-14). The sensitivity of the other afterbody flow variables can also be obtained from Eq. (VII-14). For example, the afterbody temperature is related to the Mach number through the relation

$$\frac{T_{t3}}{T_3} = 1 + \frac{\gamma-1}{2} M_3^2$$

$$\text{(VII-15)}$$

where the subscript "t" denotes total quantities. Also, since the flow is isoenergetic $T_{t3} = T_{t2} = T_{t1}$ and

$$\frac{T_{t1}}{T_1} = 1 + \frac{\gamma-1}{2} M_1^2 \qquad \text{(VII-16)}$$

Therefore

$$\frac{T_3}{T_1} = \frac{1+\frac{\gamma-1}{2}M_1^2}{1+\frac{\gamma-1}{2}M_3^2} \qquad \text{(VII-17)}$$

from which one obtains

$$\frac{\delta T_3}{T_3} - \frac{\delta T_1}{T_1} = - \frac{(\gamma-1) M_3^2}{1 + \frac{\gamma-1}{2} M_3^2} \frac{\delta M_3}{M_3} + \frac{(\gamma-1) M_1^2}{1 + \frac{\gamma-1}{2} M_1^2} \frac{\delta M_1}{M_1}$$ (VII-18)

where the second term on the left-hand side is meaningful only when the change in free-stream Mach number is caused by a change in free-stream temperature. Thus, the sensitivity of the afterbody temperature to changes in free-stream velocity is

$$\frac{\delta T_3/T_3}{\delta U_1/U_1} = \frac{(\gamma-1) M_1^2}{1 + \frac{\gamma-1}{2} M_1^2} - \left(\frac{M_2^2-1}{M_3^2-1}\right)^{1/2} \frac{(\gamma-1) M_3^2}{1 + \frac{\gamma-1}{2} M_2^2} \frac{(\delta M_2/M_2)}{(\delta U_1/U_1)}$$ (VII-19)

where the quantity $(\delta M_2/M_2)/(\delta U_1/U_1)$ is given by Eq. (VII-8). Similarly, for the sensitivity to changes in free-stream temperature, one finds that

$$\frac{(\delta T_3/T_1)}{(\delta T_1/T_1)} = \frac{1}{1 + \frac{\gamma-1}{2} M_1^2} - \left(\frac{M_2^2-1}{M_3^2-1}\right)^{1/2} \frac{(\gamma-1) M_3^2}{1 + \frac{\gamma-1}{2} M_2^2} \frac{(\delta M_2/M_2)}{(\delta T_1/T_1)}$$ (VII-20)

When determining similar expressions for the sensitivity of the afterbody pressure, it should be borne in mind that the total pressure is not conserved across the bow shock wave. Thus

$$\frac{p_{t_3}}{p_3} = \left(1 + \frac{\gamma-1}{2} M_3^2\right)^{\frac{\gamma}{\gamma-1}}$$ (VII-21)

and since the afterbody expansion is isentropic, $p_{t_3} = p_{t_2}$. However,

$$\frac{p_{t_2}}{p_{t_1}} = \left[\frac{(\gamma+1) M_1^2 \sin^2 \sigma}{(\gamma-1) M_1^2 \sin^2 \sigma + 2}\right]^{\frac{\gamma}{\gamma-1}} \left[\frac{\gamma+1}{2\gamma M_1^2 \sin^2 \sigma - (\gamma-1)}\right]^{\frac{1}{\gamma-1}}$$ (VII-22)

103

Equations (VII-21) and (VII-22) yield

$$\frac{\delta p_3}{p_3} - \frac{\delta p_{t_2}}{p_{t_2}} = - \frac{\gamma M_3^2}{1 + \frac{\gamma-1}{2} M_3^2} \frac{\delta M_3}{M_3} \tag{VII-23}$$

and

$$\frac{\delta p_{t_2}}{p_{t_2}} - \frac{\delta p_{t_1}}{p_{t_1}} = - \frac{\frac{4\gamma}{\gamma+1}\left(M_1^2 \sin^2\sigma - 1\right)^2}{\left[1 + \frac{2\gamma}{\gamma+1}\left(M_1^2 \sin^2\sigma - 1\right)\right]\left[(\gamma-1)M_1^2 \sin^2\sigma + 2\right]} \frac{\delta M_1}{M_1} \tag{VII-24}$$

Also, since p_{t_1} is related to p_1 through the relation

$$\frac{p_{t_1}}{p_1} = \left(1 + \frac{\gamma-1}{2} M_1^2\right)^{\frac{\gamma}{\gamma-1}} \tag{VII-25}$$

one obtains

$$\frac{\delta p_{t_1}}{p_{t_1}} - \frac{\delta p_1}{p_1} = \frac{\gamma M_1^2}{1 + \frac{\gamma-1}{2} M_1^2} \frac{\delta M_1}{M_1} \tag{VII-26}$$

where the second term on the left-hand side is meaningful only when the change in free-stream Mach number is caused by a change in free-stream temperature. Equations (VII-14, 23-26) can be combined to yield

$$\frac{\left(\delta p_3/p_3\right)}{\left(\delta U_1/U_1\right)} = -\left(\frac{M_2^2-1}{M_3^2-1}\right)^{1/2} \frac{\gamma M_3^2}{1 + \frac{\gamma-1}{2} M_2^2} \frac{\left(\delta M_2/M_2\right)}{\left(\delta U_1/U_1\right)}$$

$$- \frac{\frac{2\gamma}{\gamma+1}\left(M_1^2 \sin^2\sigma - 1\right)^2}{\left[1 + \frac{2\gamma}{\gamma+1}\left(M_1^2 \sin^2\sigma - 1\right)\right]\left[1 + \frac{\gamma-1}{2} M_1^2 \sin^2\sigma\right]} + \frac{\gamma M_1^2}{1 + \frac{\gamma-1}{2} M_1^2} \tag{VII-27}$$

and

$$\frac{\delta p_3 / p_3}{\delta T_1 / T_1} = -\left(\frac{M_2^2 - 1}{M_3^2 - 1}\right)^{1/2} \frac{\gamma M_3^2}{1 + \frac{\gamma - 1}{2} M_2^2} \frac{(\delta M_2 / M_2)}{(\delta T_1 / T_1)}$$

$$+ \frac{\frac{\gamma}{\gamma + 1}\left(M_1^2 \sin^2 \sigma - 1\right)^2}{\left[1 + \frac{2\gamma}{\gamma + 1}\left(M_1^2 \sin^2 \sigma - 1\right)\right]\left[1 + \frac{\gamma - 1}{2} M_1^2 \sin^2 \sigma\right]} - \frac{\frac{1}{2} M_1^2 - 1}{1 + \frac{\gamma - 1}{2} M_1^2} \qquad \text{(VII-28)}$$

Expressions for the sensitivity of the other afterbody flow variables can be obtained from Eqs. (VII-19, 20, 27, 28). In particular, the sensitivity of the afterbody density and velocity can be obtained from the relations

$$\frac{\delta \rho_3}{\rho_3} = \frac{\delta p_3}{p_3} - \frac{\delta T_3}{T_3} \qquad \text{(VII-29)}$$

and

$$\frac{\delta U_3}{U_3} = \frac{\delta M_3}{M_3} + \frac{1}{2} \frac{\delta T_3}{T_3} \qquad \text{(VII-30)}$$

The above relations show that in the limit of large Mach numbers

$$\frac{(\delta \rho_3 / \rho_3)}{(\delta U_1 / U_1)} \rightarrow 0; \quad \frac{(\delta T_3 / T_3)}{(\delta U_1 / U_1)} \rightarrow 2; \quad \frac{(\delta p_3 / p_3)}{(\delta U_1 / U_1)} \rightarrow 2; \quad \frac{(\delta M_3 / M_3)}{(\delta U_1 / U_1)} \rightarrow 0$$

$$\text{(VII-31)}$$

and

$$\frac{(\delta \rho_3 / \rho_3)}{(\delta T_1 / T_1)} \rightarrow 0; \quad \frac{(\delta T_3 / T_3)}{(\delta T_1 / T_1)} \rightarrow 0; \quad \frac{(\delta p_3 / p_3)}{(\delta T_1 / T_1)} \rightarrow 0; \quad \frac{(\delta M_3 / M_3)}{(\delta T_1 / T_1)} \rightarrow 0 \quad \text{(VII-32)}$$

The sensitivity of the afterbody density, temperature, pressure, and Mach number to changes in free-stream velocity and temperature are shown in Figs. 27, 28, 29, 30, respectively. The calculated values for the three wedge half-angles of 20°, 30°, and 40° are shown correlated in terms of the parameter $M_1 \sin \theta$. Again, it can be seen that even for the relatively large angle of forty degrees, excellent correlation is obtained beyond a

value of five for $M_1 \sin \theta$. As mentioned earlier, since for an angle of forty degrees a value of five is equivalent to a free-stream Mach number of about eight, the hypersonic similarity law is valid over the entire free-stream velocity range of interest (10,000 to 36,000 fps). Here, as before, an afterbody quantity is assumed to be independent of changes in a free-stream quantity if the proportional change in the afterbody quantity is smaller than ten per cent of the changes in the free-stream quantity. It can be seen from the figures that the afterbody density and Mach numbers become independent of the free-stream velocity at values of $M_1 \sin \theta$ of about twelve and eight, respectively. The afterbody density, temperature, pressure, and Mach number become independent of the free-stream temperature at values of $M_1 \sin \theta$ of approximately eight, eight, ten, and six, respectively.

C. ANALYSIS OF THE EQUILIBRIUM-FROZEN MODEL

1. Formulation of the Model

In the present section we will determine the sensitivity of the afterbody quantities to changes in free-stream conditions using the equilibrium-frozen model. As in the analysis of the frozen-frozen model, the analysis of the equilibrium-frozen model is also carried out in two separate steps. First, the sensitivity of the forebody quantities to changes in free-stream conditions are determined, and then the sensitivity of the afterbody quantities to changes of forebody quantities are determined.

The first step is essentially that of determining the sensitivity of conditions behind an equilibrium oblique shock wave to changes in conditions ahead of it. In order to perform the calculations for this case, equilibrium oblique shock results are needed in the range of free-stream conditions of interest. The equilibrium oblique shock calculations of Feldman[144] are unsuitable for this purpose since the atmospheric model used by Feldman differs from the more recent 1959 ARDC Standard atmospheric model to be used here[*]. Moreover, Feldman has reported solutions for U_∞ of only up

---

[*] Although the 1962 U.S. Standard Atmosphere has been used throughout the rest of this study, the desire to utilize the results reported in Ref. 129 dictated adoption of the 1959 atmosphere for this section. This introduces no appreciable error in the results presented here.

to 26,000 fps. However, Wittliff and Curtis[129] have reported extensive equilibrium normal shock solutions for the 1959 ARDC Standard Atmosphere. As mention in Section V-E, these solutions can be used to obtain the equilibrium oblique shock parameters for arbitrary flow deflection angles by using the concept of "effective specific heat ratio" developed by Trimpi and Jones[146]. However, the procedure suggested by Trimpi and Jones involves a fairly lengthy calculation, and it has not been used in the present study. Instead, an approximate method has been developed by which results of Ref. 129 can be used to generate oblique shock results for arbitrary free-stream conditions.

Exact calculations[147] show that the pressure on a nonslender wedge in supersonic flow is relatively insensitive to nonequilibrium effects; that is, the frozen and equilibrium pressures are nearly equal. This property of nonslender wedge flows has been used as a basis for the present approximation. The calculation of equilibrium oblique shock wave parameters proceeds as follows: for a fixed wedge angle and any free-stream conditions, the pressure ratio across the appropriate frozen oblique shock wave is determined from perfect gas tables. It is then assumed that this pressure ratio is identical to the pressure ratio across the corresponding equilibrium oblique shock wave. The equilibrium normal shock Mach number for this pressure ratio can then be determined from Ref. 129. This immediately yields the equilibrium oblique shock angle, as well as the other flow variables behind the shock. The accuracy of the present approximation has been checked for a thirty-degree half-angle wedge, and it was found that the average error is about five per cent and the maximum error (which occurs at the highest altitude) is under ten per cent. Therefore, the above approximation has been adopted as a reasonable one throughout the present study.

In blunt-body flows, the enthalpy is relatively insensitive to nonequilibrium effects. This property of blunt-body nonequilibrium flows was also considered in the present case as a means of obtaining approximate values of the equilibrium oblique shock wave parameters. Several sample calculations were performed to assess the accuracy of the constant enthalpy assumption. It was found that the errors introduced by this approximation were uniformly larger than the errors introduced by the constant pressure

approximation. Therefore, the constant enthalpy approximation was not given any further consideration.

The values of the equilibrium oblique shock wave parameters calculated using the constant pressure approximation described above are shown in Figs. 31 to 34. These figures show the variation of the pressure ratio, shock-wave angle, density ratio and temperature ratio with free-stream velocity for a typical wedge angle of 30° and altitudes of 0 feet and 250,000 feet. For the sake of comparison, the results obtained by Feldman[144] are also shown in these figures. Since the atmospheric model used by Feldman and the 1959 ARDC atmospheric model are identical at sea level, Feldman's exact calculations at sea level conditions should also provide a check for the accuracy of the present approximation.

It can be seen from Figs. 31 to 34 that the sea level values calculated by the present approximations show very good agreement with Feldman's results. However, it can be seen that the present results differ considerably from Feldman's results at the higher altitude. This is to be expected because of the substantial differences in atmospheric models. In particular, at an altitude of 250,000 feet, the value of the speed of sound used by Feldman is considerably in excess of the value predicted by the 1959 ARDC atmosphere. Since the present approximation is equivalent to assuming that for a given wedge angle the pressure ratio is determined uniquely by the free-stream Mach number alone, the present results and Feldman's results for the pressure ratio should agree if they are compared at the same free-stream Mach number.

In Fig. 31, Feldman's results for the 250,000-ft altitude are shown normalized to the correct value of the speed of sound. It can be seen that the agreement between the present results and the normalized results is of the same order as the agreement at sea level. Also, note that the present results and Feldman's results predict almost identical qualitative behavior for all the equilibrium oblique shock wave parameters. It is also of interest to note that while, in general, the variations of the shock-wave parameters with velocity are monotonic at sea level, they are highly nonmonotonic at the higher altitude.

Since in the equilibrium-frozen model the afterbody expansion is supposed to occur with the chemistry frozen at its level on the forebody, the appropriate forebody parameters of interest are the frozen-flow specific heat ratio and the Mach number based on frozen speed of sound. Following Whalen[199], we will take the frozen-flow specific heat ratio to be

$$\gamma_2 = \frac{3\alpha_2 + 7}{\alpha_2 + 5}$$

(VII-33)

where α_2 is the mass fraction of the gas on the forebody that is dissociated. For air, α_2 is merely $(Z_2 - 1)$ where Z_2 is the compressibility factor. The frozen-flow Mach number is given by

$$M_2 = U_2 \Big/ \left(\frac{\gamma_2 \, p_2}{\rho_2} \right)^{1/2}$$

(VII-34)

The frozen-flow Mach number and specific heat ratio on the forebody are shown plotted in Figs. 35 and 36 for a flow-deflection angle of thirty degrees. In Fig. 35, the corresponding perfect-gas Mach number is also shown for the sake of comparison. It can be seen that for an equilibrium shock wave the frozen-flow Mach number on the forebody is always higher than the corresponding perfect-gas value.

The calculations described above for a flow deflection angle of thirty degrees were also repeated for flow deflection angles of twenty and forty degrees. It has been pointed out by Cheng[33] that for real gas flows in equilibrium, the hypersonic similarity law will apply for a fixed altitude. Therefore, the results calculated above were correlated in terms of the parameter $U_1 \sin \theta$ at each altitude. A typical correlation of some calculated values of the density ratio across the shock wave are shown in Fig. 37. It can be seen that at both the 0-ft and 250,000-ft altitudes, excellent correlation is obtained between the three sets of calculated values for the entire free-stream velocity range of interest (that is, between ten and thirty-six thousand feet per second). The scatter of the points about the mean curve is well within the accuracy of the constant pressure approximation itself. Therefore, at each altitude, a single curve will suffice to

describe the variation of the density on the forebody for all flow deflection angles between twenty and forty degrees.

It should be pointed out here that while the hypersonic similarity principle is itself certainly valid for angles smaller than twenty degrees, the constant pressure approximation is not. Therefore, results obtained by using the constant pressure approximation cannot be extrapolated to smaller values of the flow deflection angle. As in the frozen-flow case, it can be seen that for equilibrium flow, also, the hypersonic similarity principle is valid for much larger angles than would be implied by the assumptions made in its derivation.

2. Sensitivity of Changes in Free-Stream Velocity

The results obtained above can be used to determine the sensitivity of the forebody quantities to changes in free-stream conditions. The continuity and momentum equations for this case are

$$\rho_1 U_1 \sin \sigma = \rho_2 U_2 \sin (\sigma - \theta) \tag{VII-35}$$

$$U_1 \cos \sigma = U_2 \cos (\sigma - \theta) \tag{VII-36}$$

$$p_1 + \rho_1 U_1^2 \sin^2 \sigma = p_2 + \rho_2 U_2^2 \sin^2 (\sigma - \theta) \tag{VII-37}$$

Thus, for a small change δU_1 in U_1, one obtains

$$\frac{\delta U_1}{U_1} + \cot \sigma \, \delta \sigma = \frac{\delta \rho_2}{\rho_2} + \frac{\delta U_2}{U_2} + \cot (\sigma - \theta) \, \delta \sigma \tag{VII-38}$$

$$\frac{\delta U_1}{U_1} - \tan \sigma \, \delta \sigma = \frac{\delta U_2}{U_2} - \tan (\sigma - \theta) \, \delta \sigma \tag{VII-39}$$

$$2 \, \frac{\tan \sigma}{\tan (\sigma - \theta)} \, \frac{\delta U_1}{U_1} = \frac{p_2}{\rho_2 U_2^2 \sin^2 (\sigma - \theta)} \frac{\delta p_2}{p_2} + 2 \frac{\delta U_2}{U_2} + \frac{\delta \rho_2}{\rho_2} \tag{VII-40}$$

where $\delta\sigma$ is the change in the equilibrium oblique shock-wave angle due to the change δU_1 and so on. Since we have assumed that the pressure is insensitive to nonequilibrium effects, the value ($\delta p_2 / p_2$) in Eq. (VII-40) can be replaced by the value given in Eq. (VII-9). Then, to the accuracy of the present approximation, one obtains from Eqs. (VII-38), (VII-39), (VII-40), and (VII-9)

$$\frac{\delta U_2 / U_2}{\delta U_1 / U_1} = \left[\left(2 + \frac{1}{\tan^2 \sigma_e} - \frac{4K}{\gamma+1} \frac{\sin^2 \sigma_f}{\sin^2 \sigma_e}\right) \frac{\rho_2}{\rho_1} - 1\right] \Bigg/ \left[\frac{\rho_2 / \rho_1}{\tan^2 \sigma_e} + 1\right] \qquad \text{(VII-41)}$$

where σ_f and σ_e are the frozen and equilibrium shock-wave angles, respectively.

The sensitivity of the forebody density to changes in free-stream velocity can be obtained from the relation

$$\frac{\delta \rho_2}{\rho_2} = \left[\frac{\rho_2 / \rho_1}{\tan^2 \sigma_e} - 1\right]\left[\frac{\delta U_2}{U_2} - \frac{\delta U_1}{U_1}\right]$$

and one obtains

$$\frac{\delta \rho_2 / \rho_2}{\delta U_1 / U_1} = 2 \left[\frac{\rho_2}{\rho_1}\left(1 - \frac{2K}{\gamma+1} \frac{\sin^2 \sigma_f}{\sin^2 \sigma_e}\right) - 1\right] \frac{\left(\frac{\rho_2 / \rho_1}{\tan^2 \sigma_e} - 1\right)}{\left(\frac{\rho_2 / \rho_1}{\tan^2 \sigma_e} + 1\right)} \qquad \text{(VII-42)}$$

Unfortunately, similar analytical expressions for the sensitivity of the forebody temperature or the dissociation fraction cannot be obtained since the law of mass action for air cannot be written down explicitly in simple terms. The sensitivities of these quantities can only be obtained in an implicit form. Since there are only two independent state variables in an equilibrium flow, one can write

$$\alpha_2 = \alpha_2 \left(p_2, \rho_2\right)$$

so that

$$\delta \alpha_2 = \left(\frac{\partial \alpha}{\partial p}\right)_{\rho,e} \delta p_2 + \left(\frac{\partial \alpha}{\partial \rho}\right)_{p,e} \delta \rho_2 \qquad \text{(VII-43)}$$

In Eq. (VII-43), the quantities $\left(\frac{\partial \alpha}{\partial p}\right)_{\rho,e}$ and $\left(\frac{\partial \alpha}{\partial \rho}\right)_{p,e}$ have to be obtained from a Mollier diagram. The subscript e has been added to the above quantities to indicate that they have to be evaluated under equilibrium conditions. Therefore, one can write

$$\frac{\delta \alpha_2}{\delta U_1/U_1} = p_2 \left(\frac{\partial \alpha}{\partial p}\right)_{\rho,e} \frac{\delta p_2/p_2}{\delta U_1/U_1} + \rho_2 \left(\frac{\partial \alpha}{\partial \rho}\right)_{p,e} \frac{\delta \rho_2/\rho_2}{\delta U_1/U_1} \qquad \text{(VII-44)}$$

where the sensitivities of the forebody pressure and density have to be evaluated from Eqs. (VII-9 and 42), respectively.

The sensitivities derived above can be related to the sensitivity of the forebody temperature by using the equation of state which gives

$$p_2 = \rho_2 R T_2 \left(1 + \alpha_2\right)$$

Therefore

$$\frac{\delta T_2/T_2}{\delta U_1/U_1} = \frac{\delta p_2/p_2}{\delta U_1/U_1} - \frac{\delta \rho_2/\rho_2}{\delta U_1/U_1} - \frac{1}{1+\alpha_2} \frac{\delta \alpha_2}{\delta U_1/U_1} \qquad \text{(VII-45)}$$

Similarly, from Eq. (VII-33), the sensitivity of the frozen-flow specific heat ratio can be expressed as

$$\frac{\delta \gamma_2}{\delta U_1/U_1} = \frac{8}{(\alpha_2 + 5)^2} \frac{\delta \alpha_2}{\delta U_1/U_1} \qquad \text{(VII-46)}$$

where the right-hand side can be evaluated from Eq. (VII-44).

The sensitivity of the forebody temperature to changes in free-stream velocity can also be obtained by numerically differencing its value calculated above. However, since the accuracy of any approximation is

112

worsened by differentiation, this procedure is, in general, not advisable.

The sensitivity of the frozen-flow Mach number is given from Eq. (VII-34) as

$$\frac{\delta M_2}{M_2} = \frac{\delta U_2}{U_2} - \frac{1}{2}\left[\frac{\delta p_2}{p_2} - \frac{\delta \rho_2}{\rho_2} + \frac{\delta \gamma_2}{\gamma_2}\right] \qquad \text{(VII-47)}$$

The only quantity in the right-hand side of Eq. (VII-47) that cannot be expressed explicitly in an analytical form is the sensitivity of the frozen-flow specific heat ratio, $\delta \gamma_2$, and it has to be obtained from Eq. (VII-46) or by numerically differencing its value. It should be noted that, in general, $\delta \gamma_2$ is small except at high altitudes and high velocities. Therefore, even if a value of $\delta \gamma_2$ obtained by numerical differencing were used in Eq. (VII-47), the errors will be less than the errors involved if the sensitivity of the Mach number were computed directly by numerically differencing the values of the Mach number itself.

Combining Eqs. (VII-9, 41, 42, and 47), one obtains

$$\frac{\delta M_2/M_2}{\delta U_1/U_1} = \frac{\rho_2}{\rho_1}\left[1 - \frac{2K}{\gamma+1}\frac{\sin^2\sigma_f}{\sin^2\sigma_e}\right]$$

$$-\frac{\frac{2\gamma}{\gamma+1}KM_1^2\sin^2\sigma_f}{1+\frac{2\gamma}{\gamma+1}\left(M_1^2\sin^2\sigma_f-1\right)} - \frac{1}{2}\frac{\delta\gamma_2/\gamma_2}{\delta U_1/U_1} \qquad \text{(VII-48)}$$

where the last term has to be obtained from Eq. (VII-46). In the limit of large Mach numbers (or more precisely when $M_1 \sin\sigma_f \gg 1$), $K \rightarrow 1$, the above expression reduces to

$$\frac{\delta M_2/M_2}{\delta U_1/U_1} = \frac{\rho_2}{\rho_1}\left[1 - \frac{2}{\gamma+1}\frac{\sin^2\sigma_f}{\sin^2\sigma_e}\right] - 1 - \frac{1}{2}\frac{\delta\gamma_2/\gamma_2}{\delta U_1/U_1} \qquad \text{(VII-49)}$$

When the shock layer is in equilibrium, it can be seen from Eq. (VII-49) that the forebody Mach number does not become independent of the free-stream velocity in the range of free-stream velocities under consideration since in this range the density ratio across the shock wave continues to increase (see Fig. 37, for example). However, when the shock layer is frozen, $\delta \gamma_2 \equiv 0$, $\sigma_e \cong \sigma_f$ and $\dfrac{\rho_2}{\rho_1} \rightarrow \dfrac{\gamma+1}{\gamma-1}$. Therefore, Eq. (VII-49) shows that in the limit of large Mach numbers, the forebody Mach number becomes independent of the free-stream velocity. This, of course, is merely a statement of the Mach number independence principle for a perfect gas and is identical to the result derived in the last section.

3. Sensitivity to Changes in Free-Stream Temperature

Expressions similar to those derived above can also be derived for the sensitivity of the forebody quantities to changes in free-stream temperature. For example, Eqs. (VII-35) -(VII-37) yield

$$\frac{\delta \rho_2}{\rho_2} + \frac{\delta U_2}{U_2} = \left[-\cot (\sigma - \theta) + \cot \sigma \right] \delta \sigma \tag{VII-50}$$

$$\frac{\delta U_2}{U_2} = \left[\tan(\sigma - \theta) - \tan \sigma \right] \delta \sigma \tag{VII-51}$$

and $\dfrac{\delta T_1}{T_1} = \dfrac{\delta p_2}{p_2} \dfrac{p_2}{p_1} + \left(\dfrac{\delta \rho_2}{\rho_2} + 2 \dfrac{\delta U_2}{U_2} \right) \left(\dfrac{\rho_1}{\rho_2} \right) \gamma M_1^2 \sin^2 \sigma$ (VII-52)

In the last of the above equations, the sensitivity of the pressure can be evaluated from Eq. (VII-10). Then, one obtains

$$\frac{\delta U_2/U_2}{\delta T_1/T_1} = -\frac{\rho_2}{\rho_1} \frac{(1-K) M_1^2 \sin^2 \sigma_f - 1}{\frac{\gamma+1}{2} M_1^2 \sin^2 \sigma_e} \bigg/ \left[\frac{\rho_2/\rho_1}{\tan^2 \sigma_e} + 1 \right] \tag{VII-53}$$

where, as before, the subscripts e and f have been used on the shock angle σ to distinguish between the equilibrium and frozen values.

The sensitivity of the density is given by

$$\frac{\delta \rho_2/\rho_2}{\delta T_1/T_1} = - \frac{\rho_2}{\rho_1} \frac{(1-K)M_1^2 \sin^2 \sigma_f - 1}{\frac{\gamma+1}{2} M_1^2 \sin^2 \sigma_e} \frac{\left(\frac{\rho_2/\rho_1}{\tan^2 \sigma_e} - 1\right)}{\left(\frac{\rho_2/\rho_1}{\tan^2 \sigma_e} + 1\right)} \qquad (VII-54)$$

The sensitivity of the forebody dissociation fraction is given by Eq. (VII-43) as

$$\frac{\delta \alpha_2}{\delta T_1/T_1} = p_2 \left(\frac{\partial \alpha}{\partial p}\right)_{\rho,e} \frac{\delta p_2/p_2}{\delta T_1/T_1} + \rho_2 \left(\frac{\partial \alpha}{\partial \rho}\right)_{p,e} \frac{\delta \rho_2/\rho_2}{\delta T_1/T_1} \qquad (VII-55)$$

The sensitivity of the frozen-flow specific heat ratio is related to the sensitivity of the dissociation fraction through a relation analogous to Eq. (VII-46). The sensitivities of the temperature and frozen-flow Mach number are

$$\frac{\delta T_2/T_2}{\delta T_1/T_1} = \frac{\delta p_2/p_2}{\delta T_1/T_1} - \frac{\delta \rho_2/\rho_2}{\delta T_1/T_1} - \frac{1}{1+\alpha_2} \frac{\delta \alpha_2}{\delta T_1/T_1} \qquad (VII-56)$$

and
$$\frac{\delta M_2/M_2}{\delta T_1/T_1} = -\frac{1}{2}\left[1 + \frac{\delta \gamma_2/\gamma_2}{\delta T_1/T_1} + \frac{\rho_2}{\rho_1} \frac{(1-K)M_1^2 \sin^2 \sigma_f - 1}{\frac{\gamma+1}{2}M_1^2 \sin^2 \sigma_e}\right.$$
$$\left. - \frac{K M_1^2 \sin^2 \sigma_f}{M_1^2 \sin^2 \sigma_f - \frac{\gamma-1}{2\gamma}}\right] \qquad (VII-57)$$

When $M_1 \sin \sigma_f \gg 1$, Eq. (VII-57) reduces to

$$\frac{\delta M_2/M_2}{\delta T_1/T_1} \approx \frac{1}{2}\left[\frac{\delta \gamma_2/\gamma_2}{\delta T_1/T_1} + \frac{1}{M_1^2} \frac{\cos \theta}{\cos(2\sigma_f - \theta)} \frac{(\rho_2/\rho_1)}{\frac{\gamma+1}{2} \sin^2 \sigma_e}\right] \qquad (VII-58)$$

Equation (VII-58) shows that when the free-stream density and velocity are kept constant, the afterbody Mach number becomes independent of free-stream temperature, which is, of course, in accordance with the Mach number independence principle.

115

It should be noted that while the sensitivity of the forebody quantities to changes in free-stream velocity can also be determined by numerically differencing their values, a similar procedure is not possible for determining the sensitivity to changes in free-stream temperature, since numerical values for variation of the forebody quantities with temperature (for fixed values of density and velocity) are not available. These sensitivities can only be determined from Eqs. (VII-53) to (VII-58).

The sensitivity of the forebody density, temperature, frozen Mach number, and frozen specific heat ratio are shown in Figs. 38-41, respectively. As before, the sensitivities are shown correlated in terms of $U_1 \sin \theta$ for a fixed altitude. Some of the calculated points are shown in Figs. 38 and 39 to display the quality of the correlation. It can be seen from the figures that the derivations of the points from the mean curves are, in general, less than five per cent over the entire range of free-stream velocities of interest. The same quality of correlation is also obtained for the specific heat ratio. Therefore, in Fig. 41 only the mean curves at each altitude are shown. Not unexpectedly, the sensitivity of the Mach number shows a systematic dependence on the angle, especially at larger angles. However, the deviations from the mean curves shown in Fig. 40 are still within the present limits of accuracy.

We next consider the sensitivity of the afterbody quantities to changes in forebody quantities for the e-f model. This case is somewhat different from the f-f model considered above even though in both cases the afterbody expansion is assumed frozen. In the present case, the frozen-flow Mach number, as well as the frozen-flow specific heat ratio, on the forebody change. Therefore, both of these are relevant variables and have to be considered separately. Also, in the present case, the total temperature is not conserved since part of the thermal energy is frozen out of the fluid flow as dissociational (and vibrational) energy. This fact will also influence the sensitivity of the afterbody flow quantities. The remarks made above are, of course, also applicable to the total pressure.

From the Prandtl-Meyer relation, Eq. (VII-13), one can write

$$\frac{\delta M_3}{M_3} = f_{1M} \frac{\delta M_2}{M_2} + f_{2M} \delta \gamma_2 \qquad \text{(VII-59)}$$

where

$$f_{1M} = \frac{1 + \frac{\gamma_2 - 1}{2} M_3^2}{1 + \frac{\gamma_2 - 1}{2} M_2^2} \left(\frac{M_2^2 - 1}{M_3^2 - 1}\right)^{1/2}$$

(VII-60)

and

$$f_{2M} = \frac{\theta + \tan^{-1}\sqrt{M_3^2 - 1} - \tan^{-1}\sqrt{M_2^2 - 1}}{(\gamma_2 + 1)(\gamma_2 - 1)} \cdot \frac{1 + \frac{\gamma_2 - 1}{2} M_3^2}{(M_3^2 - 1)^{1/2}}$$

$$+ \frac{2}{\gamma - 1}\left[\left(\frac{M_2^2 - 1}{M_3^2 - 1}\right)^{1/2} \frac{1 + \frac{\gamma - 1}{2} M_3^2}{1 + \frac{\gamma - 1}{2} M_2^2} - 1\right]$$

(VII-61)

The influence coefficient f_{1M} is, of course, identical in form to the influence coefficient derived for the frozen-frozen model.

The influence coefficients f_{1M} and f_{2M} are shown plotted in Figs. 42 and 43 for corner angles of 10°, 20°, 30°, and 40°, and for specific heat ratios of 1.4 and 1.67. Note that the functions f_{1M} and f_{2M} are always of the same sign. Thus, an increase in either the forebody Mach number or specific heat ratio will tend to increase the sensitivity of the afterbody Mach number. Since in the $e-f$ model both the frozen-flow Mach number and the frozen-flow specific heat ratio on the forebody will be higher than the corresponding values for the $f-f$ model, the sensitivity of the afterbody Mach number can be expected to be higher for the $e-f$ model than for the $f-f$ model. Finally, the sensitivity of the afterbody Mach number to changes in free-stream velocity can be written as

$$\frac{\delta M_3/M_3}{\delta U_1/U_1} = f_{1M} \frac{\delta M_2/M_2}{\delta U_1/U_1} + f_{2M} \frac{\delta \gamma_2}{\delta U_1/U_1}$$

(VII-62)

where the first term in the right-hand side has to be evaluated from Eq. (VII-48), and the second term has to be obtained from Eq. (VII-46).

From the Prandtl-Meyer relation and the isentropic relation,

$$\frac{p}{p_t} = \left(1 + \frac{\gamma-1}{2} M^2\right)^{-\frac{\gamma}{\gamma-1}} \tag{VII-63}$$

one obtains for the sensitivity of the afterbody pressure the expression

$$\frac{\delta p_3}{p_3} = f_{1p} \frac{\delta M_2}{M_2} + f_{2p} \delta \gamma_2 + \frac{\delta p_{t_2}}{p_{t_2}} \tag{VII-64}$$

where

$$f_{1p} = \frac{\gamma_2 M_3^2}{1 + \frac{\gamma-1}{2} M_2^2} \left(\frac{M_2^2 - 1}{M_3^2 - 1}\right)^{1/2} \tag{VII-65}$$

and

$$f_{2p} = \frac{1}{(\gamma_2 - 1)^2} \ln\left(1 + \frac{\gamma_2 - 1}{2} M_3^2\right) - \frac{\gamma_2}{\gamma_2 - 1} \frac{0.5 M_3^2}{1 + \frac{\gamma_2 - 1}{2} M_3^2} \tag{VII-66}$$
$$- \frac{\gamma_2 M_3^2}{1 + \frac{\gamma_2 - 1}{2} M_3^2} f_{2M} \quad.$$

Similarly, for the sensitivity of the afterbody temperature, one obtains

$$\frac{\delta T_3}{T_3} = f_{1T} \frac{\delta M_2}{M_2} + f_{2T} \delta \gamma_2 + \frac{\delta T_{t_2}}{T_{t_2}} \tag{VII-67}$$

where

$$f_{1T} = - \frac{(\gamma_2 - 1) M_3^2}{1 + \frac{\gamma_2 - 1}{2} M_3^2} \left(\frac{M_2^2 - 1}{M_3^2 - 1}\right)^{1/2} \tag{VII-68}$$

and

$$f_{2T} = - \frac{(\gamma_2 - 1) M_3^2}{1 + \frac{\gamma_2 - 1}{2} M_3^2} f_{2M} - \frac{0.5 M_3^2}{1 + \frac{\gamma_2 - 1}{2} M_3^2} \tag{VII-69}$$

In Eqs. (VII-64) and (VII-67), the last terms on the right-hand side represent the sensitivities of the forebody total pressure and total temperature, respectively.

118

Before the sensitivities of the afterbody pressure and temperature
to changes in free-stream velocity can be determined in an explicit form,
the last terms on the right-hand sides of Eqs. (VII-64) and (VII-67) have to
be related to the change in free-stream velocity. As pointed out earlier,
the total temperature is not conserved across the bow shock in the $e-f$
model, since part of thermal energy is frozen out of the flow as dissociation
energy. Similarly, the total pressure in the forebody is different from the
value for the corresponding $f-f$ case. The sensitivities of these total
quantities to changes in free-stream velocity can be obtained as follows.

The total pressure and total temperature on the forebody are
related to the other forebody flow quantities through the relations[*]

$$\frac{p_{t_2}}{p_2} = \left(1 + \frac{\gamma_2 - 1}{2} M_2^2\right)^{\frac{\gamma_2}{\gamma_2 - 1}} \qquad \text{(VII-70)}$$

and

$$\frac{T_{t_2}}{T_2} = \left(1 + \frac{\gamma_2 - 1}{2} M_2^2\right) \qquad \text{(VII-71)}$$

Therefore

$$\frac{\delta p_{t_2}}{p_{t_2}} = \frac{\delta p_2}{p_2} + \frac{\gamma_2 M_2^2}{1 + \frac{\gamma_2 - 1}{2} M_2^2} \frac{\delta M_2}{M_2} + \left\{ \frac{\gamma_2}{\gamma_2 - 1} \frac{0.5 M_2^2}{1 + \frac{\gamma_2 - 1}{2} M_2^2} \right.$$

$$\left. - \frac{1}{(\gamma_2 - 1)^2} \ln\left(1 + \frac{\gamma_2 - 1}{2} M_2^2\right) \right\} \delta \gamma_2 \qquad \text{(VII-72)}$$

and

$$\frac{\delta T_{t_2}}{T_{t_2}} = \frac{\delta T_2}{T_2} + \frac{(\gamma_2 - 1) M_2^2}{1 + \frac{\gamma_2 - 1}{2} M_2^2} \frac{\delta M_2}{M_2} + \frac{0.5 M_2^2}{1 + \frac{\gamma_2 - 1}{2} M_2^2} \delta \gamma_2 \qquad \text{(VII-73)}$$

---

[*] The total quantities referred to here are the values that would be attained
if the gas were isentropically brought to rest with the chemical composition
frozen. These are the values that are relevant for a frozen-shoulder expansion.

Finally, Eqs. (VII-64, 72, 67, 73) can be combined to yield

$$\frac{\delta p_3/p_3}{\delta U_i/U_i} = \frac{\delta p_2/p_2}{\delta U_i/U_i} + \left\{ f_{1p} + \frac{\gamma_2 M_2^2}{1 + \frac{\gamma_2 - 1}{2} M_2^2} \right\} \frac{\delta M_2/M_2}{\delta U_i/U_i} \qquad \text{(VII-74)}$$

$$+ \frac{\delta \gamma_2}{\delta U_i/U_i} \left\{ f_{2p} + \frac{\gamma_2}{\gamma_2 - 1} \frac{0.5 M_2^2}{1 + \frac{\gamma_2 - 1}{2} M_2^2} + \frac{1}{(\gamma_2 - 1)^2} \ln \left(1 + \frac{\gamma_2 - 1}{2} M_2^2 \right) \right\}$$

and

$$\frac{\delta T_3/T_3}{\delta U_i/U_i} = \frac{\delta T_2/T_2}{\delta U_i/U_i} + \left\{ f_{1T} + \frac{(\gamma_2 - 1) M_2^2}{1 + \frac{\gamma_2 - 1}{2} M_2^2} \right\} \frac{\delta M_2/M_2}{\delta U_i/U_i}$$

$$+ \left\{ f_{2T} + \frac{0.5 M_2^2}{1 + \frac{\gamma_2 - 1}{2} M_2^2} \right\} \frac{\delta \gamma_2}{\delta U_i/U_i} \qquad \text{(VII 75)}$$

In the foregoing equations, the sensitivity of the forebody Mach number is given by Eq. (VII-48), and the sensitivity of the forebody temperature and specific heat ratio have to be obtained from Eqs. (VII-45) and (VII-46), respectively. Consistent with our approximation, the sensitivity of the forebody pressure can be evaluated from Eq. (VII-9).

Equations (VII-74) and (VII-75) can be written in the convenient form

$$\frac{\delta p_3/p_3}{\delta U_i/U_i} = \frac{\delta p_2/p_2}{\delta U_i/U_i} + F_{1p} \frac{\delta M_2/M_2}{\delta U_i/U_i} + F_{2p} \frac{\delta \gamma_2}{\delta U_i/U_i} \qquad \text{(VII-74a)}$$

and

$$\frac{\delta T_3/T_3}{\delta U_i/U_i} = \frac{\delta T_2/T_2}{\delta U_i/U_i} + F_{1T} \frac{\delta M_2/M_2}{\delta U_i/U_i} + F_{2T} \frac{\delta \gamma_2}{\delta U_i/U_i} \qquad \text{(VII-75a)}$$

where the influence coefficients F_{1p}, F_{2p}, F_{1T} and F_{2T} are defined in an obvious manner. These influence coefficients are shown plotted in Figs. 44 to 47 for corner angles of 10°, 20°, 30°, and 40° and specific heat ratios of 1.4 and 1.67. Again, note that the pairs of influence coefficients for each variable are of the same sign. That is, an increase in either the forebody frozen Mach number or the forebody frozen-flow specific heat ratio has the same qualitative effect on the afterbody quantities.

The sensitivities of the other afterbody flow quantities can be expressed in terms of the sensitivities derived above. Thus, since $p_3' = \rho_3 R T_3 (1 + \alpha_3)$, one obtains

$$\frac{\delta \rho_3}{\rho_3} = \frac{\delta p_3}{p_3} - \frac{\delta T_3}{T_3} - \frac{\delta \alpha_3}{1 + \alpha_3} \qquad \text{(VII-76)}$$

Since the afterbody expansion is frozen, $\alpha_3 \equiv \alpha_2$ and Eq. (VII-33) yields

$$\delta \alpha_3 = \frac{(\alpha_2 + 5)^2}{8} \delta \gamma_2 \qquad \text{(VII-77)}$$

Eq. (VII-76) can be written as

$$\frac{\delta \rho_3}{\rho_3} = \frac{\delta p_3}{p_3} - \frac{\delta T_3}{T_3} - \frac{(\alpha_2 + 5)^2}{8(1 + \alpha_3)} \delta \gamma_2 \qquad \text{(VII-78)}$$

All the quantities in the right-hand side of Eq. (VII-78) are, of course, known quantities.

Similarly, the sensitivity of the afterbody velocity is given by

$$\frac{\delta U_3}{U_3} = \frac{\delta M_3}{M_3} + \frac{1}{2} \left(\frac{\delta p_3}{p_3} + \frac{\delta \gamma_2}{\gamma_2} - \frac{\delta \rho_3}{\rho_3} \right) \qquad \text{(VII-79)}$$

The expressions for the sensitivity of the afterbody pressure and temperature to changes in free-stream temperature are formally similar to Eqs. (VII-74) and (VII-75) except that here the appropriate values of the forebody sensitivities have to be used. Thus, one can write for the sensitivity of the pressure

$$\frac{\delta p_3 / p_3}{\delta T_1 / T_1} = \frac{\delta p_2 / p_2}{\delta T_1 / T_1} + F_{1p} \frac{\delta M_2 / M_2}{\delta T_1 / T_1} + F_{2p} \frac{\delta \gamma_2}{\delta T_1 / T_1}$$

where the sensitivities of the forebody pressure, Mach number and specific heat ratio are given by Eqs. (VII-58), (-10), and (-55), respectively. It

can be seen from the above equation that the sensitivity of afterbody pressure to changes in free-stream temperature is usually greater than the sensitivity of the forebody pressure since the quantity $(\delta M_2/M_2)\big/(\delta T_1/T_1)$ is negative.

The sensitivities of the afterbody density, temperature, pressure, and Mach number are shown in Figs. 48 and 51. Since, as before, the quantities correlate excellently in terms of $U_1 \sin \theta$ at each altitude, only the mean curves are shown.

We will close the present section with a discussion of the results given above for the equilibrium-frozen model. It can be seen from Figs. 42a and 42b that, for a given corner angle, the influence coefficient f_{1M} increases with increasing forebody Mach number, and that it becomes infinite at some critical value of the forebody Mach number. This critical Mach number, of course, corresponds to the condition at which the given corner angle represents the maximum-flow turning angle for the forebody flow. In other words, this critical forebody Mach number corresponds to the condition at which the afterbody temperature, pressure and density tend to zero while the Mach number tends to infinity. Any further increase in the forebody Mach number beyond this critical value will cause the flow to leave the afterbody. It can be seen from Figs. 42a and 42b that, for a given corner angle, the critical Mach number decreases with increasing forebody frozen specific heat ratio.

Conclusions similar to those given above can be seen to be valid for the influence coefficients F_{1p} and F_{1T} also (see Figs. 44 and 45). Clearly, all the afterbody flow quantities will be very sensitive to changes in forebody Mach number when its value is close to the critical one.

The influence coefficients f_{2M} , F_{2T} and F_{2p} shown in Figs. 43, 46, and 47 determine the sensitivity of the afterbody flow quantities to changes in forebody specific heat ratio. Here again, it can be seen that the afterbody flow quantities are extremely sensitive to changes in forebody specific heat ratio when the forebody Mach number is close to its critical value.

The sensitivity of the afterbody density, temperature, pressure and Mach number with respect to changes in free-stream velocity are shown in Figs. 48a, 49a, and 50a and 51a. As the free-stream velocity is increased, more and more of gas behind the leading-edge shock wave dissociates, and the forebody frozen-flow Mach number and frozen-flow specific heat ratio increase continuously (see Figs. 35 and 36). Thus, the forebody Mach number approaches its critical value, and the afterbody density, temperature and pressure decrease rapidly while the afterbody Mach number increases rapidly. Under these conditions, a further increase in the free-stream velocity will cause large changes in the afterbody quantities. It can be seen from Figs. 48a, 49a, 50a, and 51a that this effect is especially pronounced at the higher altitude. Physically, the above behavior arises because as the free-stream velocity is increased, more and more energy is frozen out of the fluid flow as dissociation energy, and a relatively smaller isentropic expansion will suffice to convert all the available flow energy into kinetic energy on the afterbody.

For the sake of comparison, the corresponding values for the frozen-frozen case are also shown in Figs. 48a, 49a, 50a, and 51a and are labeled "perfect gas". For the frozen-frozen model, the forebody Mach number reaches a limiting value which is considerably lower than the critical value, so that the influence coefficients are never too large. Moreover, since the forebody quantities reach limiting values of some large value of the free-stream velocity, the afterbody quantities reach limiting values also.

The sensitivity of the afterbody flow quantities to changes in free-stream temperature are shown in Figs. 48b, 49b, 50b, and 51b. It can be seen that for this case the flow reaches Mach number independence as expected. However, note that the flow does not become Mach number independent until after fairly large free-stream velocities are reached.

D.   ANALYSIS OF THE EQUILIBRIUM-EQUILIBRIUM MODEL

The analysis of the sensitivity of the forebody quantities to changes in free-stream conditions for this case is identical to that for the equilibrium-frozen model discussed above. Therefore, the analysis of the sensitivity of the afterbody quantities to changes in forebody quantities is the only additional problem that need be considered here.

The analysis of this case is complicated by the fact that no explicit solutions exist for an equilibrium Prandtl-Meyer expansion. Even numerical calculations of equilibrium Prandtl-Meyer expansions are rather lengthy and involved because of the continuous exchange of energy, within the fan, between the active and relaxing internal degrees of freedom. Therefore, in this section, an approximate method of solving equilibrium Prandtl-Meyer flows is developed, based on the fact that in nonequilibrium expanding flows the density is relatively insensitive to nonequilibrium effects; in other words, the frozen and equilibrium flow densities are nearly equal[200].

The solution for the equilibrium-equilibrium flow model then proceeds as follows. The conditions behind the leading-edge equilibrium oblique shock are determined using the analysis developed for the equilibrium-frozen model. For these conditions (that is, the Mach number based on frozen speed of sound and the frozen-flow specific heat ratio), the density on the afterbody after an expansion through the given angle is determined assuming frozen flow and using perfect-gas tables. It is then assumed that this density is the same for an equilibrium expansion also. Since the equilibrium expansion is isentropic, the entropy on the afterbody will be the same as that on the forebody. Thus, the state of the flow on the afterbody is completely determined since in an equilibrium flow there are only two independent state variables. In a practical example, the final state is determined from the Mollier diagram by making use of the fact that the final state point has to fall on the vertical line (that is, the constant entropy line) passing through the initial state point. The final state point can be fixed on this constant entropy line since the final value of the density is known, and the other state variables can be read off the Mollier diagram.

The accuracy of the present approximation has not been checked by comparing the approximate and exact solutions. However, exact calculations like the one carried out by Heims[200], indicate that the density in an expanding flow is indeed insensitive to the flow chemistry.

The values of the afterbody flow quantities calculated, using the method described above, are shown in Fig. 52 for flow deflection angles of 20°, 30°, and 40°. As before, the results are shown correlated in terms of $U, \sin \theta$ and only the mean curves are shown.

The sensitivity of the afterbody flow variables can be calculated as follows. Since in an equilibrium flow there are only two independent state variables, any afterbody state variable can be expressed as a function of two other state variables. Thus, one can write

$$p_3 = p_3 \left(\rho_3, S_3 \right) \quad , \tag{VII-80}$$

so that

$$\delta p_3 = \left. \frac{\partial p_3}{\partial S_3} \right|_{\rho, e} \delta S_3 + \left. \frac{\partial p_3}{\partial \rho_3} \right|_{S, e} \delta \rho_3 \tag{VII-81}$$

Since $(\partial p / \partial \rho)_{S,e}$ is merely the equilibrium speeds of sound, a_e, one obtains

$$\delta p_3 = \frac{\partial p}{\partial S} \left(\rho_3, S_3 \right) \delta S_3 + a_{e_3}^2 \, \delta \rho_3 \tag{VII-82}$$

Similarly,

$$\delta p_2 = \frac{\partial p}{\partial S} \left(\rho_2, S_2 \right) \delta S_2 + a_{e_2}^2 \, \delta \rho_2 \tag{VII-83}$$

However, $S_2 \equiv S_3$, and Eqs. (VII-82) and (VII-83) can be combined to give

$$\frac{\delta p_3}{p_3} = \gamma_{e_3} \frac{\delta \rho_3}{\rho_3} + \frac{p_2}{p_3} \frac{\frac{\partial p}{\partial S}\left(\rho_3, S_2 \right)}{\frac{\partial p}{\partial S}\left(\rho_2, S_2 \right)} \left[\frac{\delta p_2}{p_2} - \gamma_{e_2} \frac{\delta \rho_2}{\rho_2} \right] \tag{VII-84}$$

where γ_e is the equilibrium specific heat ratio defined as $\gamma_e = a_e^2 \rho_e / p_e$.
Since we have assumed that the density is insensitive to nonequilibrium
effects, the first term in the right-hand side of Eq. (VII-84) can be evaluated,
using the results of the equilibrium-frozen model (see Eq. (VII-78)). The
derivative $(\partial p / \partial s)_\rho$ and the values of γ_{e_2} and γ_{e_3} can be evaluated
from the Mollier diagram. Thus, the sensitivity of the afterbody pressure
to a change in free-stream velocity can be written as

$$\frac{\delta p_3 / p_3}{\delta U_1 / U_1} = \gamma_{e_3} \frac{\delta \rho_3 / \rho_3}{\delta U_1 / U_1} + \frac{p_2}{p_3} \frac{\frac{\partial p}{\partial s}(\rho_3, S_2)}{\frac{\partial p}{\partial s}(\rho_2, S_2)} \left[\frac{\delta p_2 / p_2}{\delta U_1 / U_1} - \gamma_{e_2} \frac{\delta \rho_2 / \rho_2}{\delta U_1 / U_1} \right] \quad \text{(VII-85)}$$

where the terms

$$\frac{\delta \rho_3 / \rho_3}{\delta U_1 / U_1} \quad , \quad \frac{\delta p_2 / p_2}{\delta U_1 / U_1} \quad \text{and} \quad \frac{\delta \rho_2 / \rho_2}{\delta U_1 / U_1}$$

have to be determined from Eqs. (VII-78), (VII-9), and (VII-42), respectively.

Similar expressions can be written down for the other sensitivities
also. The expressions for the sensitivity of the afterbody quantities to changes
in free-stream temperature are formally similar to the equations derived
above. Thus, one can write

$$\frac{\delta p_3 / p_3}{\delta T_1 / T_1} = \gamma_{e_3} \frac{\delta \rho_3 / \rho_3}{\delta T_1 / T_1} + \frac{p_2}{p_3} \frac{\frac{\partial p}{\partial s}(\rho_3, S_2)}{\frac{\partial p}{\partial s}(\rho_2, S_2)} \left[\frac{\delta p_2 / p_2}{\delta T_1 / T_1} - \gamma_{e_2} \frac{\delta \rho_2 / \rho_2}{\delta T_1 / T_1} \right]$$

$$\text{(VII-86)}$$

where the terms

$$\frac{\delta \rho_3 / \rho_3}{\delta T_1 / T_1} \quad , \quad \frac{\delta p_2 / p_2}{\delta T_1 / T_1} \quad \text{and} \quad \frac{\delta \rho_2 / \rho_2}{\delta T_1 / T_1}$$

have to be determined from Eqs. (VII-78), (VII-10), and (VII-54),
respectively.

The sensitivities of the afterbody flow quantities for the range of
free-stream conditions of interest are shown in Figs. 53 to 55. These figures
show the sensitivities of afterbody pressure, temperature, and dissociation
fraction to changes in free-stream velocity, as well as temperature. The
sensitivity of the afterbody density is not shown since, by assumption, it is the
same as that for the equilibrium-frozen model.

It can be seen from the above figures that the qualitative behaviors of the sensitivities for this case are somewhat similar to those of the equilibrium-frozen model. However, in the present case,the magnitudes of the sensitivities are considerably smaller. Even though a substantial recombination of the dissociated atoms occurs during the afterbody equilibrium expansion process, it can be seen from Fig. 52 that the dissociation fraction on the afterbody is still considerable. Therefore, a substantial fraction of the total energy is still contained in the dissociation mode, and the values of the afterbody state variables will decrease rapidly with increasing velocity.

E. EXTENSION OF THE PRESENT RESULTS TO MORE
GENERAL TWO-DIMENSIONAL BODIES

As mentioned previously, the results derived above for the wedge-nosed flat plate can be extended to more general body shapes by using the tangent-wedge approximation or the more accurate shock-expansion method. In fact, this was one of the main reasons for considering the analysis of the blunt-nosed flat plate in two separate steps, namely, the analysis of the sensitivity of the forebody variables to changes in free-stream conditions and the analysis of the sensitivity of the afterbody flow variables to changes in forebody conditions.

In the tangent-wedge approximation, the surface pressure at any point on a two-dimensional body is taken to be equal to the value on a wedge whose half-angle is equal to the local inclination of the body streamline with respect to the free-stream direction. Accordingly, we take the sensitivity of the surface pressure at a point to changes in any free-stream condition to be the same as the sensitivity of the pressure on the equivalent wedge. Thus, the results obtained above can be directly applied to the case of any general slender body. The tangent-wedge approximation is based on the assumption that at hypersonic speeds the pressure,as well as the streamline inclination, can be taken to be constant across the shock layer. Since this assumption is equally valid for both frozen and equilibrium flows, solutions for the sensitivity of frozen,as well as equilibrium,pressure fields around general airfoil shapes can be obtained by applying the tangent-wedge approximation to the

results derived above. However, since the results derived above assumed that the frozen and equilibrium oblique shock pressure ratios were equal, the frozen and equilibrium solutions will be identical for the present case.

The tangent-wedge approximation neglects two important effects, namely, the centrifugal effects of streamline curvature and the effects of changes in the streamline inclination across the shock layer. For this reason, the tangent-wedge approximation yields inaccurate results in regimes where the aforementioned effects are important. A somewhat more accurate method for solving the flow fields about slender airfoils with attached shock waves is the shock-expansion method. Essentially, the shock-expansion method is based on the assumption that the Mach number at any point in the flow field downstream of the nose shock wave can be related to the local flow inclination angle through the Prandtl-Meyer relation. This assumption is equivalent to neglecting the reflected disturbances from the shock wave itself, as well as the vorticity layers produced by the curvature of the shock. The limitations of this assumption are discussed at length in Ref. 25 (pp. 265-277). Even though the shock-expansion method is generally applied to perfect gas flows only, it can be equally well applied to equilibrium flows provided the equilibrium Prandtl-Meyer relation is used to relate the local Mach number to the local streamline inclination.

As an example of the application of the results for the wedge-nosed flat plate to more general bodies, consider the biconvex airfoil shown in Fig. 56. Let us first consider the zero angle of attack case. Let θ_o denote the half-angle of the leading edge of the airfoil and let θ_P be the inclination of the surface at any point P to the free-stream direction. The sensitivity of the pressure at point P to changes in free-stream velocity is given by the tangent-wedge approximation as

$$\frac{\delta p_P / p_P}{\delta U_1 / U_1} = \left(\frac{\delta p_2 / p_2}{\delta U_1 / U_1} \right)_{\theta = \theta_P} \tag{VII-87}$$

where the right-hand side has to be evaluated from Eq. (VII-9) with $\theta = \theta_P$ for both frozen and equilibrium flows. Therefore, within the scope of the

tangent-wedge approximation, the sensitivity of the pressure at any point in the body to changes in free-stream conditions is the same for both frozen and equilibrium flows. However, the tangent-wedge approximation can be used in conjunction with the results derived for the wedge-nosed flat plate only for points close to the leading edge of the airfoil; that is, only when θ_P is not less than about fifteen degrees. As pointed out earlier, the approximation that the equilibrium and frozen pressures are nearly equal is not valid for slender bodies.

The shock-expansion method can be used in conjunction with the results derived above as follows. Let the subscript "o" denote the conditions at the point 0 which is at the leading edge of the airfoil and immediately behind the bow shock wave. Then, for the free-stream conditions, the conditions at 0 will correspond to conditions on the forebody of a wedge-nosed flat plate with half-angle θ_o. Since shock-expansion theory assumes that the expansion from 0 to P takes place isentropically, the conditions at P will be equivalent to conditions after a Prandtl-Meyer expansion (from state 0) through an angle equal to $(\theta_o - \theta_P)$. Thus, for frozen flow, the sensitivity of the pressure at any point P on the airfoil to changes in free-stream velocity is given by Eq. (VII-27) as

$$
\frac{\delta p_P / p_P}{\delta U_1 / U_1} = \frac{\gamma M_1^2}{1 + \frac{\gamma - 1}{2} M_1^2} - \frac{\frac{2\gamma}{\gamma + 1} \left(M_1^2 \sin^2 \sigma_o - 1 \right)}{\left[1 + \frac{2\gamma}{\gamma + 1} \left(M_1^2 \sin^2 \sigma_o - 1 \right) \right] \left[1 + \frac{\gamma - 1}{2} M_1^2 \sin^2 \sigma_o \right]}
$$
$$
- \left(\frac{M_o^2 - 1}{M_P^2 - 1} \right)^2 \frac{\gamma M_P^2}{1 + \frac{\gamma - 1}{2} M_o^2} \frac{\delta M_o / M_o}{\delta U_1 / U_1}
$$

(VII-88)

where σ_o is the shock angle corresponding to a flow deflection angle of θ_o at the given free-stream conditions, and the term $\left(\delta M_o / M_o \right) / \left(\delta U_1 / U_1 \right)$ has to be determined from Eq. (VII-8) with $\theta = \theta_o$ and $\sigma = \sigma_o$.

Similarly, when the flow is in equilibrium everywhere, Eq. (VII-85) gives

$$\frac{\delta p_P/p_P}{\delta U_1/U_1} = \gamma_{e_P} \frac{\delta \rho_P/\rho_P}{\delta U_1/U_1} + \frac{p_o}{p_P} \frac{\frac{\partial p}{\partial S}(\rho_P, S_o)}{\frac{\partial p}{\partial S}(\rho_o, S_o)} \left[\frac{\delta p_o/p_o}{\delta U_1/U_1} - \gamma_{e_o} \frac{\delta \rho_o/\rho_o}{\delta U_1/U_1} \right] \quad \text{(VII-89)}$$

Similar results can also be derived for the sensitivity of the afterbody pressure to changes in free-stream temperature.

The equilibrium-frozen model is not considered here since it is unrealistic for the case of the biconvex airfoil where the expansion behind the shock wave occurs quite gradually.

The results derived above for zero angle of attack can be easily generalized to cases with angle of attack. The sensitivity of the aerodynamic forces and moments for the biconvex airfoil can also be obtained from Eqs. (VII-88) and (VII-89) in a straightforward manner by integrating these equations over the surface of the airfoil.

Fig. 56 shows the sensitivity of the pressure on a 15% thickness biconvex airfoil to changes in free-stream conditions. Both the results of the tangent-wedge and shock-expansion approximations are shown for frozen and equilibrium flows. It can be seen that the pressure at points closer to the leading edge are more sensitive to changes in free-stream velocity while the pressure at points closer to the center of the airfoil are more sensitive to changes in temperature.

F.   ANALYSIS OF FLOW ABOUT CONICAL-NOSED CYLINDERS

So far, we have restricted our attention to two-dimensional shapes. In Sections B, C, and D, flows past wedge-nosed flat plates were considered using three idealized chemistry models, and, in Section E, it was shown how these results can be extended to more generalized slender bodies. In the present section, an analogous procedure for three-dimensional bodies will be outlined. The basic geometry that will be considered here is the conical-nosed cylinder. The results for the conical-nosed cylinder can be extended to more general three-dimensional slender bodies by using the tangent-cone or the shock-expansion methods.

The analysis of the conical-nosed cylinder is complicated by the fact that neither the forebody quantities nor the afterbody quantities can be expressed explicitly in terms of the free-stream conditions even for the relatively simple case of perfect gas flow. The forebody quantities cannot be expressed explicitly in terms of the free-stream conditions because the flow behind the shock wave is not uniform, only part of the compression takes place across the shock wave, and the remainder is accomplished behind it isentropically. The solution has to be obtained by fitting an isentropic conical flow to a conical shock. However, extensive numerical solutions have been reported by Kopal[154] for the flow about cones, and the sensitivity of the forebody quantities to changes in free-stream conditions can be obtained by numerically differencing these results.

The afterbody quantities cannot be related to the forebody quantities in a straightforward manner since the afterbody expansion is nonsimilar even in the simplified case of frozen-flow chemistry. The expansion right at the shoulder is locally two-dimensional. However, the flow overexpands at the shoulder and, subsequently, suffers an isentropic compression, and the variation of the flow quantities along the afterbody cannot be determined in a simple way. In general, this variation can be determined exactly only by some numerical technique, such as the method of characteristics. However, the exact numerical calculations of Ehret et al[26] show that the variation of pressure along the afterbody is nearly exponential for slender bodies. Therefore, for our purpose, it will be sufficiently accurate to assume that the variation of pressure on the afterbody is exponential. In fact, this approach was used by Syvertson and Dennis[201] in conjunction with a second-order shock-expansion method.

When the assumption is made that the variation of pressure along the afterbody is exponential, the variation of the pressure is uniquely determined by the value of the pressure at the shoulder (which can be obtained from two-dimensional theory) and a characteristic length, L , which depends on the initial gradient of the pressure at the shoulder. Thus, the variation of pressure along the afterbody can be written as

$$p = p_1 - (p_1 - p_3) e^{-x/L}$$

<div align="right">(VII-90)</div>

where

$$L = \frac{p_1 - p_3}{(\partial p / \partial x)_{x=0}}$$

<div align="right">(VII-91)</div>

In Eqs. (VII-90) and (VII-91), p_1 represents the free-stream pressure, p_3 represents the pressure on the afterbody at the shoulder ($x = 0$), and x is the distance along the afterbody. Equation (VII-90) shows that, in accordance with shock-expansion theory, the pressure on the afterbody will tend to the free-stream pressure far downstream of the shoulder. To determine the characteristic length L, one must determine the initial gradient of the pressure at the shoulder. Johannsen and Meyer[202] have developed a method of determining this gradient by expanding all the flow variables in terms of a certain nondimensional distance from the shoulder. However, the method used by Johannsen and Meyer involves numerical calculations, and a somewhat simpler, but approximate, value for the initial gradient has been obtained by Syvertson and Dennis by using a quasi-one-dimensional stream tube approach. Syvertson and Dennis[201] give

$$\left(\frac{\partial p}{\partial x}\right)_{x=0} = \frac{\gamma_2 p_3 M_3^2}{2(M_3^2 - 1)R} \left[\frac{\Omega_2}{\Omega_3} \sin \theta\right]$$

<div align="right">(VII-92)</div>

where

$$\Omega = \frac{1}{M} \left[\frac{1 + \frac{\gamma-1}{2} M^2}{\frac{\gamma+1}{2}}\right]^{\frac{\gamma+1}{2(\gamma-1)}}$$

<div align="right">(VII-93)</div>

In Eq. (VII-92), γ_2 is the specific heat ratio and R is the radius of the afterbody. Equations (VII-91) and (VII-92) can be combined to give

$$\frac{L}{R} = \frac{2}{\gamma_2 \sin \theta} \frac{\Omega_3}{\Omega_2} \left(\frac{p_1}{p_3} - 1\right)\left(1 - \frac{1}{M_3^2}\right)$$

<div align="right">(VII-94)</div>

Thus, the sensitivity of the pressure at any point on the afterbody to changes in forebody conditions can be described completely in terms of the sensitivities of the pressure (p_3) at the shoulder and the characteristic length L . Since the afterbody expansion is locally two-dimensional at the shoulder, the sensitivity of the shoulder pressure to changes in free-stream Mach number can be obtained by using Fig. 44, and one can write

$$ \frac{\delta p_3 / p_3}{\delta M_1 / M_1} = \frac{\delta p_2 / p_2}{\delta M_1 / M_1} + F_{1p} \frac{\delta M_2 / M_2}{\delta M_1 / M_1} \tag{VII-95} $$

where, now, M_2 and p_2 are the Mach number and pressure on the surface of the cone. The sensitivities of the cone pressure and Mach number to changes in free-stream Mach number have to be obtained by numerically differencing the values given in Ref. 167. The sensitivity of p_3 to changes in free-stream Mach number can be related to the sensitivities of p_3 to changes in free-stream velocity and temperature by using the relations given on page 99.

The sensitivity of the characteristic length L to changes to free-stream conditions can be derived from Eqs. (VII-94) and (VII-93), and one obtains

$$ \frac{\delta L}{L} = \frac{2 \delta M_3 / M_3}{M_3^2 - 1} + \frac{\delta M_3}{M_3} \left[\frac{M_3^2 - 1}{1 + \frac{\gamma - 1}{2} M_3^2} \right] - \frac{\delta M_2}{M_2} \left[\frac{M_2^2 - 1}{1 + \frac{\gamma - 1}{2} M_2^2} \right] $$

$$ + \frac{(p_1 / p_3)}{(p_1 / p_3) - 1} \left[\frac{\delta p_1}{p_1} - \frac{\delta p_3}{p_3} \right] \tag{VII-96} $$

where the term $\delta p_1 / p_1$ is relevant only when a change in free-stream Mach number is caused by a change in free-stream temperature. The term $\delta M_3 / M_3$ can be eliminated from Eq. (VII-96) by using Eq. (VII-14), so that

$$\frac{\delta L}{L} = \left[\left(\frac{2}{M_3^2 - 1} + \frac{M_3^2 - 1}{1 + \frac{\gamma - 1}{2} M_3^2} \right) \left(\frac{M_2^2 - 1}{M_3^2 - 1} \right)^{1/2} \frac{1 + \frac{\gamma - 1}{2} M_3^2}{1 + \frac{\gamma - 1}{2} M_2^2} \right.$$

$$\left. - \frac{M_2^2 - 1}{1 + \frac{\gamma - 1}{2} M_2^2} \right] \frac{\delta M_2}{M_2} + \frac{p_1/p_3}{(p_1/p_3) - 1} \left[\frac{\delta p_1}{p_1} - \frac{\delta p_3}{p_3} \right]$$

(VII-97)

where the terms $\delta M_2 / M_2$ and $\delta p_3 / p_3$ have to be obtained from numerical differencing and from Eq. (VII-95), respectively.

A corresponding analysis for the equilibrium-frozen model is further complicated by the fact that information on equilibrium conical flows is much less extensive than that for the frozen flow case. Of course, when considering the afterbody expansion in this case, the forebody specific heat ratio has to be included as a relevant parameter. The sensitivity of the forebody quantities to changes in free-stream conditions can be determined by using the isothermal solution of Zienkiewicz[203], the "incompressible" results of Feldman[204], or the tabulated numerical results of Romig[173]. However, no detailed calculations for the equilibrium-frozen model have been carried out in the present study. Since no analytical solutions are known for the equilibrium expansion around a three-dimensional corner, the equilibrium-equilibrium model is also not analyzed in the present study.

The results for the conical-nosed cylinder for the frozen-frozen model reported above can also be extended to other slender bodies by using the tangent-cone or shock-expansion methods. The procedure is completely analogous to that in the two-dimensional case, and it will not be dealt with in detail here.

G. EFFECTS OF FREE-STREAM DISSOCIATION

So far in our analyses, we have not considered the effects of free-stream dissociation. In fact, we have assumed throughout that the free stream is undissociated and has a constant specific heat ratio, γ, equal to the perfect gas value of 1.4. This assumption is certainly realistic in atmospheric flight where ambient dissociation levels are usually negligible. However, as discussed in Sec. II-D, the generation of hypersonic airflows in wind tunnels is usually accompanied by a certain level of dissociation in the test section because of freezing of the chemical reactions. Therefore, for the proper interpretation of the test data, the effects of ambient dissociation on the flow field must be understood. In this section, we will discuss briefly the effects of ambient dissociation on the flow fields about slender bodies by using the approximate chemical models developed above.

In general, the driving force for chemical relaxation behind a strong shock wave arises because of the difference between the actual value of the local mass fraction and a pseudo-equilibrium value based on any two of the local state variables (say, pressure and temperature). In fact, all linearized theories of relaxation processes assume that the rate of approach to equilibrium is directly proportional to this difference between the local and pseudo-equilibrium values of the mass fraction. When the free stream is undissociated, the maximum value of this difference occurs immediately behind the shock wave since the value of the mass fraction is zero immediately behind the shock wave and since the temperature is highest there. Along a particle path this difference becomes progressively smaller as the relaxation proceeds, and the flow reaches equilibrium far downstream of the shock wave where this difference asymptotically tends to zero.

When the free stream is dissociated, the difference between the actual and pseudo-equilibrium values of the dissociation fraction will usually be less than that in the corresponding case when the free stream is undissociated. Therefore, there will be a correspondingly smaller amount of relaxation in this case. In fact, when the shock wave is of such strength that the pseudo-equilibrium value of the dissociation fraction immediately behind

it is identically equal to the free-stream value, the flow will equilibrate immediately behind the shock wave. Such cases for the flow past wedges have been considered by Vincenti[205], Capiaux and Washington[155], and Lee[206]. Also, it is clear that when this equilibrated gas is subjected to an afterbody expansion, "freezing" would most likely occur since the gas is now being processed through an expansion of strength equal to that of the compression through which the free-stream gas was processed. Note that in the simplified case considered above, the dissociation fraction remains constant throughout the flow field with the result that there is no exchange of energy between the fluid mechanical and chemical modes. The gas will behave like a perfect gas everywhere with a value of the specific heat ratio that is determined completely by the value of the free-stream dissociation fraction alone.

It is clear from the arguments given above that even when the simplified conditions described here do not exist, the most appropriate flow model to be used will be the equilibrium-frozen model. In the present section, we will analyze the effects of free-stream dissociation on the afterbody flow quantities of a wedge-nosed flat plate by using the equilibrium-frozen model. Since in the equilibrium-frozen model it is assumed that the pressure ratio is the same as that for the corresponding frozen-flow case, we first need to consider the sensitivity of the pressure behind a frozen oblique shock wave to changes in the dissociation fraction in front of it. In the frozen-flow case, the only effect of the free-stream dissociation fraction will be to change the specific heat ratio for the flow field. Again, as in Eq. (VII-33), the relation between the dissociation fraction and the specific heat ratio is given by

$$\gamma_1 = \frac{3\alpha_1 + 7}{\alpha_1 + 5} \quad ,$$

(VII-98)

so that

$$\delta\gamma_1 = \frac{8}{(\alpha_1 + 5)^2} \delta\alpha_1$$

(VII-99)

The pressure ratio across frozen oblique shock wave is given by

$$\frac{p_2}{p_1} = 1 + \frac{2\gamma_1}{\gamma_1 + 1}\left(M_1^2 \sin^2 \sigma_f - 1\right)$$

(VII-100)

Therefore, one obtains

$$\frac{\delta p_2}{p_1} = \frac{4\gamma_1}{\gamma_1 + 1}\left(\frac{\delta M_1}{M_1} + \cot \sigma_f \, \delta \sigma_f\right) + \frac{2}{\gamma_1 + 1}\left(M_1^2 \sin^2 \sigma_f - 1\right)\frac{\delta \gamma_1}{\gamma_1 + 1}$$

(VII-101)

where δM_1 and $\delta \sigma_f$ are the changes in the free-stream Mach number and the frozen shock-wave angle due to the change in α_1.

The definition of the Mach number yields

$$\frac{\delta M_1}{M_1} = -\frac{1}{2}\frac{\delta \gamma_1}{\gamma_1}$$

(VII-102)

and Eq. (VII-2) yields

$$\delta \sigma = \frac{(\gamma_1 M_1^2 \sin^2 \sigma_f + 1)\cos(\sigma_f - \theta)\sin \sigma_f}{M_1^2 \sin^2 \sigma_f \cos(2\sigma_f - \theta) + \cos \theta}\quad \frac{\delta \gamma_1}{\gamma_1(\gamma_1 + 1)}$$

(VII-103)

Equations (VII-101), (VII-102), and (VII-103) can be combined to give

$$\frac{\delta p_2}{p_2} = \frac{2K}{\gamma_1 + 1}\frac{1 + \gamma_1 M_1^2 \sin^2 \sigma_f}{1 + \frac{2\gamma_1}{\gamma_1 + 1}\left(M_1^2 \sin^2 \sigma_f - 1\right)}\frac{\cos \theta}{\cos(2\sigma_f - \theta)}\frac{\delta \gamma_1}{\gamma_1 + 1}$$

(VII-104)

where K is given by Eq. (VII-5b).

Now, for an equilibrium oblique shock wave, Eqs. (VII-35), (VII-36), and (VII-37) give

$$\frac{\delta \rho_2}{\rho_2} + \frac{\delta U_2}{U_2} = \left[\cot \sigma_e - \cot(\sigma_e - \theta)\right]\delta \sigma_e$$

(VII-105)

$$\frac{\delta U_2}{U_2} = \left[\tan(\sigma_e - \theta) - \tan \sigma_e\right]\delta \sigma_e$$

(VII-106)

and

$$\frac{p_2}{\rho_2 U_2^2 \sin^2(\sigma_e - \theta)} \frac{\delta p_2}{p_2} + \frac{\delta \rho_2}{\rho_2} + 2 \frac{\delta U_2}{U_2} = 0$$

(VII-107)

Consistent with our approximation, the term $\delta p_2 / p_2$ in Eq. (VII-107) can be evaluated using Eq. (VII-104). Then, one obtains

$$\frac{\delta U_2 / U_2}{\delta \gamma_1} = -\frac{\rho_2}{\rho_1} \frac{K(\gamma_1 M_1^2 \sin^2 \sigma_e + 1)}{\left[\frac{\gamma_1 + 1}{2} M_1^2 \sin^2 \sigma_e\right] \left[\frac{\rho_2 / \rho_1}{\tan^2 \sigma_e} + 1\right]} \frac{\cos \theta}{\cos(2\sigma_e - \theta)} \frac{1}{\gamma_1(\gamma_1 + 1)}$$

(VII-108)

and

$$\frac{\delta \rho_2 / \rho_2}{\delta \gamma_1} = -\frac{\rho_2}{\rho_1} \frac{K(\gamma_1 M_1^2 \sin^2 \sigma_e + 1)\left(\frac{\rho_2 / \rho_1}{\tan^2 \sigma_e} - 1\right)}{\left(\frac{\gamma_1 + 1}{2} M_1^2 \sin^2 \sigma_e\right)\left(\frac{\rho_2 / \rho_1}{\tan^2 \sigma_e} + 1\right)} \frac{\cos \theta}{\cos(2\sigma_e - \theta)} \frac{1}{\gamma_1(\gamma_1 + 1)}$$

(VII-109)

The sensitivity of the forebody frozen-flow specific heat ratio can be obtained from Eq. (VII-43), and one obtains

$$\frac{\delta \gamma_2}{\delta \gamma_1} = \frac{8}{(\alpha_2 + 5)^2} \left[p_2 \left(\frac{\partial \alpha}{\partial p}\right)_{\rho,e} \frac{\delta p_2 / p_2}{\delta \gamma_1} + \rho_e \left(\frac{\partial \alpha}{\partial \rho}\right)_{p,e} \frac{\delta \rho_2 / \rho_2}{\delta \gamma_1} \right]$$

(VII-110)

The sensitivity of the afterbody frozen-flow Mach number is given by Eq. (VII-47).

The sensitivity of the afterbody quantities can be obtained from the above results by using equations similar to Eqs. (VII-74a) and (VII-75a). Thus,

$$\frac{\delta p_3 / p_3}{\delta \gamma_1} = \frac{\delta p_2 / p_2}{\delta \gamma_1} + F_{1p} \frac{\delta M_2 / M_2}{\delta \gamma_1} + F_{2p} \frac{\delta \gamma_2}{\delta \gamma_1}$$

(VII-111)

$$\frac{\delta T_3 / T_3}{\delta \gamma_1} = \frac{\delta T_2 / T_2}{\delta \gamma_1} + F_{1T} \frac{\delta M_2 / M_2}{\delta \gamma_1} + F_{2T} \frac{\delta \gamma_2}{\delta \gamma_1}$$

(VII-112)

In the above equations the quantity $(\delta M_2 / M_2) / \delta \gamma_1$ has to be determined from Eqs. (VII-104), (VII-108), and (VII-109).

Note that the quantities $(\delta M_2 / M_2) / \delta \gamma_1$ and $\delta \chi_2 / \delta \gamma_1$ do not become small at large values of the free-stream velocity. Also, since, as mentioned previously, the influence coefficients $F_{1\varphi}$, F_{1T}, $F_{2\varphi}$ and F_{2T} increase with increasing forebody Mach number and specific heat ratio, the sensitivities of the afterbody quantities to changes in free-stream specific heat ratio are likely to be substantial. Hence, in supersonic flows over blunt-nosed slender bodies, the effects of free-stream dissociation are likely to be quite important.

H.   SUMMARY

We have considered above the effects of nonduplication of certain free-stream conditions on the afterbody flow quantities of a class of slender bodies by using three simplified chemical models. The problem was studied in detail for the case of a wedge-nosed flat plate and it was demonstrated how the results for this simplified geometry could be extended to more general bodies. Only a preliminary analysis of the corresponding three-dimensional problem of the conical-nosed wedge was possible since equilibrium conical flow fields are considerably more difficult than wedge flows and since the afterbody expansion for the conical cylinder is nonsimilar.

The analysis of the sensitivity of the afterbody quantities on the wedge-nosed flat plate to changes in free-stream velocity and temperature showed that for all of the three chemical models the more important parameter to be duplicated was the velocity. For all the three chemical models, the sensitivity of the afterbody quantities to changes in free-stream velocity was higher than the sensitivity to changes in free-stream temperature over almost the entire free-stream velocity range of interest. This is not surprising since at hypersonic speeds the kinetic energy constitutes a large part of the total enthalpy.

It was found that the sensitivities to changes in free-stream temperature were higher in the cases of the equilibrium-frozen and equilibrium-equilibrium models than the corresponding sensitivities for the frozen-frozen model.

Also, it was found that the flow fields were not Mach number independent over a substantial range of free-stream velocities, especially for the lower wedge angles. For the frozen-frozen model, it was found that all the sensitivities correlated in terms of the hypersonic similarity parameter $M_1 \sin \theta$, even at the fairly large angles involved, and the values of the hypersonic similarity parameter at which each afterbody variable became Mach number independent were delineated. Similar delineations were also made for the other two models.

In Sec. E, it was shown how the above results could be generalized to other slender bodies. The only restriction for the generalization is that the flow field about the body in question must satisfy the requirements of either the tangent-wedge or the shock-expansion approximations. For the tangent-wedge approximation to apply, the body must be such that the centrifugal effects and the variation of the pressure across the shock layer are small. For the shock-expansion approximation to apply, the body must be such that the flow field around it can be analyzed in terms of a single family of characteristics alone; that is, the reflection of disturbances from the shock wave and the vorticity layers must be negligible.

In the present study, we have considered only the sensitivity of the afterbody flow quantities immediately behind the shoulder. In particular, we have not considered the "blast-wave" effect which will be present some distance downstream of the shoulder. The analysis of this downstream influence of leading-edge bluntness for perfect gas flows by using the so-called blast-wave analogy is well known[207, 208]. A corresponding analysis to include real gas effects will, of course, be of great practical interest. Whalen[199] has made a start in this direction by using the equilibrium-frozen chemical model. However, even for this simplified case, Whalen was not able to obtain any general results since now the blast-wave effect is no longer self-similar and, in fact, depends on the details of the nose shape.

Finally, one further word need be said about the range of applicability of the results presented here. The present analysis is strictly valid only when small deviations from the free-stream conditions are considered. This analysis is analogous in spirit to a linearized analysis in which squares and

products of the derivations from a reference condition are neglected. Thus, within an accuracy of ten percent, deviations from the free-stream conditions of up to thirty percent can be considered since the error involved will be approximately equal to the square of the deviations.

VIII BLUNT BODIES

A.   INTRODUCTION

Because of its importance to reentry vehicle technology, the blunt-body flow field has received considerable attention in recent years. As cited earlier, the flow over a blunt body exhibits hypersonic characteristics at fairly low Mach numbers. The flow field is characterized by a strong, detached shock wave with a mixed subsonic, supersonic region behind. Moreover, throughout the velocity-altitude range of interest, real gas effects play an important role in determining shock-layer properties.

The stagnation-point boundary layer has also been extensively studied for hypersonic, blunt-body flows, the main purpose of these studies being to predict the surface heat-transfer rate. In addition to the state of the boundary layer, the state of the inviscid shock layer and the wall properties can significantly affect the heat-transfer rate.

In this section, the theoretical solutions to the blunt-body problem are noted. Pressure distributions and forces are discussed first in relation to Newtonian theory. The features of the flow field, including flow-field chemistry, are described next, first for the stagnation region and then for the afterbody flows. For the stagnation region, the results of not duplicating free-stream conditions are presented.

B.   NEWTONIAN THEORY FOR BLUNT-BODY FLOWS

Newtonian theory, which is described in Refs. 25, 40, and 184, assumes that the normal component of momentum of the flow is destroyed at the body surface and that the tangential component is unaltered. This leads to the Newtonian formula for the pressure distributions

$$C_p = 2 \sin^2 \theta$$

(VIII-1)

where θ is the angle of the surface relative to the free stream. The agreement of the Newtonian formula with experimental data is improved by an empirical modification suggested by Lees[24, 209]

$$C_P = C_{P_c} \sin^2 \theta$$

(VIII-2)

where C_{P_c} is the exact stagnation-point pressure coefficient. The agreement of this modified Newtonian formula for surface pressures with experimental data is very good, as Lees and many others have shown. Furthermore, this agreement extends to cases in which real gas effects are significant as is demonstrated, for example, by Rose[210]. Flax[18] has shown that real gas effects on the stagnation-point pressure behind a normal shock are much less than on the static pressure ratio across the shock. Thus, it can be concluded that the pressure and drag on sufficiently blunt bodies are very little influenced by real gas effects. Further evidence of this is provided by Gravalos et al[211] who have compared ideal and real air pressure distributions at $M_\infty = 15$ on a 30° half-angle cone having a spherical nose. The modified Newtonian formula gave good agreement with numerical calculations for both real and ideal gases. Also Chernyi[184] has shown that Eq. (VIII-2) works quite well for the front side of a circular cylinder at Mach numbers as low as 3 or 4. When the bow shock angle differs appreciably from the body angle, the modified Newtonian formula fails to provide good agreement with experiment.

The success of Newtonian theory has led to several extensive compilations of force coefficients based on this theory for various simple shapes (see, e.g., Refs. 187, 190, 212-215). It has also been used as the basis for calculating minimum drag bodies (see, e.g., Ref. 216). There is a large body of literature comparing Newtonian theory with experimental data on relatively blunt bodies. Typical, is the paper by Geiger[217] reporting extensive shock-tunnel tests of lift and drag measurements on half-sphere

cone models over a wide angle of attack range. Geiger found that the experimental data generally followed the trends predicted by simple Newtonian theory. In general, it is found that when viscous effects are unimportant, Newtonian theory can predict aerodynamic forces on blunt bodies with reasonable accuracy. In discussing the limitations of Newtonian theory, Larson[218] has pointed out that Newtonian theory applies if the vehicle's length is less than its diameter. Since this theory exhibits Mach number independence, it is only necessary that model and flight vehicle have the same geometry and that density-altitude and velocity be duplicated.

C. STAGNATION REGION

1. General Features

The flow in the stagnation region of a blunt body is very much like the flow behind a strong normal shock wave. It is just this fact which is responsible for the accuracy of the shock-mapping technique[48]. In the stagnation region, the fluid is strongly compressed and has low velocity. As the gas is strongly compressed and heated, it begins to dissociate and ionize. On the basis of normal shock wave results, it can be seen that for the lower altitudes of the altitude-velocity map a substantial portion of the shock layer is in thermochemical equilibrium. As the altitude increases, a smaller region surrounding the inviscid stagnation point will be in equilibrium.

Another feature of the high-altitude stagnation region is that the boundary layer thickens and its interaction with the shock layer can no longer be ignored. Hence, the shock layer and boundary layer can no longer be treated separately. Furthermore, the rates of chemical reaction in the stagnation-point boundary layer vary widely in the present range of interest. At the lower altitudes, the boundary layer is expected to be in chemical equilibrium. At the higher altitudes, where the boundary-layer thickness becomes large relative to the shock-layer thickness, the chemical reactions become unimportant relative to diffusion processes.

Establishing a precise boundary where the boundary layer can no longer be considered thin and an equilibrium stagnation point does not exist must await a solution which accounts simultaneously for finite-rate chemistry and higher-order viscous effects. For the purpose of examining the effect of not duplicating flight conditions, the presence of an inviscid, equilibrium stagnation point and a separate boundary layer will be assumed. For the region of the altitude-velocity map where test-flow nonequilibrium effects are important, the boundary layer will be assumed frozen. For the region where altitude and velocity cannot be fully duplicated, the boundary layer will be assumed in equilibrium.

Quite naturally, the same numerical methods have been employed for chemically-reacting shock layers as for the ideal gas case. Solutions for the axisymmetric, reacting flow field behind a bow shock wave have been obtained using the inverse method[45, 138] and the method of integral relations[219]. The inverse method has been used extensively. The computer program of Ref. 138 has been used specifically to verify the shock-mapping[48] and binary-scaling analysis[44]. The results obtained for nonequilibrium, inviscid flows behind bow shock waves have been discussed in detail before[45, 138].

Several investigators have obtained solutions for the stagnation-point boundary layer for various combinations of gas-phase reaction rates and wall catalycity. Notable among these studies are the works of Fay and Riddell[51] and Inger[67]. Fay and Riddell obtained numerical solutions of the stagnation-point boundary layer by using a binary model of air. Solutions were obtained for a wide range of the recombination-rate parameter and the limits of completely catalytic and non-catalytic walls. Correlation formulas were given for the limiting cases of frozen and equilibrium flow in the boundary layer. Inger later obtained solutions for the stagnation-point boundary layer for arbitrary values of the gas-phase reaction rate and surface catalycity.

These studies have shown that for Lewis numbers near unity and a catalytic wall, the surface heat-transfer rate is almost independent of the gas-phase chemistry. Further, for equilibrium flow and a reasonably cold wall, the heat transfer is independent of the surface catalycity.

2. Effects of Nonduplication of Altitude-Velocity Conditions

Using the similarity between normal-shock flows and the heat-transfer correlation formulas, some effects of not duplicating altitude and velocity conditions can be examined. First, consider the departure from full duplication likely in the lower-altitude region, i. e. , a mismatch in free-stream temperature while preserving free-stream velocity and density. At the lower boundary of this region, the shock layer and boundary layer can be assumed to be in equilibrium.

As cited in Section II-E-2, equilibrium normal-shock solutions have been computed in order to assess the effect of mismatch in static temperature. Since the corresponding stagnation temperature differs only slightly from the equilibrium temperature behind the shock and density in the stagnation region is virtually constant, stagnation-point properties for blunt bodies can be found from these results. The stagnation pressures have been computed from the formula[129]

$$\frac{p_o'}{p_\infty} = 1 + \frac{\rho_\infty U_\infty^2}{p_\infty} \left(1 - \frac{1}{2} \frac{\rho_\infty}{\rho_s} \right)$$

(VIII-3)

for the test-flow conditions given in Table II-1. The results are compared with those for the corresponding flight velocity and altitude[129,131] in the following table. The barred symbols denote the test flow or tunnel values. The unbarred symbols denote the flight or full duplication values.

TABLE VIII-1
COMPARISON OF FLIGHT AND TUNNEL VALUES OF STAGNATION PRESSURE

U_∞, Kfps	Altitude, Kft	p_o', atm	$\bar{p}_o'$, atm	Error, %
10	50	16. 2	17. 2	6. 2
15	50	36. 7	39. 0	6. 2
20	50	65. 7	69. 8	6. 2
25	88	16. 7	17. 6	6. 2
30	125	4. 29	4. 46	4. 2
35	170	0. 948	0. 941	<1. 0

This table shows the expected trends. The effect of the mismatch in static temperature (and pressure) on pitot pressure is compensated by attendant increases in velocity for $h_v = 50,000$ ft. Since Newtonian theory[25] predicts that the drag is proportional to pitot pressure, these results also indicate the error in drag measurements resulting from the postulated mismatches in static temperature.

The results of the normal shock calculations described in Sec. II-E-2 can also be used to calculate the effects of mismatch in static temperature on stagnation-point heat transfer. This has been done, assuming the equilibrium stagnation-point properties are given by those obtained from the normal shock solutions and Fay and Riddell's correlation formula for an equilibrium boundary layer. For a constant Lewis number, the heat-transfer rate is given by [51]

$$ q = \frac{0.76}{Pr^{0.6}} \left(\rho_w \mu_w \right)^{0.1} \left(\rho_s \mu_s \right)^{0.4} \left\{ 1 + \left(Le^{0.52} - 1 \right) \frac{H_D}{H_s} \right\} \left(H_s - H_w \right) \sqrt{du_e/ds} $$

(VIII-4)

For a stagnation-point flow, modified Newtonian theory yields[25]

$$ \frac{du_e}{ds} = \frac{1}{R_N} \sqrt{\frac{2 \left(p_s - p_\infty \right)}{\rho_s}} $$

(VIII-5)

Also, assuming a cold wall ($H_w \ll H_s$) and neglecting p_∞ relative to p_s , this formula reduces to

$$ q = \frac{0.76}{Pr^{0.6}} \left(\rho_w \mu_w \right)^{0.1} \left(\rho_s \mu_s \right)^{0.4} \left\{ 1 + \left(Le^{0.52} - 1 \right) \frac{H_D}{H_s} \right\} \frac{H_s}{\sqrt{R_N}} \sqrt[4]{\frac{2 p_s}{\rho_s}} $$

(VIII-6)

Again letting the bar symbols denote the tunnel case and the unbarred symbols the flight case, consider $\bar{q}/q$ when Eq. (VIII-6) is used for the heat-transfer rate. If it is assumed that

$$ \rho_s \mu_s = \bar{\rho}_s \bar{\mu}_s , \qquad Pr = \bar{Pr} $$

(VIII-7)

and

$$\frac{1 + \left(\overline{Le}^{\,0.52} - 1\right) \dfrac{\bar{H}_D}{\bar{H}_s}}{1 + \left(Le^{0.52} - 1\right) \dfrac{H_D}{H_s}} \cong 1 \qquad , \tag{VIII-8}$$

then

$$\frac{\bar{q}}{q} \cong \frac{\bar{H}_s}{H_s} \sqrt[4]{\frac{\bar{p}_s}{p_s} \frac{\rho_s}{\bar{\rho}_s}} \tag{VIII-9}$$

Since the mismatches in static temperature considered are known not to lead to significantly different stagnation-point properties, the above assumptions should be accurate.

The values of the ratios of stagnation-point enthalpy, velocity gradient $\sqrt{\bar{p}_s \rho_s / p_s \bar{\rho}_s}$ for equal nose radii and heat transfer are shown in the following table for the tunnel and flight conditions of Table II-1, Section II-E-2.

Table VIII-2

EFFECT OF MISMATCH IN AMBIENT TEMPERATURE ON STAGNATION-
POINT ENTHALPY, VELOCITY GRADIENT,
AND HEAT TRANSFER

U_∞, Kfps	Altitude, Kft	$\sqrt{\dfrac{\bar{p}_s}{p_s} \dfrac{\rho_s}{\bar{\rho}_s}}$	$\dfrac{\bar{H}_s}{H_s}$	$\dfrac{\bar{q}}{q}$
10	50	1.07	1.11	1.15
15	50	1.07	1.09	1.13
20	50	1.06	1.08	1.11
25	88	1.05	1.02	1.05
30	125	1.06	1.01	1.04
35	180	1.01	1.00	1.00

The results presented in Tables VIII-1 and 2 indicate that preserving velocity and density-altitude within the limits of tunnel performance assumed here can lead to moderate errors in the observable quantities of blunt-body flow fields. These effects are most pronounced at the lower boundary of the velocity-altitude range of interest. It should be emphasized that the effects of mismatch in ambient temperature will be appreciably greater for less optimistic assumptions for tunnel performance.

It is helpful to consider the above results further in the light of results for normal shock waves. Throughout the flight altitude-velocity map of interest, the real gas normal shock solutions show that the density ratio, ρ_∞ / ρ_s , is much less than the ideal gas value of 1/6, and that the stagnation conditions immediately behind the shock are very nearly those given by the equilibrium conditions behind the shock. Thus, since the strong shock approximation is also valid in this altitude-velocity range,

$$ H_s \cong \frac{1}{2} U_\infty^2 \qquad\qquad p_s \cong \rho_\infty U_\infty^2 \qquad\qquad \text{(VIII-10)} $$

From these relations it can be seen that the error made in H_s and p_s by preserving density-altitude and velocity stems from the higher values of p_∞ and T_∞ . For the postulated tunnel performance, the required values of $\overline{T}_\infty$ and $\overline{p}_\infty$ are sufficiently high that

$$ \overline{H}_s = \overline{H}_\infty + \frac{1}{2} \overline{U}_\infty^2 \qquad\qquad \text{(VIII-11)} $$

$$ \overline{p}_s = \overline{p}_\infty + \overline{\rho}_\infty \overline{U}_\infty^2 \qquad\qquad \text{(VIII-12)} $$

where $\overline{H}_\infty$ and $\overline{p}_\alpha$ are no longer negligible compared to $\frac{1}{2} \overline{U}_\infty^2$ and $\overline{\rho}_\infty \overline{U}_\infty^2$.

Another conclusion which may be drawn concerning lack of duplication in the lower altitude region is that duplicating total enthalpy will not simulate stagnation pressure and stagnation-point heat transfer. The above discussed mismatches in static temperature resulted from trying to preserve density-altitude and velocity. If instead, total enthalpy and

density were matched, then the attendant mismatch in velocity would affect both the stagnation pressure and heat transfer.

Equilibrium normal shock calculations were also performed for the total enthalpy and density-altitude corresponding to U_∞ = 10,000, 15,000 and 20,000 fps at 50,000 ft altitude. The test-flow velocity was the highest attainable for the assumed tunnel performance limit. The resulting tunnel values of stagnation pressure and heat transfer are shown in the following table.

Table VIII-3

ERRORS IN STAGNATION PRESSURE AND HEAT TRANSFER FOR TOTAL
ENTHALPY AND DENSITY-ALTITUDE
DUPLICATION FOR 50,000 FT ALTITUDE

U_∞, Kfps	$\bar{U}_\infty$, Kfps	$\bar{p}_o'/p_o'$	$\bar{\rho}_2/\rho_2$	$\bar{q}/q$
10	9.17	0.902	0.865	1.01
15	14.2	0.957	0.913	1.01
20	19.1	0.975	0.928	1.01

As can be seen from this table, duplicating total enthalpy and density-altitude leads to smaller errors in stagnation-point heat transfer than when velocity and density-altitude are duplicated. The error in stagnation pressure is lower for the higher velocities at a given altitude. Both of these behaviors are direct consequences of the assumed facility capability. The assumed performance limit on a Mollier diagram (see Fig. 6) has a larger slope than the constant density lines. Thus, the error in velocity and, hence, pitot pressure is lower for the higher velocities ($p_o' \cong \rho_\infty U_\infty^2$). The error in velocity would be larger for less optimistic assumptions on tunnel performance. The larger errors in velocity would in turn lead to larger errors in heat transfer.

3. Effects of Test-Flow Nonequilibrium

Analytical studies of the effects of test-flow nonequilibrium have been done by previous investigators. Inger[152] has examined the effect of free-stream nonequilibrium on the frozen and equilibrium flow behind normal and oblique shock waves. On the basis of these studies, Inger[220] further examined the effects of free-stream nonequilibrium on viscous and inviscid stagnation flows. Gibson[50] has treated the effect of ambient dissociation on the nonequilibrium flows over blunt bodies using his earlier work on shock-mapping [48]. For streamlines away from the stagnation streamline, the results also depend on his earlier results of binary scaling [44].

For application to wind-tunnel testing, it is useful to compare a free-flight and tunnel flow of the same total enthalpy. Thus, assuming that if equilibrium were maintained in the nozzle expansion of the test flow, the flight conditions would be fully duplicated; nonequilibrium effects result in the following differences between the tunnel and flight ambient streams. The ratio of tunnel to flight velocity is given by

$$\frac{\overline{U}_\infty}{U_\infty} = \sqrt{1 - \frac{\overline{H}_f}{H_o}}$$

(VIII-13)

This equation assumes that the thermal contribution to the static enthalpy is negligible in the test section. The static temperature and pressure are lower for the nonequilibrium test flow, perhaps as much as an order of magnitude [9]. However, the mass flux $\rho_\infty U_\infty$ will be virtually unaffected by nonequilibrium effects.

For equilibrium and nonequilibrium test flows having the same total enthalpy, Inger[220] considered the nonequilibrium effects on such quantities as shock density-ratio, stagnation-point velocity gradient, stagnation pressure, and stagnation-point heat transfer. Inger's results are applicable here when the nonequilibrium effect is considered in terms of H_f. However, Inger related H_f to α_∞ by assuming a binary model

150

for air. In the present work, the composition of the test flow has been related to H_f through the results of numerical solutions for nonequilibrium nozzle flows (see Section II-D).

Using the same approach as was used to assess the effects of mismatch in static temperature, some approximate results may be easily obtained for the effects of free-stream nonequilibrium. As discussed previously, test flow nonequilibrium is expected to be important at the higher altitudes in the range of interest. Thus, the strong-shock approximations will be valid for the velocities being considered.

In the previous section, the effects of not duplicating velocity and altitude conditions was to increase the static pressure and temperature so that the strong-shock approximations broke down. However, nonequilibrium effects decrease the static temperature and pressure. The chemical contribution to the static enthalpy may not be negligible. Hence, the strong shock approximation remains valid for the momentum equation, but not the energy equation.

Consider the strong shock approximation for p_o', i.e.,

$$p_o' = \rho_\infty U_\infty^2 \left(1 - \frac{1}{2} \frac{\rho_\infty}{\rho_s}\right) \qquad \text{(VIII-14)}$$

Further assuming $\rho_\infty/\rho_s \ll 1$ for both tunnel and flight cases and that $\rho_\infty U_\infty = \bar{\rho}_\infty \bar{U}_\infty$, then

$$\frac{\bar{p}_o'}{p_o'} = \frac{\bar{U}_\infty}{U_\infty} = \sqrt{1 - \frac{\bar{H}_f}{H_o}} \qquad \text{(VIII-15)}$$

Using this equation, the approximate nonequilibrium effect on pitot pressure may be found for the altitude-velocity map of Fig. 2. The maximum effect observed for the postulated relation of nonequilibrium effects and flight conditions would be 13% (where $H_f/H_o = 0.25$).

The effect of test-flow nonequilibrium on stagnation-point heat transfer can also be estimated. Fay and Riddell's correlation formula[51]

151

for frozen flow is used in this case because of the higher altitudes involved. Fay and Riddell give for a frozen boundary layer and a catalytic wall

$$\left(\frac{Nu}{\sqrt{Re}}\right)\bigg/\left(\frac{Nu}{\sqrt{Re}}\right)_{Le=1} = 1 + \left(Le^{0.63} - 1\right)\frac{H_D}{H_s} \qquad \text{(VIII-16)}$$

Since for $Le = 1$ the frozen and equilibrium results for the stagnation-point heat transfer are the same, then for a frozen boundary layer and a cold wall

$$q = \frac{0.76}{Pr^{0.6}}\left(\rho_w \mu_w\right)^{0.1}\left(\rho_s \mu_s\right)^{0.4}\left\{1 + \left(Le^{0.63} - 1\right)\frac{H_D}{H_s}\right\}\frac{H_s}{\sqrt{R_N}}\sqrt[4]{\frac{2 p_s}{\rho_s}} \qquad \text{(VIII-17)}$$

Then, since we are comparing flight and tunnel flows for a given total enthalpy and equal nose radii

$$\frac{\bar{q}}{q} \cong \frac{1 + \left(Le^{0.63} - 1\right)\bar{H}_D/H_s}{1 + \left(Le^{0.63} - 1\right)H_D/H_s}\sqrt[4]{\frac{\bar{p}_s}{p_s}\frac{\rho_s}{\bar{\rho}_s}} \qquad \text{(VIII-18)}$$

where it has been assumed that $\overline{\rho\mu} = \rho\mu$ and $\bar{P}_r = P_r$. Since the stagnation enthalpy is the same for both cases, and, as seen above, the effect of ambient dissociation on stagnation pressure is not large, then $\bar{H}_D$ should not be appreciably different from H_D. Assuming $\bar{H}_D \cong H_D$ and noting that, for $Le \cong 1$, the factor $\left(Le^{0.63} - 1\right)$ further reduces the difference between $\bar{H}_D$ and H_D

$$\frac{\bar{q}}{q} \cong \sqrt[4]{\frac{\bar{p}_s}{p_s}\frac{\rho_s}{\bar{\rho}_s}} \qquad \text{(VIII-19)}$$

Using the result in Eq. (VIII-15) for the effect on pitot pressure,

$$\frac{\bar{q}}{q} = \sqrt[4]{\frac{\bar{U}_\infty}{U_\infty}\frac{\rho_s}{\bar{\rho}_s}} = \left(1 - \frac{\bar{H}_f}{H_o}\right)^{1/8}\left(\frac{\rho_s}{\bar{\rho}_s}\right)^{1/4} \qquad \text{(VIII-19a)}$$

152

Now, since it has been assumed that $\rho_\infty U_\infty = \bar{\rho}_\infty \bar{U}_\infty$, then

$$\frac{\rho_\infty}{\bar{\rho}_\infty} = \gamma\sqrt{1 - \frac{\bar{H}_f}{H_o}} \qquad \text{(VIII-20)}$$

so that

$$\frac{\bar{q}}{q} = \gamma\sqrt[4]{\left(1 - \frac{\bar{H}_f}{H_o}\right)\left(\frac{\bar{\rho}_\infty}{\bar{\rho}_s}\right)\left(\frac{\rho_s}{\rho_\infty}\right)} \qquad \text{(VIII-21)}$$

Inger[220] obtained results for the effect of free-stream non-equilibrium on the equilibrium density-ratio across a normal shock wave. He shows that for a comparison at fixed total enthalpy, the effect of ambient dissociation is to increase ρ_∞/ρ_s . Thus, it can be seen from Eq. (VIII-22) that the effect on stagnation-point heat transfer is less severe than the effect on pitot pressure. Inger states that $\bar{H}_f$ must be greater than 0.1 times the total enthalpy to have an observable affect on the density-ratio. However, for $\bar{H}_f > 0.1\,H_o$, $\bar{\rho}_\infty/\bar{\rho}_s$ increases appreciably with increasing $\bar{H}_f$. For $\bar{H}_f$ greater than about $0.5\,H_o$, $\left(\bar{\rho}_\infty/\bar{\rho}_s\right)\big/\left(\rho_\infty/\rho_s\right)$ can be as high as 2 or 3.

The nonequilibrium effects on the density-ratio and on $\bar{H}_f$ have opposing effects on the stagnation-point heat transfer. On the basis of Inger's results for $\left(\bar{\rho}_\infty/\bar{\rho}_s\right)\big/\left(\rho_\infty/\rho_s\right)$ and the present assumptions for nozzle non-equilibrium effects, the maximum effect of ambient dissociation on $\bar{q}/q$ is about 10%. For example, for $\bar{H}_f/H_o = 0.25$ which is the value obtained at $U_\infty = 10,000$ fps and 250,000 ft (Fig. 5) and assuming $\left(\bar{\rho}_\infty/\bar{\rho}_s\right)\big/\left(\rho_\infty/\rho_s\right) = 2$ as an upper bound, then $\bar{q}/q = 1.1$.

Inger[220] points out that if the nonequilibrium effect on ρ_∞/ρ_s is too severe, the strong-shock assumptions may break down (see Eq. (VIII-14)). It should be mentioned that if the effect on ρ_∞/ρ_s is large, then the further assumption made here, i.e.,

$$\frac{1 + \left(Le^{0.63} - 1 \right) \dfrac{\overline{H_D}}{H_s}}{1 + \left(Le^{0.63} - 1 \right) \dfrac{H_D}{H_s}} \cong 1$$

will also break down. For the tunnel performance postulated here, it is likely that very large values of H_f will not be the limiting assumption. The model of a thin boundary layer and an equilibrium stagnation point may well be a more suspect assumption.

The validity of the thin, stagnation-point boundary layer assumption has been discussed in Section IV-B-2. It has been noted that vorticity interaction begins to be important for $\rho_\infty \sqrt{H_o} \, R/\mu_\infty > 10^4$. For nose radii of the order of 1 ft, this parameter is of this order for the upper portion of the present altitude-velocity map[58]. For small test-model nose radii, say $\ll 1$ ft, the stagnation region may be a fully viscous layer at the higher altitudes of interest here.

Using a frozen-flow approximation and Cheng's thin shock-layer model,[58] Buckmaster[75] has examined the effects of ambient dissociation on viscous stagnation flows. These studies were done for a diatomic gas and showed that for large free-stream dissociation fractions, α_∞, the convective heat transfer could be significantly altered. The assumption of frozen, viscous stagnation flow again may not be valid except for very small bodies in the altitude range of interest. As yet, no solutions for stagnation-point heat transfer are available for the case where viscous-layer effects and gas-phase reaction are important.

Before going on to discuss afterbody flows, some further results on the effects of free-stream nonequilibrium deserve mention. As cited earlier, Gibson determined the effects of ambient dissociation on the non-equilibrium flow behind shock waves in air[50]. For a comparison of dissociated and undissociated free streams at fixed enthalpy, the effects of free-stream dissociation decay as chemical equilibrium is approached[137]. Near the shock, however, the species concentrations may be appreciably different. Consequently, the radiation properties would also differ markedly. A

highly dissociated, slightly ionized free stream also results in a substantially different shock-layer electron distribution. Such effects would be important in any spectroscopic or microwave studies of blunt-body stagnation flows.

D. AFTERBODY FLOWS

There is not as yet as much information available on nonequilibrium afterbody flow fields as there is for the stagnation region. Some solutions have been obtained using the method of characteristics. For a reacting gas flow, the computations are far more complex than for the supersonic flow of an ideal gas. Both the method of solution and representative results are given in Refs. 221 and 222. Most of the studies of nonequilibrium afterbody flows have used a streamtube approximation [45, 137, 223, 224], usually specifying the streamline pressure distribution. The pressure distributions employed have been the experimental values or those obtained from ideal gas computations.

Hall, Eschenroeder, and Marrone[45] reported solutions for inviscid-afterbody flows over hemisphere cylinders. They assumed the surface pressure distribution to be the Newtonian result for the forebody and a matched blast-wave value for the afterbody. The method of numerical solution employed was a modification of that originally developed for nozzle flows by Eschenroeder, Boyer, and Hall[8]. Using this same method, further calculations for a hemisphere cylinder and a blunted cone were done by Burke, Curtis, and Boyer[137].

Some justification exists for using quasi-one-dimensional streamtube computations with a specified pressure distribution. In Reference 221, equilibrium, nonequilibrium, and frozen solutions were presented for flows over conical afterbodies with spherical and ogival nose shapes. These results show the pressure distribution to be insensitive to real gas effects. Furthermore, nonequilibrium streamtube calculations for the body stream-line were compared with the corresponding characteristics solution. Good agreement was observed for both the gas dynamic quantities and the flow composition.

The results obtained in Ref. 45 for a hemisphere-cylinder show that the flow freezes rapidly in the expansion downstream of the stagnation point. The behavior is much like that in a nonequilibrium nozzle expansion. However, the results obtained in Ref. 137 for a blunted cone indicate that as the pressure approaches the cone pressure, the flow chemistry begins to relax toward equilibrium. The pressure distribution assumed there for the blunted cone typified a case for which overexpansion occurred on the afterbody. The temperature and the O_2 and NO concentrations follow the variations in surface pressure. The N_2 and O concentrations remained constant at essentially their undissociated and fully dissociated values, respectively.

On the basis of studies of ideal gas flows over blunted cones, the possibility of a significant overexpansion in the afterbody flow is known to exist[225]. The comparison of a characteristics solution and surface stream-tube result for a blunted cone, which was discussed in Ref. 221, did not exhibit this overexpansion. The validity of using an ideal gas pressure distribution as an input to a nonequilibrium streamtube calculation has not been established, in general. It is not known how nonequilibrium phenomena will affect the overexpansion observed in blunted-cone flows.

The method of solution developed by Curtis and Strom[222] also accounts for the displacement effects of the boundary layer. No details of the boundary-layer flow are computed, but, using the assumption of local similarity, the boundary-layer displacement effects on the inviscid flow are determined as that solution proceeds.

Thus far, the solutions for the real gas boundary layer on blunted cones have been obtained using the simplifying assumption of local similarity. Lees[59] first applied this approach to the calculation of the heat transfer on blunt bodies. Lees observed that for relatively large angle cones (half-angles of 30°-40°) the heat-transfer-rate distribution is almost the same as for the "equivalent sharp-nosed cone". For slender cones, however, the heat-transfer rate is expected to be lower than the equivalent cone value aft of the shoulder. The question of correlating heat-transfer rates on slender cones is also discussed in Sections IV and VI.

As for the forebody region, the afterbody flow on a blunt vehicle will be almost fully viscous at the higher altitudes of interest here. Cheng[58] has studied the viscous flow of an ideal gas over blunted cones. To date, there are no solutions available for the case where the shock layer is fully viscous and nonequilibrium effects are important.

Although the above methods of solution exist for afterbody flows, there has not as yet been a systematic study of the influence of variations in free-stream conditions. Consequently, it is not possible without further study to estimate the effects of not duplicating free-stream conditions on afterbody pressure and heat-transfer distributions.

At the lower altitudes of the pertinent altitude-velocity map, it has been theorized that facility limits will be the cause of not duplicating flight conditions. In this region, simulating either the stream velocity or ambient static temperature may have to be relaxed. Only at the lower limit of this region would Cheng's equilibrium flow similitude studies[58] (see Sec. IV-D) be applicable to the whole flow field. However, since it is for this region that the assumption of a thin boundary layer remains valid, it should be possible to apply the existing methods described above to this problem. For example, nonequilibrium streamtube calculations could be combined with locally similar boundary-layer solutions to assess the effect of different free-stream conditions on heat-transfer rates. Furthermore, additional justification for assuming ideal gas pressure distributions could be obtained using existing methods for computing afterbody flows. Such a result may well be combined with the correlation scheme developed for nonequilibrium nozzle flows[9] in order to predict inviscid, afterbody flow properties. That is, for a given geometry, the nonequilibrium surface streamline flow may depend only on the entropy at the equilibrium stagnation point. In addition to blunted cones, which are currently receiving much attention, these procedures could also be applied to other blunt bodies such as the hemisphere cylinder.

At the higher altitudes in the region of interest, significant departures from equilibrium are expected in the corresponding test flows. This is also the region of the altitude-velocity map for which both viscous and real gas effects are prominent. An investigation of the effects of free-stream non-

equilibrium on viscous, nonequilibrium afterbody flows must await further research on this problem.

IX.   EFFECTS OF SEEDING TEST FLOW FOR MHD AUGMENTATION

A.   INTRODUCTION

In order to use MHD acceleration of test flows, the electrical conductivity of air must be increased [2]. Alkali-metal seeding is an effective method because these elements are easily ionized. In this section, the effects of seeding a test flow with up to 1% by weight of alkali metal are examined. The influence of the seed on the test-flow properties are first described. Then, the effects on typical model flow-field quantities are estimated. Finally, the question of seed condensation is considered and the possible consequences discussed.

B.   EFFECT OF SEED ON TEST-FLOW PROPERTIES

Nonequilibrium expansions of ionized air through hypersonic nozzles have been studied previously[226]. Numerical solutions are available for the variation of the thermodynamic properties and species concentrations along a nozzle. A limited number of unpublished solutions for airflows seeded with alkali metals have been calculated at CAL.

In nonequilibrium nozzle expansions of ionized air the electron concentration remains significantly above the equilibrium-flow value. However, the electron concentration does not freeze to the extent that dominant neutral species concentrations do[226]. The reason that the electron concentration does not exhibit the rapid freezing behavior is that the governing deionization paths are bimolecular reactions.

The numerical solutions which have been obtained accounting for the effects of alkali-metal seed have included sodium, potassium, or cesium as the additive elements. In general, these solutions indicate that the

seeding does not affect the thermodynamic properties or velocity of the flow. Furthermore, the neutral-species chemistry is not appreciably altered. The electron density is significantly enhanced because the alkali metals are more readily ionized than the air species.

One of the solutions which has been published is for cesium-seeded air[227]. This solution is for the expansion of air from equilibrium reservoir conditions of 7400°K, 340 atm, through the CAL 6-ft shock tunnel nozzle. Results were obtained for pure air and air plus 0.001 mole fraction of cesium (0.005% by weight). The effect of adding the seed on the test-section values of the gasdynamic variables and dominant neutral species was less than 1%. On the other hand, the electron density was increased by a factor of 500.

Another solution, performed for AEDC by CAL and communicated privately[228], considered potassium seeding (0.0025% by weight). This computation was for the flow in a conical nozzle located downstream of an MHD accelerator. The conditions at the accelerator exit were $T = 5000$ °K; $p = 70$ atm and $H_o/R = 1.2 \times 10^5$ °K. In this case, the gasdynamic variables and dominant neutral-species concentrations were virtually unaffected by the presence of the seed. The electron density at the exit of the conical nozzle was increased from approximately 10^{10} per cc. to about 5×10^{12} per cc.

While the above-mentioned solutions are for smaller seed concentrations than of interest here, the conclusions concerning the effects on test-flow properties remain valid. The following arguments may be advanced to justify extrapolating the above conclusions to slightly higher seed concentrations and other test-flow conditions in the range of interest. First of all, the addition of 1% by weight of seed (which corresponds to mole fractions of less than 1%) cannot significantly affect the molecular weight of the mixture. Hence, the thermal equation of state is not altered by the seed. Furthermore, for the test-flow velocities of interest, the energy required to completely ionize the seed element is negligible compared with the total enthalpy of the flow. Thus, the ionization reactions involving the seed element are thermally unimportant.

C. SEEDING EFFECTS ON FLOW-FIELD SIMULATION

In this section, the influence of 1% by weight of alkali-metal seed on the measurement of typical flow-field quantities, such as pressure and heat transfer, is considered. The same arguments given in the previous section for the seed having a negligible effect on the gasdynamic variables and neutral-species chemistry in nozzle flows also apply to blunt-body flows. However, the number density of electrons can be significantly affected. These arguments can be supported with a limited number of numerical solutions.

The most striking evidence for the alkali-metal seed not affecting the gasdynamic variables and neutral-species chemistry in body flow fields appears in Ref. 227. While the main concern in that study was MHD inter- action in the stagnation region of a blunt body, numerical solutions were obtained for the zero field case, with and without the presence of seed. The solutions were obtained for the stagnation streamline using normal shock- wave solutions and the shock-mapping technique[48]. One solution for the forebody shock layer was obtained by the inverse method and the results near the stagnation streamline were compared with the shock-mapping solu- tion. The agreement again confirmed the validity of this technique[227].

Specifically, the blunt-body stagnation-region solutions of Ref. 227 were for a 6-in. diameter sphere and used the results of the nozzle-flow solutions mentioned in the previous section to obtain the free-stream condi- tions. For both the seeded and unseeded cases, the free-stream conditions were $U_\infty = 16,200$ fps, and $\rho_\infty = 1.52 \times 10^{-8}$ gms/cc. The variation of the density, temperature, and neutral-species concentrations along the stagnation streamline were affected very little by the presence of the seed. The electron density at the stagnation point was slightly more than a factor of 10 higher in the seeded case.

Since the gasdynamic variables were unaffected by the presence of the metallic seed, force or pressure-distribution measurements will, in turn, also be unaffected. A substantial increase in the electron density in the flow field, however, precludes studies involving electromagnetic signal propagation

through the flow. While the above-mentioned effects of seed on the gasdynamic properties can be expected to be small throughout the range of flow conditions of interest, the effects on electron density may not. An indication of the variation of the effect of seed on electron concentration for the flight conditions of interest is obtained below.

An upper bound for the effect of seed on the number density of electrons at equilibrium behind a strong normal shock can be obtained as follows. Assume that all the seed species present are in the form of singly-ionized atoms and that the thermodynamic-state variables are unchanged from the pure-air normal-shock values. With this assumption and 1% by weight of seed, the number density of the seed-produced electrons is

$$\bar{n}_{seed} = \frac{0.01 \, N_0 \, \rho}{\mathcal{m}_{seed}}$$

<div align="right">(IX-1)</div>

where N_0 is Avogadro's number, ρ the gas density at equilibrium behind a normal shock in air, and $\mathcal{m}_{seed}$ is the atomic weight of the seed element. Using this equation and tables of Wittliff and Curtis[129] and Marrone[131], the number density of seed-produced electrons can be compared with the number density of electrons behind shock waves in air. Results for typical flight conditions in the range of interest and for Na, K and Cs as the seed elements are presented in the following table.

<div align="center">

TABLE IX-1

COMPARISON OF UPPER BOUND ON NUMBER DENSITY OF
SEED-PRODUCED ELECTRONS WITH VALUES BEHIND
NORMAL SHOCK WAVES IN UNSEEDED AIR

</div>

Altitude (Kft)	U_∞ (Kfps)	Seed-produced electrons (#/cc)			Pure Air Electron Density (#/cc)
		Na	K	Cs	
50	10	4.1×10^{17}	2.4×10^{17}	7.1×10^{16}	$\ll 10^{15}$
50	20	5.6×10^{17}	3.4×10^{17}	1.0×10^{17}	3.8×10^{16}
250	10	1.1×10^{14}	6.5×10^{13}	1.9×10^{13}	$\ll 10^{11}$
250	20	1.7×10^{14}	1.0×10^{14}	3.0×10^{14}	3.9×10^{12}
250	30	1.9×10^{14}	1.2×10^{14}	3.4×10^{13}	2.9×10^{14}

These results indicate that for the higher flight velocities, the number density of free electrons in the stagnation region of a blunt body may be unaffected by seeding the test flow. However, the results for the lower velocities show the opposite trend, and furthermore, suggest that the number of electrons in the flow about slender bodies would be significantly increased at the higher velocities.

Although the amount of seeding considered here is not expected to affect the gasdynamic variables in test-flow fields, this was not felt to be sufficient justification for neglecting its effect on the measurement of surface heat transfer. The effect of electron-ion recombination on the surface may add to the heat transfer obtained without seeding. To investigate this effect, the influence of seeding on stagnation-point heat transfer has been estimated.

As discussed above, the presence of 1% by weight of seed has negligible influence on the thermodynamic properties and composition of air. Also, this amount of seed will not significantly alter the frozen thermal conductivity of air[229]. If it is further assumed that the wall is cold and, hence, the thermal energy of the seed species near the wall is negligible, the stagnation-point heat transfer in the presence of seed can be written

$$q_w = \bar{q}_w + \left(\rho c_i V_i h_i^o \right)_w$$

(IX-2)

where $\bar{q}_w$ is the stagnation-point heat transfer in unseeded air, and c_i, V_i, and h_i^o are the mass fraction, diffusion velocity, and formation energy of singly-ionized seed atoms.

Since it is desired to simply estimate the maximum effect of seed, it is reasonable to assume that all of the seed exists as singly-ionized atoms at the edge of the boundary layer, that no gas-phase recombination of the ion occurs in the boundary layer, and that the ion-concentration profiles are similar. With these assumptions, the equation expressing conservation of singly-ionized seed atoms becomes, in the usual compressible boundary layer coordinates[59],

$$\left[\frac{l}{Sc_i}\mathcal{S}_{i\eta}\right]_\eta + f\mathcal{S}_{i\eta} = 0$$

(IX-3)

where $l = \rho\mu/\rho_w\mu_w$, Sc_i = Schmidt number based on diffusion coefficient of ions into the mixture, f is the dimensionless stream function and $\mathcal{S}_i = c_i/c_{ie}$ is the dimensionless concentration variable.

Further assuming that l/Sc_i is a constant decouples the equation for $\mathcal{S}_i$ from the remaining conservation equations. In addition, assuming a completely catalytic wall, i.e., $\mathcal{S}_i(0) = 0$ permits Eq. (IX-3) to be integrated to

$$\mathcal{S}_i(\eta) = \frac{\int_0^\eta exp\left\{-\frac{Sc_i}{l}\int_0^\beta f(\alpha)d\alpha\right\}d\beta}{\int_0^\infty exp\left\{-\frac{Sc_i}{l}\int_0^\beta f(\alpha)d\alpha\right\}d\beta}$$

(IX-4)

For a stagnation point $u_e = Ks$ and the seed contribution to the heat transfer may be written

$$q_{seed} = \left(\rho c_i V_i h_i^o\right)_w = \sqrt{2\mu_w\rho_w K}\,\frac{l}{Sc_i}h_i^o c_{ie}\frac{\partial\mathcal{S}_i}{\partial\eta}\bigg)_{\eta=0}$$

(IX-5)

Evaluating $\partial\mathcal{S}_i/\partial\eta)_{\eta=0}$ from Eq. (IX-4),

$$\frac{\partial\mathcal{S}_i}{\partial\eta}\bigg)_{\eta=0} = \frac{1}{\int_0^\infty exp\left\{-\frac{Sc_i}{l}\int_0^\beta f(\alpha)d\alpha\right\}d\beta}$$

(IX-6)

The denominator of Eq. (IX-6) may integrated, using the Fage-Falkner approximation, $f(\eta) \cong f''(0)\eta^2/2$ which had previously been applied successfully to reacting boundary layers[230]. Then

$$\frac{\partial\mathcal{S}_i}{\partial\eta}\bigg)_{\eta=0} = \frac{3}{\Gamma(1/3)}\left[\frac{Sc_i\,f''(0)}{6l}\right]^{1/3}$$

(IX-7)

which can be used in Eq. (IX-5) to obtain q_{seed}.

Using this result for q seed' and Hoshizaki's[231] correlation formula

$$\bar{q}_w = \frac{2.59 \times 10^4}{\gamma R_N} \left(\frac{K R_N}{U_\infty}\right)^{1/2} (\rho_\infty)^{1/2} \left(\frac{U_\infty}{10^4}\right)^{3.19} \text{BTU/ft}^2\text{-sec}$$

(IX-8)

where $[U_\infty]$ = fps, $[R_N]$ = ft, $[\rho_\infty]$ = slugs/ft^3, the ratio $q_{seed}/\bar{q}_w$ can be written as

$$\frac{q_{seed}}{\bar{q}_w} = \frac{3\sqrt{2\rho_w \mu_w} \left(\frac{\ell}{Sc_i}\right)^{2/3} h_i^o \varkappa_{i_e} \left(\frac{f''(0)}{6}\right)^{1/3}}{2.59 \times 10^4 \, \Gamma(1/3) \sqrt{\frac{\rho_\infty}{U_\infty}} \left(\frac{U_\infty}{10^4}\right)^{3.19}}$$

(IX-9)

Assuming the seed ion to be $K^+\left(h_i^o = 4.6 \times 10^3 \text{ BTU/lb}\right)$, T_w = 300°K (μ_w = 3.87 x 10^{-7} lbs sec/ft^2), the following numerical data

$$f''_{s.p.}(0) = 0.58 \qquad \frac{\ell}{Sc_i} = 2 \qquad \varkappa_{i_e} = 0.01$$

reduce Eq. (IX-9) to

$$\frac{q_{seed}}{\bar{q}_w} = \frac{4.1 \times 10^{-5} \sqrt{\rho_w/\rho_\infty} \sqrt{U_\infty}}{\left(U_\infty/10^4\right)^{3.19}}$$

(IX-10)

Now, using $\rho_w = \rho_s T_s/T_w$,

$$\frac{q_{seed}}{\bar{q}_w} = \frac{4.1 \times 10^{-5} \sqrt{\frac{\rho_s}{\rho_\infty} \frac{T_s}{T_w}} \sqrt{U_\infty}}{\left(U_\infty/10^4\right)^{3.19}}$$

(IX-11)

Next, using Eq. (IX-11) and the tables of Wittliff and Curtis[129] and Marrone[131], $\frac{q_{seed}}{\bar{q}_w}$ has been evaluated for the following velocity and altitude conditions of interest. The results are given in the following table.

TABLE IX-2
COMPARISON OF STAGNATION-POINT HEAT TRANSFER
DUE TO SEED-PRODUCED ELECTRON WITH UNSEEDED AIR

U_∞ (Kfps)	Altitude (Kft)	$q_{seed}/\bar{q}_w$
10	50	3.2×10^{-2}
10	250	3.4×10^{-2}
20	50	7.8×10^{-3}
35	170	2.6×10^{-3}
35	250	2.6×10^{-3}

Although the analysis leading to the evaluation of $q_{seed}/\bar{q}_w$ is idealized, it is not expected to underestimate the effect of seeding by more than an order of magnitude. Consequently, in light of the values predicted for $q_{seed}/\bar{q}_w$, it is concluded that 1% by weight alkali-metal seeding will not affect the measurement of stagnation-point heat transfer.

The above results indicate that if the seed has negligible effect on the gasdynamic variables, the effect on surface heat transfer is also negligible. Hence, in summary, the addition of 1% by weight of alkali-metal seed is not expected to disturb pressure distribution or heat-transfer measurements. However, the resulting increases in the number density of free electrons preclude meaningful measurements of electromagnetic signal propagation. Another aspect of the seeding question, that of condensation, is considered in the ensuing section.

D.   CONDENSATION EFFECTS DUE TO TEST-FLOW SEEDING

In using MHD augmentation of nozzle test flows, it is possible that the metallic vapor used to seed the flow may condense either in the nozzle expansion or on a model surface. Condensation in the expansion process may occur via two alternative mechanisms, either homogeneous or heterogeneous condensation[232,233]. In homogeneous condensation, molecules of the condensible vapor form nuclei upon which condensation may occur, resulting in sub-micron-size droplets. In heterogeneous condensation, dust particles or, in other words, foreign nuclei control the condensation process in a

supersaturated vapor. In this case, condensation occurs on a limited number of nuclei and results in the production of larger, micron-size drops. If condensation occurs, there will be a heat release to the flow. Also, the formation of droplets will result in a reduction of kinetic energy due to a drag on the drops. The order of magnitude of the heat release which may occur if all the metallic vapor condenses can be compared to the total enthalpy of the nozzle flow. Letting h_{f_g} denote the heat of vaporization, C the mass fraction of metallic vapor and neglecting the difference in specific heats of the vapor and gas stream, then $C h_{f_g} / H_o$ represents the fractional increase in flow enthalpy if all the seed condenses. For both sodium and potassium seed concentrations of 0.01, this ratio is less than 10^{-3}. Since for small concentrations of metallic vapor the slippage between condensed particles and the gas stream is also unimportant, condensation will not have a significant effect on the test-flow nozzle expansion.

Another aspect of the condensation question is the collection of condensible vapor on a model. If condensation does not occur in the nozzle expansion, then it is likely to occur on the surface of a cold blunt-nosed model. For some of the velocity-altitude conditions of interest, the stagnation pressures on blunt-nosed bodies are higher than the vapor pressures of sodium and potassium at about 300°K.

If condensation does occur in the nozzle expansion then, depending on the size of drops which are formed, the condensed seed may follow the flow streamlines around the model. For instance, if homogeneous nucleation is the dominant process in the nozzle expansion, the submicron-size drops which are formed will follow streamlines around a body. On the other hand, if heterogeneous condensation occurs, the droplets will be larger and may impinge on body surface. In fact, this behavior formed the basis for using a pitot-probe to determine droplet size in the experiments of Ref. 236.

In summary, if condensation of metallic seed occurs in the expansion, it will not significantly affect the test-flow properties. Depending on whether or not condensation occurs in the expansion and, if it occurs, on the specific mechanism, condensed metallic seed may collect on a model. However, in a short-duration facility, the amount of condensed seed collected on a model should be negligible.

X. ABLATION PHENOMENA

A.   INTRODUCTION

The regime of flight at altitudes below 250,000 ft and flight velocities in excess of 10,000 fps contains a region where extensive ablation of material surfaces must be expected.   For that reason,any aerodynamic test facility designed to duplicate the flight conditions must take account of the processes of material removal by ablation.

Usually, short-duration test facilities are considered to be incapable of producing any realistic ablation information.   Comments along these lines can be found in many papers (see,for example, Refs. 234 and 235).   In this section of the report, the difficulty of simulating ablation in a short-duration test facility is examined, and the uncertainties introduced by failure to simulate it are considered.

Previously, in Sec. IV, certain general similitudes applicable to flows with mass addition were discussed. Here, the general requirements for similitude of ablation phenomena are briefly reviewed in Section B below, and a discussion of potential similitude methods is then given in Section C. This sec tion of the report then closes with some summary comments in Section B.

B.   REVIEW OF SIMILITUDE REQUIREMENTS

1.   General Features

There are two general areas in which ablation phenomena are of interest.   The first has to do with the heat-load-bearing capabilities of a given ablation material and with the amount of such material needed to thermally protect a given flight vehicle.   The second area in which ablation plays a role has to do with aerodynamic effects that are associated with the introduction of mass into the flow field.

2. Thermal Protection

The heat-load capability of a material is of little interest as far as aerodynamic test facilities are concerned. The area of primary interest in determining the heat-bearing capabilities of an ablator is that of stagnation-point flows. For flows of this type, the similitude parameters have been studied by Lees[82, 236] and by Adams[83] and consist essentially of duplicating the stagnation enthalpy of the stream. Extensive measurements of the ablative properties of various materials have been conducted in arc-jet facilities. The net result of such studies is to produce a quantity called the effective heat of ablation, defined as follows

$$\hbar_{eff} = \frac{q)_{\dot{m}=0}}{\dot{m}} \qquad (X-1)$$

In this relation, the heat-transfer rate is that to a nonablating body. An alternative parameter used by some authors (see, e.g., Ref. 57) to classify the heat-load capability of an ablator is the so-called intrinsic heat of ablation, defined in the following manner

$$\hbar_{a} = \frac{q)_{\dot{m}\neq 0}}{\dot{m}} \qquad (X-2)$$

In this relation, the heat-transfer rate is that appropriate to the flow with mass addition. The aerodynamic effects associated with heat-transfer reduction are contained entirely in the expression for the heat transfer, while the properties which pertain only to the material are included in the heat of ablation.

Design estimates for the ablator thickness required for bodies of relatively general shape can be made by using either of the two formulas above. In the first, one calculates the heat-transfer distribution to a non-ablating body, and uses it together with the effective heat of ablation. Such a procedure raises the question whether the quantity $\hbar_{eff}$ determined in stagnation-point tests is truly applicable to conditions along a slender body. Although this approach has been applied with reasonable success to slender-cone models by Stetson[237], its limits of applicability, however, are unknown.

The second procedure is to use the intrinsic heat of ablation in conjunction with the actual heat transfer occurring with mass addition present. This approach has a more satisfactory division of the aerodynamic and materials factors, but is complicated by the necessity for a mass-transfer, heat-transfer-reduction correlation, and requires an iterative solution.

3. Aerodynamic Effects

The second general area of interest to ablation phenomena, namely, that dealing with aerodynamic effects, is not nearly as well understood. The problems encountered can be divided in two categories, according to whether the flow is steady or unsteady.

a. Steady Flows

When measurements of static aerodynamic coefficients are made on a nonablating body, and are then used to predict the aerodynamic performance of a flight vehicle which will experience ablation, it is necessary to estimate the changes in aerodynamic coefficients associated with the mass injection. It is known that moderate rates of mass addition have little effect on the pressure distribution and, consequently, on aerodynamic forces (although it does have a pronounced effect on heat transfer), but the level of mass injection at which significant aerodynamic effects are to be expected is not very well known. For the case of a stagnation-point flow, the work of Cresci and Libby[88] and that of Kaattari[90], discussed previously in Sec. IV-D, gives some indication of the mass-injection level at which aerodynamic effects are encountered. However, the extrapolation of this criterion to the case of slender bodies and to flows at relatively low density has no experimental basis as yet.

There are other problems concerning static aerodynamic tests, such as the clogging of hinge lines by condensing flow of the melted surface material, the effects of body forces such as deceleration, discussed, for example, by Ostrach[238], and finally the effect of shear on the ablation rate, as discussed by Graves.[239]

In general, it can be stated that small rates of mass addition do not falsify the measured aerodynamic coefficients, but a general criterion giving the level of mass addition which can be tolerated has not yet been developed.

b.   Unsteady Flows

For the case of dynamic stability testing, the problems are even more severe. In recent years, evidence has accumulated that the stability of slender reentry configurations can be adversely affected by the presence of ablation. Reports of such instability have been presented by Sachs and Schurmann [240], Grimes and Casey [241], Colosimo [242]*, Pettus [243], and Syvertson and McDevitt[244]. Divergent oscillations of cone-shaped models in hypersonic wind tunnels have been reported by Stalmach and Pope [245], Grimes and Casey [241], and Colosimo [242]. Further considerations of this problem can be found in a recent workshop on Dynamic Stability Testing held at AEDC in 1965 [246].

Theoretical attempts to predict such instabilities have been presented by Thyson [247], and Thyson and Schurmann [248], and Colosimo [242]. Other more elaborate theories have been set forth by Li and Gross [249]. These theoretical efforts span the full spectrum from routine application of classical boundary-layer theory to more complicated efforts, such as that of Li and Gross[249] which include some of the low-density second-order effects. However, there is no satisfactory general theory at present.

C.   POTENTIAL SIMILITUDE METHODS

1.   General Considerations

The fact that there does not exist a complete rational theory describing the role of various parameters, such as Mach number, Reynolds

---

number, shear-stress level, molecular weight of the injected gases, body
shape, and the like, means that it is impossible to provide any experimental
technique which reliably simulates the phenomena associated with ablation.
In spite of this fact, however, there is still some point in attempting to
produce at least a partial similitude by adding mass to the flow. At a very
minimum, one can add mass in a manner in which the Reynolds number
and the mass-addition rate are duplicated. There are essentially two
methods presently in use in long-duration test facilities, by which mass is
added. The first is the use of relatively low-temperature subliming
materials, such as camphor, naphthalene, and paradichlorobenzene (moth
balls). The second method is that of forced injection through a porous model
surface. In the comments below, both of these methods are discussed
briefly in the light of possible application to short-duration, high-enthalpy
test facilities.

2.   Low-Temperature Sublimers; Testing Time Limitations

The use of low-temperature subliming materials would appear, at
first glance, to offer some advantages   since it produces a natural ablation
distribution over the model surface. However, its use in short-duration
facilities is usually dismissed because of the problem of the time required
to reach steady-state ablation conditions. Criteria for the attainment of a
steady state have been discussed, among others, by Brogan[239] and by
Denison[254] and have the following general form:

$$t_{steady-state\ ablation} = \frac{k}{\rho c}\left(\frac{\rho h_{eff}}{q}\right)^2 \tag{X-3}$$

Here k , ρ and c are the thermal conductivity, density, and specific
heat of the solid. It can be seen from this equation that whenever a facility
has an extremely high heat-transfer-rate capability and when materials with
a small heat of ablation are available, one must necessarily reexamine the
question of the time required to reach steady-state conditions. For par-
adichlorobenzene, the heat of ablation is on the order of 200 BTU/lbm,

(Ref. 251-253) while k , ρ and c are approximately 4×10^{-4} cal/cm-sec-°K, 1.46 gm/cm^3, and 0.2 cal/gm-°K, respectively [254, 255]. Thus, $k/\rho c$ is about 1.5×10^{-3} cm^2/sec $\simeq 1.5 \times 10^{-6}$ ft^2/sec. A model with a one-inch nose radius, immersed in a flow which duplicates an altitude of 100,000 ft, and a velocity of 20,000 fps, experiences a stagnation-point heat-transfer rate of approximately 3000 BTU/ft^2-sec [130]. According to the formula above, steady-state conditions would be reached in approximately 50 microseconds in such a case. Thus, one cannot dismiss the possibility that a short-duration, high enthalpy facility might bring a low-temperature sublimer up to steady-state ablation conditions during the useful test duration.

There are at least two other problems which present themselves, in addition to the question of the time required to reach steady ablation. The first is concerned with the possibility that a so-called low-temperature sublimer may, in fact, melt under conditions of high heat-transfer rate. The second arises from the fact that the kinetics of the sublimation process introduce a relaxation length which is characteristic of the material and which does not necessarily duplicate the analogous property of the material being used on the flight vehicle. Both of these possibilities are discussed at greater length in the paragraphs below.

5. Low-Temperature Sublimers; Melting Problems

It can be assumed that the presence of a liquid molten film flowing over the body surface destroys any hope of simulating the behavior of a charring ablator. Thus, the suitability of a low-temperature sublimer depends on whether its surface temperature will exceed the melting point in the interval during which steady-state conditions are established. An analytical determination of the steady-state surface temperature reached in such an ablation process does not appear to have been treated in the literature. Instead, one usually finds quoted values of the observed wall temperature.

The evidence suggesting the possibility of surface melting comes from an estimate of the initial rate of rise of surface temperature. For a step-function heat-transfer rate of magnitude q_o , the surface temperature

rise is [42]

$$\Delta T_w = \frac{2 q_0 \sqrt{t}}{\sqrt{\pi k \rho \varkappa}} \qquad (X-4)$$

Using the properties of paradichlorobenzene listed above, and expressing t in seconds, q_0 in BTU/ft^2-sec, and T_w in Kelvin degrees,

$$\Delta T_w = 27.1 \ q_0 \ \sqrt{t} \qquad (X-5)$$

For the conditions cited above, R_N = 1 inch, U_∞ = 20,000 ft/sec, altitude = 100,000 ft, q_0 = 3000 BTU/ft^2-sec, this becomes

$$\Delta T_w = 8.1 \times 10^4 \ \sqrt{t} \ [sec] \qquad (X-6)$$

At this rate of increase, the temperature would rise from an initial value of, say, 20°C to melting point of 53°C in about 16 nanoseconds.

A time interval as short as this obviously calls for a more detailed study; for example, the rise time of the heat pulse itself should be taken into account in any refined estimate. The general conclusion, however, is that melting would probably occur in less than one microsecond, unless the ablation process is both fast enough and strong enough to prevent it. The sort of unsteady analysis that would be required to settle this question is indicated below.

At time zero, the model surface is at some given temperature, and may be in equilibrium with its vapor depending on the ambient pressure. Under these conditions, the initial rate of mass loss is zero, since the rate at which molecules evaporate from the surface is balanced by the rate at which they condense on it. The vapor pressure of these materials is relatively high, however (for moth balls it is about 1 mm Hg at room temperature), so for shock-tunnel operation at extremely low initial pressures, a non-zero rate of mass loss would occur even before exposure to the high-enthalpy air stream.

When the flow starts, the stagnation point is initially subjected to the heat-transfer rate for zero mass addition, the wall temperature begins to climb, and this is reflected in an increased mass-addition rate. The mass addition reduces the heat-transfer rate, which in turn reduces the rate of increase of surface temperature and of mass addition. The whole process ultimately approaches a steady condition in which the temperature distribution in the solid no longer changes, and in which the constant heat-transfer and surface-recession rates are related by the heat of ablation.

It might be possible to construct an approximate analytical description of this process, by assuming the boundary-layer flow to be quasi-steady, and by taking the time dependence into account only in calculating the transient temperature distribution in the body. The dependence of heat transfer on mass addition could be taken from Howe and Sheaffer[57]. To find the mass-addition rate, the analysis of Scala and Vidale[256] could be used. These authors have presented an approximate analysis of the stagnation-point boundary layer for a three-species model, consisting of "air atoms", "air molecules", and vaporizing molecules. By assuming a value for the mass fraction of the vaporizing species at the surface, they were able to solve for mass-addition rate. They present correlated results for the parameter $\dot{m}\sqrt{R_N}/(\kappa_\ell)_w$ as a function of altitude and flight velocity

$$\frac{\dot{m}\sqrt{R_N}}{(\kappa_\ell)_w} = fcn \left(alt., U_\infty\right)$$

(X-7)

Here, $(\kappa_\ell)_w$ denotes the wall value of the vaporizing species' mass fraction, which is as yet undetermined. In order to determine it, Scala and Vidale use the kinetic-theory expression for the interphase mass transfer

$$\dot{m}_\ell = \frac{\alpha \, p_e \, \bar{m}}{\sqrt{2\pi R \, m_\ell T_w}} \left\{ (\kappa_\ell)_{eq} - \kappa_\ell \right\}_w$$

(X-8)

where α is an evaporation coefficient, p_e is the (constant) pressure in the boundary layer $\overline{m}$ and m_{ℓ} the molecular weights of the mixture and of the vaporizing species, R the universal gas constant, and T_w the wall temperature. The symbol $(c_{\ell})_{eq}$ denotes the equilibrium mass fraction, which is related to the vapor pressure p_{ℓ} by

$$(c_{\ell})_{eq} = \frac{p_{\ell}}{p_e} \frac{m_{\ell}}{\overline{m}} \tag{X-9}$$

The equilibrium vapor pressure, in turn, is a function only of the wall temperature. A simultaneous solution of Eqs. (X-7) and (X-8) will now yield $(c_{\ell})_w$ and, hence, $\dot{m}$ as functions of T_w for any given set of free-stream conditions. Knowledge of $\dot{m}$, in turn, can be used in conjunction with some relation giving the dependence of heat transfer on mass addition (e.g., that of Howe and Sheaffer, Eq. (IV-8)).

To complete the solution, a second relation between T_w and $\dot{q}$ must be provided. This relation comes from the solution of the transient heat-conduction problem in the solid, with mass addition included. If there were no mass addition, the solution would be the well-known relation[42]

$$\Delta T_w(t) = \frac{1}{\sqrt{\pi k \rho c}} \int_0^t \frac{\dot{q}(\lambda) \, d\lambda}{\sqrt{t - \lambda}} \tag{X-10}$$

Unfortunately, the counterpart to this equation that applies when mass addition is present does not seem to have been treated in the literature. The integral-method solution described by Goodman[257] appears to come closest, and could probably be extended to the case of interest here. Alternatively, it would be of interest to try a further approximation, in which Eq. (X-10) is used, but with $\dot{q}$ replaced by ($\dot{q} - \dot{m}L$), where L is the latent heat of vaporization.

Thus, it appears that an approximate analytical theory could be constructed, leading to an estimate of the steady-state temperature reached by a low-temperature sublimer in a high heat-transfer environment. While the difficulties involved in developing such a theory are not trivial, nevertheless it would appear to be a useful topic for further study.

4.   Low-Temperature Sublimers; Kinetic Problems

A second shortcoming of low-temperature sublimers as a simulation technique is associated with the relaxation length appropriate to the heterogeneous   chemical reaction rate contained in Eq. (X-8) above. The role of this length has been discussed by Charwat [258]. In most applications of the boundary-layer theory to interphase mass transfer, such as that of Scala and Gilbert [96], for example, the equation containing the mass-addition kinetics is bypassed altogether and is replaced either by a rate-controlled approximation or by a diffusion-controlled approximation. The first of these corresponds to neglect of the ambient mass fraction at the wall, so that the mass-addition kinetics are entirely those of the forward reaction. At the opposite end of the scale, one assumes that the evaporation coefficient and the other terms multiplying the bracket in Eq. (X-8) are so large that the slope of the kinetic relation, as shown in the sketch below, is quite large.
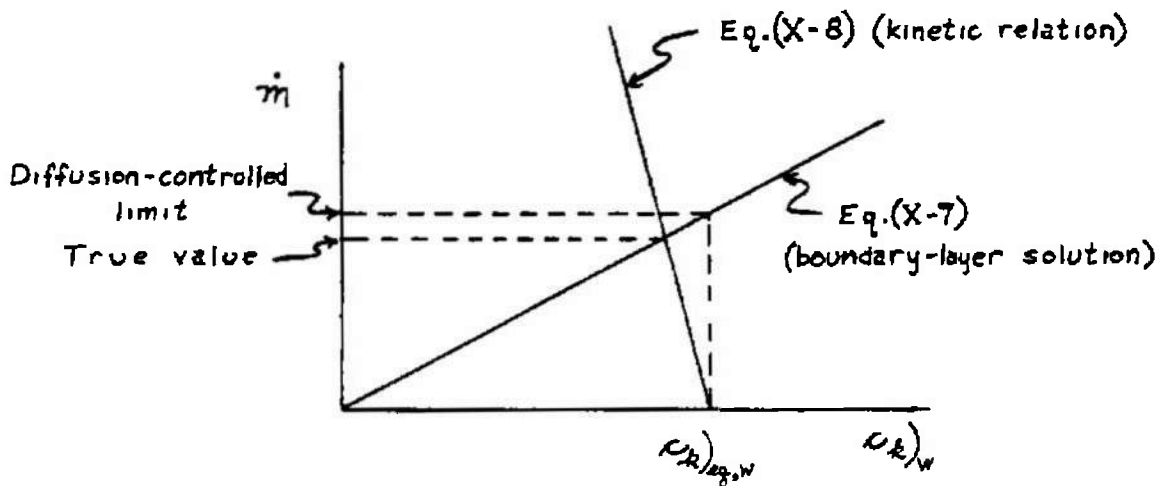
Since this is the case, it is a reasonable approximation to assume that the surface mass fraction of the ablating species is that appropriate to equilibrium at the given wall temperature.

The essence of the contribution made by Charwat[258] was to call attention to the fact that a certain relaxation distance is required to complete the transition from the situation in which the mass-addition kinetics are entirely rate-controlled to the opposite extreme in which they are diffusion-controlled. Charwat presented an approximate analysis leading to estimates of the relaxation distance and of the surface-temperature distribution for steady flows. He concluded that the use of some low-temperature sublimers (among them camphor, as used in tests by Kubota[259]) did not properly simulate a flight situation, in that practically the entire length of the wind-tunnel model lay in a transitional regime, whereas the flight configuration would be expected to be almost entirely diffusion-controlled.

The addition of a time-dependent environment, as envisioned in the considerations above, further complicates the problem that Charwat has discussed. Any theoretical treatment of the suitability of a low-temperature sublimer should consider the relaxation length, in addition to the time-dependent effects.

It must be kept in mind that the relaxation-length considerations described above, complicated as they are, are nevertheless appropriate only to the relatively simple case in which a sublimation reaction is the only type of surface kinetics present. In a case of realistic ablating materials, the surface kinetics are further complicated by the presence of heterogeneous reactions, in addition to the sublimation of the solid species. Thus, in practical cases, one has not a single surface reaction to consider, but a relatively large number of them, each with its own relaxation length. Spalding[260] has considered the same problem as that treated by Charwat, including the case where heterogeneous reactions can occur at the surface, in addition to the sublimation of the solid material. In contrast to Charwat's result, Spalding concludes that certain sublimation reactions will likely reach the diffusion-controlled limit in model tests. On the other hand, he points out that the relaxation distances associated with some of the heterogeneous chemical reactions will not reach equilibrium.

The type of unsteadiness contemplated in the remarks above is that associated with the heating-up time of a low-temperature sublimer in an

177

otherwise steady flow. If one considers the use of this method for unsteady dynamic testing, then the problem is even more complicated and one must then attempt to duplicate the time lags of the full-scale configuration.

5.   Low-Temperature Sublimers: Shear Effects

Finally, one limitation of low-temperature sublimers that is not well understood at the moment is the influence of surface shear stresses in removing material. The process by which evaporation or sublimation takes place consists of the liberation of molecular-sized fragments. It is also true, however, that in the presence of a high-shear environment, materials with a relatively low shear strength allow the removal of material, not only in relatively large flakes, but also in microscopic frag-ments which have dimensions large compared to the molecular scale. The influence of this mechanism in augmenting the material-removal rate is not understood at present.

6.   Forced Injection

The second potential similitude method for mass-injection studies is that of forced injection through a porous model. This technique has long been used to simulate ablation in steady-flow, long-duration test facilities, and has been applied successfully by Burke and Ryder[261] in a shock-tunnel facility. The technique has also been successfully applied by Stalmach and Pope[245] to an oscillating model in which the mass in-jection from the top and bottom surfaces of a porous cone could be adjusted in phase or out of phase with the cone's oscillation.

There are at least two problems associated with the application of this technique to a short-duration test facility. The first is to determine whether the distribution of mass addition appropriate to natural ablation is sufficiently smooth that one could hope to design a model porosity dis-tribution to duplicate it. The second question has to do with the testing time available and the time required to establish the boundary layer in the presence of fluid injection.

The first of these problems does not appear to be very serious. To a very good approximation, the distribution of mass injection over the surface is exactly the same as the distribution of heat-transfer rate to a nonablating surface. This general conclusion is drawn, for example, by Stetson[237]. Because the distributions of heat transfer over a relatively smooth contoured body are themselves quite smooth, it can be expected that the distribution of mass addition will also exhibit no large discontinuities.

Thus, the major obstacle to the application of mass injection in a short-duration test facility is that associated with the testing time. For steady-flow tests, there appears to be no reason why the technique developed by Burke and Ryder could not be extended, so as to provide mass addition over the entire model surface. On the other hand, for dynamic tests the requirements are considerably more severe. Even for the case of a non-ablating model, the difficulty of carrying on dynamic testing in a shock tunnel is very large. The essence of the problem, as discussed, for example, by Bird[262], by Martin[263], or by Urban[264], is to achieve a sufficient number of cycles of oscillation during the short test time. One is naturally led to high-frequency suspensions, and with these come the problem of large flexural stiffness, and a consequent limitation of the maximum amplitude of oscillation if undue stresses are to be avoided.

D.   SUMMARY

Natural mass addition by means of low-temperature sublimers is faced with some rather extensive development problems and also requires the development of a rather substantial body of theory before it can be properly understood. On the other hand, the use of forced injection appears to offer no significant problems for steady flows, but its application to dynamic testing is considerably more difficult.

To put the whole matter in perspective, it is appropriate to mention in concluding this chapter that the present state of knowledge is not sufficient to permit a realistic assessment of the ablation rate at which significant aerodynamic effects are likely to be encountered. Thus, the penalty for

failure to simulate ablation cannot be reliably judged at the present time. A second general comment that must be made is to point out that no simulation technique, either in long-duration or in short-duration wind tunnels, can be said to rest on a firm theoretical basis. The problems of interpretation that affect the nonablating short-duration facility are by no means entirely eliminated in a long-duration facility. While the latter facilities do partially simulate the ablation phenomena, it is nontheless impossible, within the confines of the present state of art, to make a quantitative determination of the degree to which their partial simulation is satisfactory.

XI.   TEST TIME REQUIREMENTS

A.   INTRODUCTION

The minimum test time required to obtain valid data in a hypervelocity tunnel is governed by the tunnel performance, the instrumentation and the type of test being conducted. Since we are concerned primarily with a shock-tunnel type of facility, we include under tunnel performance the time to establish a quasi-steady flow in the test section, as well as the duration of the air supply. Here, we are concerned only with nonablating model tests. Limitations due to instrumentation are presumed to be imposed only by the sensors and not the recorders. The time requirements introduced by the instrumentation are, in general, related to the type of test, e.g., pressure distribution or dynamic stability. In the following discussion, consideration is given to each of these items and their interrelationship. Finally, the results are summarized.

B.   TUNNEL PERFORMANCE

An important part of the design of any short-duration wind tunnel, such as a shock tunnel, concerns providing a quasi-steady air supply to the nozzle and test section for a duration that exceeds the nozzle starting time

plus the required test time. In a conventional shock tunnel, this requirement dictates the lengths of the driver and driven tubes.

A study of the flow phenomena involved in starting and stopping a hypersonic shock tunnel has been reported by Glick, Hertzberg and Smith.[265] They have shown that the starting and stopping times for a hypersonic nozzle are very brief and their theoretical estimates have proven adequate for engineering estimates. Hertzberg, Wittliff and Hall have reported that the testing-time loss associated with nozzle starting and stopping is less than a millisecond for all CAL shock tunnels.[14] This is at least an order of magnitude less than the flow establishment times reported for the AEDC hotshot tunnels.[266] The nozzles of these latter tunnels have length-to-diameter ratios which are at least twice those of the CAL shock tunnels. However, this in itself cannot account for the large differences in flow establishment times.

Once the nozzle and test-section flows are established, they must be maintained for a time period dictated by the instrumentation and/or the type of test being made. An important aspect of this is that the flow must not only be steady as regards its gasdynamic properties, but also must be homogeneous, i.e., of constant chemical composition. This latter consideration introduces the matter of mixing at the interface between the test gas and the driver or buffer gas. Hilton et al[267] report that in operating the CAL 6-foot hypersonic shock tunnel at high enthalpy this interface mixing strongly influences the available test time. Unfortunately, there is no theoretical analysis of interface mixing which will predict the loss in test time caused by that phenomenon. One can only utilize the limited amount of empirical data, such as that reported in Ref. 267, in attempting to make allowances for such mixing in the design of a new facility.

C.   INSTRUMENTATION

The existence of cathode-ray-tube oscilloscopes precludes any time limitations as far as recording instrumentation is concerned. Hence, the only problem is that of having sensors whose response time is less than the available test time. Consideration is given, therefore, to the type of instrumentation used to measure the various quantities of interest.

In shock tubes and hypersonic shock tunnels, heat-transfer rates are commonly measured using either thin-film[268] or thick-film[269] resistance thermometers to sense surface temperature history. Both types of instrumentation have response times of less than one microsecond and, hence, impose no significant time requirement on the flow duration. The thin-film thermometer has been more widely used for several reasons: its response time is about 0.1 μ sec [268]; its greater sensitivity allows the measurement of heat-transfer rates[270] as low as 0.02 BTU/ft² -sec; the use of analogue circuits[271] permits the direct recording of heat-transfer rates; such equipment is relatively simple to build and calibrate. The thick-film thermometer finds primary application where the heat-transfer rates are extremely high-- sufficient to produce melting of the glass-backing material used with thin-film gauges. Its other advantages are: rapid response (about 1 μ sec), its relatively large thickness makes it insensitive to erosion, its low electrical impedance makes it less sensitive to spurious electrical interference. The important point here is that instrumentation exists for measuring heat-transfer rates as low as 2×10^{-2} BTU/ft²-sec and as high as 2.2×10^{4} BTU/ft²-sec with response times of 1 μ sec or less.

The measurement of pressure distributions on models in hypersonic shock tunnels is commonly made with piezoelectric crystal transducers. The latest type in current use at CAL has a flush diaphragm and is 1/4-inch in diameter by 1/8-inch thick. This transducer has a frequency response of 25 Kcps or a response time of about 10 μ sec. Its sensitivity permits pressure measurements from 10^{-4} to 15 psia. Other transducers are available for measuring pitot pressures of several hundred psia. These are mounted behind an orifice in the model surface and have a somewhat slower response time because of lag introduced by the orifice. In a recent research study, the flush transducer has been used to obtain meaningful data in flows lasting 300 μ sec [272]. Thus, it can be concluded that pressure instrumentation imposes a time requirement of, at most, 300 μ sec on the flow duration.

Forces and moments have been measured in hypersonic shock tunnels by two distinct methods. One technique allows the model to fly freely during the test while photographing its motion. The forces and moments are then

inferred from the model's trajectory. The time requirement inherent in this technique is that the displacement of the model during its flight be sufficient to allow an accurate determination of the trajectory. In practice, this has meant a test time of several milliseconds (see, e.g., Ref. 217). The other technique involves the more conventional use of internal force balances. The balances in use at CAL have piezoelectric crystals as force sensors and accelerometers to compensate for the model inertia [273]. Such balances have a nominal frequency response of 600 cps or a rise time of about 1/4 of a millisecond. This implies a steady-flow requirement of 1 msec or greater.

A skin-friction transducer has also been developed at CAL with a frequency response to 5000 cps [274]. The corresponding rise time of about 32 μ sec requires a test-flow duration of several hundred microseconds.

Dynamic-testing techniques have been used to obtain static aero-dynamic stability coefficients and, in some cases, damping coefficients in hypersonic shock tunnels. Experience at CAL has indicated that force and moment balance systems are most suitable for determining the static derivatives [262]. A free-oscillation technique with mechanical restoring moments provided has been judged to be most practical for determining the longitudinal dynamic derivative ($Cm_q + Cm_{\dot{\alpha}}$) although the free-flight method may be feasible [262]. The free-oscillation technique, as developed at CAL, requires a steady-flow duration of 12 milliseconds in order to obtain at least 3 cycles of oscillation at 250 cps.

D.   TYPE OF TEST

The influence of the type of test on the minimum flow time has, to some degree, been covered in the preceding discussion of instrumentation. It is seen that heat-transfer rates can be measured in flows lasting only a few microseconds, whereas the measurement of dynamic stability derivatives requires a flow time of 12 milliseconds. A point that was not considered in that discussion is the matter of flow establishment about the model. Here, we make two distinctions: namely, flows that are completely attached to the model, and flows involving separation and/or wakes. In the first case, it is reasonable to assume that the flow-development time can be expressed in terms of model lengths of flow. Perhaps the most striking illustration of how rapidly this can

occur is boundary layer development on a flat-plate model mounted in a shock tube. In this case, the phenomenon is not complicated by nozzle-starting processes and one can truly measure model flow establishment times. In such tests, the heat-transfer rates on the forward portion of the model are established at their steady-state values before the incident shock wave has reached the model trailing edge. Conservatively, the flow-establishment time is equivalent to two model lengths of flow. This also illustrates why in shock tunnel tests the flow establishment about models occurs concurrent with the nozzle-starting process. Experience at CAL has shown that attached model flows, both viscous and inviscid, are established within the time the quasi-steady test-section flow is established.

Whenever separated flows or wakes are involved, one would expect a somewhat longer flow-establishment time. However, measurements of heat-transfer rates on the rear half of a circular cylinder mounted transverse to the flow[270] and on the lee side of cones at angles of attack greater than the cone half-angle[181] indicate steady-state values are obtained as soon as the nozzle flow is established. In fact, the only tests wherein this is not the case are some recent separated-flow studies at CAL. These studies involved a flat-plate model with a compression wedge [275]. Both pressure and heat-transfer measurements were made as the wedge angle was varied from 0 to 32 degrees. For wedge angles from 0° to 16° there was no separation present and the boundary-layer flow was established during the one-millisecond nozzle-starting time. At wedge angles sufficient to produce a well-separated flow in the interaction region between the flat plate and the wedge, an examination of the pressure and heat-transfer records indicated that these flows can take up to 2 milliseconds to stablize, or about one millisecond longer than the nozzle starting time. The records show that a separated region is created during the starting process of the tunnel and the separation point moves forward slightly during the steady running time. For wedge angles close to the incipient separation condition, the pressure and heat-transfer records from gauges immediately ahead of the flat plate-wedge junction increase and decrease, respectively, in an approximately linear manner with time from their initial flat-plate values to reach a steady-state value in approximately 2.5 m sec, or 1.5 $m$sec after the nozzle has started.

These tests were conducted at a free-stream Mach number of 19.9 and Reynolds number of 0.5×10^4 per inch. The total available test time was 3 m sec after the nozzle had started.

E.   SUMMARY

Nozzle starting times for hypersonic shock tunnels are predictable for engineering purposes by the theoretical results obtained by Glick et al [265]. The overall design of the shock tunnel then determines the duration of steady flow obtainable after the nozzle starting process. If the flow of interest contains no separated flows other than at the model base, pressure, heat transfer and skin friction measurements require no more than one millisecond of steady flow and, in fact, can be made in flows lasting only several hundred microseconds. The flapped plate experiments discussed above indicate that, if there are separated flows or conditions of incipient separation on the model, then an additional 1 or 1-1/2 m sec of test time is required for these flows to stabilize.

While it may be possible to obtain force data with a piezoelectric crystal balance in a steady flow of 1 millisecond duration, several milliseconds are more desirable. The use of the "free-flight" technique also requires several milliseconds of test time.

The longest test-time requirement results when dynamic stability measurements are desired. In this case, there is little experience available; however, a free-oscillation technique has been developed at CAL which requires 12 milliseconds of steady flow.

XII.   CONCLUDING REMARKS

It is obvious that the hypervelocity flight regime considered in this study encompasses a wide range of gasdynamic and thermochemical phenomena.   The limitations of present wind tunnels prohibit full duplication of flight conditions throughout this regime.   Hence, careful attention must be paid to the detailed similitude requirements for the various flow phenomena. In many cases, these similitude requirements are so restrictive as to preclude the possibility of meaningful testing.   Thus, it is most important that the similitude requirements themselves be evaluated from the standpoint of determining the possible degree of relaxation of duplicating the less important parameters.   Such a quantitative evaluation can only be made on the basis of pertinent theoretical solutions or experimental data.   Unfortunately, such information is totally lacking in many instances.   As a result, all of the initial objectives of this study cannot be fulfilled within our limited present-day knowledge.   On the other hand, this study does provide guidelines for the future research necessary to accomplish these objectives.

In review, it is worthwhile to summarize some of the more important results that have been obtained:

1.   The flight regime of interest has been subdivided into two regions on the basis of an assumed wind-tunnel performance capability. In one region, the wind tunnel is capable of producing the proper nozzle reservoir conditions for duplicating flight altitude and velocity.   However, nonequilibrium phenomena in the nozzle expansion prevent complete duplication of the flight conditions in the test flow.   In this 'full-duplication" region the nonequilibrium effects on velocity, density and gas composition are small.   Furthermore, the nonnegligible effects on pressure and temperature can be correlated with entropy (i.e., the flight altitude).

2. Binary scaling has been found valid throughout almost all of the relaxation zone behind strong normal shock waves.

3. Normal shock-wave solutions provide a suitable approximation (for engineering purposes) to the nonequilibrium flow about nonslender wedges.

4. Additional theoretical solutions for slender, blunt-nosed wedges and cones are required before the nonequilibrium similitude established by Inger can be accurately evaluated, particularly with respect to relaxing the requirement that the free-stream thermodynamic state be duplicated.

5. The analysis of blunted slender bodies for three models of limiting flow chemistry has shown that the duplication of free-stream velocity is more important than ambient temperature. However, the nonduplication of free-stream static temperature can also introduce significant errors. Furthermore, the flow fields were not Mach-number independent over a substantial range of the flight velocities considered.

6. In the region where flight conditions must be simulated, the stagnation-region flow of blunt bodies is better simulated by duplicating total enthalpy and density-altitude than by duplicating velocity and density-altitude.

7. Although seeding the flow with alkali-metal vapor can have an appreciable effect on the number density of the electrons in the flow field, the effect on stagnation-point heat transfer is negligible.

8. Ablation phenomena can alter the aerodynamic characteristics of a vehicle. Hence, for certain types of testing, simulation of ablation may be important. Existing theory does not provide the appropriate similitude parameters, however.

9. Except for dynamic testing, test times from 5 to 10 m secs are adequate for other aerodynamic measurements provided ablation is not important.

In conclusion, a few general comments are appropriate. It is clear that for the flight regime considered here substantial regions of nonequilibrium flows will exist for many flight vehicles. Simulation of such flows has been found to be extremely complex. When flight velocity is duplicated, correct gas composition in the flow field depends on having correct density, and any geometrical scaling of tunnel models will introduce departures from correct density if flow transit times are scaled. The implication is that not only should flight velocities be duplicated, but that nearly full-scale models are ultimately desirable. Finally, it should be pointed out that the hypothetical wind-tunnel performance used in this study far exceeds that of any existing facility. Hence, the similitude problems studied here will be more acute for facilities falling short of this performance.

XIII. REFERENCES

1. Masson, D. J. and Gazley, C., Jr., "Surface Protection and Cooling Systems for High-Speed Flight." Aero. Eng. Rev. 15, pp. 46-55, November 1956.

2. Ring, L. E., "General Considerations of MHD Acceleration for Aerodynamic Testing." AEDC-TDR-64-256, December 1964.

3. Harris, C. J., Marsten, C. H., Rogers, D. A., Mallin, J. R. and Warren, W. R., "A High Density Shock Tunnel Augmented by a Faraday MHD Accelerator." Proc. 4th Hypervelocity Techniques Symposium, Arnold Air Force Station, November 1965.

4. Trimpi, R. L., "A Preliminary Theoretical Study of the Expansion Tube, A New Device for Producing High-Enthalpy Short-Duration Hypersonic Gas Flows." NASA TR R-133, 1962.

5. Jones, J. J., "Some Performance Characteristics of the LRC 3 3/4-inch Pilot Expansion Tube Using an Unheated Hydrogen Driver." Proc. 4th Hypervelocity Techniques Symposium, Arnold Air Force Station, November 1965.

6. Norfleet, G. D., Lacey, J. J., Jr. and Whitfield, J. D., "Results of an Experimental Investigation of the Performance of an Expansion Tube." Proc. 4th Hypervelocity Techniques Symposium, Arnold Air Force Station, November 1965.

7. Stoddard, F. J., Hertzberg, A. and Hall, J. G. "The Isentropic Compression Tube: A New Approach to Generating Hypervelocity Test Flows with Low Dissociation." Proc. 4th Hypervelocity Techniques Symposium, Arnold Air Force Station, November 1965.

8. Eschenroeder, A. Q., Boyer, D. W. and Hall, J. G., "Exact Solutions for Nonequilibrium Expansions of Air with Coupled Chemical Reactions." CAL Rept. No. AF-1413-A-1, May 1961.

9. Lordi, J. A. and Mates, R. E., "Nonequilibrium Expansions of High-Enthalpy Airflows." ARL 64-206 (CAL Rept. AD-1716-A-3), November 1964. (also AIAA Journ. 3, pp 1972-1974, October 1965).

10. Emanuel, G. and Vincenti, W. G., "Method for Calculation of the One-Dimensional Nonequilibrium Flow of a General Air Mixture Through a Hypersonic Nozzle." AEDC TDR 62-131, June 1962.

11. Brainerd, J. J. and Levinsky, E. S., "Viscous and Nonviscous Nonequilibrium Nozzle Flows." AIAA Journal, 1, pp. 2474-2481, November 1963.

12. Reinhardt, W. A. and Baldwin, B.S., Jr., "A Model for Chemically Reacting Nitrogen-Oxygen Mixtures with Application to Nonequilibrium Air Flow." NASA TN D-2971, August 1965.

13. Harris, C.J. and Warren, W.R., "Correlation of Nonequilibrium Chemical Properties of Expanding Air Flows." G. E. Rept. R64SD92, December 1964. (also AIAA Journ. 4, pg. 1148, June 1966).

14. Hertzberg, A., Wittliff, C. E. and Hall, J.G., "Development of the Shock Tunnel and its Application to Hypersonic Flight." Hypersonic Flow Research, (Edit. F. R. Riddell), pp. 701-758, Academic Press, New York, 1962.

15. "Mollier Diagram for Equilibrium Air." ARO, Inc., March 1964.

16. U.S. Standard Atmosphere, 1962, U.S. Government Printing Office Washington, D. C., 1962.

17. Harney, D.J., "Chemical Kinetic Regimes of Hypersonic Flight Simulation." AEDC-TDR-63-3, January 1963.

18. Flax, A. H., "Similarity and Flight Simulation in Hypersonic Test Facilities." Proc. 7th Anglo-American Aeronaut. Conf., 1959.

19. Cheng, H. K., "Recent Advances in Hypersonic Flow Research." AIAA Journ. 1, pp. 295-310, February 1963.

20. Stalder, J.R. and Seiff, A., "The Simulation and Measurement of Aerodynamic Heating at Supersonic and Hypersonic Mach Numbers." AGARD AF19/P9, 7th Meeting of the Wind Tunnel and Model Testing Panel, Ottawa, Canada, June 1955.

21. Charwat, A. F., "A Generalized Analysis of the Performance Characteristics and Operating Ranges of Hypersonic-Flow Test Facilities." Rand Corp. Rept. R-432-PR, January 1965.

22. Tsien, H.S., "Similarity Law of Hypersonic Flow." J. Math & Phys. 25, pp. 247-251, 1946.

23. Hayes, W.D., "On Hypersonic Similitude." Quart. Appl. Math. 5, pp. 105-106, 1947.

24. Lees, L., "Hypersonic Flow." Fifth International Aeronaut. Conf. (Los Angeles, Calif., June 20-23, 1955), pp. 241-276, I. A.S.

25. Hayes, W.D. and Probstein, R.F., Hypersonic Flow Theory, Academic Press, New York, 1959.

26. Ehret, D.M., Rossow, V.J. and Stevens,V.I., "An Analysis of the Applicability of the Hypersonic Similarity Law to the Study of the Flow about Bodies of Revolution at Zero Angle of Attack." NACA TN 2250, December, 1950.

27. Neice, S.E. and Ehret, D.M., "Similarity Laws for Slender Bodies of Revolution in Hypersonic Flows." J. Aero. Sci. $\underline{18}$, pp. 527-530, August 1951.

28. Rossow, V.J., "Applicability of the Hypersonic Similarity Rule to Pressure Distributions Which Include the Effects of Rotation for Bodies of Revolution at Zero Angle of Attack." NACA TN 2399, June 1951.

29. Hamaker, F.M., Neice, S.E. and Eggers, A.J., Jr., "The Similarity Law for Hypersonic Flow About Slender Three-Dimensional Shapes." NACA TN 2443, August 1951.

30. Hamaker, F.M. and Wong, T.J., "The Similarity Law for Nonsteady Hypersonic Flows and Requirements for the Dynamic Similarity of Related Bodies in Free Flight." NACA TN 2631, February 1952.

31. Van Dyke, M.D., "The Combined Supersonic-Hypersonic Similarity Rule." J. Aero. Sci. $\underline{18}$, pp. 499-500, July 1951.

32. Hindes, J.W. and Augustine, N.R., "The Applicability of the Hypersonic Similarity Laws to a Complete Missile Configuration." Paper No. 61-212-1906 presented at Nat'l. IAS-ARS Joint Mtg., Los Angeles, Calif., June 1961.

33. Cheng, H.K., "Similitude of Hypersonic Real-Gas Flows Over Slender Bodies with Blunted Noses." J. Aero. Sci. $\underline{26}$, pp. 575-585, September 1959.

34. Inger, G.R., "Similitude of Hypersonic Flows Over Slender Bodies in Nonequilibrium Dissociated Gases." AIAA Journ. $\underline{1}$, pp. 46-53, January 1963.

35. Lighthill, M.J., "Dynamics of a Dissociating Gas, Part 1. Equilibrium Flow." J. Fluid Mech. $\underline{2}$, pp. 1-32, January 1957.

36. Lighthill, M.J., "Dynamics of a Dissociating Gas, Part 2. Quasi-equilibrium Transfer Theory." J. Fluid Mech. $\underline{8}$, pp. 161-182, June 1960.

37. Freeman, N.C., "Nonequilibrium Flow of an Ideal Dissociating Gas." J. Fluid Mech. $\underline{4}$, pp. 407-425, August 1958.

38. Gibson, W.E. and Sowyrda, A., "An Analysis of Nonequilibrium Inviscid Flows." AEDC-TDR-62-172, August 1962.

39. Oswatitsch, K., "Similarity Laws for Hypersonic Flow." Royal Inst. for Tech., Tech. Note No. 16, Stockholm, 1950.

40. Cox, R. N. and Crabtree, L. F., Elements of Hypersonic Aerodynamics, p. 28, Academic Press, New York, 1965.

41. Hodges, A. J., "The Drag Coefficient of Very High Velocity Spheres." J. Aero. Sci. 24, pp. 755-758, October 1957.

42. Vidal, R. J., Wittliff, C. E., Bartlett, G. E., and Logan, J. G., "Investigation of Stagnation Point Heat Transfer in the CAL Hypersonic Shock Tunnel." CAL Rept. No. AA-966-A-1, November 1955.

43. Rose, P. H. and Stark, W. I., "Stagnation Point Heat Transfer Measurements in Dissociated Air." J. Aero. Sci. 25, pp. 86-97, February 1958.

44. Gibson, W. E., "Dissociation Scaling for Nonequilibrium Blunt-Nose Flows." ARS Journal 32, pp. 285-287, February 1962; also, AEDC TDR 62-25, February 1962.

45. Hall, J. G., Eschenroeder, A. Q., and Marrone, P. V., "Blunt-Nose Inviscid Airflows with Coupled Nonequilibrium Processes." J. Aero. Sci. 29, pp. 1038-1051, September 1962.

46. Gibson, W. E. and Marrone, P. V., "A Similitude for Nonequilibrium Phenomena in Hypersonic Flight," The High Temperature Aspects of Hypersonic Flow (Edit. W. C. Nelson) AGARDograph 68, pp. 105-132, Macmillan, New York, 1964.

47. Gibson, W. E. and Marrone, P. V., "Nonequilibrium Scaling Criterion for Inviscid Hypersonic Airflows." CAL Rept. No. QM-1626-A-8, November 1962.

48. Gibson, W. E. and Marrone, P. V., "Correspondence Between Normal Shock and Blunt-Body Flows." Phys. Fluids, 5, pp. 1649-1656, December 1962 (also CAL Rept. No. QM-1626-A-7, June 1962).

49. Ellington, D., "Binary Scaling Limits for Hypersonic Flight." CARDE T.R. 499/64, May 1964.

50. Gibson, W. E., "The Effect of Ambient Dissociation on Equilibrium Shock-Layers." ARL 64-42, March 1964. (also I.A.S. Paper No. 63-70, January 1963).

51. Fay, J. A. and Riddell, F. R., "Theory of Stagnation Point Heat Transfer in Dissociated Air." J. Aero. Sci. 25, pp. 73-85, February 1958.

52. Ferri, A. and Libby, P. A., "Note on an Interaction Between the Boundary Layer and the Inviscid Flow." J. Aero. Sci. 21, p. 130. February 1954.

53. Rott, N. and Lenard, M., "Vorticity Effect on the Stagnation Point Flow of a Viscous Incompressible Fluid." J. Aero. Sci. 26, pp. 542-543, August 1959.

54. Van Dyke, M. D., "Second-Order Compressible Boundary-Layer Theory with Application to Blunt Bodies in Hypersonic Flow." Hypersonic Flow Research, (Edit, F. R. Riddell), pp. 37-76, Academic Press, 1962.

55. Van Dyke, M. D., "A Review and Extension of Second-Order Hypersonic Boundary-Layer Theory." Rarefied Gas Dynamics, Vol. II, (Edit. J. A. Laurmann), pp. 212-227, Academic Press, 1963.

56. Ferri, A., Zakkay, V., and Ting, L., "Blunt-Body Heat Transfer at Hypersonic Speed and Low Reynolds Numbers." J. Aero. Sci. 28, pp. 962-971, December 1961.

57. Howe, J. T. and Sheaffer, Y. S., "Mass Addition in the Stagnation Region for Velocity up to 50,000 Ft/Sec." NASA TR R-207, 1964.

58. Cheng, H. K., "The Blunt-Body Problem in Hypersonic Flow at Low Reynolds Number." CAL Rept. No. AF-1285-A-10, June 1963.

59. Lees, L., "Laminar Heat Transfer Over Blunt-Nosed Bodies at Hypersonic Flight Speeds." Jet Propulsion 26, pp. 259-269, 274, April 1956.

60. Kemp, N. H., Rose, P. H., and Detra, R. W., "Laminar Heat Transfer Around Blunt Bodies in Dissociated Air." J. Aero. Sci. 26, pp. 421-430, July 1959.

61. Griffith, B. J. and Lewis, C. H., "Laminar Heat Transfer to Spherically Blunted Cones at Hypersonic Conditions." AIAA Journal 2, pp. 438-444, March 1964.

62. Lewis, C. H. and Whitfield, J. D., "Theoretical and Experimental Studies of Hypersonic Viscous Effects." AEDC TR-65-100, May 1965.

63. Whitfield, J. D. and Griffith, B. J., "Hypersonic Viscous Drag Effects on Blunt Slender Cones." AIAA Journal 2, pp. 1714-1722, October 1964.

64. Crawford, D. R., "Wall Temperature Effects on the Zero-Lift Viscous Drag of Blunted Cones in Rarefied Supersonic Flow." University of California, Berkeley, Institute of Engineering Research Rept. AS-65-15, September 1965.

65. Dayman, B., "Hypersonic Viscous Effects on Free-Flight Slender Cones." AIAA Journal 3, pp. 1391-1400, August 1965.

66. Waldron, H. F., "Viscous Hypersonic Flow over Pointed Cones at Low Reynolds Numbers." AIAA Paper 66-34, January 1966.

67. Inger, G. R., "Nonequilibrium Stagnation Point Boundary Layers with Arbitrary Surface Catalycity." AIAA Journal 1, pp. 1776-1784, August 1963.

68. Inger, G. R., "Nonequilibrium Hypersonic Stagnation Flow at Low Reynolds Numbers." Aerospace Corp. Rept. SSD-TDR-64-118, September 1964.

69. Hartunian, R. A. and Thompson, W. P., "Nonequilibrium Stagnation Point Heat Transfer Including Surface Catalysis." AIAA Paper 63-464, 1963.

70. Carden, W. H., "Experimental Heat Transfer to Hemispheres in Nonequilibrium Dissociated Hypersonic Flow with Surface Catalysis and Second-Order Effects." AIAA Paper 66-3, January 1966.

71. Rosner, D. E., "Scale Effects and Correlations in Nonequilibrium Convective Heat Transfer." AIAA Journal 1, pp. 1550-1555, July 1963.

72. Chung, P. M. and Liu, S. W., "An Approximate Analysis of Simultaneous Gas-Phase and Surface Atom Recombination for Stagnation Boundary Layer." Aerospace Corp. Rept. TDR-169(3230-12)TN-4, November 1962.

73. Inger, G. R., "Analytical Prediction of Nonequilibrium Heat Transfer Around Blunt-Nosed Bodies." J. Spacecraft and Rockets 3, pp. 439-441, March 1966.

74. Cheng, H. K. "Hypersonic Shock Layer Theory of the Stagnation Region at Low Reynolds Number." CAL Rept. No. AF-1285-A-7, April 1961.

75. Buckmaster, J. D., "The Effects of Ambient Dissociation on Frozen Hypersonic Stagnation Flow." CAL Rept. No. AF-1560-A-7 (AEDC-TDR-64-142), June 1964.

76. Rae, W. J., "A Solution for the Nonequilibrium Flat-Plate Boundary Layer." AIAA Journ. 1, pp. 2279-2288, October 1963.

77. Chung, P. M., "Chemically Reacting Nonequilibrium Boundary Layers." Advances in Heat Transfer, Vol. 2, (Edit. J. P. Hartnett and T. F. Irvine, Jr.) pp. 109-270, Academic Press, 1965.

78. Levinsky, E. S. and Fernandez, F. L., "Approximate Nonequilibrium Air Ionization in Hypersonic Flows Over Sharp Cones." AIAA Journ. 2, pp. 565-568, March 1964.

79. Mondrzyk, R. J., "Nonsimilar, Nonequilibrium Laminar Boundary Layers for Sharp Conical Bodies." Boeing Company Rept. D2-36398-1 December 1965.

80. Flax, A. H., "Simulation Capabilities of the Wave Superheater with Respect to Ionization Phenomena on Ballistic Missiles." Appendix B of "Gas Dynamics of a Wave Superheater Facility for Hypersonic Research and Development" by R. C. Weatherston, A. L. Russo, W. E. Smith and P. V. Marrone, CAL Rept. No. AD-1118-A-1, February 1959.

81. Glick, H. S., "Interaction of Electromagentic Waves with Plasmas of Hypersonic Flows." ARS Journ. 32, pp. 1359-1364, September 1962.

82. Lees, L., "Ablation in Hypersonic Flows." I. A. S. Paper 59-146, October 1959.

83. Adams, M. C., "Recent Advances in Ablation." ARS Journ. 29, pp. 625-632, September 1959.

84. Georgiev, S., Hidalgo, H., and Adams, M. C., "On Ablation for the Recovery of Satellites." Proc. 1959 Heat Trans. and Fluid Mech. Inst. pp. 171-180, Stanford University Press, June 1959.

85. Baron, J. R., "The Binary-Mixture Boundary Layer Associated with Mass Transfer Cooling at High Speeds." MIT NSL Technical Rept. 160, May 1956.

86. Reshotko, E. and Cohen, N. B., "Heat Transfer at the Forward Stagnation Point of Blunt Bodies." NACA TN 3513, July 1955.

87. DeRienzo, P. and Pallone, A., "Convective Stagnation Point Heating for Reentry Speeds up to 70,000 Ft/Sec Including Effects of Large Blowing Rates." AVCO RAD-TM -65-58, January 1965.

88. Cresci, R. J. and Libby, P. A., "The Downstream Influence of Mass Transfer at the Nose of a Slender Cone." J. Aero. Sci. 29, pp. 815-826, July 1962.

89. Libby, P. A., "The Homogeneous Boundary Layer at an Axisymmetric Stagnation Point with Large Rates of Injection." J. Aero. Sci. 29, pp. 48-60, January 1962.

90. Kaattari, G. E., "The Effect of Simulated Ablation-Gas Injection on the Shock Layer of Blunt Bodies at Mach Nos. of 3 and 5." NASA TN D-2954, August 1965.

91. Katzen, E. D. and Kaattari, G. E. , "Flow Around Blunt Bodies Including Effects of High Angles of Attack, Nonequilibrium Flow, and Vapor Injection. " AIAA Entry Technology Conference, AIAA Pulbication CP-9, pp. 106-117, October 1964.

92. Barber, E. A. , "An Experimental Investigation of Stagnation Point Injection." J. Spacecraft and Rockets 2, pp. 770-774, September-October 1965.

93. Lam, S. H. , "Interaction of a Two-Dimensional Inviscid Incompressible Jet Facing a Hypersonic Stream. " Princeton University, AFOSR Rept. TN 59-274, March 1959.

94. Hoshizaki, H. , "Mass Transfer and Shock-Generated Vorticity. " ARS Journ. 30, pp. 628-634, July 1960.

95. Martin, E. D. , "Possible Occurrence of Boundary Shock Waves." NASA TN D-3195, January 1966.

96. Scala, S. M. and Gilbert, L. M. , "Sublimation of Graphite at Hypersonic Speeds." AIAA Journ. 3, pp. 1635-1644, September 1965.

97. Vojvodich, N. S. and Pope, R. B. , "The Influence of Ablation on Stagnation Region Convective Heating for Dissociated and Partially Ionized Boundary-Layer Flows." Proc. 1965 Heat Tran. and Fluid Mech. Inst. pp. 114-137, Stanford University Press, 1965.

98. Hickman, R. S. and Giedt, W. H. , "Heat Transfer to a Hemisphere-Cylinder at Low Reynolds Number." AIAA Journ. 1, pp. 665-671, March 1963.

99. Swenson, B. L. , "An Approximate Analysis of Film Cooling on Blunt Bodies by Gas Injection Near the Stagnation Point." NASA TN D-861, September 1961.

100. King, H. H. and Talbot, L. , "Effect of Mass Injection on the Drag of a Slender Cone in Hypersonic Flow." AIAA Journ. 2, pp. 836-844, May 1964.

101. Lewis, C. H. , Marchand, E. O. and Little, H. R. , "Mass Transfer and First-Order Boundary-Layer Effects on Sharp Cone Drag." AIAA Paper 66-33, January 1966.

102. Wray, K. L. , Rose, P. H. and Koritz, H. E. , "Measurements of the Radiation from an Ablation Contaminated Boundary Layer under Simulated Flight Conditions." AVCO Everett Research Rept. 226, August 1965.

103. Wray, K.L. and Kemp, N. H., "The Ablating Boundary Layer on a Teflon Plate in an Arc-Heated Airstream." AIAA Paper 66-56, January 1966.

104. Williams, F. A., "Production of Trace Species in Boundary Layers." Heterogeneous Combustion, (Edit. H. G. Wolfhard, I. Glassman, and L. Green), Progress in Aeronautics and Astronautics, Vol. 15, pp. 609-642, Academic Press, 1964.

105. Eschenroeder, A. Q., "Nonequilibrium Scaling of High-Enthalpy Gas Flows." GM DRL TR 64-02C, June 1964.

106. Stetson, K. F., "Boundary-Layer Transition on Blunt Bodies with Highly Cooled Boundary Layers." J. Aero. Sci. 27, pp. 81-91, February 1960.

107. Anon., "Final Technical Report: NOL Ballistics Range Program on ABRES Research." Naval Ordnance Laboratory Report, AD 475971, October 20, 1965.

108. Reshotko, E., "Transition Reversal and Tollmien-Schlichting Instability." Physics of Fluids 6, pp. 335-342, March 1963.

109. Potter, J. L. and Whitfield, J. D., "Effects of Slight Nose Bluntness and Roughness on Boundary-Layer Transition in Supersonic Flows." J. Fluid Mech. 12, pp. 501-535, April 1962.

110. Wilkins, M. E. and Tauber, M. E., "Boundary-Layer Transition on Ablating Cones at Speeds up to 7 km/sec." AIAA Paper 66-27, January 1966.

111. Powers, J. O. and Albacete, L. M., "Laminar Boundary-Layer Stability with Foreign Gas Injection." Paper No. F7, 1965 Divisional Meeting, Division of Fluid Dynamics, American Physical Society, 22-24 November 1965, Case Institute of Technology, Cleveland, Ohio.

112. Seiff, A. and Tauber, M. E., "Optimum Conical Bodies for Grazing Hyperbolic Entry." AIAA Journ. 4, pp. 61-67, January 1966.

113. Rose, P. H., Probstein, R. F. and Adams, M. C., "Turbulent Heat Transfer through a Highly Cooled, Partially Dissociated Boundary Layer." J. Aero. Sci. 25, pp. 751-760, December 1958.

114. Probstein, R. F., Adams, M. C. and Rose, P. H., "On Turbulent Heat Transfer through a Highly Cooled, Partially Dissociated Boundary Layer." Jet Propulsion 28, pp. 56-58, January 1958.

115. Murphy, J. D. and Rubesin, M. W., "Reevaluation of Heat Transfer Data Obtained in Flight Tests of Heat Sink Shielded Reentry Vehicles." J. of Spacecraft and Rockets 3, pp. 53-60, January 1966.

116. Rose, P. H., Probstein, R. F. and Adams, M. C., "Turbulent Heat Transfer on Highly Cooled, Blunt-Nosed Bodies of Revolution in Dissociated Air." Proc. 1958 Heat Trans. and Fluid Mech. Inst. pp. 143-155, 1958.

117. Phillips, R. L., "A Summary of Several Techniques used in the Analysis of High Enthalpy Level, High Cooling Ratio, Turbulent Boundary Layers on Blunt Bodies of Revolution." Ramo-Wooldridge Corp. GM-TM-194, September 1957.

118. Burnell, J. A., Goodwin, F. K., Nielsen, J. N., Rubesin, M. W. and Sacks, A. H., "Effects of Supersonic and Hypersonic Aircraft Speed Upon Aerial Photography." Vidya Report 28, October 1960.

119. Spalding, D. B. and Chi, S. W., "The Drag of a Compressible Turbulent Boundary Layer on a Smooth, Flat Plate With and Without Heat Transfer." J. Fluid Mech. 18, pp. 117-143, January 1964.

120. Spalding, D. B., Auslander, D. M. and Sundaram, T. R., "The Calculation of Heat and Mass Transfer Through the Turbulent Boundary Layer on a Flat Plate at High Mach Numbers, With and Without Chemical Reaction." Supersonic Flow, Chemical Processes and Radiative Transfer, (Edit. D. B. Olfe and V. Zakkay) pp. 211-276, Macmillan Company, 1964.

121. Lin, S. C., "A Bimodal Approximation for Reacting Turbulent Flows, I: Description of the Model, II: Example of Quasi-One-Dimensional Wake Flow." AIAA Journ. 4, pp. 202-216, February 1966.

122. Eschenroeder, A. Q., "Turbulence Spectra in a Reacting Gas." AIAA Journ. 3, pp. 1839-1846, October 1965.

123. AIAA Conference on the Aerothermochemistry of Turbulent Flows, San Diego, December 13-15, 1965.

124. Meroney, R. N., "The Effect of Mass Injection on Heat Transfer from a Partially Dissociated Gas Stream." Ph. D. Thesis, University of California, Berkeley, AD 467171, May 1965.

125. Danberg, J. E., Winkler, E. M. and Chang, P. K., "Heat and Mass Transfer in a Hypersonic Turbulent Boundary Layer." Proc. 1965 Heat Trans. and Fluid Mech. Inst., pp. 87-113, Stanford University Press, 1965.

126. Kane, J. J., "Nonequilibrium Sodium Ionization in Laminar Boundary Layers." AIAA Journ. 2, pp. 1651-1653, October 1964.

127. Brant, D. N. and Burke, A. F., "Ablative Effects on the Turbulent Boundary Layer of Conical Bodies." CAL Rept. No. UB-1376-S-123, August 1965.

128. Ames Research Staff, "Equations, Tables and Charts for Compressible Flow." NACA Report 1135, 1953.

129. Wittliff, C. E. and Curtis, J. T., "Normal Shock Wave Parameters in Equilibrium Air." CAL Rept. No. CAL-111, November 1961.

130. Lewis, C. H. and Burgess, E. G., III, "Altitude-Velocity Table and Charts for Imperfect Air." AEDC-TDR-64-214, January 1965.

131. Marrone, P. V., "Normal Shock Waves in Air: Equilibrium Composition and Flow Parameters for Velocities from 26,000 to 50,000 ft/sec." CAL Rept. No. AF-1792-A-2, August 1962.

132. Lewis, C. H. and Burgess, E. G., III, "Charts of Normal Shock Wave Properties in Imperfect Air." AEDC-TDR-64-43, March 1964.

133. Bond, J. W., Jr., "Structure of a Shock Front in Argon." Phys. Rev. 2nd Series 105, pp. 1683-1694, March 1957.

134. Duff, R. E. and Davidson, N., "Calculation of Reaction Profiles Behind Steady-State Shock Waves. II. The Dissociation of Air." J. Chem. Phys. 31, pp. 1018-1027, October 1959.

135. Batchelder, R. A., "Normal Shock Waves in Air with Chemical and Vibrational Relaxation Effects." Douglas Rept. SM-37627, July 1960.

136. Lin, S. C. and Teare, J. D., "Rate of Ionization Behind Shock Waves in Air. II. Theoretical Interpretation." AVCO Res. Rept. 115, September 1962.

137. Burke, A. F., Curtis, J. T. and Boyer, D. W., "Nonequilibrium Flow Considerations in Hypervelocity Wind Tunnel Testing." CAL Rept. No. AA-1632-Y-1, May 1962.

138. Marrone, P. V., "Inviscid, Nonequilibrium Flow Behind Bow and Normal Shock Waves, Part I. General Analysis and Numerical Examples." CAL Rept. No. QM-1626-A-12 (I), May 1963.

139. Treanor, C. E., "Vibrational Relaxation Effects in Dissociation Rate-Constant Measurements." CAL Rept. No. AG-1729-A-1, August 1962.

140. Treanor, C. E., "Coupling of Vibration and Dissociation in Gasdynamic Flows." AIAA Paper No. 65-29, January 1965.

141. Dunn, M. G., Daiber, J. W., Lordi, J. A. and Mates, R. E., "Estimates of Nonequilibrium Ionization Phenomena in the Inviscid Apollo Plasma Sheath." CAL Rept. No. AI-1972-A-1, September 1965.

142. Hammitt, A. G. and Murthy, K. R. A., "Approximate Solutions for Supersonic Flow Over Wedges and Cones." Princeton Univ. Rept. No. 449, April 1959.

143. Moeckel, W. E., "Oblique-Shock Relations at Hypersonic Speeds for Air in Chemical Equilibrium." NACA TN 3895, January 1957.

144. Feldman, S. "Hypersonic Gas Dynamic Charts for Equilibrium Air." AVCO Res. Rept. 40, January 1957.

145. Batchelder, R. A., et al., "Normal and Oblique Shock Characteristics at Hypersonic Speeds." Douglas Engineering Rept. LB-25599, December 1957.

146. Trimpi, R. L. and Jones, R. A., "A Method of Solution with Tabulated Results for the Attached Oblique Shock-Wave System for Surfaces at Various Angles of Attack, Sweep, Dihedral in an Equilibrium Real Gas Including the Atmosphere." NASA TR R-63, 1960.

147. Spurk, J.H., Gerber, N. and Sedney, R., "Characteristics Calculation of Flowfields with Chemical Reactions." AIAA Journ. 4, pp. 30-37, January 1966.

148. Sedney, R. "Some Aspects of Nonequilibrium Flows." J. Aero. Sci., 28, pp. 189-196, March 1961.

149. Epstein, M., "Dissociation Relaxation Behind a Plane, Oblique, Shock Wave." J. Aero. Sci. 28, pp. 664, 665, August 1961.

150. Hsu, C. T. and Anderson, J.E., "Nonequilibrium Dissociating Flow Over a Cusped Body." AIAA Journ. 1, pp. 1784-1789, August 1963.

151. Chu, C. W., "Equivalence of Nonequilibrium Flows Behind Normal and Oblique Shock Waves." AIAA Journ. 2, p. 1833, October 1964.

152. Inger, G. R., "Nonequilibrium Flow Behind Strong Shock Waves in a Dissociated Ambient Gas." Douglas Rept. SM 38936, January 1962.

153. Yalamanchili, J., "Normal and Oblique Shock Wave Parameters with Dissociated Ambient Conditions in Hypersonic Flow with Various Chemical States Across the Shock." Honeywell Rept. U-RD-6333, March 1964.

154. Linnell, R. D., "Two-dimensional Airfoils in Hypersonic Flows." J. Aero. Sci. 16, pp. 22-30, January 1949.

155. Capiaux, R. and Washington, M., "Nonequilibrium Flow Past a Wedge." AIAA Journ. 1, pp. 650-660, March 1963.

156. South, J. C., Jr., "Application of the Method of Integral Relations to Supersonic Nonequilibrium Flow Past Wedges and Cones." NASA TR R-205, August 1964.

157. Lee, R.S., "A Unified Analysis of Supersonic Nonequilibrium Flow over a Wedge: I. Vibrational Nonequilibrium." AIAA Journ. 2, pp. 637-646, April 1964.

158. Newman, P.A., "A Modified Method of Integral Relations for Supersonic Nonequilibrium Flow over a Wedge." NASA TN D-2654, February 1964.

159. Sedney, R.J., South, J.C., Jr., and Gerber, N., "Characteristic Calculation of Nonequilibrium Flows." The High-Temperature Aspects of Hypersonic Flow (Edit. W.C. Nelson), pp. 89-104, Macmillan Co., New York, 1964.

160. Zhigulev, V.N., "The Relaxation Boundary Layer Effect." Soviet Physics-Doklady I, pp. 463-465, December 1962.

161. Thommen, H.U., "Nonequilibrium Flow of Dilute Reacting Gases." Trans. ASME - Journ. Appl. Mech. Series E, 32, pp. 169-176, March 1965.

162. Moore, F.K. and Gibson, W.E., "Propagation of Weak Disturbances in a Gas Subject to Relaxation Effects." J. Aero. Sci., 27, pp. 117-127, February 1960.

163. Clarke, J.F., "The Linearized Flow of a Dissociating Gas." J. Fluid Mech. 7, pp. 577-595, April 1960.

164. Sundaram, T.R. "The Flow of a Dissociating Gas Past a Convex Corner, Part I-Linearized Theory." ARL 65-106, May 1965.

165. Cheng, H.K., Hall, J.G., Golian, T.C. and Hertzberg, A., "Boundary-Layer Displacement and Leading-Edge-Bluntness Effects in High-Temperature Hypersonic Flow." J. Aero. Sci. 28, pp. 353-381, May 1961.

166. Taylor, G.I. and Maccoll, J.W., "The Air Pressure on a Cone Moving at High Speeds." Proc. Roy. Soc. (London), Sec. A 139, 1933.

167. Kopal, Z., "Tables of Supersonic Flow Around a Cone." MIT Dept. of Elect. Eng. Tech. Rept. No. 1, 1947.

168. Sims, J.L., "Supersonic Flow Around Right Circular Cone Tables for Zero Angles of Attack." Army Ball. Missile Agency Rept. ABMA DA-TR-11-60, March 1960.

169. Simon, W.E. and Walter, L.A., "Approximations for Supersonic Flow over Cones." AIAA Journ. 1, pp. 1696-1698, July 1963.

170. Zumwalt, G. W. and Tang, H. H., "Mach Number Independence of the Conical Shock Pressure Coefficient." AIAA Journ. 1, pp. 2389-2391, October 1963.

171. Blick, E. F., "Similarity Rule Estimation Methods for Cones." AIAA Journ. 1, pp. 2415-2416, October 1963.

172. Linnell, R. D. and Bailey, J. Z., "Similarity-Rule Estimation Methods for Cones and Parabolic Noses." J. Aero. Sci. 23, pp. 796-797, August 1956.

173. Romig, M. F., "Conical Flow Parameters for Air in Dissociation Equilibrium: Final Results." Convair Res. Note 14, January 1958.

174. Sedney, R. and Gerber, N., "Nonequilibrium Flow over a Cone." AIAA Journ. 1, pp. 2482-2486, November 1963.

175. Lee, R. S., "Hypersonic Nonequilibrium Flow over Slender Bodies." J. Fluid Mech. 22, pp. 417-431, July 1965.

176. Probstein, R. F., "Interacting Hypersonic Laminar Boundary-Layer Flow over a Cone." Brown Univ. Tech. Rept. AF 2798/1, March 1955.

177. Peter, R. A., High, M. D., and Blick, E. F., "Viscous Flow Properties on Slender Cones." AIAA Journ. 3, pp. 572-573, March 1965.

178. Talbot, L., Koga, T. and Sherman, P. M., "Hypersonic Viscous Flow over Slender Cones." NACA TN 4327, September 1958.

179. King, H. H., "Hypersonic Flow over a Slender Cone with Gas Injection." Univ. of California, Berkeley, TR HE-150-205, 1962.

180. Probstein, R. F. and Elliot, D., "The Transverse Curvature Effect in Compressible Axially Symmetric Laminar Boundary-Layer Flow." J. Aero. Sci. 23, pp. 208-224, March 1956.

181. Wittliff, C. E. and Wilson, M. R., "Heat Transfer to Slender Cones in Hypersonic Air Flow, Including Effects of Yaw and Nose Bluntness." J. Aero. Sci. 29, pp. 761-774, July 1962.

182. Lukasiewicz, J., "Hypersonic Flow-Blast Analogy." AEDC-TR-61-4, June 1961.

183. Cheng, H. K., "Hypersonic Flow with Combined Leading-Edge Bluntness and Boundary-Layer Displacement Effect." CAL Rept. No. AF-1285-A-4, August 1960.

184. Chernyi, G. G., *Introduction to Hypersonic Flow*, Academic Press, 1961.

185. Lewis, C. H., "Pressure Distribution and Shock Shape over Blunted Slender Cones at Mach Numbers from 16 to 19." AEDC - TN -61-81, August 1961.

186. Burke, A. F. and Curtis, J. T., "Blunt-Cone Pressure Distributions at Hypersonic Mach Numbers." J. Aero. Sci. 29, pp. 237-238, February 1962.

187. Wells, W. R. and Armstrong, W. O., "Tables of Aerodynamic Coefficients Obtained from Developed Newtonian Expressions for Complete and Partial Conic and Spheric Bodies at Combined Angles of Attack and Sideslip with Some Comparisons with Hypersonic Experimental Data." NASA TR R-127, 1962.

188. Whitfield, J. D. and Wolny, W., "Hypersonic Static Stability of Blunt Slender Cones." AEDC-TDR-62-166, August 1962.

189. Edenfield, E. E., "Comparison of Hotshot Tunnel Force, Pressure, Heat-Transfer and Shock Shape Data with Shock Tunnel Data." AEDC-TDR-64-1, January 1964.

190. Trimmer, L. L., "Equations and Charts for the Evaluation of Forces on Spherically Blunted Cones by the Newtonian Theory." AEDC-TR-66-16 April 1966.

191. Wilkinson, D. B. and Harrington, S. A., "Hypersonic Force, Pressure and Heat Transfer Investigations of Sharp and Blunt Slender Cones." AEDC-TDR-63-177, August 1963.

192. Lyons, W. C., Brady, J. J. and Levensteins, Z. J., "Hypersonic Drag, Stability and Wake Data for Cones and Spheres." AIAA Journ. 2, pp. 1948-1956, November 1964.

193. Wilson, R. E., "Laminar Boundary-Layer Growth on Slightly Blunted Cones at Hypersonic Speeds." J. Spacecraft and Rockets 2, pp. 490-496, July-August 1965.

194. Ellett, D. M., "Pressure Distributions on Sphere Cones." Sandia Corp. Rept. RR-64-1796, January 1965.

195. Roberts, J. F., Lewis, C. H. and Reed, M., "Ideal Gas Spherically Blunted Cone Flow Field Solutions at Hypersonic Conditions." AEDC-TR-66-121, August 1966.

196. Jenkins, B. Z., "Real Gas Flow Field Properties Around Blunt Cones Vol. II." Army Missile Command Rept. RF-TR-63-18, December 1963.

197. Eggers, A.J., Jr. and Savin, R.C., "Approximate Methods for Calculating the Flow About Nonlifting Bodies of Revolution at High Supersonic Speeds." NACA TN 2579, December 1951.

198. Eggers, A.J., Jr., Savin, R.C., and Syvertson, C.A., "The Generalized Shock Expansion Method and Its Application to Bodies Traveling at High Supersonic Speeds." J. Aero. Sci., 22, pp. 231-238, April 1955.

199. Whalen, R.J., "Viscous and Inviscid Nonequilibrium Gas Flows." J. Aero. Sci., 29, pp. 1222-1237, October 1962.

200. Heims, S.P., "Prandtl-Meyer Expansion of Chemically reacting Gases in Local Chemical and Thermodynamic Equilibrium." NACA TN 4230, March 1958.

201. Syvertson, C.A. and Dennis, D.H., "A Second Order Shock Expansion Method Applicable to Bodies of Revolution Near Zero Lift." NACA Rept. 1328, 1957.

202. Johannsen, N.H. and Meyer, R.E., "Axially-Symmetric Supersonic Flow Near the Center of an Expansion." Aero. Quart, 2, pp. 127-142, August 1950.

203. Zienkiewicz, H.K., "Flow About Cones at Very High Speeds." Aero. Quart, 8, pp. 384-394, November 1957.

204. Feldman, S.R., "Hypersonic Conical Shocks for Dissociated Air In Thermodynamic Equilibrium." Jet Propulsion, 27, pp. 1253-1255, December 1957.

205. Vincenti, W.G., "Linearized Flow Over a Wedge in Nonequilibrium Oncoming Strean." Journal de Mecanique, 1, pp. 193-211, 1962.

206. Lee, R.S., "A Study of Supersonic Nonequilibrium Flow over a Wedge." Stanford Univ. Rept. SUDAER No. 160, June 1963.

207. Lees, L. and Kubota, T., "Inviscid Hypersonic Flow Over Blunt-Nosed Slender Bodies." J. Aero. Sci. 24, pp. 195-202, March 1957.

208. Cheng, H.K. and Pallone, A.J., "Inviscid Leading-Edge Effects in Hypersonic Flow." J. Aero. Sci. 23, pp. 700-702, July 1956.

209. Lees, L., "Recent Developments in Hypersonic Flow." Jet Propulsion, 27, pp. 1162-1178, November 1957.

210. Rose, P.H., "Physical Gas Dynamics Research at the AVCO Research Laboratory." AVCO Res. Rept. 9, May 1957.

211. Gravalos, F. G., Edelfelt, I. H., and Emmons, H. W., "The Supersonic Flow About a Blunt Body of Revolution for Gases at Chemical Equilibrium." Proc. IX International Astronautical Congress, Amsterdam, Vol. 1, pp. 312-322, August 1958.

212. Rainey, R. W., "Working Charts for Rapid Prediction of Force and Pressure Coefficients on Arbitrary Bodies of Revolution by Use of Newtonian Concepts." NASA TN D-176, December 1959.

213. Margolis, K., "Theoretical Evaluation of the Pressures, Forces and Moments at Hypersonic Speeds Acting on Arbitrary Bodies of Revolution Undergoing Separate and Combined Angle-of-Attack and Pitching Motions." NASA TN D-652, June 1961.

214. Fisher, L. R., "Equations and Charts for Determining the Hypersonic Stability Derivatives of Combinations of Cone Frustrums Computed by Newtonian Impact Theory." NASA TN D-149, November 1959.

215. Clark, E. L. and Trimmer, L. L., "Equations and Charts for the Evaluation of the Hypersonic Aerodynamic Characteristics of Lifting Configurations by the Newtonian Theory." AEDC-TDR-64-25, March 1964.

216. Miele, A., _Theory of Optimum Aerodynamic Shapes_, Academic Press, New York, 1965.

217. Geiger, R. E., "Experimental Lift and Drag of a Series of Glide Configurations at Mach Numbers 12.6 and 17.5." J. Aero. Sci. 29, pp. 410-419, April 1962.

218. Larson, H. K., "The Hypersonic Shape." Space/Aeronautics, 45, pp. 69-75, September 1965.

219. Shih, W. E. L. and Baron, J. R., "Nonequilibrium Blunt-Body Flow Using the Method of Integral Relations." AIAA Journ. 2, pp. 1062-1071, June 1964.

220. Inger, G. R., "Viscous and Inviscid Stagnation Flow in a Dissociating Hypervelocity Free Stream." Aerospace Corp. Rept. TDR-69 (2230-06) TR-2, July 1962.

221. Wood, A. D., Springfield, J. F., and Pallone, A. J., "Chemical and Vibrational Relaxation of an Inviscid Hypersonic Flow." AIAA Journ. 2, pp. 1697-1706, October 1964.

222. Curtis, J. T. and Strom, C. R., "Applications of Numerical Methods to the Problems of Hypersonic Flow Fields." Paper presented at the SIAM Symposium on _Numerical Solution of Nonlinear Differential Equations_, Univ. of Iowa. May 9-11, 1966.

223.   Vaglio-Laurin, R. and Bloom, M.H., "Chemical Effects in External Hypersonic Flows." Hypersonic Flow Research (Edit., F.R. Riddell), pp. 205-254, Academic Press, New York, 1962.

224.   Lin, S.C. and Teare, J.D., "A Streamtube Approximation for Calculations of Reaction Rates in the Inviscid Flow Field of Hypersonic Objects." AVCO Res. Note 223, August 1961.

225.   Tragott, S.C., "Some Features of Supersonic and Hypersonic Flow About Blunted Cones." J. Aero. Sci., 29, pp. 389-399, April 1962.

226.   Eschenroeder, A.Q., "Ionization Nonequilibrium in Expanding Flows." ARS Journ. 32, pp. 196-203, February 1962.

227.   Boyer, D.W., "Ionization Nonequilibrium Effects on the Magnetogasdynamic Interaction in the Stagnation Region of an Axisymmetric Blunt Body." CAL Rept. No. AG-1547-Y-1, June 1963.

228.   Nonequilibrium Nozzle Expansion Calculations for ARO Inc. - Communicated to Dr. W. Norman of ARO by D.W. Boyer of CAL.

229.   Fay, James A., "Hypersonic Heat Transfer in the Air Laminar Boundary Layer." The High Temperature Aspects of Hypersonic Flow (Edit., W.C. Nelson), pp. 583-606, AGARDograph 68, Macmillan New York, 1964. (Also Everett Res. Lab. Rept. AMP 71, March 1962.)

230.   Chambré, P.L. and Acrivos, A. "On Chemical Surface Reactions in Laminar Boundary Layer Flows." J. of App. Physics, 27, pp. 1322-1328, November 1956.

231.   Hoshizaki, H. "Heat Transfer in Planetary Atmospheres at Super-Satellite Speeds." ARS Journ. 32, pp. 1544-1552, October 1962.

232.   Merritt, G.E. and Weatherston, R.C., "Condensation of Mercury Vapor and Drop Growth Processes in a Nitrogen Flow." AIAA Paper No. 66-85, January 1966.

233.   Hill, P.G., Witting, H., Demetri, E.P., "Condensation of Metal Vapors During Rapid Expansion." Trans-ASME, 62-WA-123, 1962.

234.   Brogan, T.R., "The Electric Arc Wind Tunnel - A Tool for Atmospheric Reentry Research." ARS Journ. 29, pp. 648-653, July 1959.

235.   Georgiev, S., "The Relative Merits of Various Test Facilities with Regard to Simulation of Hypersonic Ablation Phenomena." Proceedings of the IAS National Symposium on Hypervelocity Techniques, Denver, Colorado, October 1960.

236.   Lees, L., "Similarity Parameters for Surface Melting of a Blunt-Nosed Body in a High-Velocity Gas Stream." ARS Journ. 29, pp. 345-354, May 1959.

237.   Stetson, K.F., "Preliminary Cone-Ablation Results." J. Spacecraft and Rockets, 2, pp. 232-238, March - April 1965.

238.   Ostrach, S., Goldstein, A.W., and Hamman, J., "Analysis of Melting Boundary Layers on Decelerating Bodies." NASA TN D-1312, July 1962.

239.   Graves, K.W., "Ablation in a High Shear Environment." AIAA Journ. 4, pp. 853-857, May 1966.

240.   Sachs, I, and Schurmann, E.E., "Aerodynamic Phenomena Associated with Advanced Reentry Systems." AVCO RAD TM-63-79, December, 1963.

241.   Grimes, J.H. and Casey, J.J., "Influence of Ablation on the Dynamics of Slender Reentry Configurations." J. Spacecraft and Rockets, 2, pp. 106-108, January - February 1965.

242.   Colosimo, D.D., "The Effects of Mass Transfer on the Dynamic Stability of Slender Cones." CAL Rept. 141, May 1965.

243.   Pettus, J.J., "Persistent Reentry Vehicle Roll Resonance." AIAA Paper No. 66-49, January 1966.

244.   Syvertson, C.A. and McDevitt, J.B., "Effects of Mass Addition on the Stability of Slender Cones at Hypersonic Speeds." AIAA Journ. 1, pp. 939-940, April 1963.

245.   Stalmach, C.J. and Pope, T.C., "Preliminary Investigation of the Effects of Mass Injection on Dynamic Stability at M = 17." LTV Report 2-59740/3R-479, October 1963.

246.   "Transactions of the Second Technical Workshop on Dynamic Stability Testing." AEDC Report, April 1965.

247.   Thyson, N., "A Linearized Analysis Concerning Boundary-Layer Effects on the Static and Dynamic Behavior of Slender Ablating and Nonablating Bodies." AVCO RAD TM-64-34, 29 July 1964.

248.   Thyson, N. A. and Schurmann, E.E.H., "Blowing Effects on Pressure Interaction Associated with Cones." AIAA Journ. 1, pp. 2179-2180, September 1963. See Comments by Li and Gross and Author's Reply, AIAA Journ. 2, pp. 1868-1869, October 1964.

249. Li, T. Y. and Gross J. F., "Hypersonic Viscous Interaction on a Slender Body of Revolution with Surface Mass Transfer." Rand Corporation Report P-2977-1, April 1965.

250. Denison, M. R., "Estimating Transient Temperature Distributions During Ablation." ARS Journ. 30, pp. 562-563, June 1960.

251. Bedingfield, C. H. and Drew, T. B., "Analogy Between Heat Transfer and Mass Transfer - A Psychrometric Study." Industrial and Engineering Chemistry, 42, pp. 1164-1173, 1950.

252. Sogin, H. H., "Sublimation from Discs to Airstreams Flowing Normal to Their Surfaces." Trans. ASME, 80, pp. 61-69, January 1958.

253. Walsh, P. N. and Smith N. O., "Sublimation Pressure of α- p-Dichloro-, β-p-Dichloro-, p-Dibromo-, and p-Bromochloro-benzene." Journ. of Chemical Engineering Data, 6, pp. 33-35, 1961.

254. Ravich, G. B. and Burtsev, Yu. N., "The Effect of Polymorphism on Thermal Conductivity." DAN SSR 137, No. 5, pp. 1155-1157, April 1961 (In Russian). Translation in Proceedings of the Academy of Sciences, USSR, Physical Chemistry Section 137, pp. 1-6, March-April 1961, pp. 337-339, Consultants Bureau, New York.

255. Ueberreiter, K. and Orthmann, H. J., "Spezifische warme, Spezifisches volumen, temperatur-und Warmeleitfahigkeit einiger disubstituierter benzole und polycyclischer systeme." Zeitschrift fur Naturforschung 5a, pp. 101-108, 1950.

256. Scala, S. M. and Vidale, G. L., "Vaporization Processes in the Hypersonic Laminar Boundary Layer." International Journ. of Heat and Mass Transfer 1, pp. 4-22, January 1960.

257. Goodman, T. R., "The Heat-Balance Integral and Its Application to Problems Involving a Change of Phase." Trans. ASME 80, 335-342, February 1958.

258. Charwat, A. F., "The Effect of Surface-Evaporation Kinetics on the Sublimation into a Boundary Layer." Rand Corp. Memorandum RM-3291-PR, June 1964.

259. Kubota, T., "Ablation with Ice Model at M = 5.8." ARS Journ. 30, pp. 1164-1169, December 1960.

260. Spalding, D. B., "The Prediction of Mass Transfer Rates when Equilibrium does not Prevail at the Phase Interface." International Journ. of Heat and Mass Transfer 2, pp. 283-313, June 1961.

261. Burke, A. F. and Ryder, M. O., "Further Shock Tunnel Studies of Pressure, Heat Transfer and Skin Friction Distributions on Slender Cones at Angles of Attack Including the Effects of Nose Transpiration Cooling." CAL Report AA/1747-Y-2, April 1964.

262. Bird, K. D., "Dynamic Stability Testing in a Hypersonic Shock Tunnel." Paper presented at AFBSD-GE Technical Workshop on Hypersonic Dynamic Stability Testing, Philadelphia, Pa., July 16-17, 1963.

263. Martin, J. F., "Dynamic Stability Research in the Cornell Aeronautical Laboratory 24" Hypersonic Shock Tunnel." Paper presented at the Thirteenth Meeting of the Supersonic Tunnel Association, Dallas, Texas, April 1960.

264. Urban, R. H., "A Dynamic Stability Balance for Hypervelocity (Hotshot) Tunnels." AEDC TR-65-222, October 1965.

265. Glick, H. S., Hertzberg, A., and Smith, W. E., "Flow Phenomena in Starting a Hypersonic Shock Tunnel." CAL Rept. AD-789-A-3, AEDC TN 55-16, March 1955.

266. Lukasiewicz, J., Whitfield, J. D., and Jackson, R., "Aerodynamic Testing at Mach Numbers from 15 to 20." Hypersonic Flow Research (Edit., F. R. Riddell), pp. 473-512, Academic Press, New York, 1962.

267. Hilton, J., Golian, T., Somers, L., Wilson, M., and Fabian, G., "Development and Performance of the CAL 6-Foot Hypersonic Shock Tunnel." CAL Rept. No. 120. (To be published)

268. Vidal, R. J., "Model Instrumentation-Techniques for Heat Transfer and Force Measurements in a Hypersonic Shock Tunnel." CAL Rept. AD-917-A-1, WADC TN 56-315, February 1956.

269. Rose, P. H., "Development of the Calorimeter Heat Transfer Gage for Use in Shock Tubes." AVCO Res. Rept., 17 February 1958.

270. Vidal, R. J. and Wittliff, C. E., "Hypersonic Low Density Studies of Blunt and Slender Bodies." Rarefied Gas Dynamics, Third Symposium, Vol. II, (Edit., J. A. Laurmann), pp. 343-378, Academic Press, New York, 1963.

271. Skinner, G. T., "Analog Network to Convert Surface Temperature to Heat Flux." CAL Rept. CAL-100, February 1960. (Also, ARS Journ. 30, pp. 569-570, June 1960.)

272. Vidal, R. J., Skinner, G. T., and Bartz, J. A., "Speed-Ratio Measurements in Nonequilibrium Nozzle and Free-Jet Expansions." CAL Rept. No. AF-2041-A-1, AFOSR 66-1975, October 1966.

273. Martin, J. F., Duryea, G. R., and Stevenson, L. M., "Instrumentation for Force and Pressure Measurements in a Hypersonic Shock Tunnel." Advances in Hypervelocity Techniques (Edit. A. M. Krill) Plenum Press, New York, 1962.

274. MacArthur, R. C., "Transducer for Direct Measurement of Skin Friction in the Hypersonic Shock Tunnel." CAL Rept. No. 129, August 1963.

275. Holden, M. S., "Theoretical and Experimental Studies of Separated Flows Induced by Shock Wave-Boundary Layer Interaction." Paper presented at the AGARD Specialists Meeting on "Separated Flows", Brussels, Belgium, May 9-11, 1966.
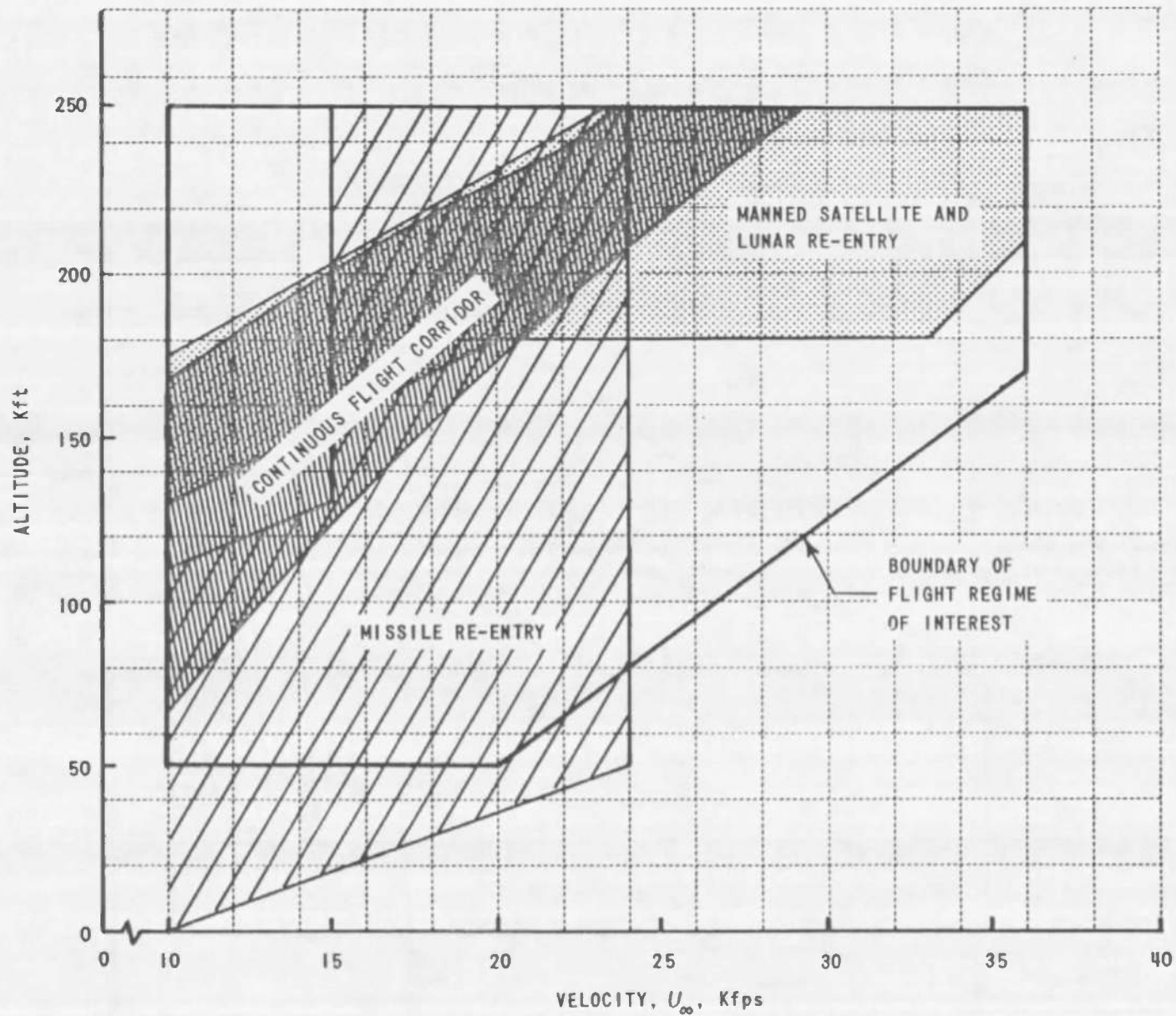
Figure 1   ALTITUDE-VELOCITY MAP OF FLIGHT REGIME OF INTEREST
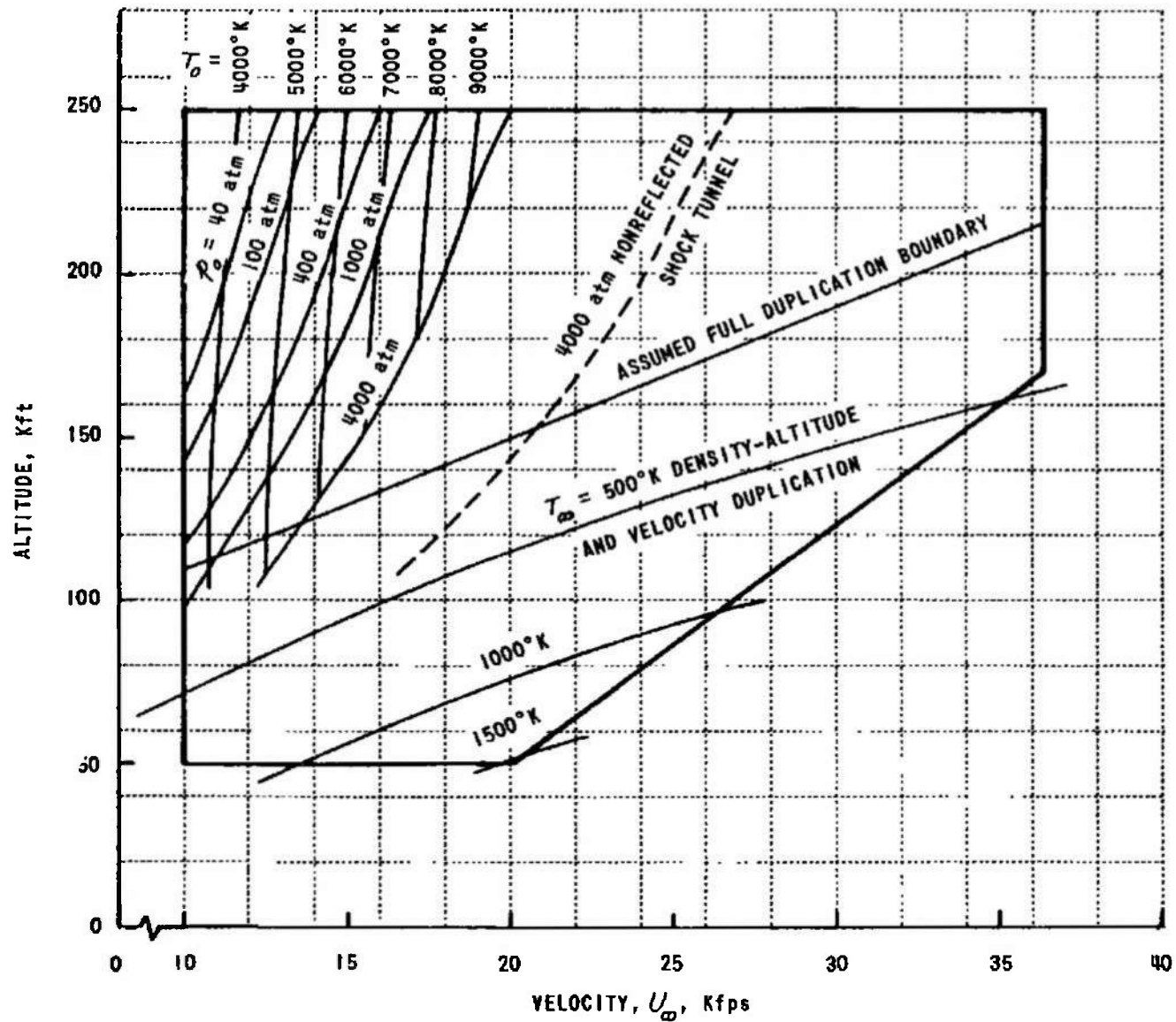
Figure 2 ALTITUDE-VELOCITY MAP SHOWING WIND TUNNEL PERFORMANCE
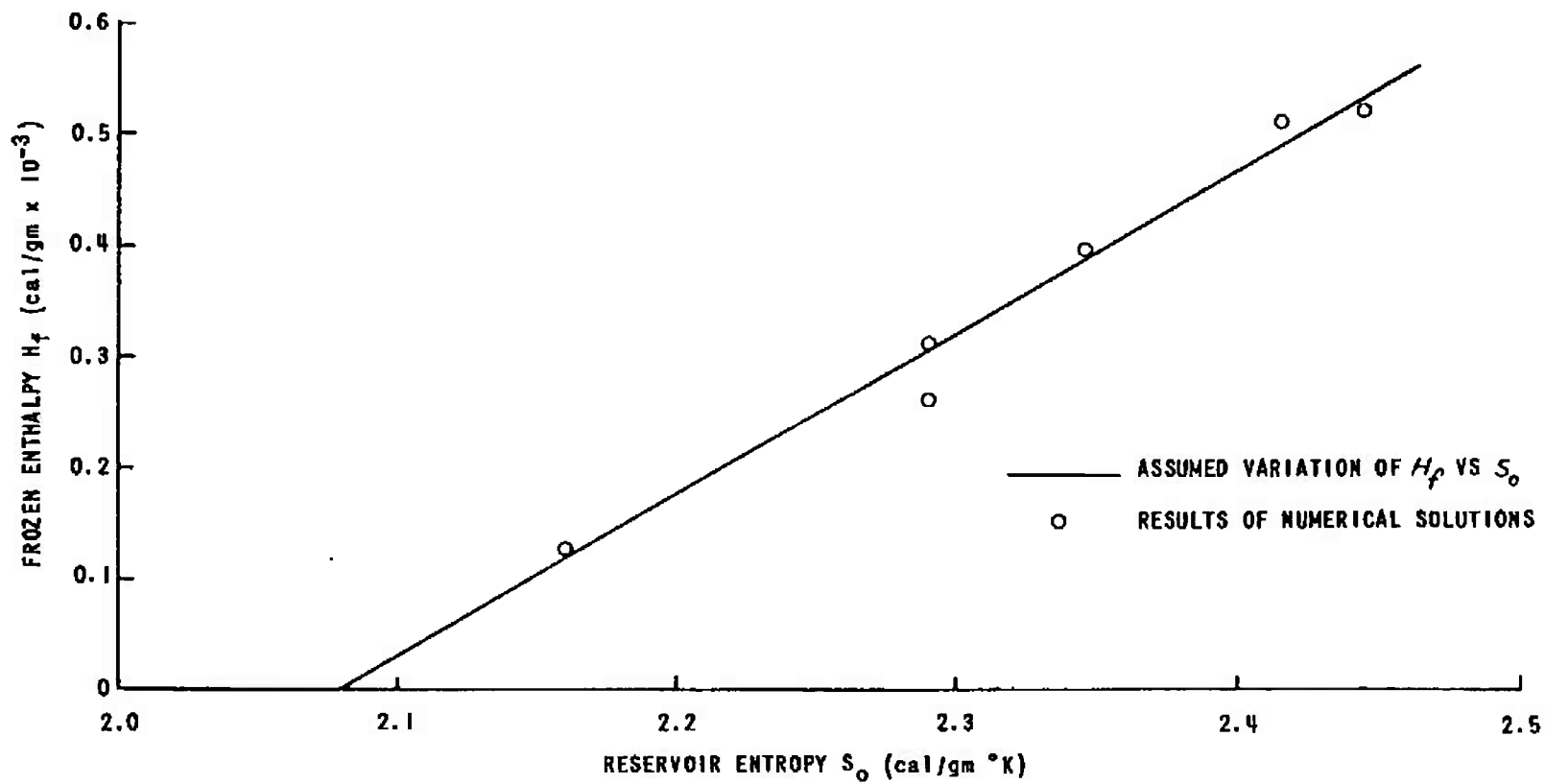
Figure 3   CORRELATION OF FROZEN ENTHALPY WITH RESERVOIR ENTROPY (TAKEN FROM REF. 9)
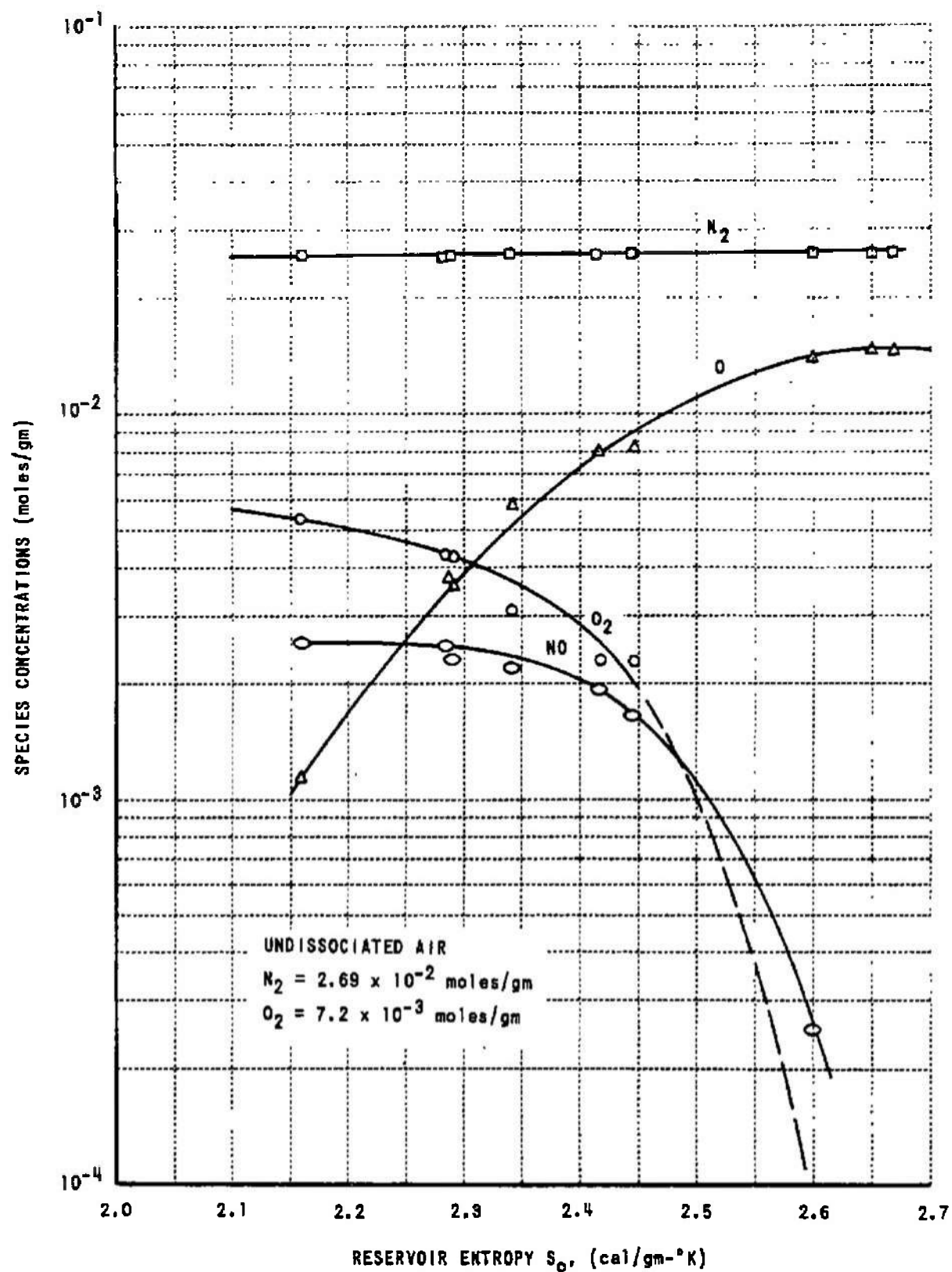
Figure 4 CORRELATION OF NOZZLE FLOW RESULTS FOR FROZEN SPECIES CONCENTRATIONS
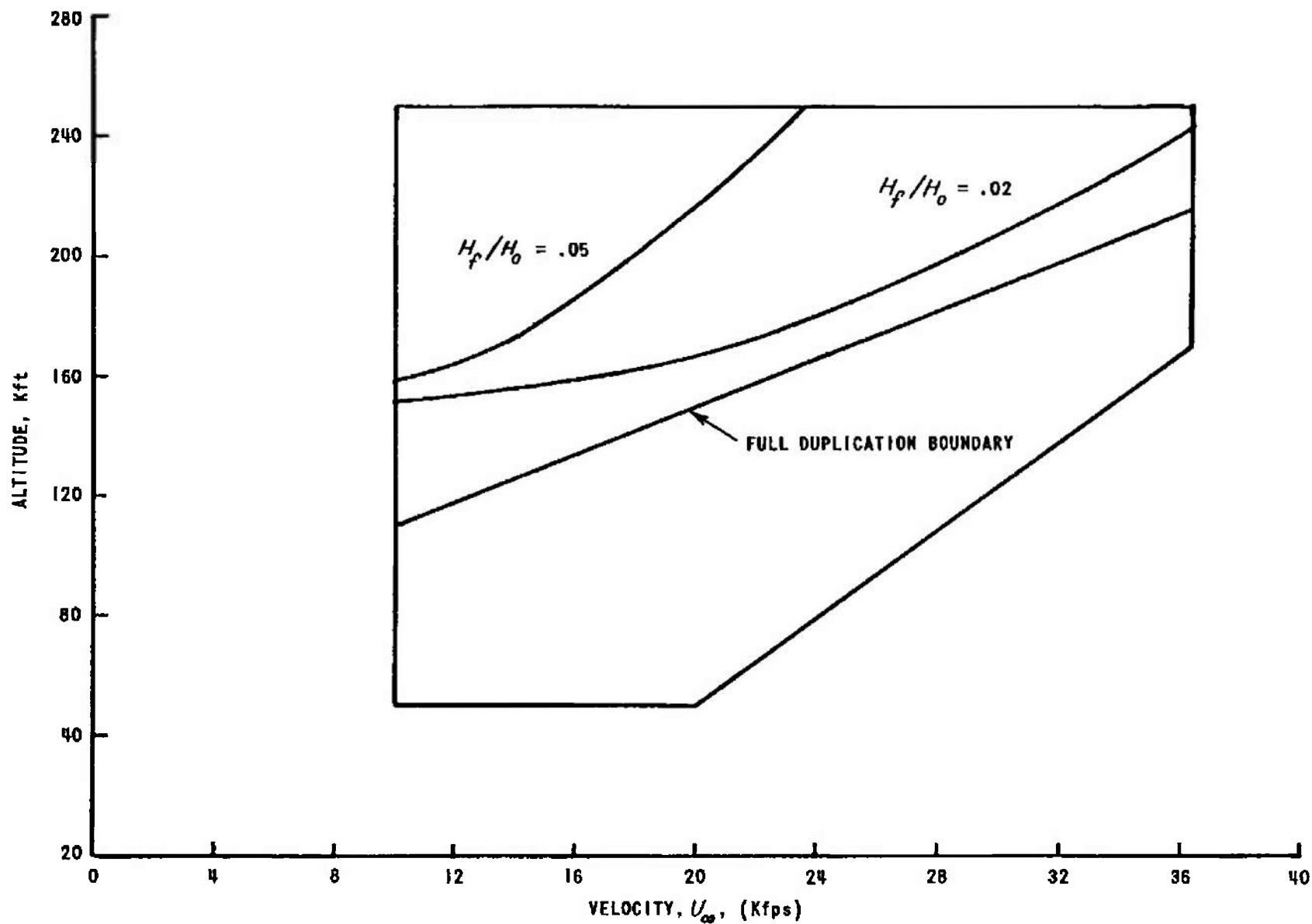
Figure 5 REGIONS OF SIGNIFICANT TEST FLOW NONEQUILIBRIUM AND FULL VELOCITY –
ALTITUDE DUPLICATION
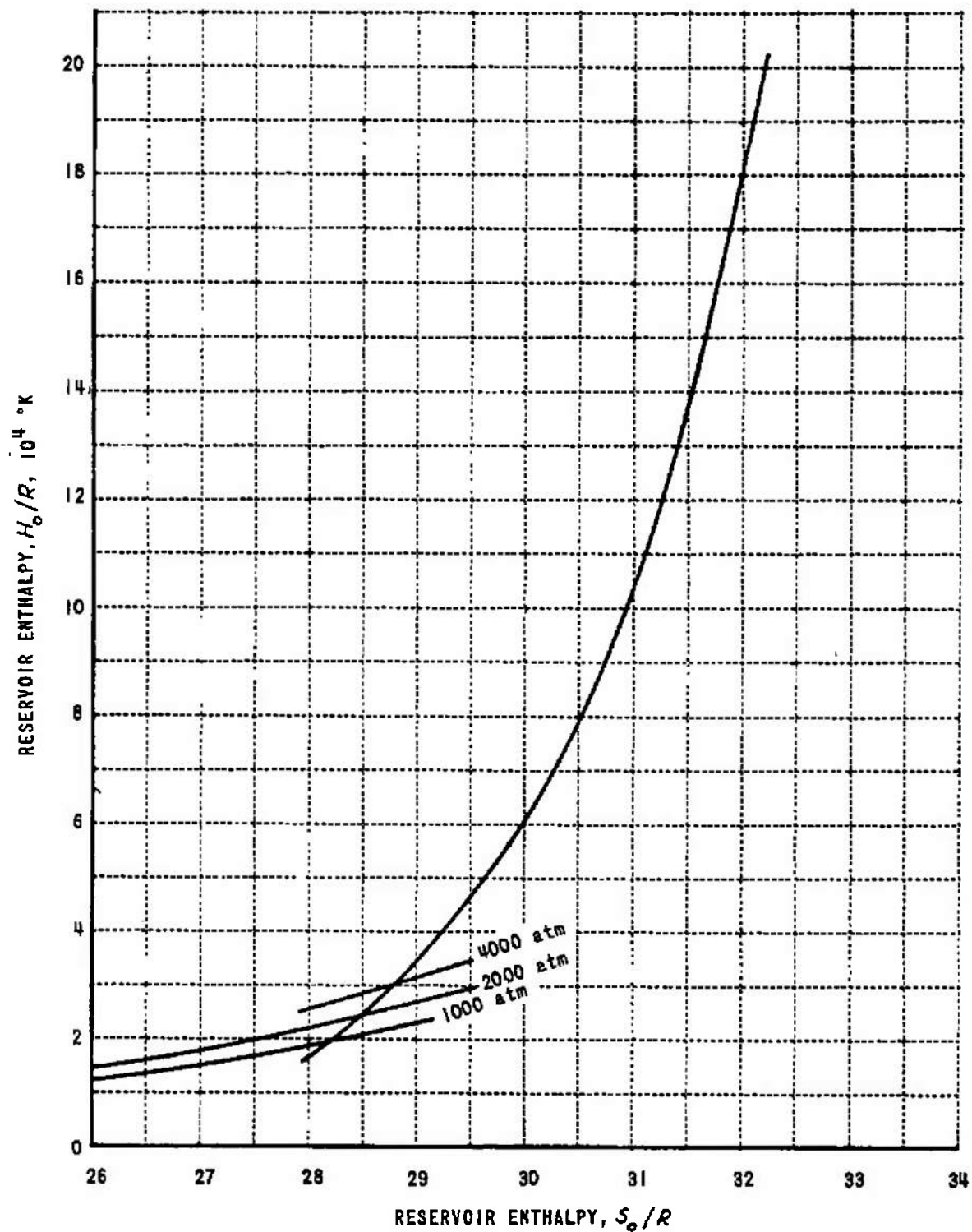
Figure 6   MAXIMUM RESERVOIR ENTHALPY AS A FUNCTION OF ENTROPY FOR HYPOTHETICAL WIND TUNNEL
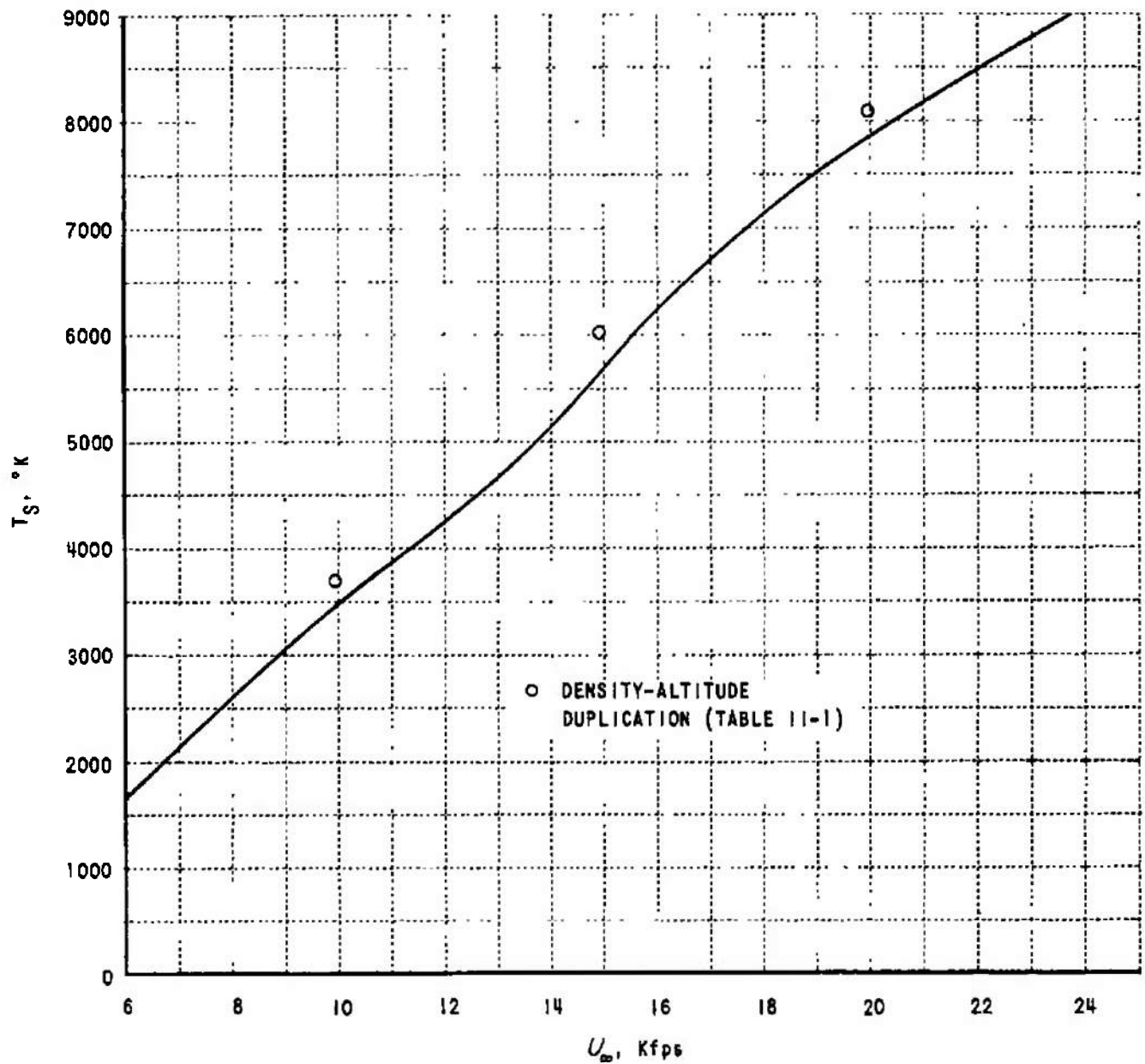
Figure 7a   COMPARISON WITH FLIGHT CASE FOR 50,000 ft ALTITUDE OF
TEMPERATURE BEHIND AN EQUILIBRIUM NORMAL SHOCK WHEN
DENSITY-ALTITUDE IS DUPLICATED
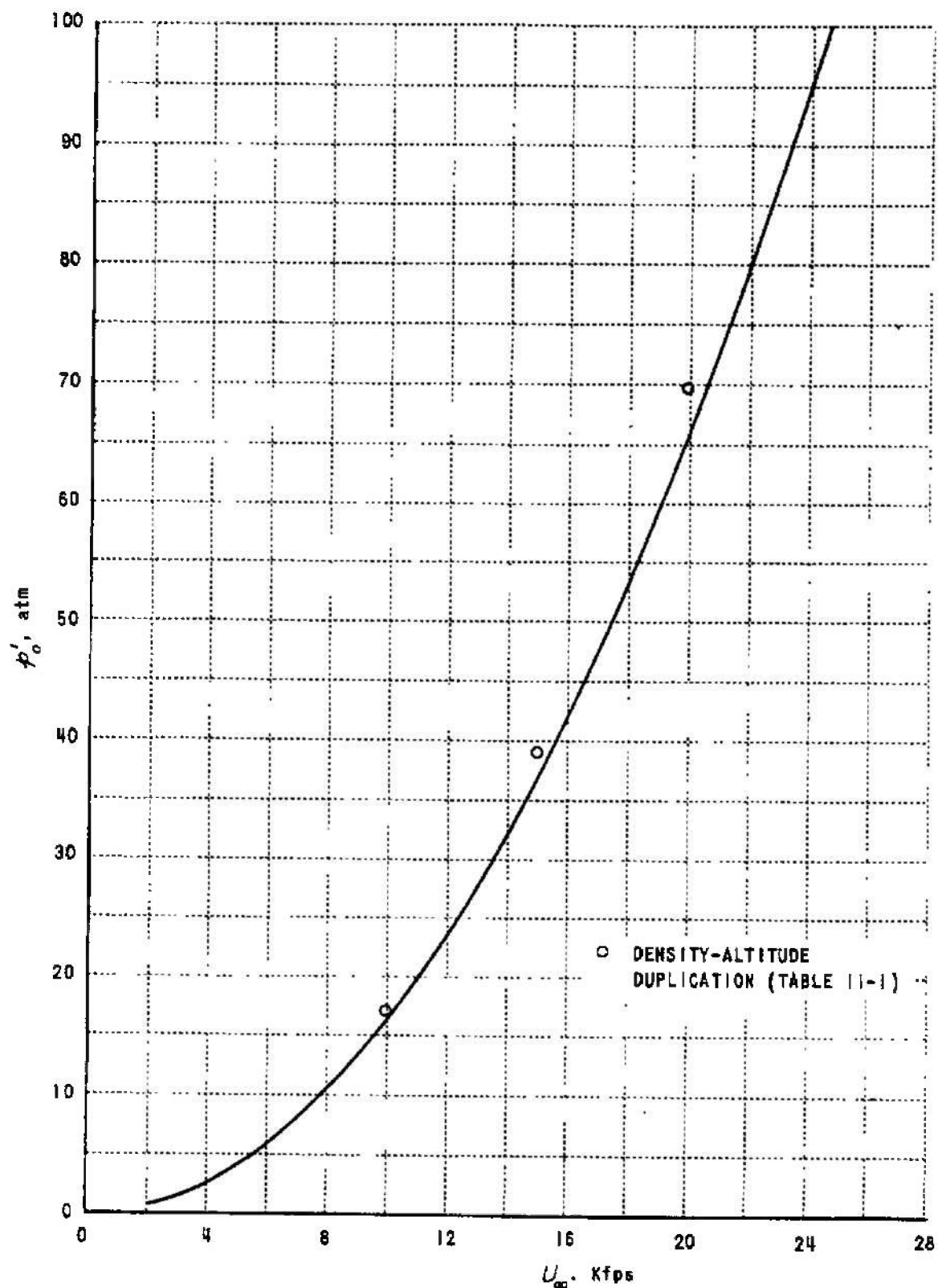
Figure 7b   COMPARISON WITH FLIGHT CASE FOR 50,000 ALTITUDE OF PITOT
PRESSURE BEHIND AN EQUILIBRIUM NORMAL SHOCK WHEN DENSITY-
ALTITUDE IS DUPLICATED
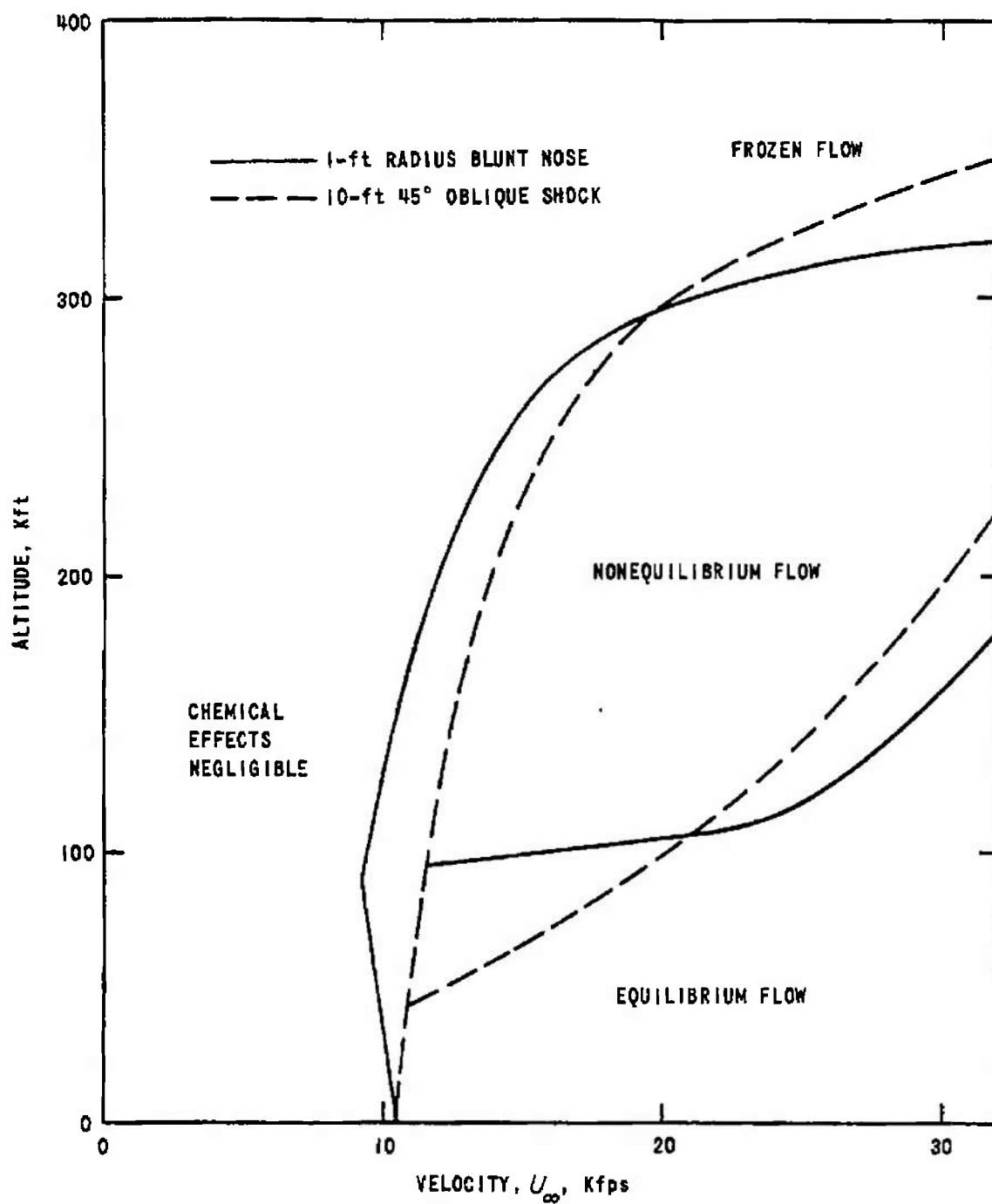
Figure 8 CHEMICAL KINETIC REGIMES OF HYPERSONIC FLOW
ACCORDING TO HARNEY (REF. 17)
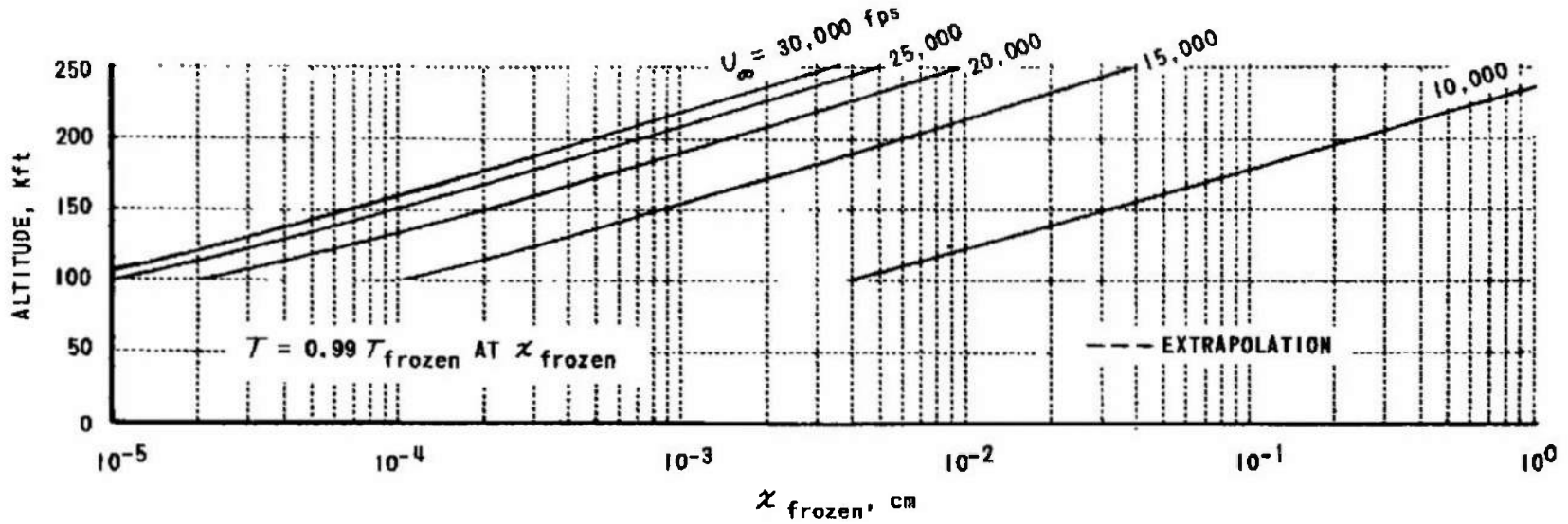
Figure 9a   EXTENT OF FROZEN FLOW BEHIND A NORMAL SHOCK WAVE
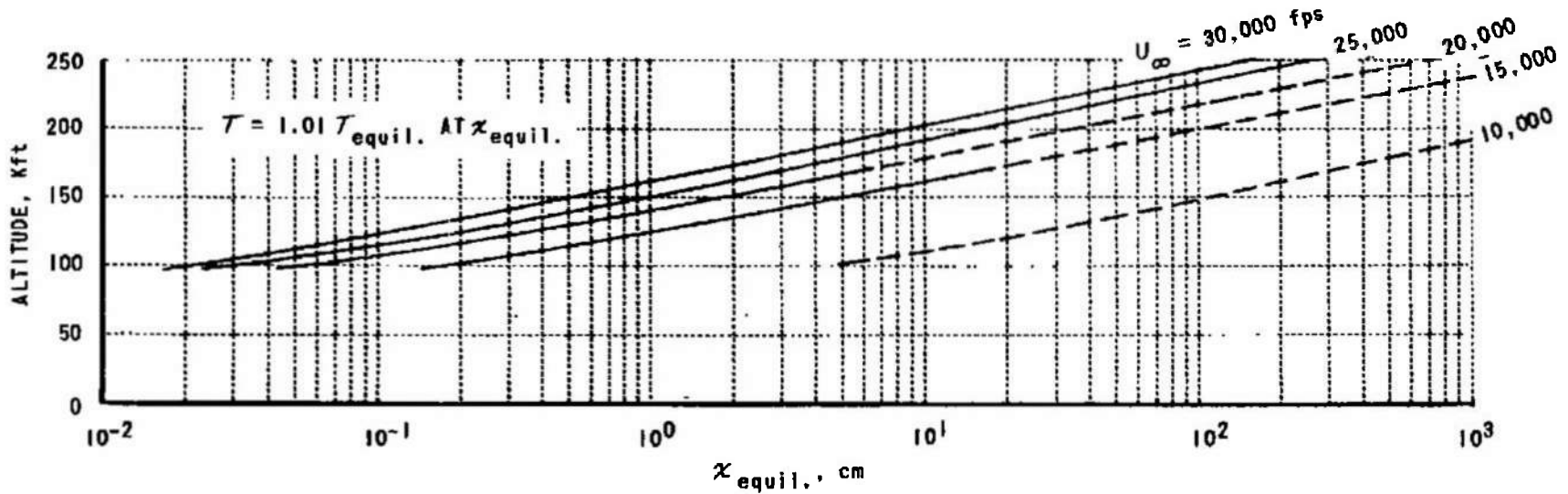
Figure 9b   DISTANCE TO REACH EQUILIBRIUM BEHIND A NORMAL SHOCK WAVE
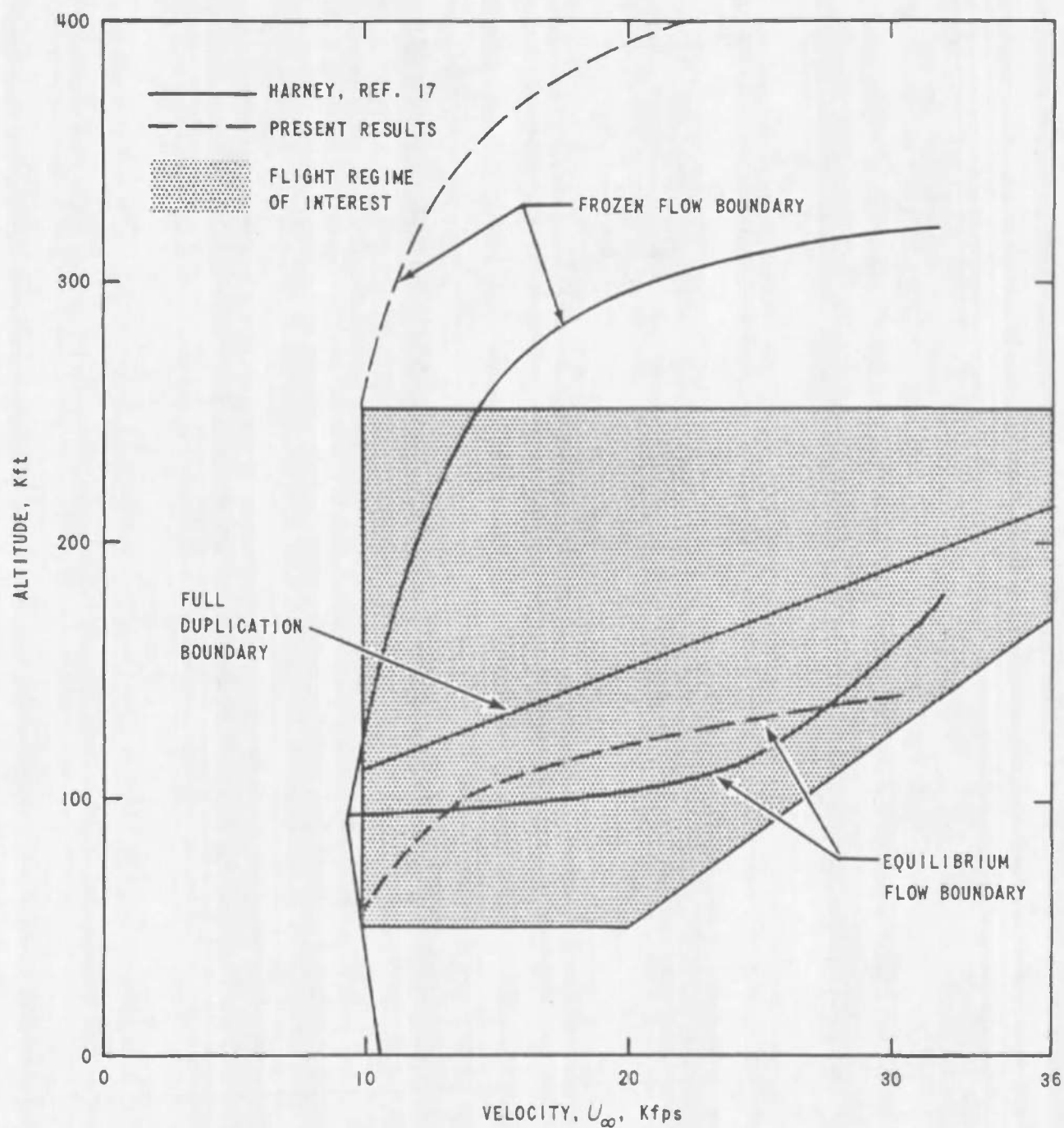
Figure 10 COMPARISON OF CHEMICAL KINETIC FLOW REGIMES
FOR BLUNT-NOSE FLOW
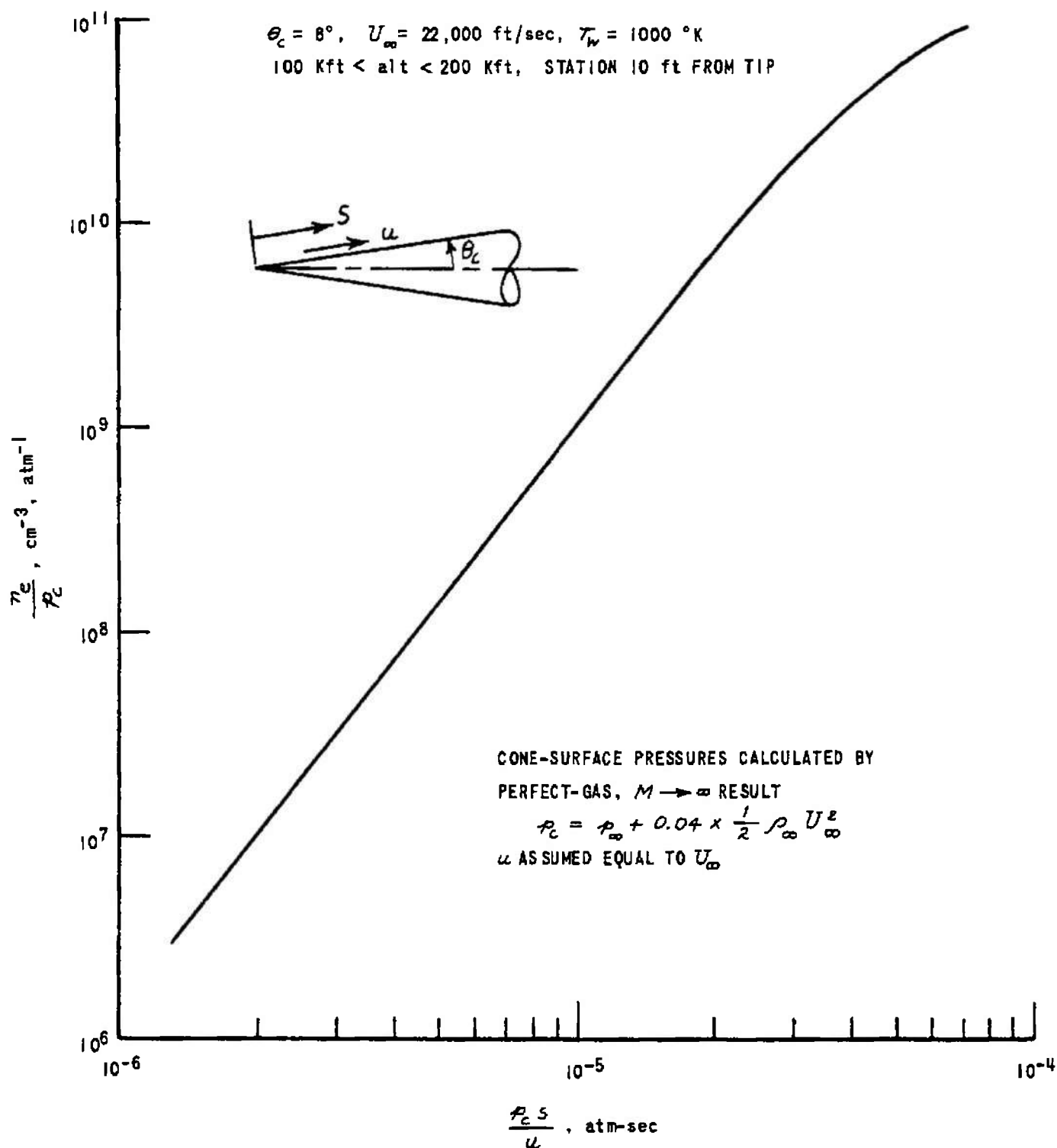
Figure II   BINARY SCALING OF PEAK ELECTRON DENSITY ON A SHARP CONE
            (RESULTS TAKEN FROM REF. 79)

$$-f_w)_{H-S} = \left(\frac{8}{3} \frac{\rho_\infty}{\rho_s}\right)^{1/4} \left(\frac{\rho_w \mu_w}{\rho_e \mu_e}\right)^{1/2} f_w)_{DR-P} \qquad \frac{\rho_\infty}{\rho_s} \text{ TAKEN AS } 1/15$$

DASHED CURVE IS THE HOWE-SHEAFFER CORRELATION

$$\frac{q)_{f_w \neq 0}}{q)_{f_w = 0}} = exp\left\{-b(-f_w)_{H-S}^{3/2}\right\}$$

$$U \leq 30,000 \ ft/sec$$
$$b(U_\infty) = \frac{45}{\bar{U}^2}\left(1 - \frac{300}{\bar{U}^6}\right)$$
$$\bar{U} = \frac{U_\infty [ft/sec]}{10,000}$$

$$U \geq 30,000 \ ft/sec$$
$$b(U_\infty) = 0.706 + 1.6\bar{U} - 0.28\bar{U}^2$$
$$\bar{U} = \frac{U_\infty [ft/sec]}{10,000}$$
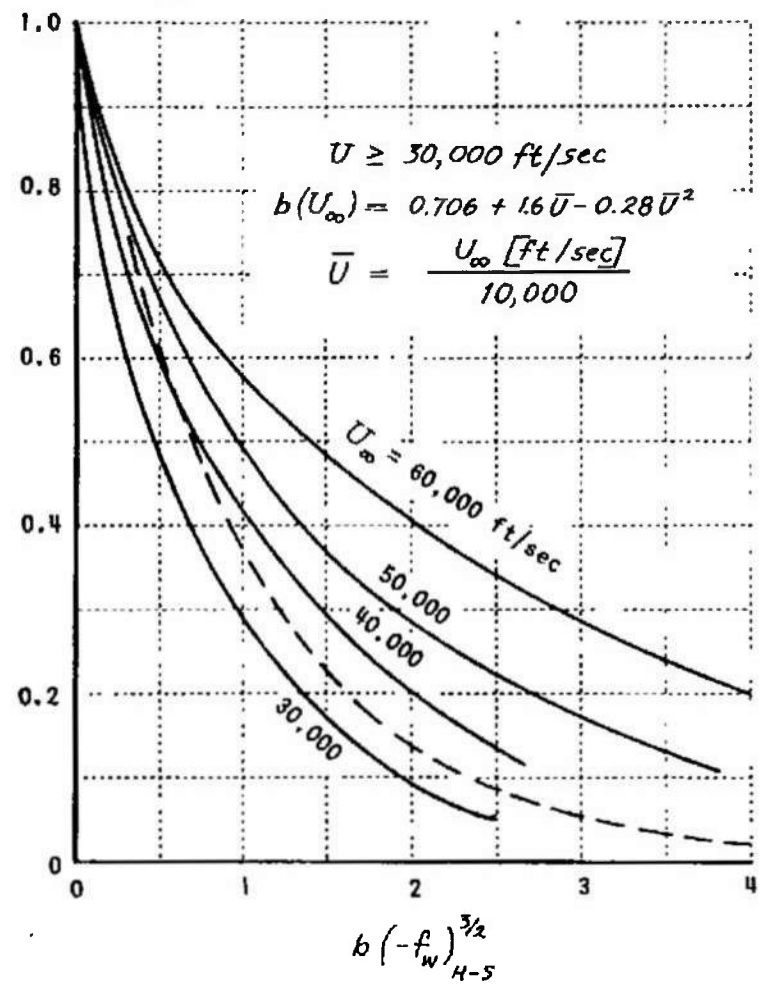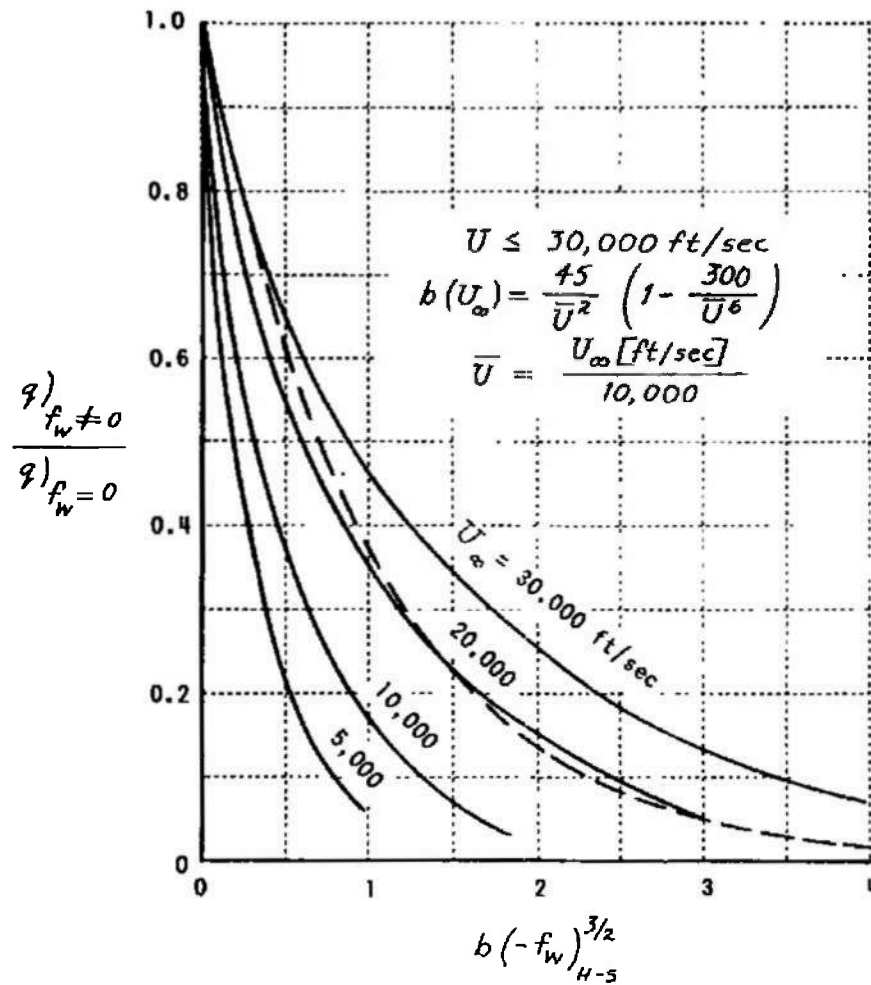
Figure 12 HEAT-TRANSFER, MASS-TRANSFER CORRELATION OF HOWE AND SHEAFFER (REF. 57)
APPLIED TO RESULTS OF DE RIENZO AND PALLONE (REF. 87)
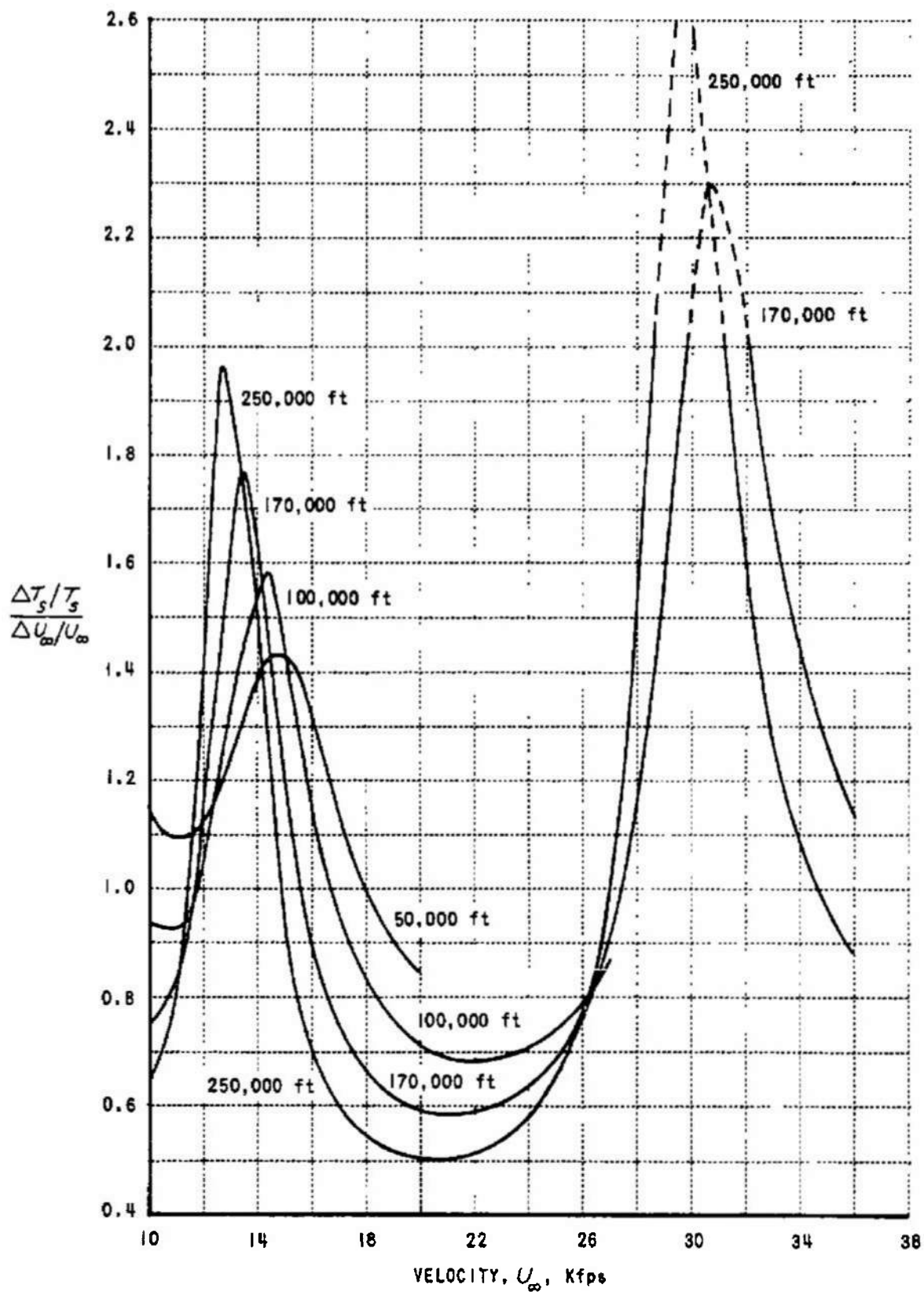
Figure 13 SENSITIVITY OF TEMPERATURE BEHIND AN EQUILIBRIUM NORMAL SHOCK WAVE
TO CHANGES IN FREE STREAM VELOCITY
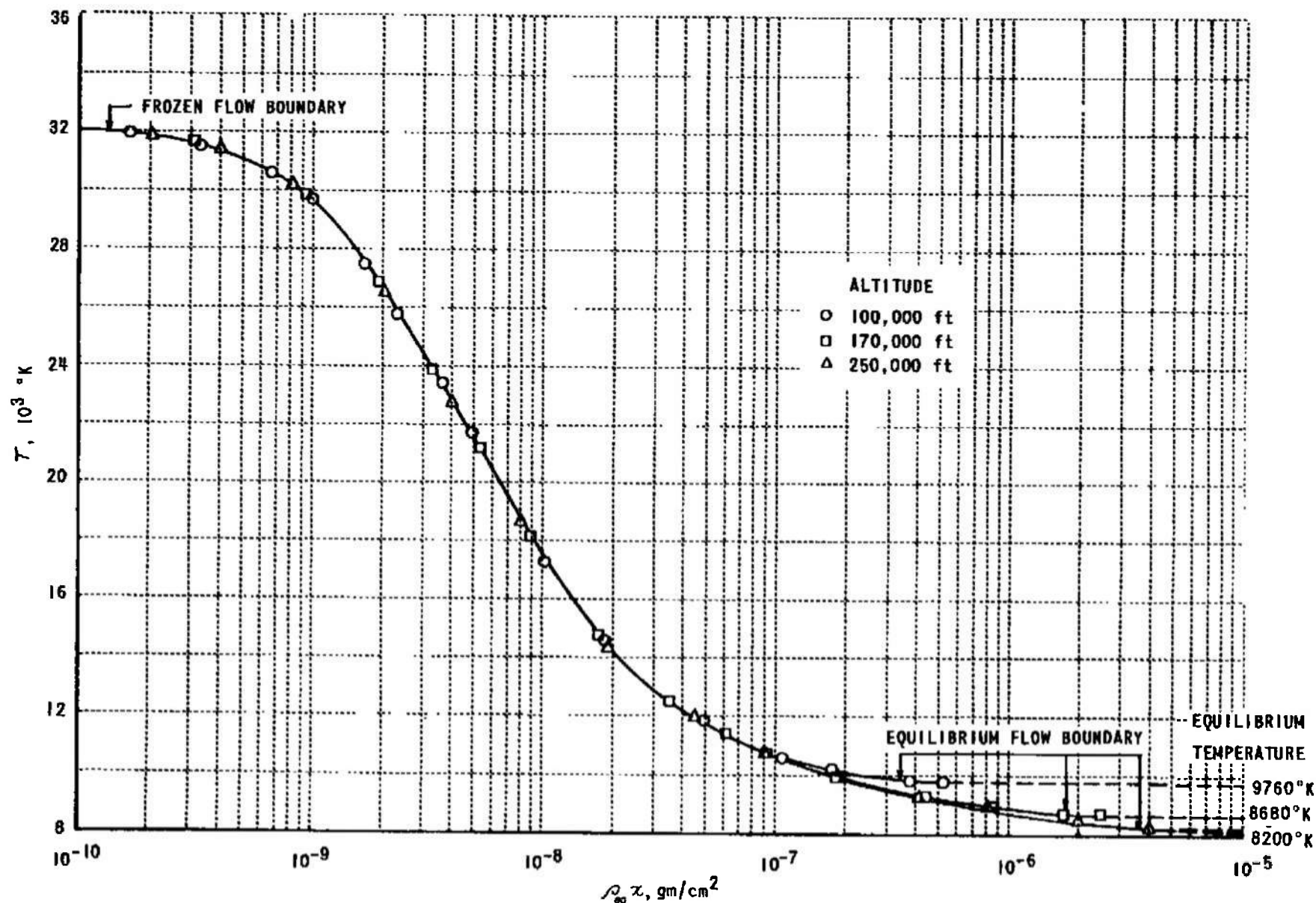
Figure 14 CORRELATION OF TEMPERATURES IN RELAXATION ZONE BEHIND NORMAL SHOCK AT 30,000 fps

225

AEDC-TR-67-72
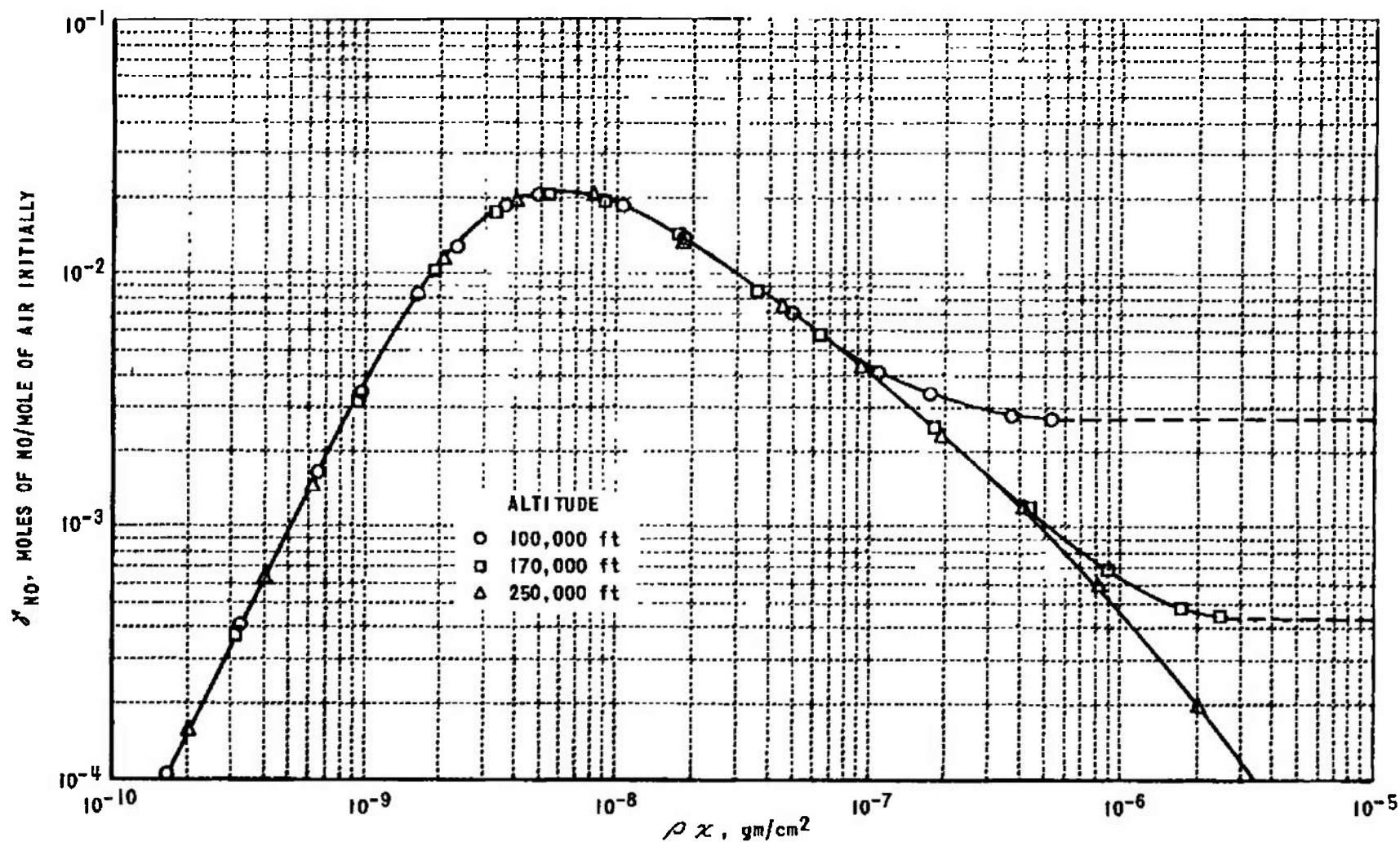
Figure 15   CORRELATION OF NO SPECIES CONCENTRATIONS BEHIND A NORMAL SHOCK WAVE IN
NONEQUILIBRIUM AIR FOR U_∞= 30,000 fps
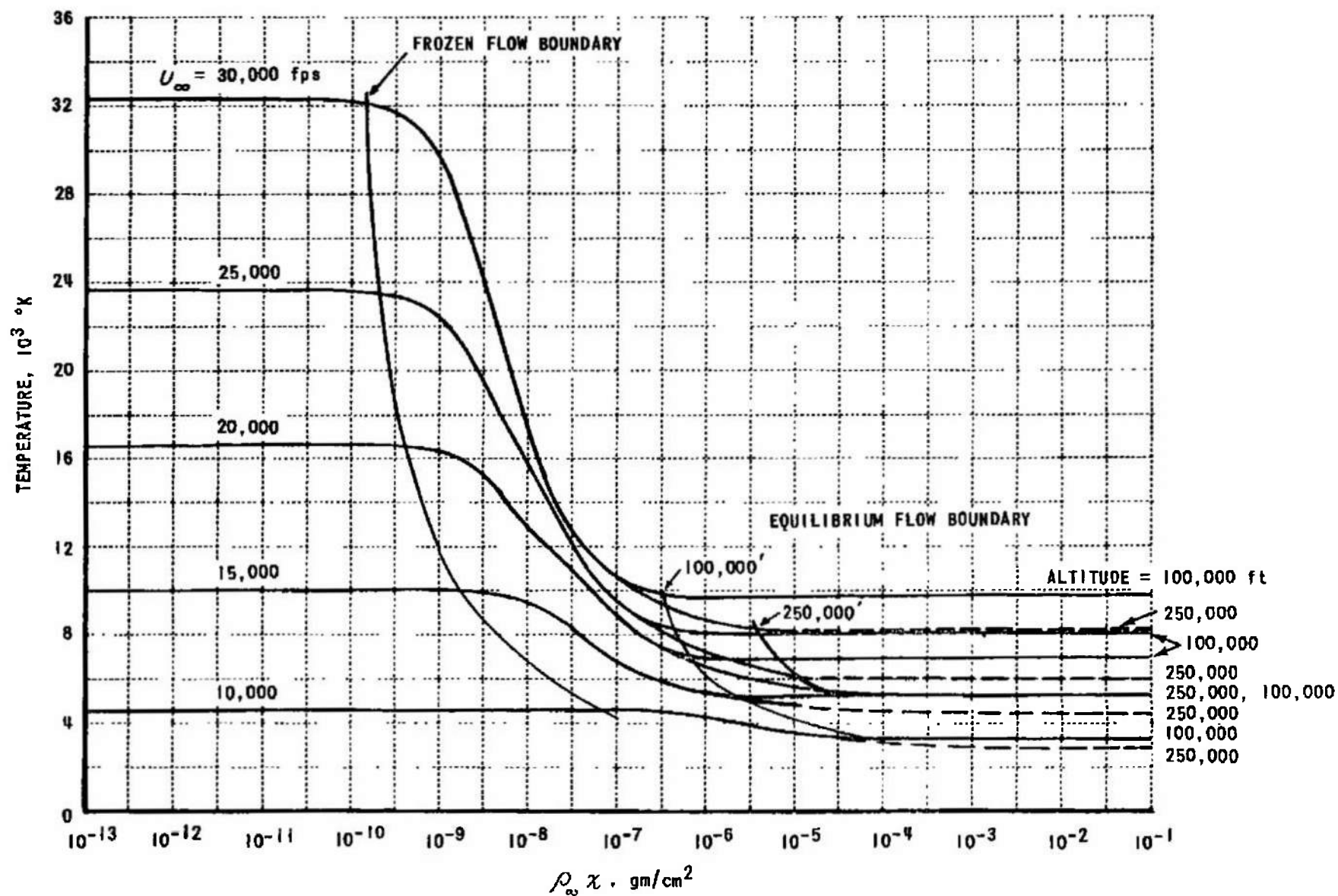
Figure 16 CORRELATION OF TEMPERATURE BEHIND NORMAL SHOCK WAVE BY BINARY SCALING
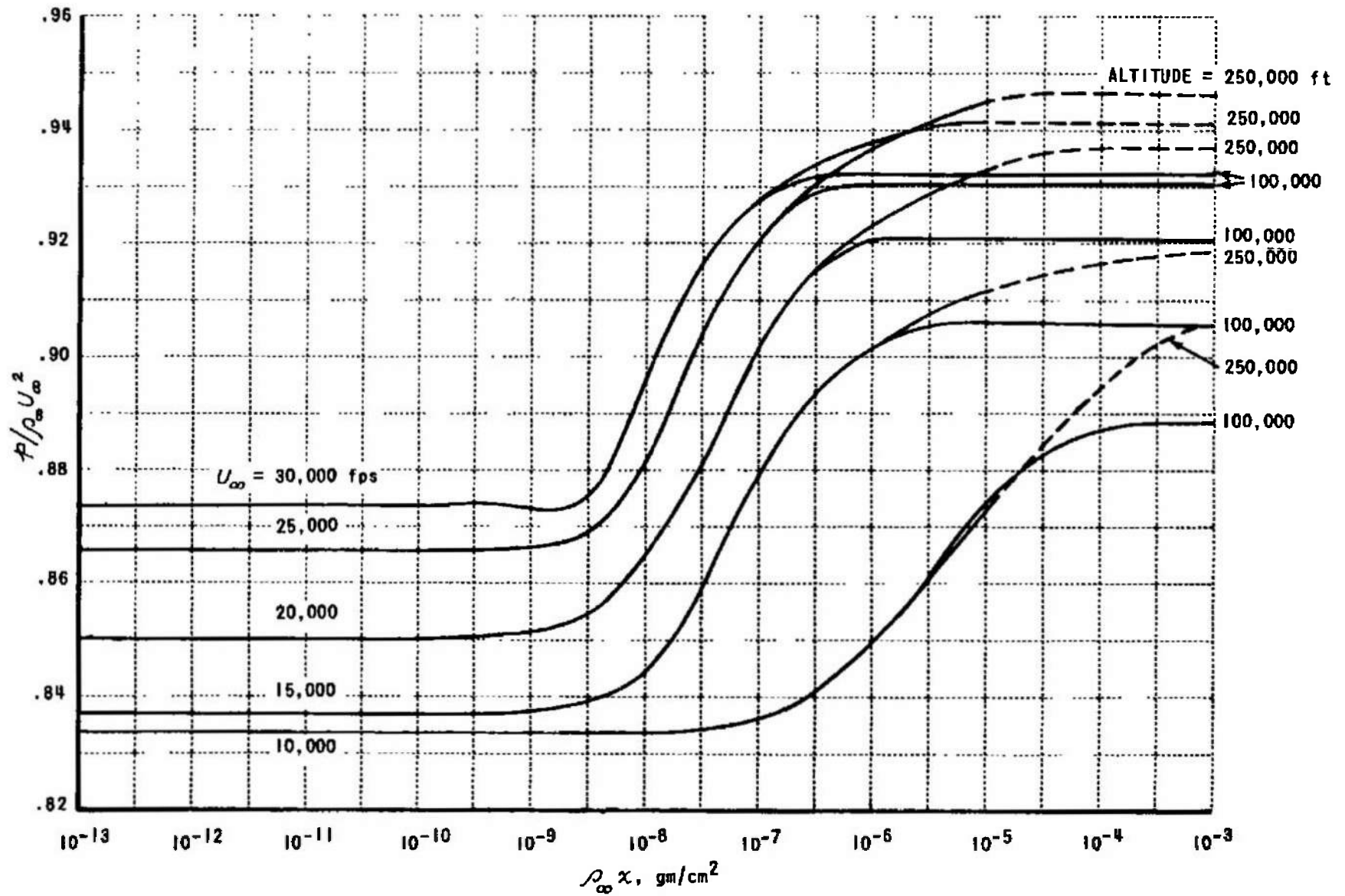
Figure 17 CORRELATION OF PRESSURE BEHIND NORMAL SHOCK WAVE BY BINARY SCALING
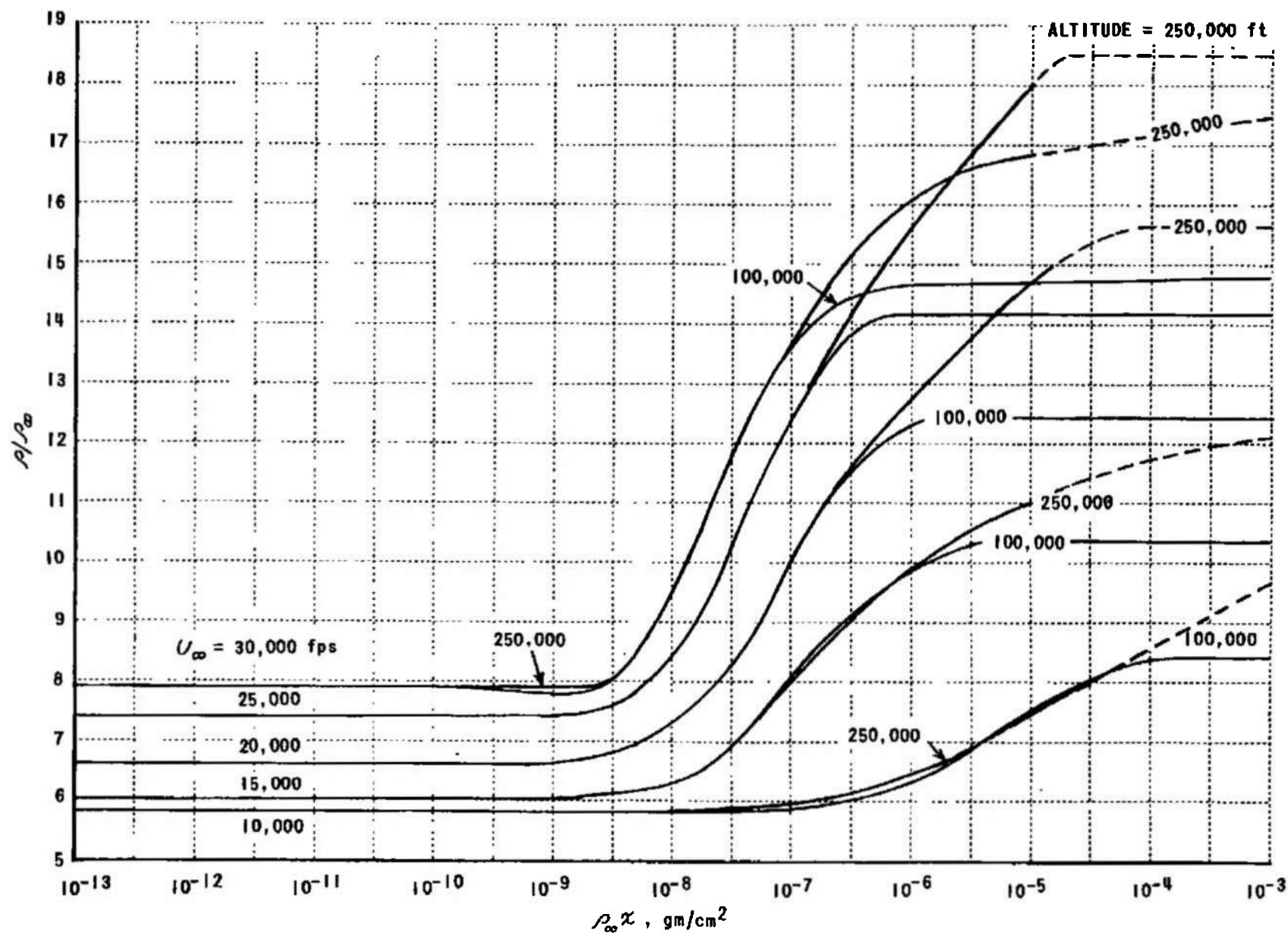
Figure 18 CORRELATION OF DENSITY BEHIND A NORMAL SHOCK WAVE BY BINARY SCALING

AEDC-TR-67-72
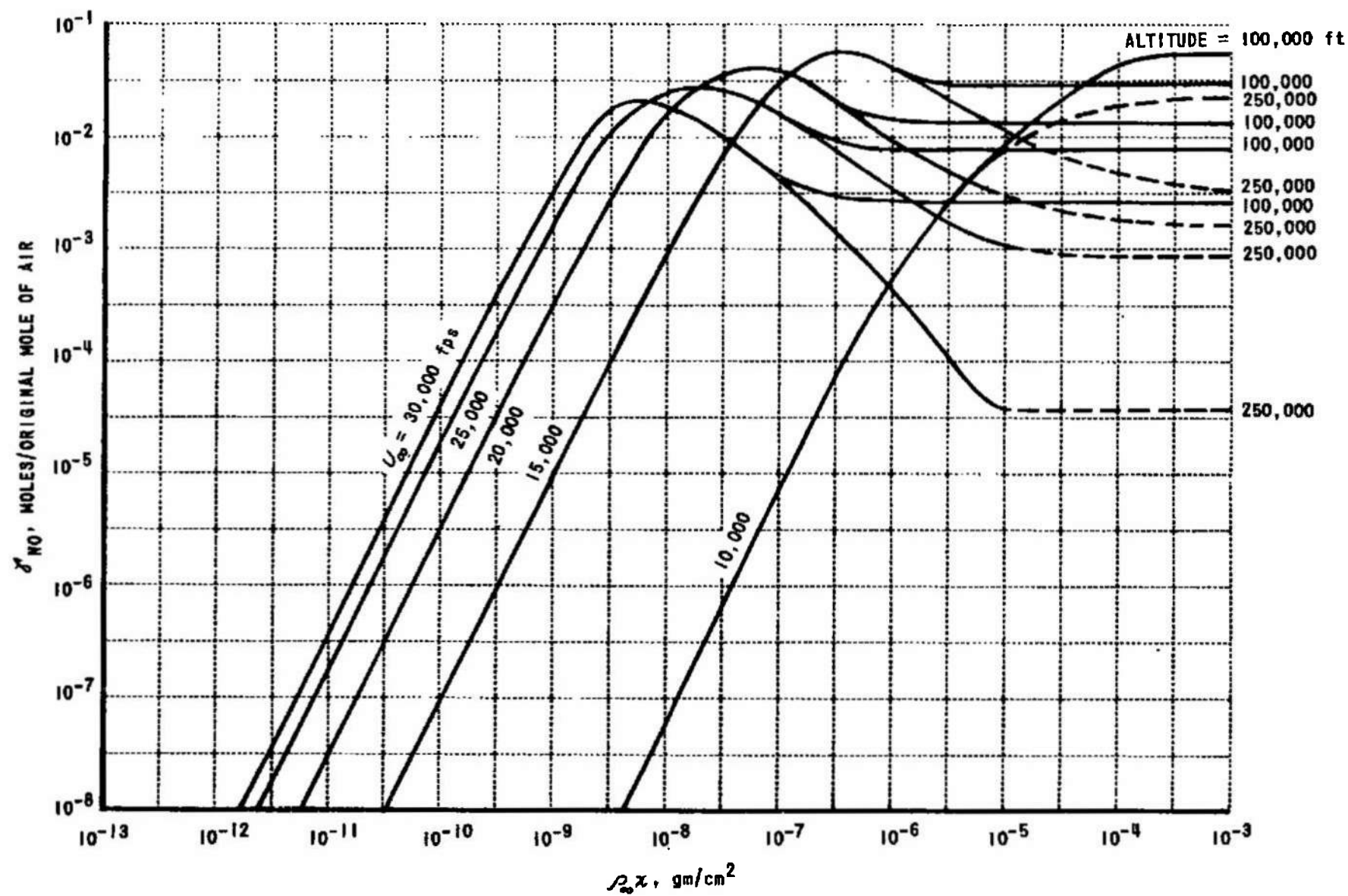
Figure 19 CORRELATION OF NITRIC OXIDE CONCENTRATION BEHIND NORMAL SHOCK WAVE BY BINARY SCALING
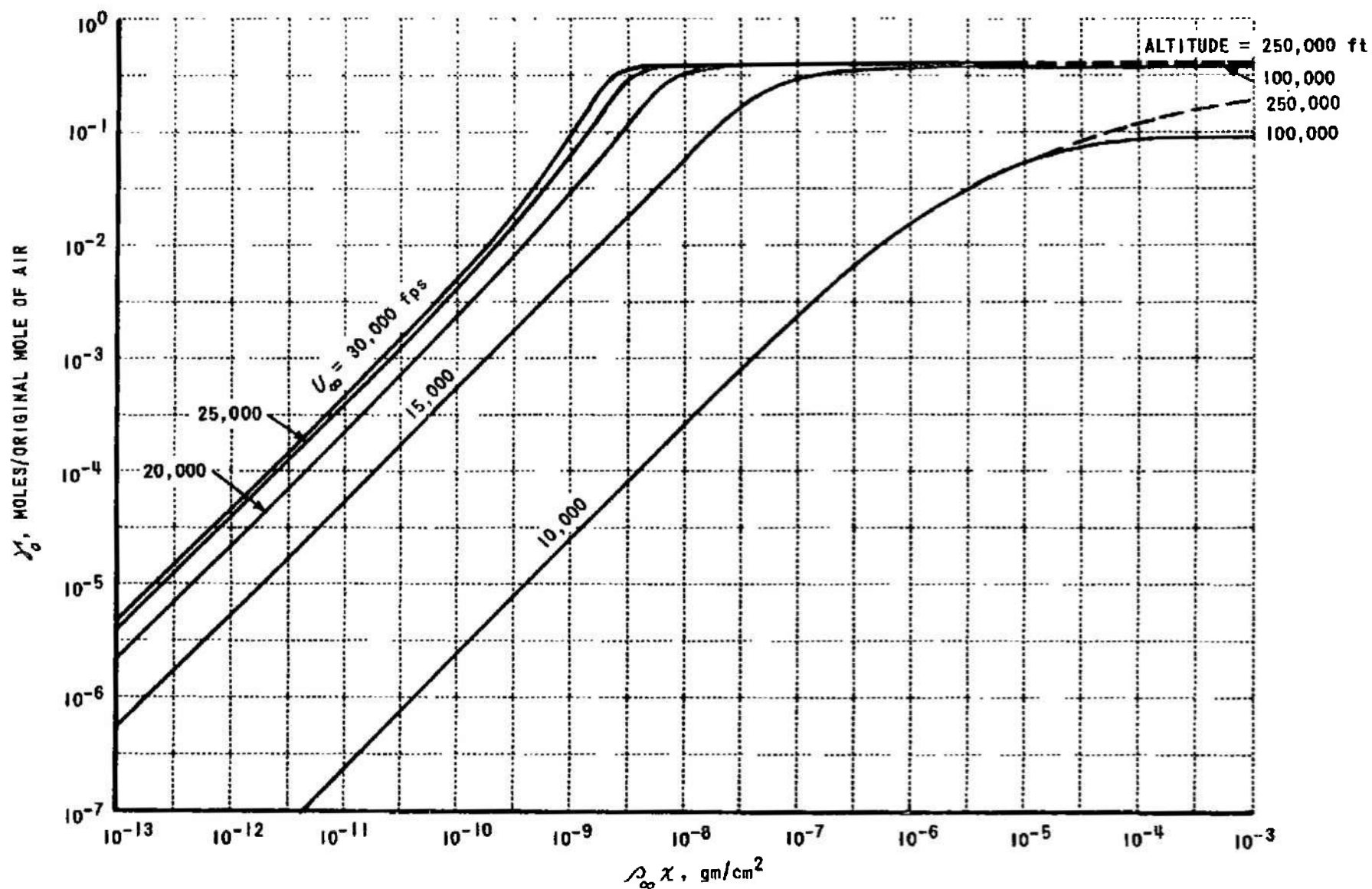
Figure 20 CORRELATION OF OXYGEN ATOM CONCENTRATION BEHIND NORMAL SHOCK WAVE BY BINARY SCALING
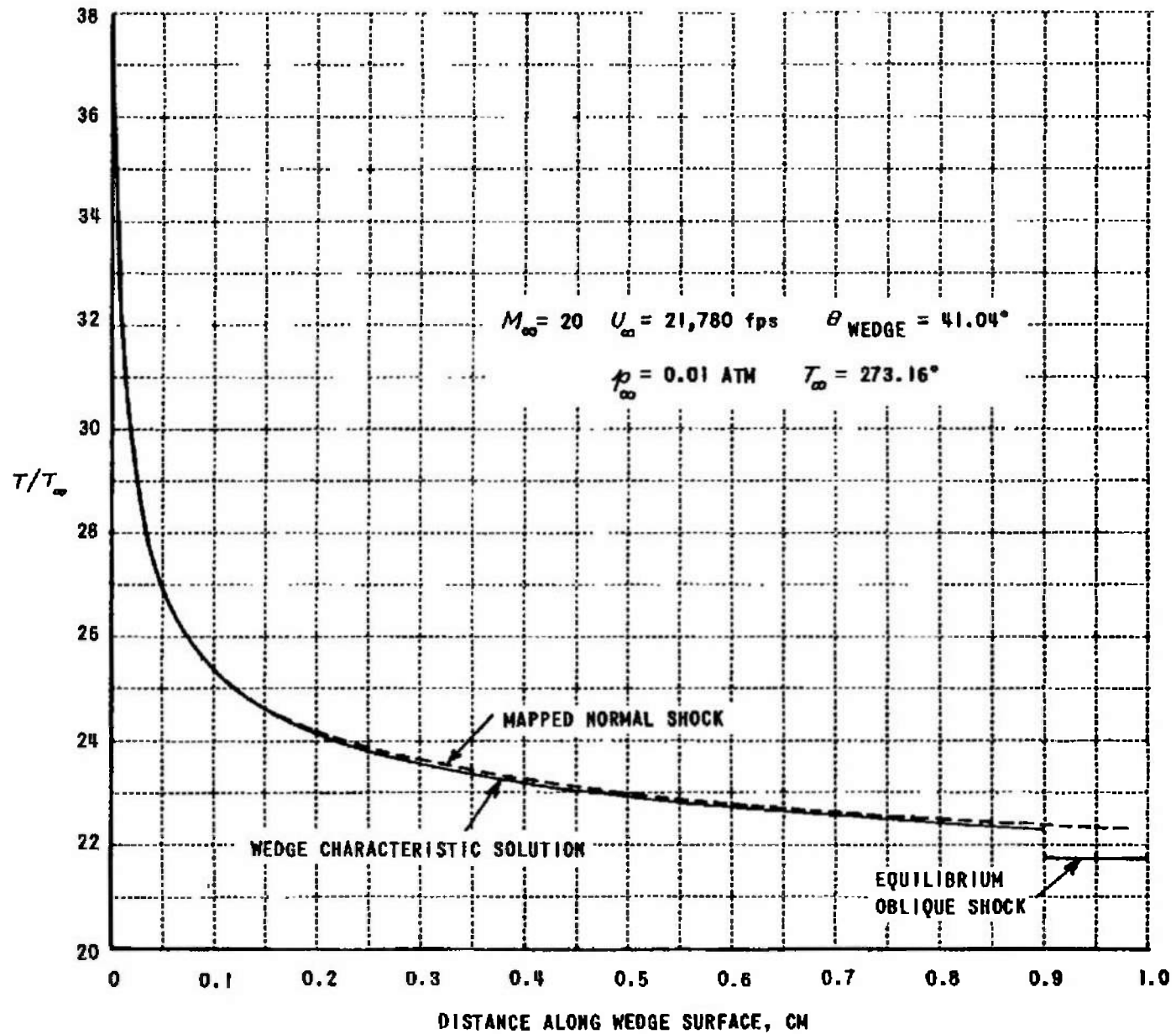
Figure 21a   COMPARISON OF WEDGE CHARACTERISTICS SOLUTION WITH MAPPED NORMAL SHOCK SOLUTION

$M_\infty = 20$ $U_\infty = 21,780$ fps θ WEDGE = 41.04°

$p_\infty = 0.01$ ATM $T_\infty = 273.16°$ K
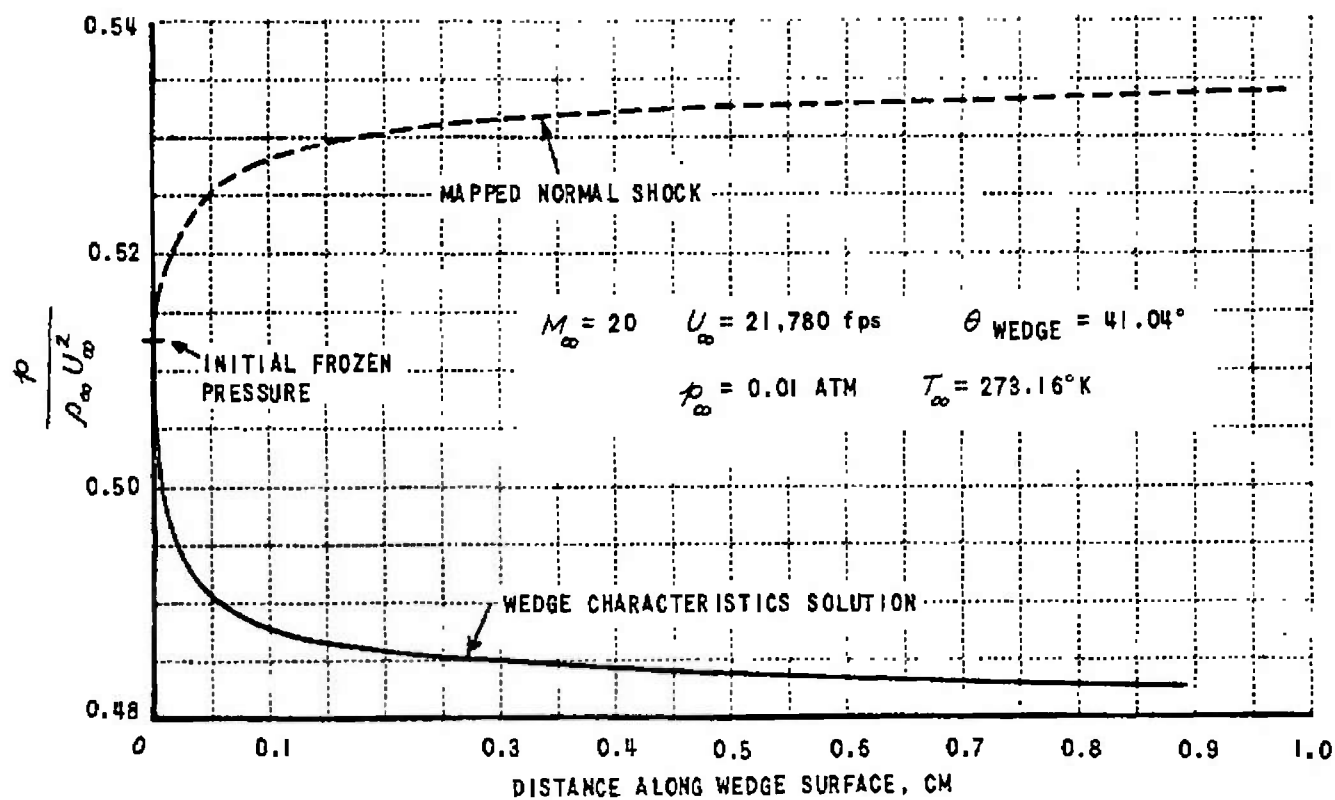
21(b)   PRESSURE
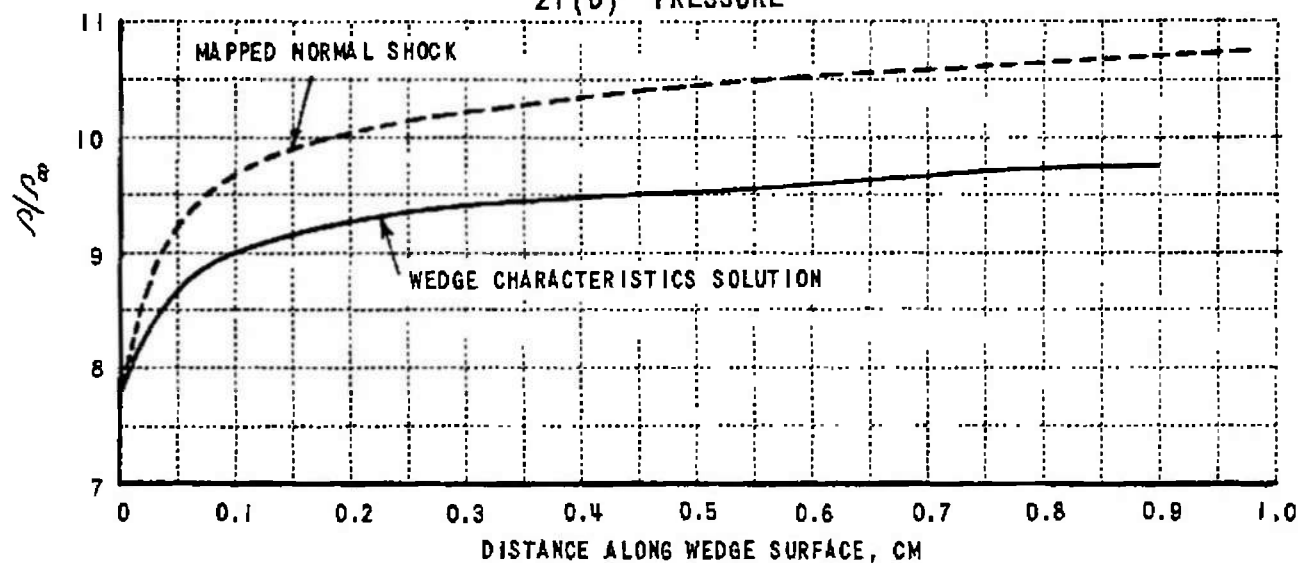
21(c)   DENSITY

Figure 21   COMPARISON OF WEDGE CHARACTERISTICS SOLUTION WITH
MAPPED NORMAL SHOCK SOLUTION
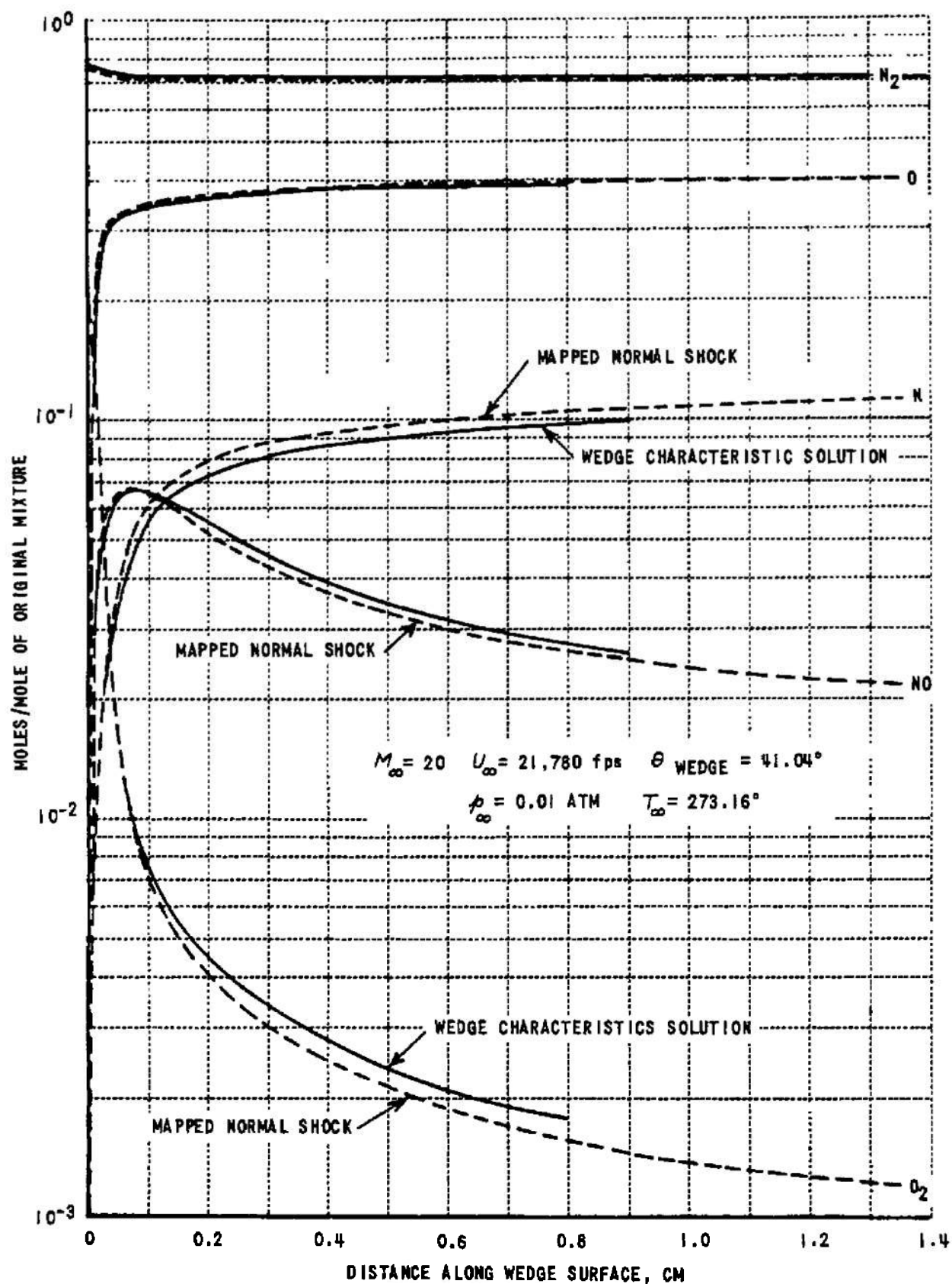
Figure 21d   COMPARISON OF WEDGE CHARACTERISTICS SOLUTION WITH
MAPPED NORMAL SHOCK SOLUTION
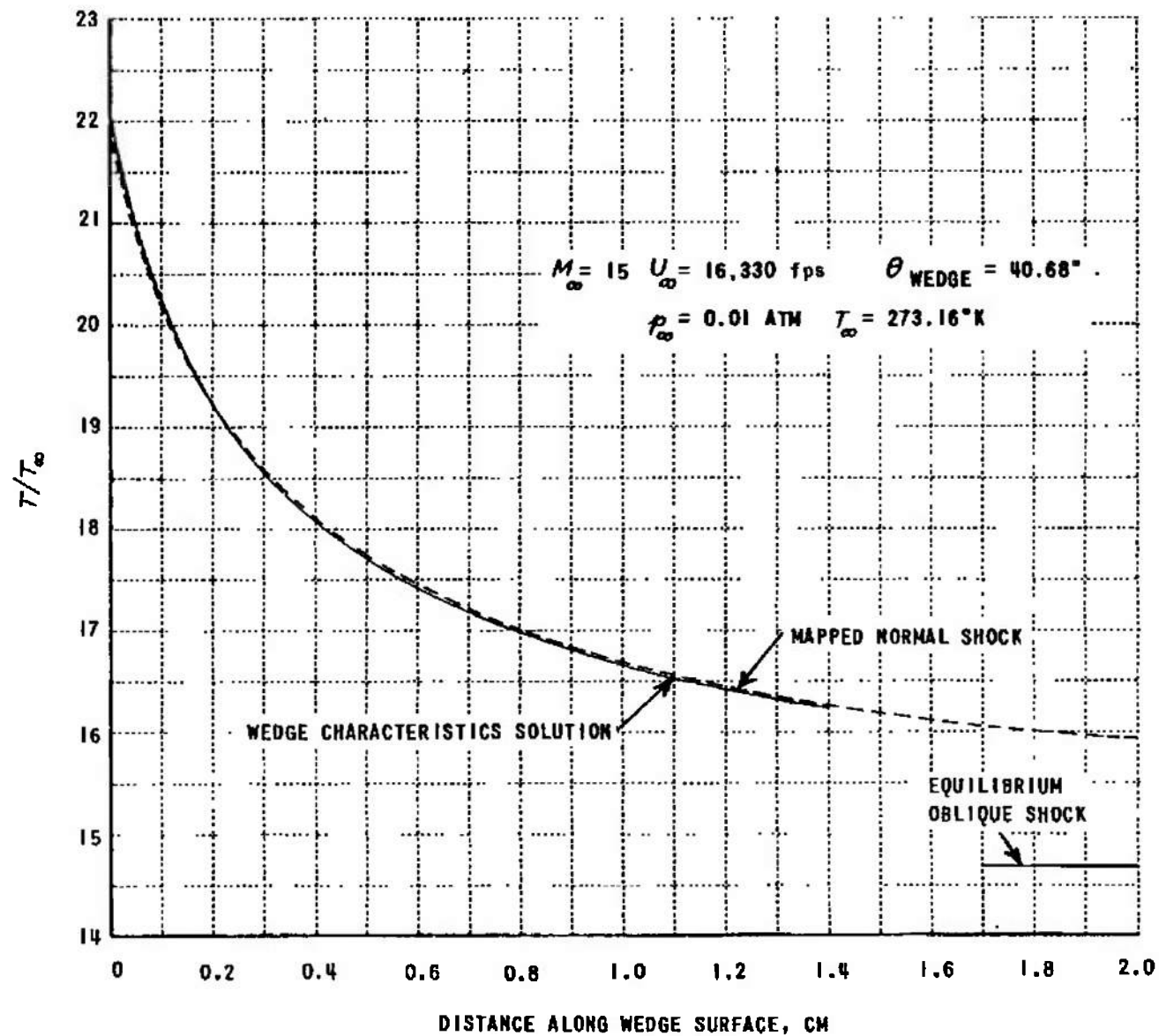
Figure 22a COMPARISON OF WEDGE CHARACTERISTICS SOLUTION WITH MAPPED NORMAL SHOCK SOLUTION
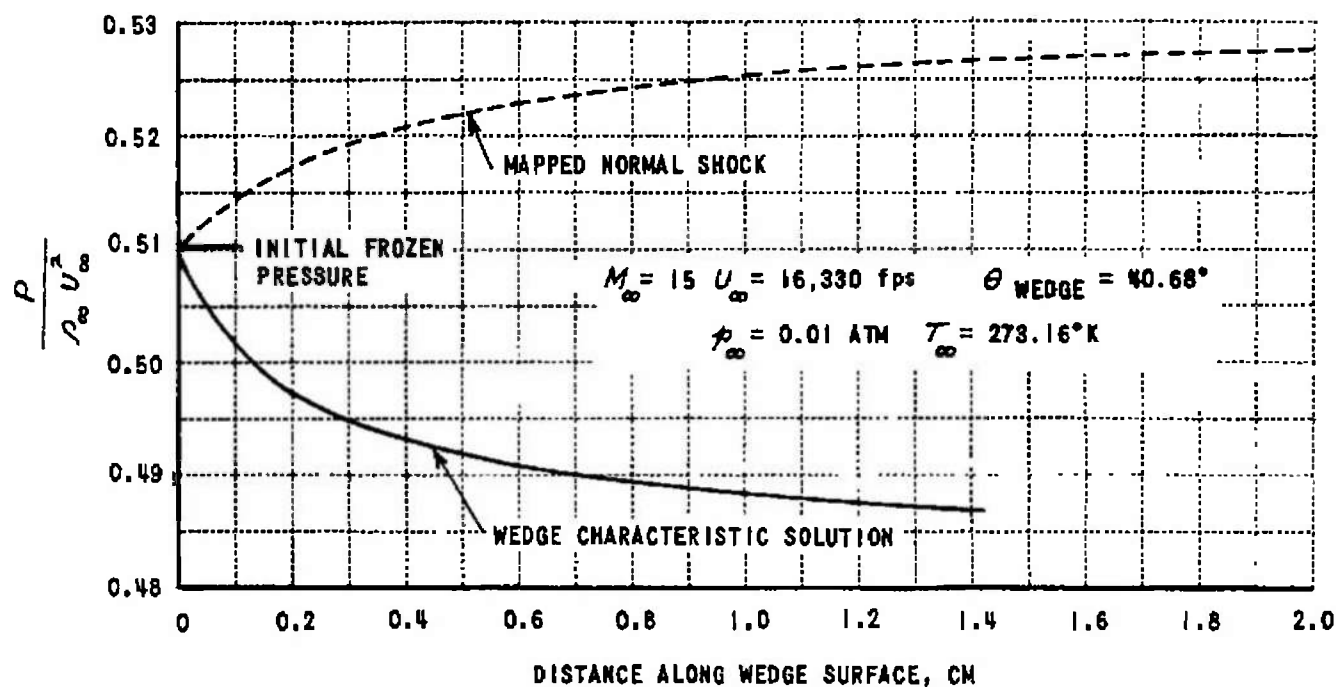
22(b) PRESSURE
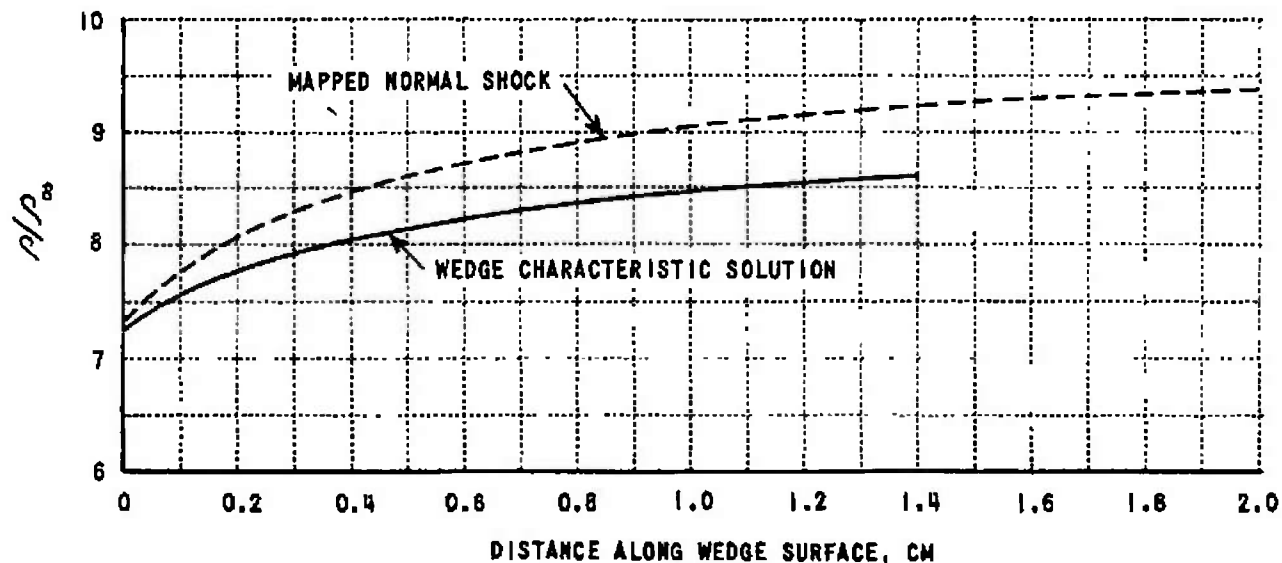
22(c) DENSITY

Figure 22   COMPARISON OF WEDGE CHARACTERISTICS SOLUTION WITH
MAPPED NORMAL SHOCK SOLUTION
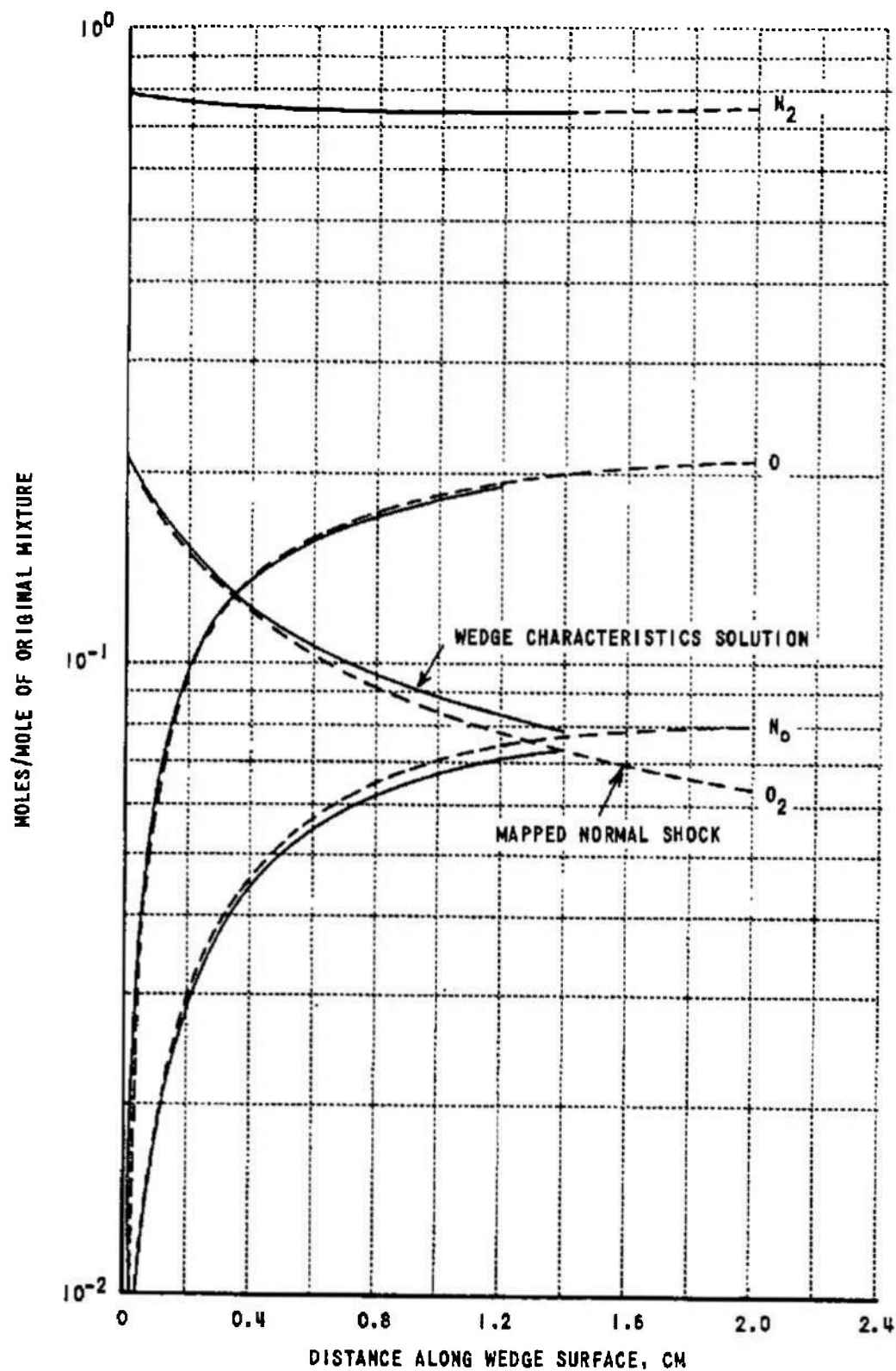
Figure 22d   COMPARISON OF WEDGE CHARACTERISTICS SOLUTION
WITH MAPPED NORMAL SHOCK SOLUTION
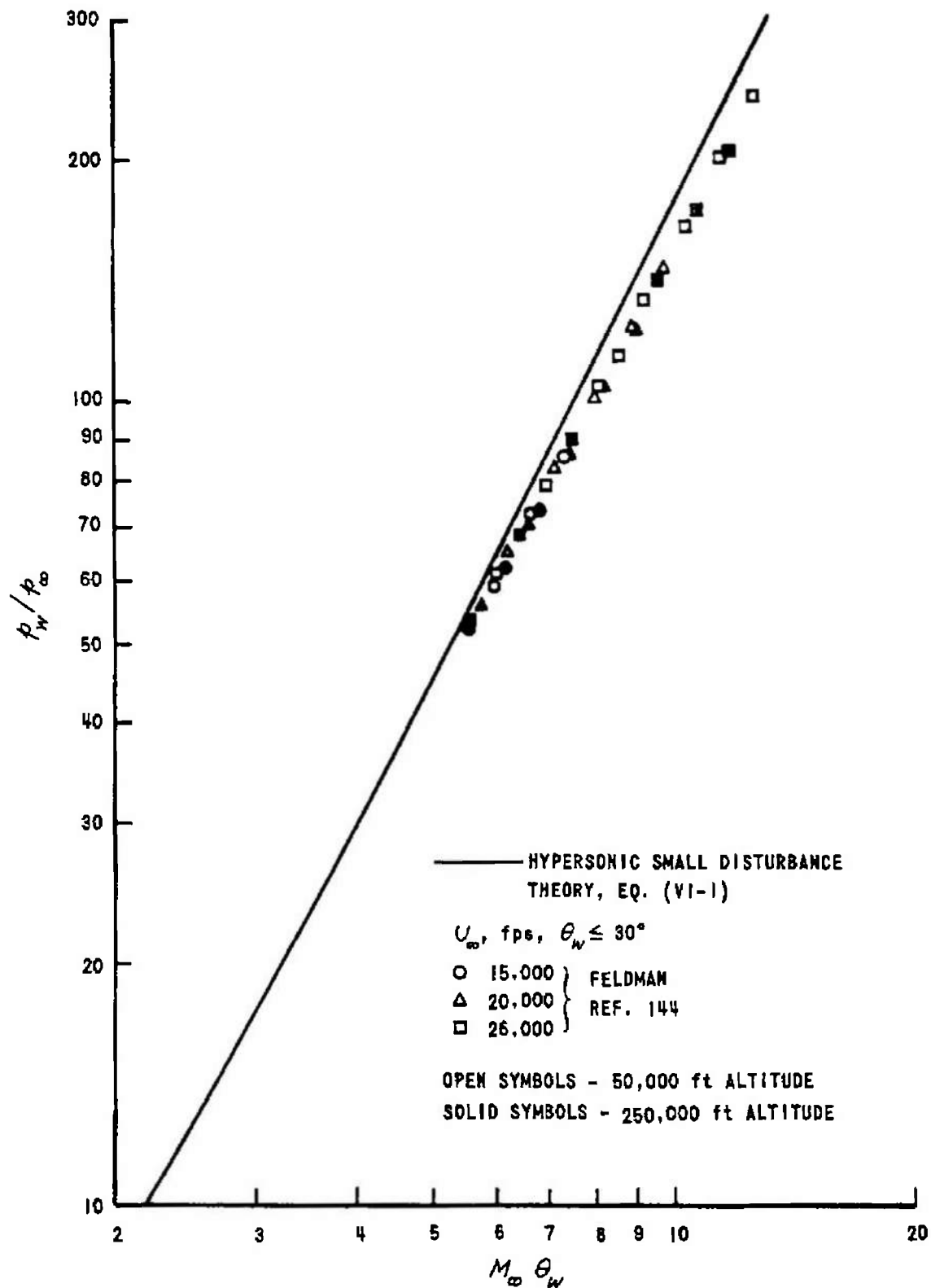
Figure 23 CORRELATION OF WEDGE PRESSURE WITH HYPERSONIC SIMILARITY PARAMETER
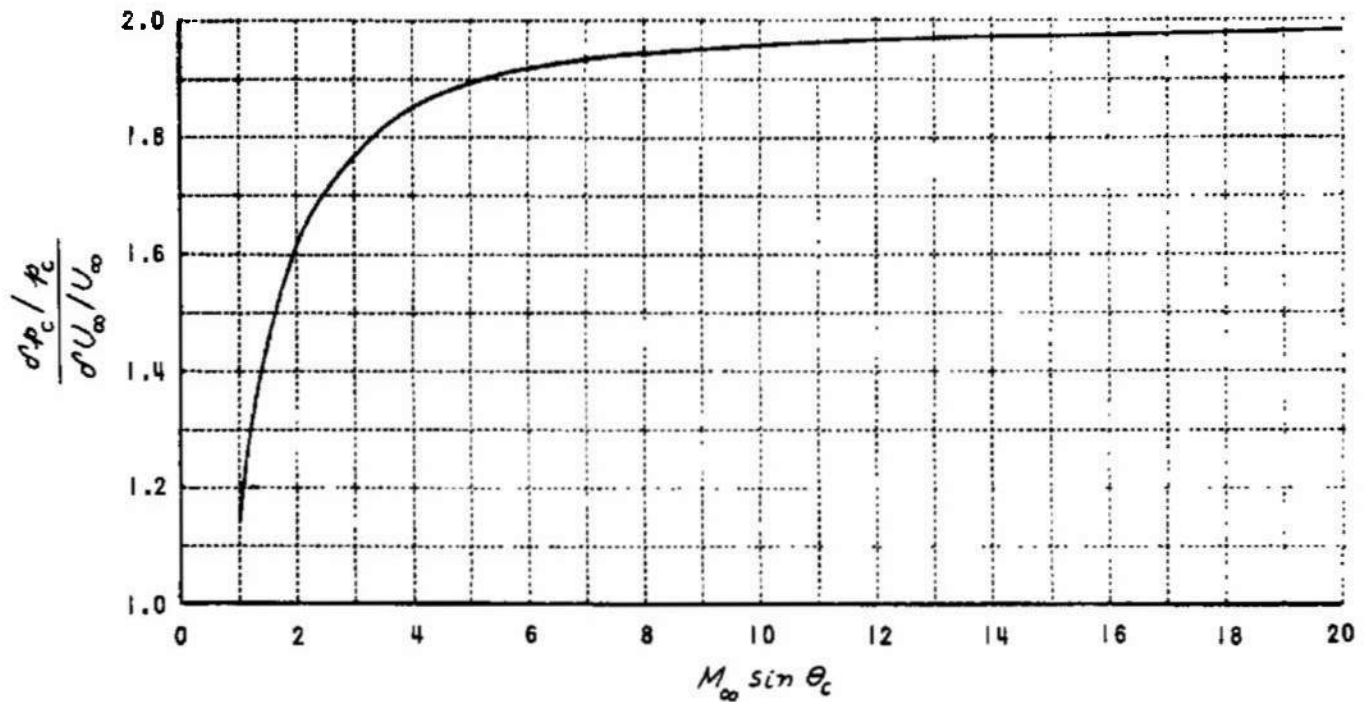
Figure 24a   SENSITIVITY OF CONE PRESSURE TO CHANGES IN FREE STREAM VELOCITY
AS A FUNCTION OF THE HYPERSONIC SIMILARITY PARAMETER
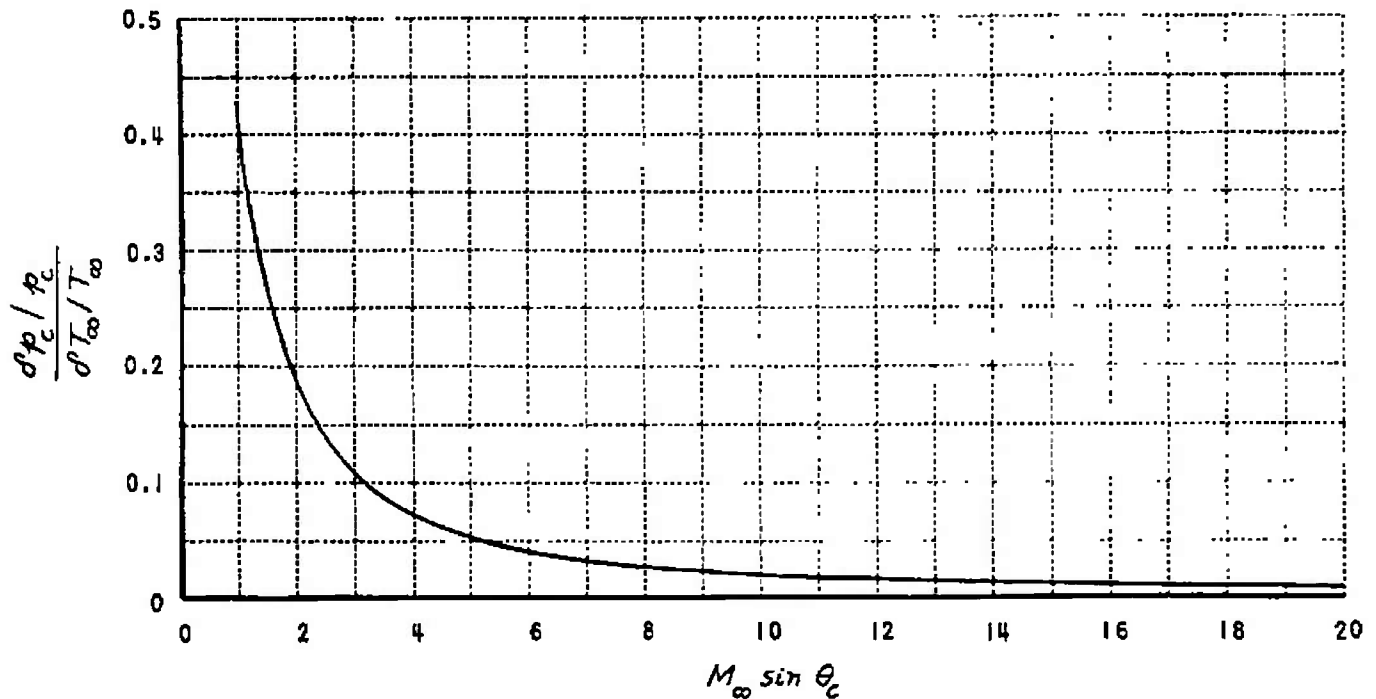
Figure 24b   SENSITIVITY OF CONE PRESSURE TO CHANGES IN FREE-STREAM TEMPERATURE
AS A FUNCTION OF THE HYPERSONIC SIMILARITY PARAMETER
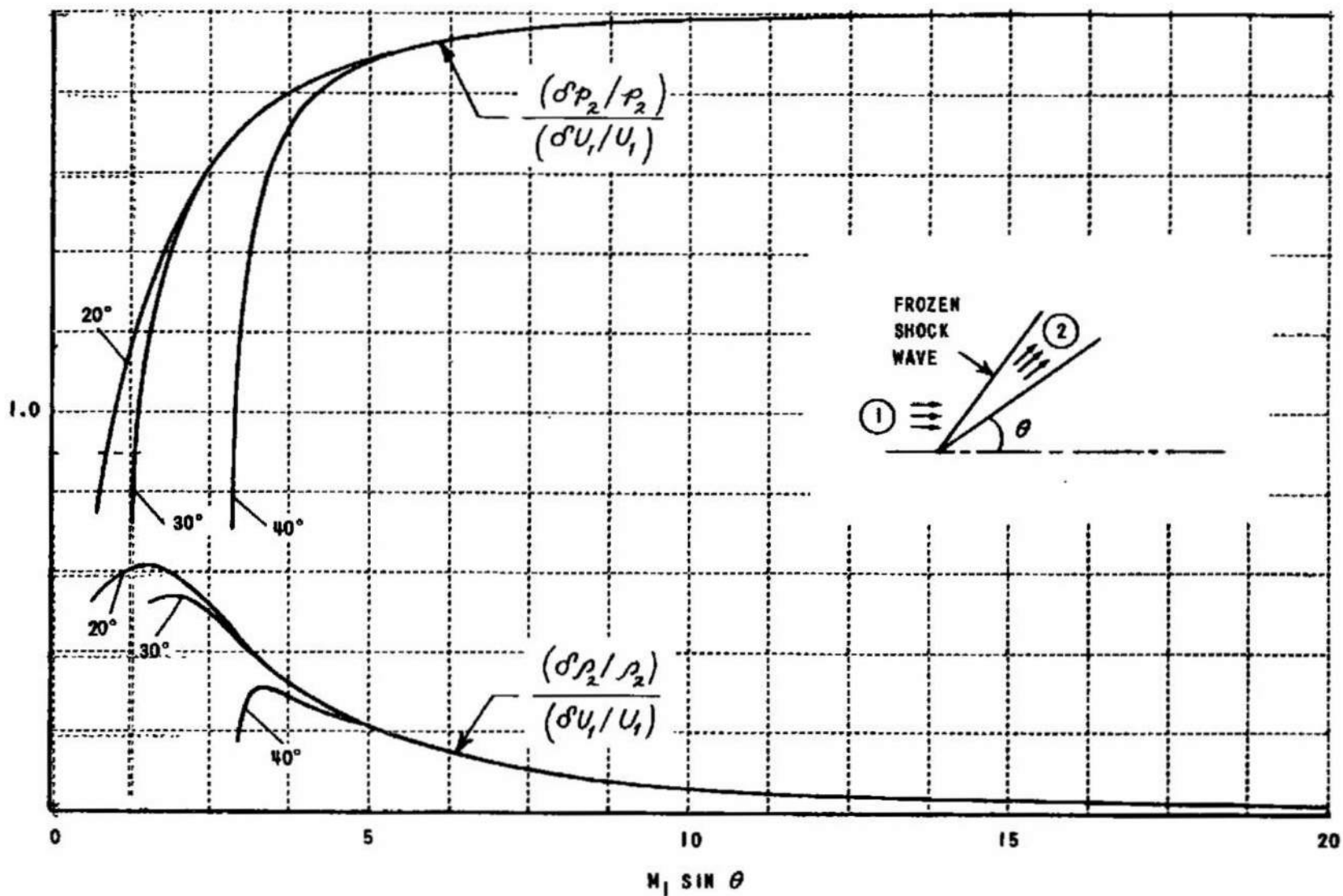
Figure 25   SENSITIVITY OF FROZEN OBLIQUE SHOCK WAVE PARAMETERS TO CHANGES IN
FREE-STREAM VELOCITY
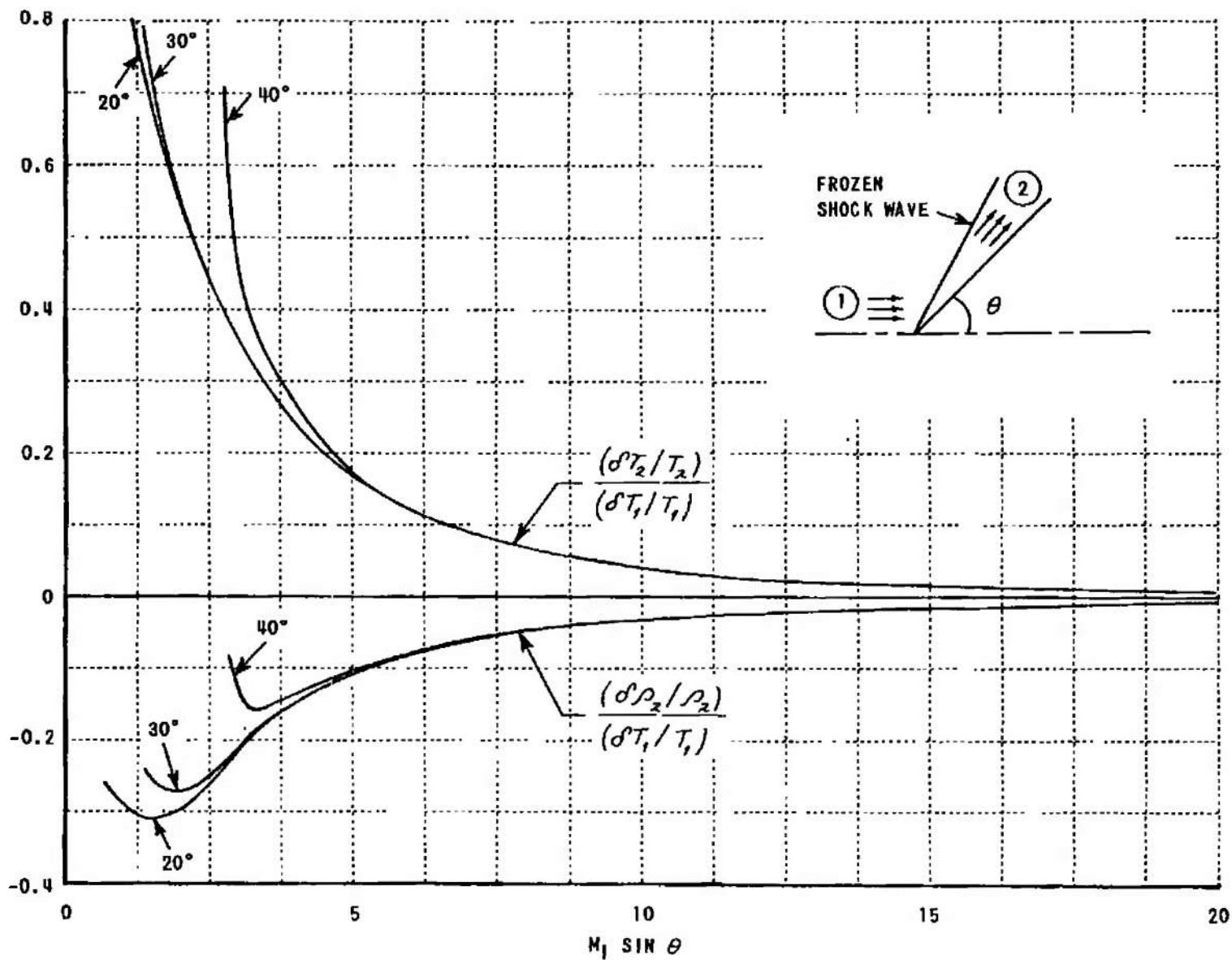
Figure 26   SENSITIVITY OF FROZEN OBLIQUE SHOCK WAVE PARAMETERS TO CHANGES
IN FREE-STREAM TEMPERATURE
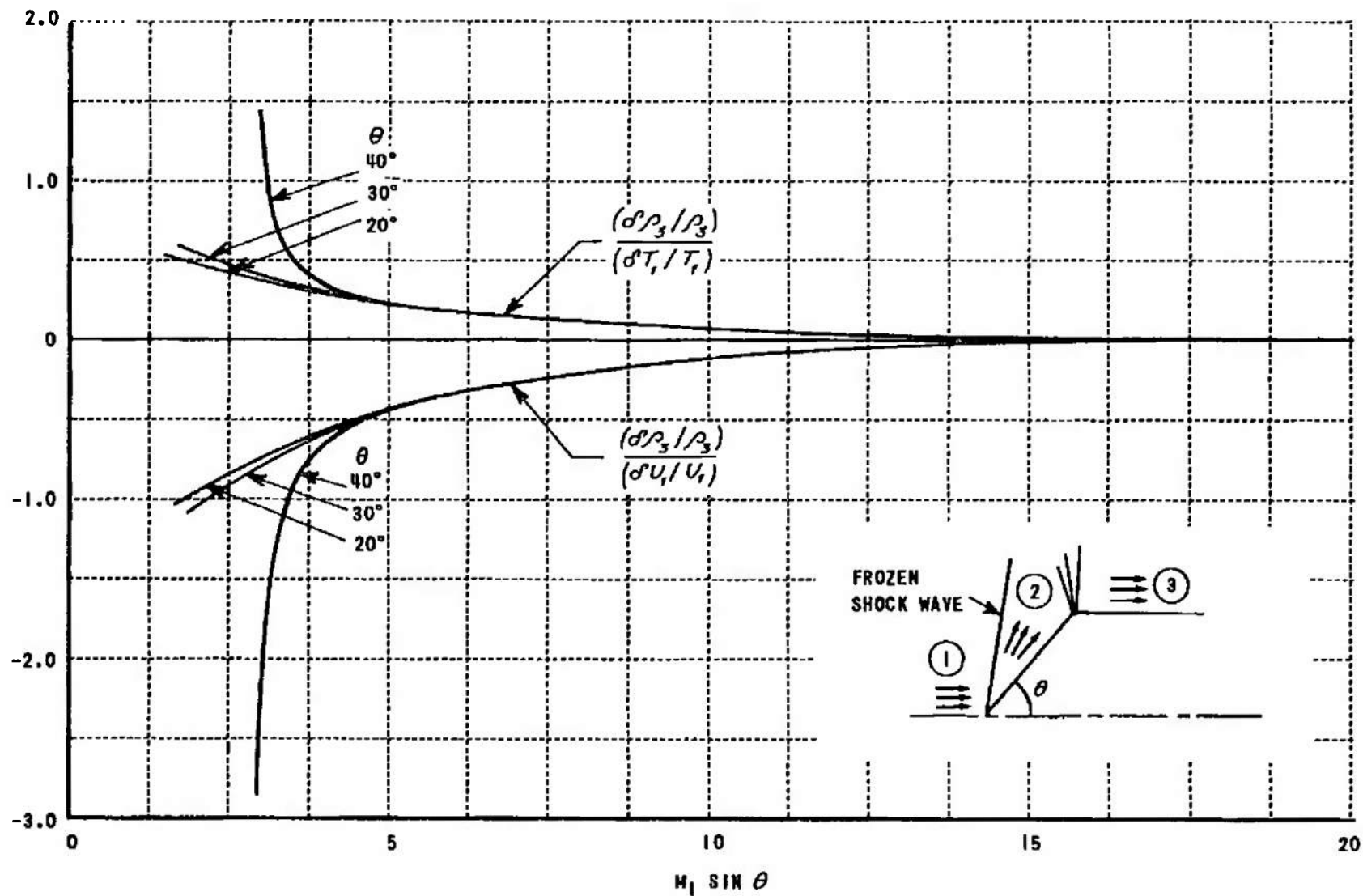
Figure 27 SENSITIVITY OF THE AFTERBODY DENSITY TO CHANGES IN FREE-STREAM VELOCITY
AND TEMPERATURE FOR THE f-f MODEL
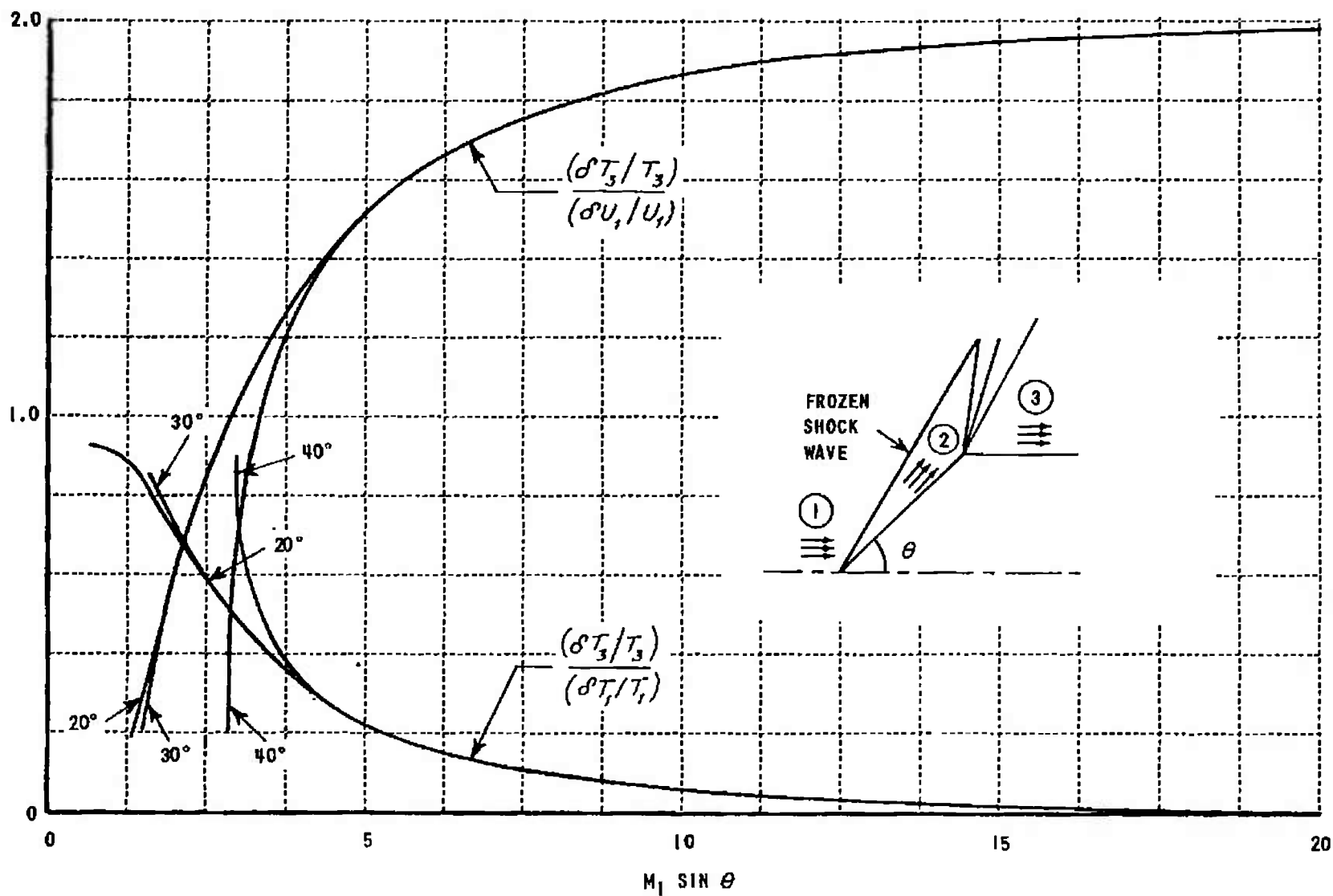
Figure 28 SENSITIVITY OF THE AFTERBODY TEMPERATURE TO CHANGES
IN FREE-STREAM VELOCITY AND TEMPERATURE FOR f-f MODEL
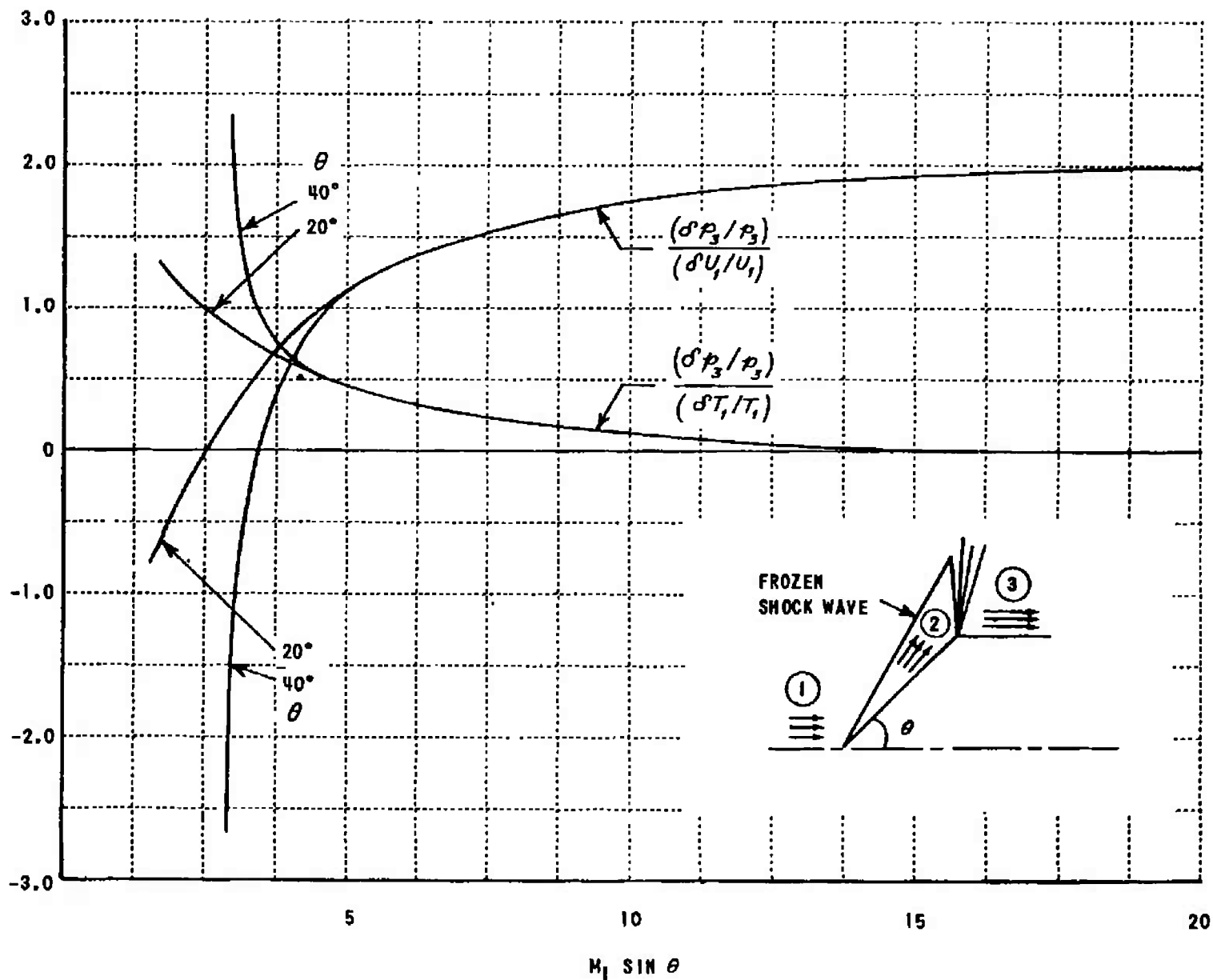
Figure 29 SENSITIVITY OF AFTERBODY PRESSURE TO CHANGES IN FREE-STREAM VELOCITY
AND TEMPERATURE FOR f-f MODEL
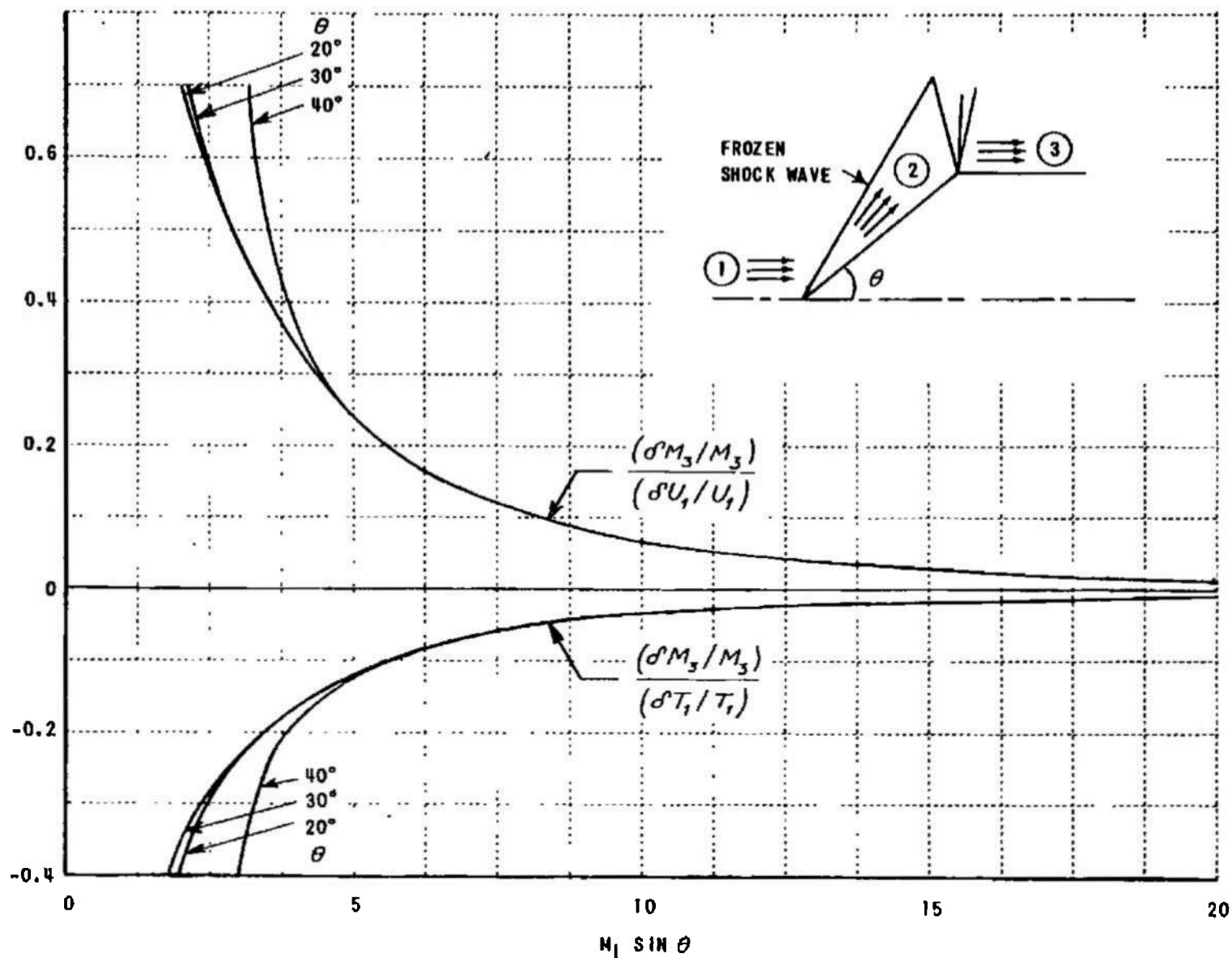
Figure 30 SENSITIVITY OF AFTERBODY MACH NUMBER TO CHANGES IN FREE-STREAM
VELOCITY AND TEMPERATURE FOR THE f-f MODEL
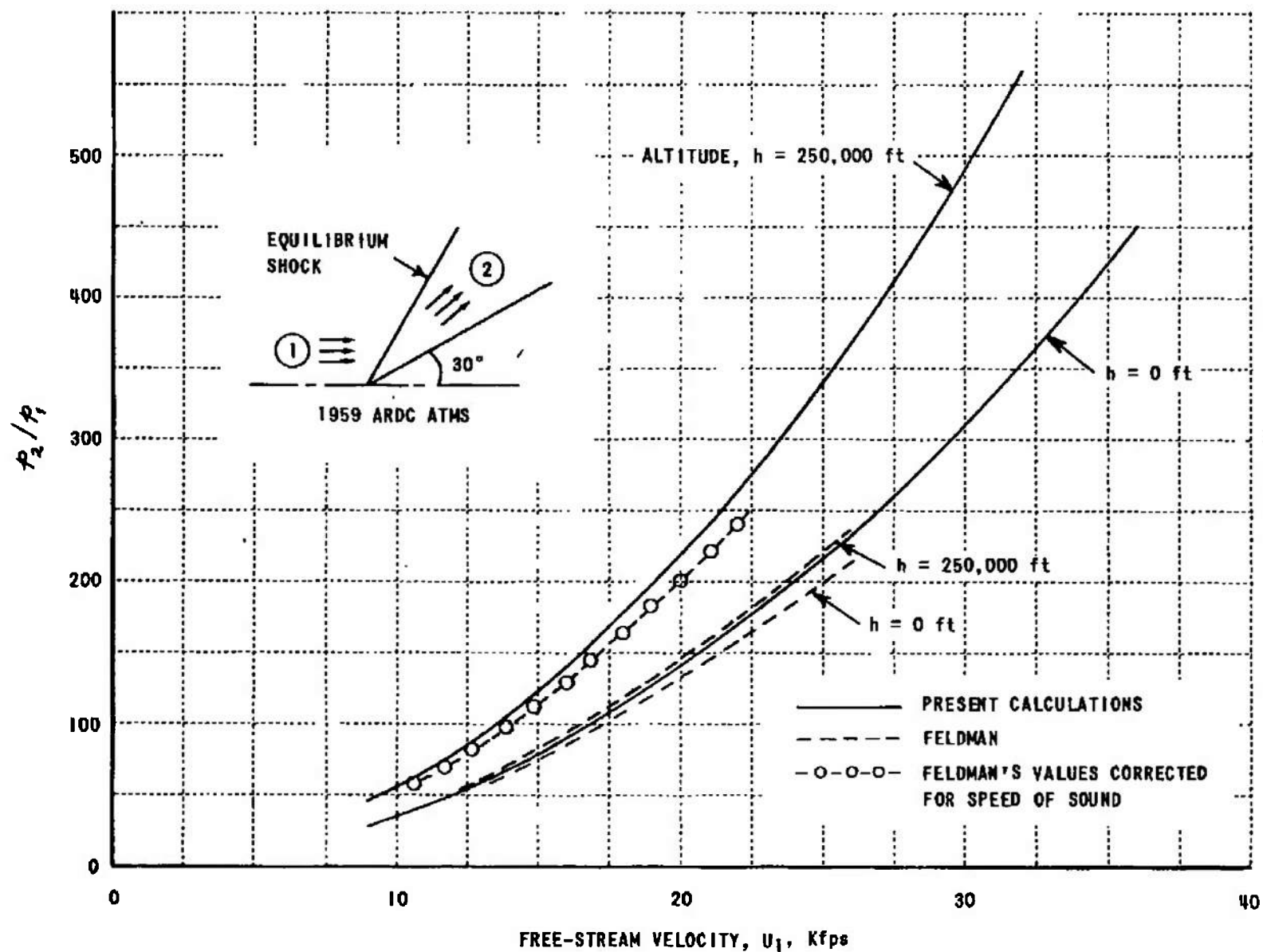
Figure 31 VARIATION OF PRESSURE BEHIND AN EQUILIBRIUM OBLIQUE SHOCK WAVE, $\theta = 30°$
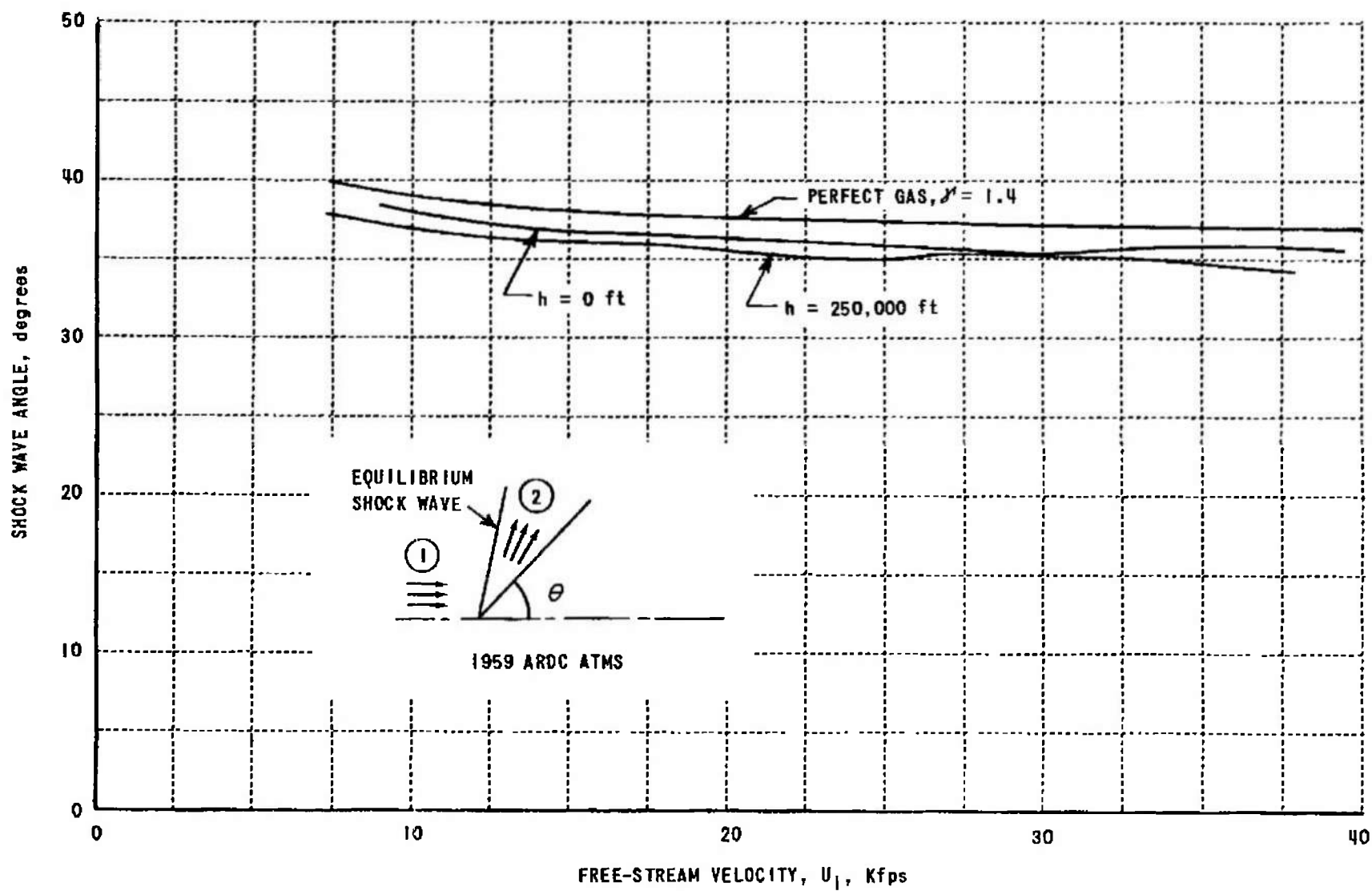
Figure 32 COMPARISON OF EQUILIBRIUM AND FROZEN SHOCK WAVE ANGLES FOR A WEDGE, $\theta = 30°$
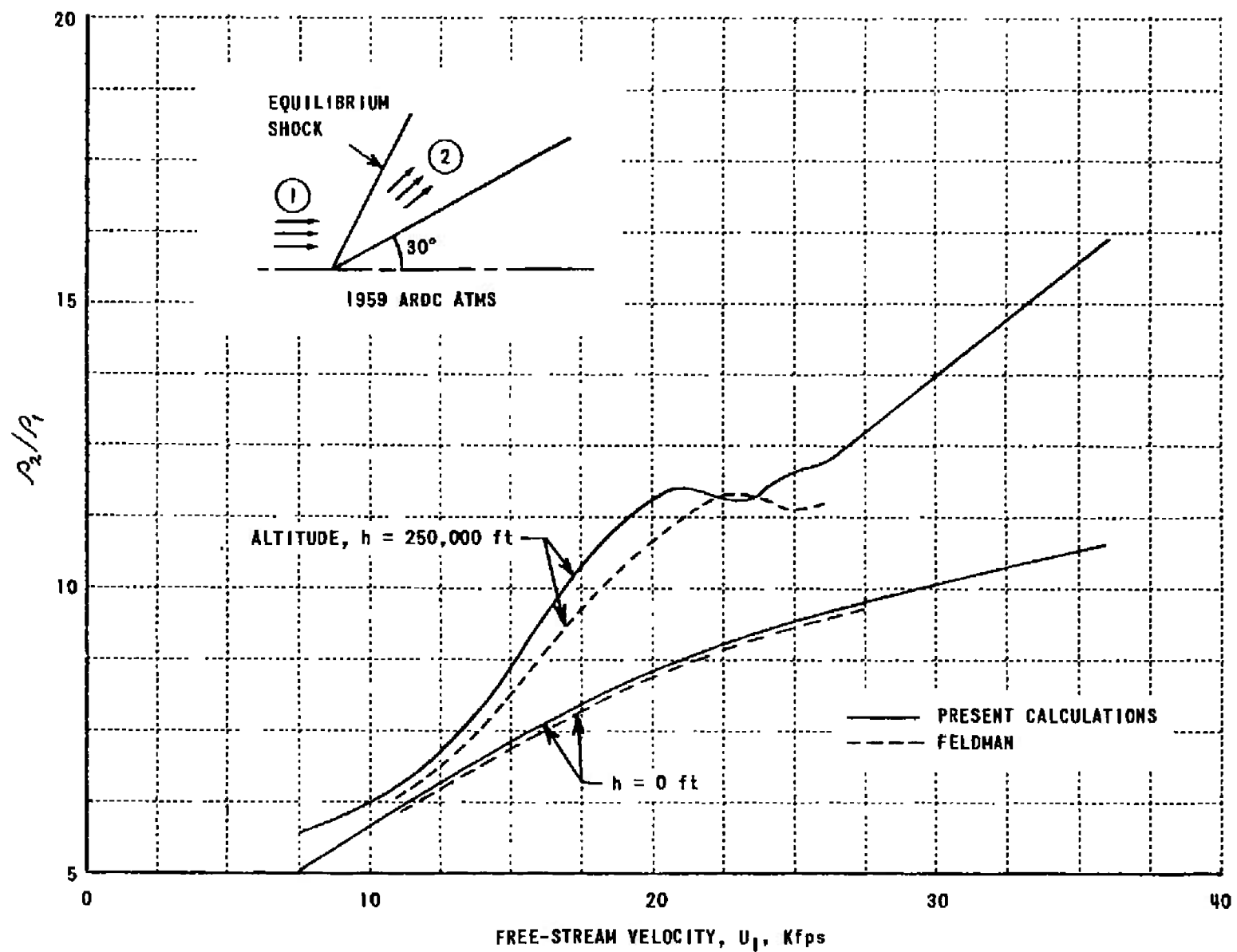
Figure 33 VARIATION OF DENSITY BEHIND EQUILIBRIUM OBLIQUE SHOCK WAVE, θ = 30°
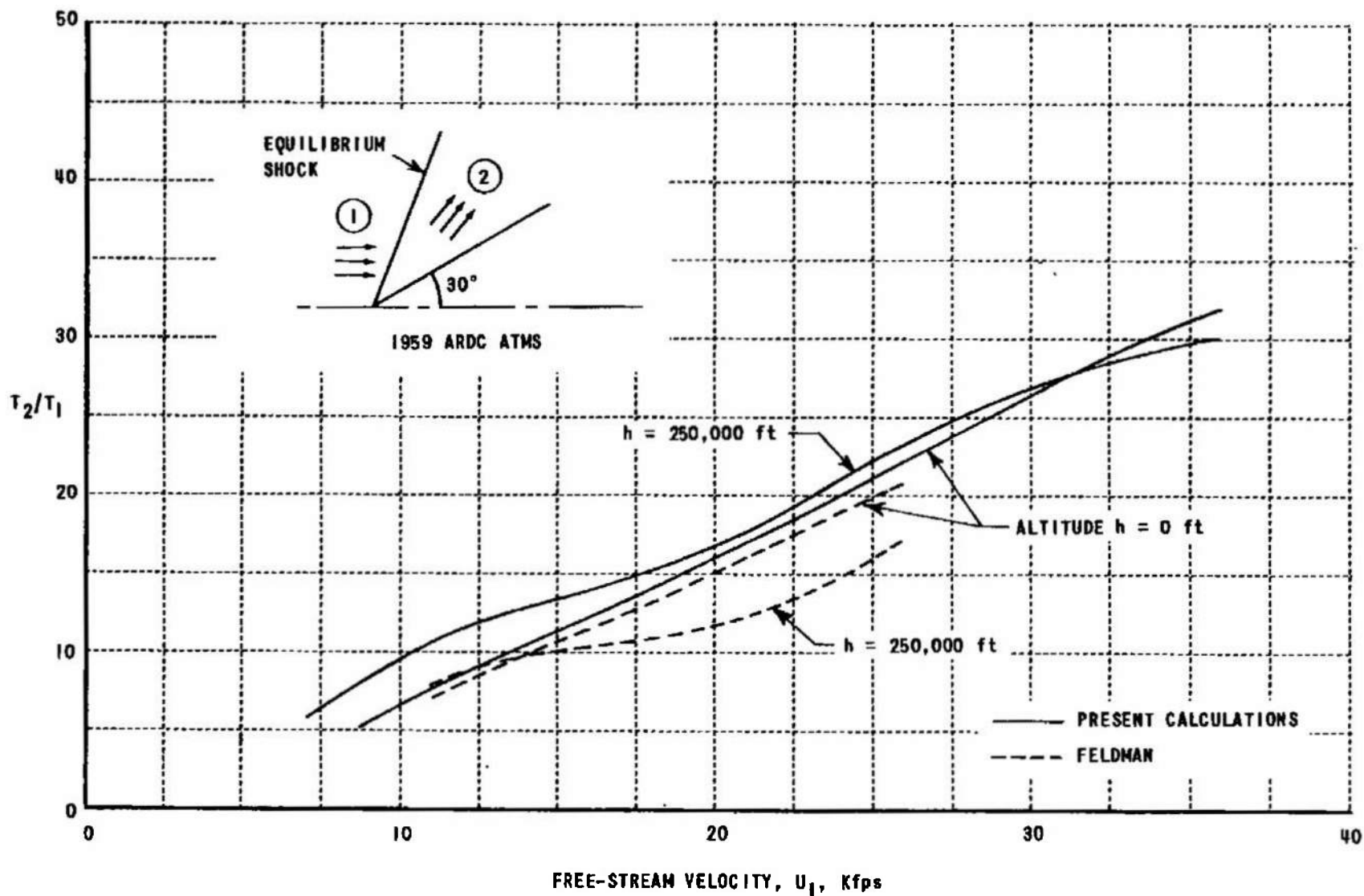
Figure 34   VARIATION OF TEMPERATURE BEHIND AN EQUILIBRIUM OBLIQUE SHOCK WAVE, θ = 30°
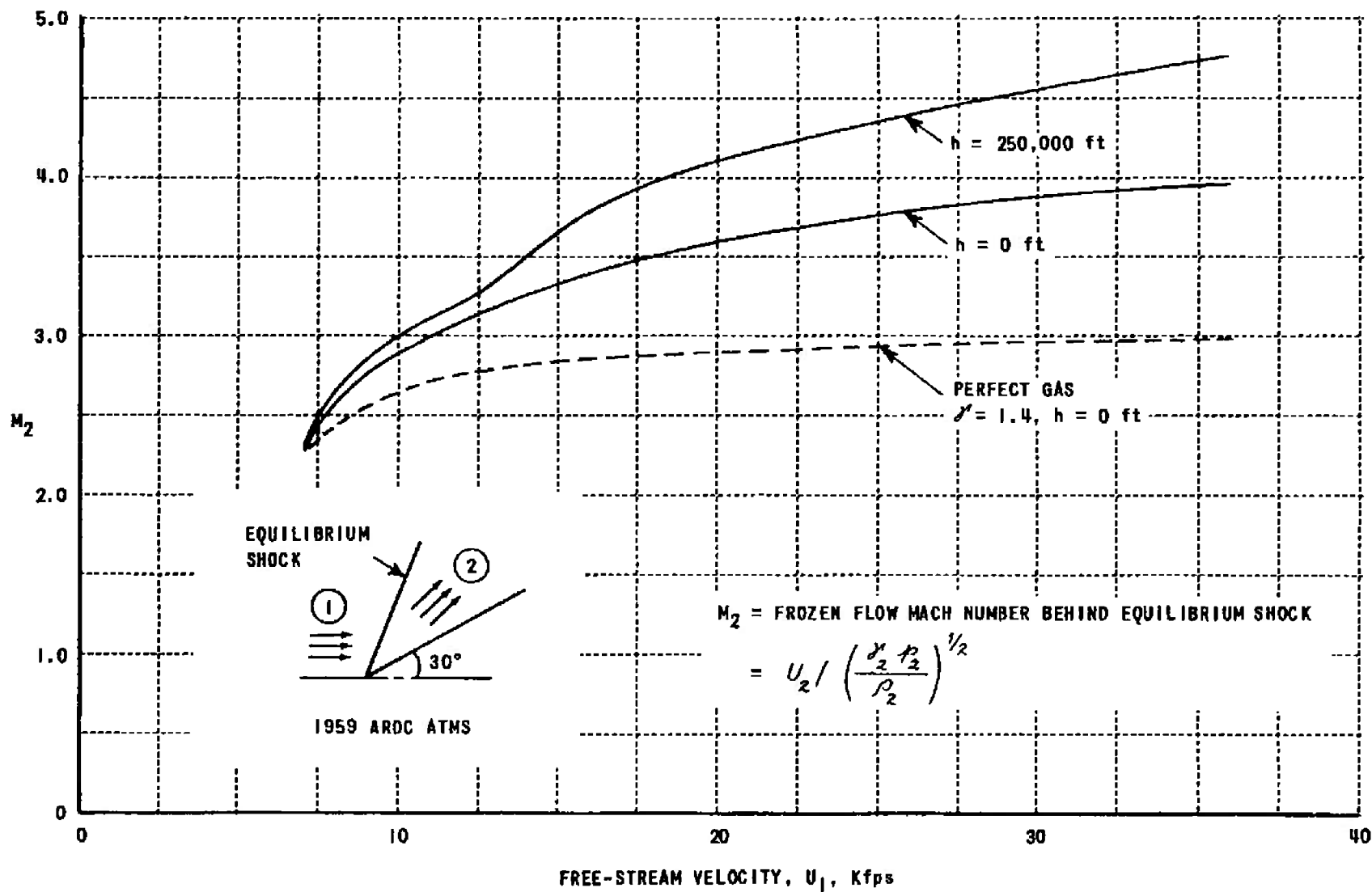
Figure 35 VARIATION OF FROZEN MACH NUMBER BEHIND AN EQUILIBRIUM OBLIQUE SHOCK WAVE, $\theta = 30°$
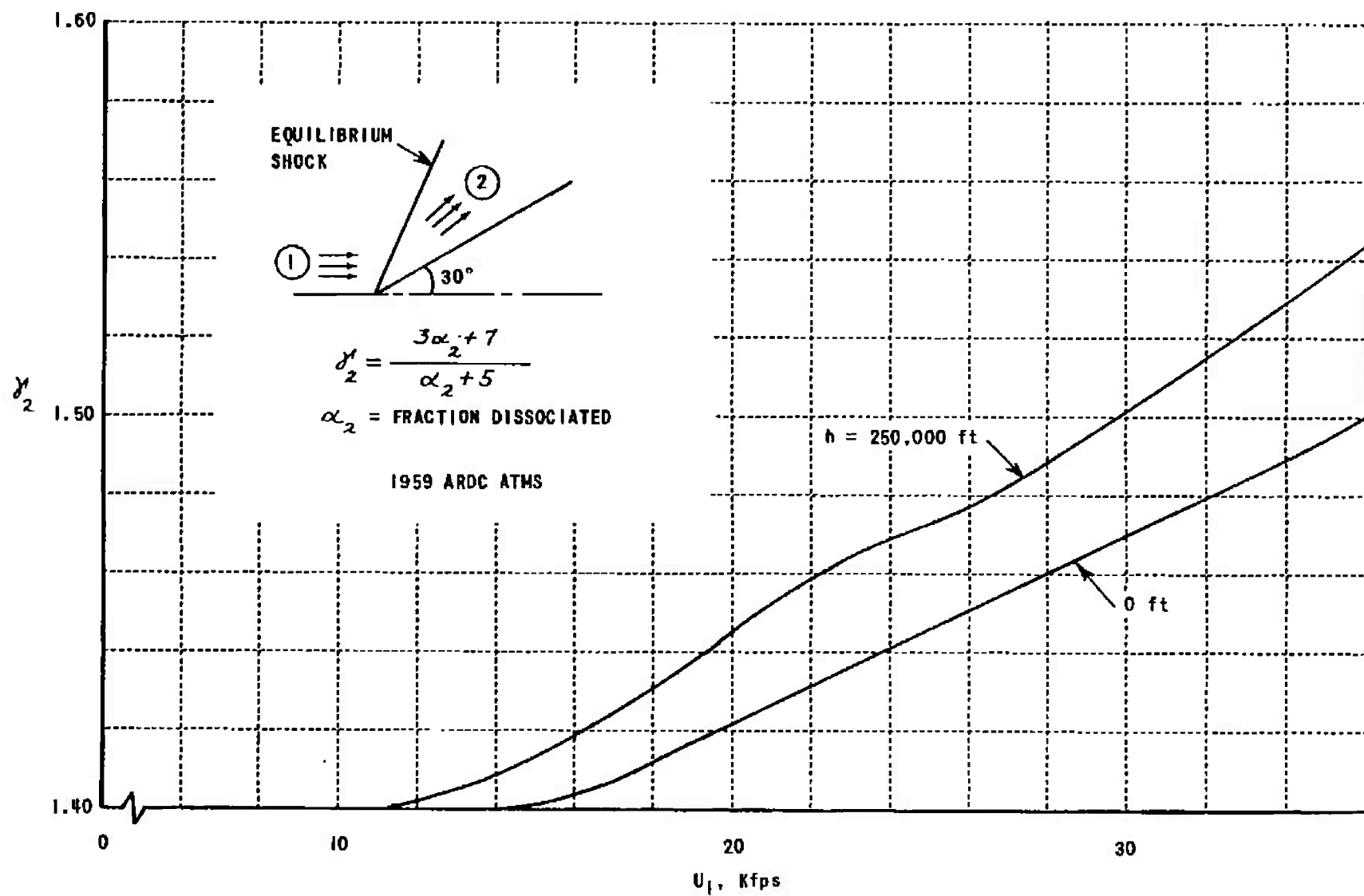
Figure 36   VARIATION OF FROZEN SPECIFIC HEAT RATIO BEHIND EQUILIBRIUM OBLIQUE SHOCKS, $\theta = 30°$
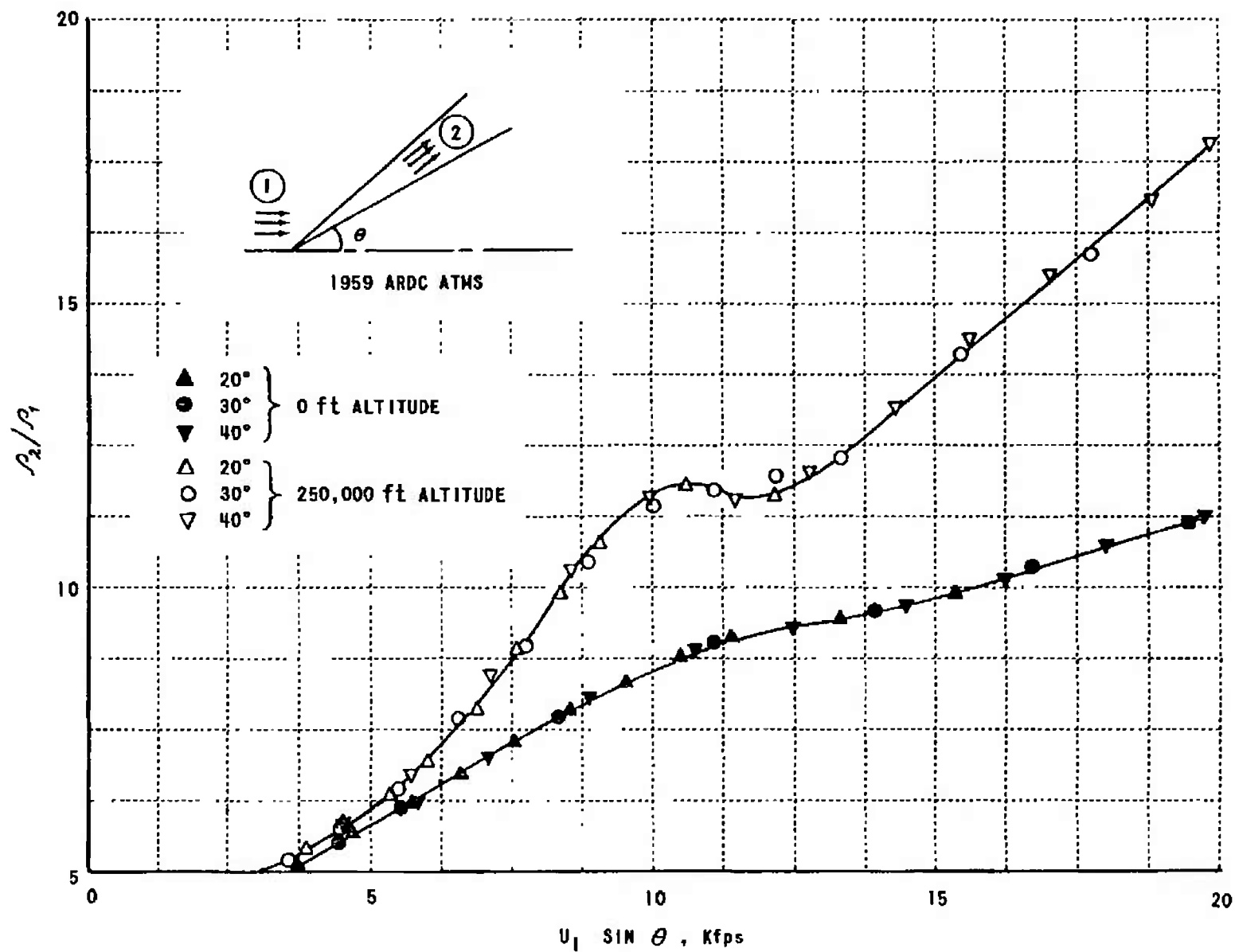
Figure 37   CORRELATION OF DENSITY RATIO ACROSS AN EQUILIBRIUM OBLIQUE SHOCK WAVE
IN TERMS OF THE HYPERSONIC SIMILARITY PARAMETER
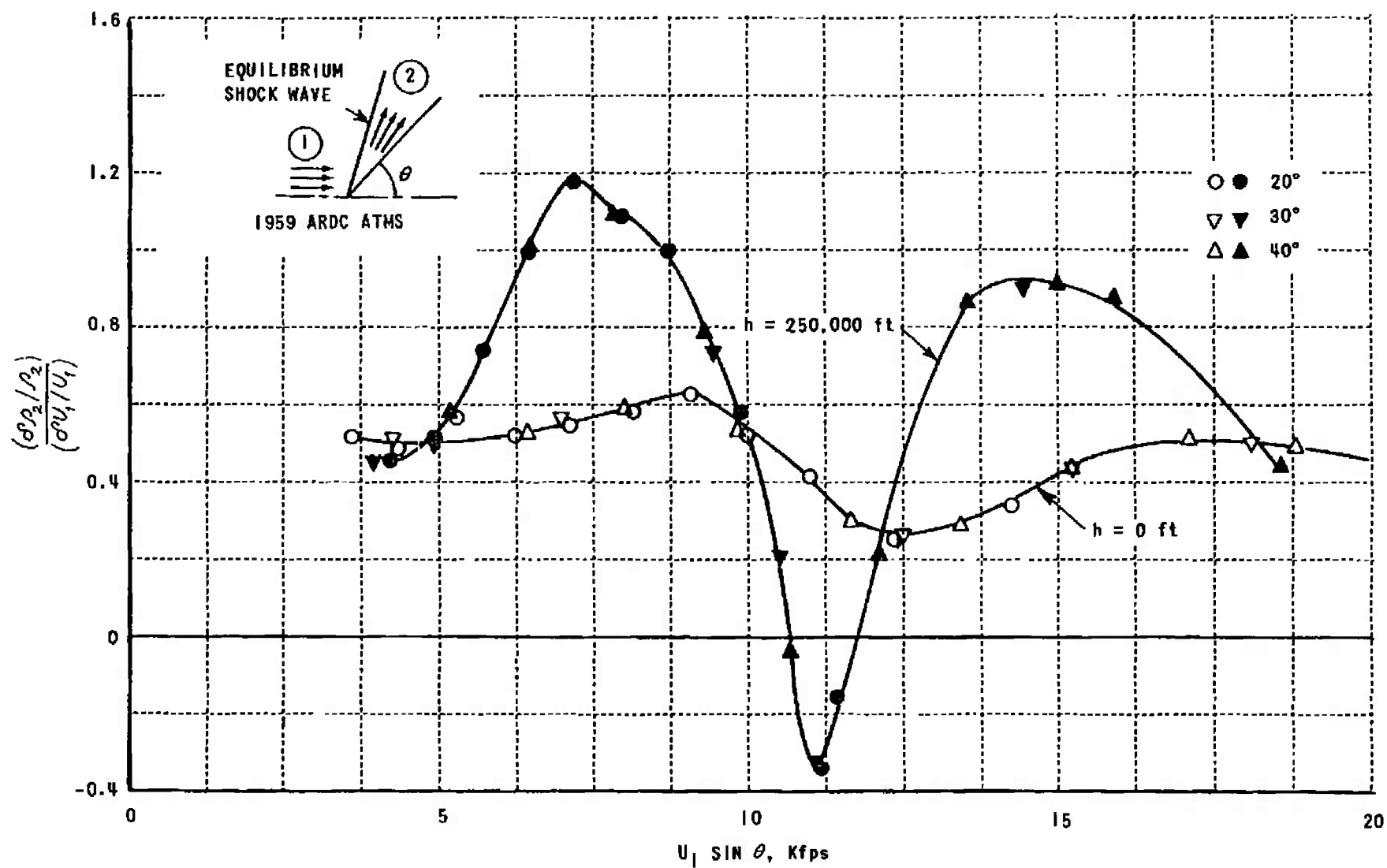
Figure 38a   SENSITIVITY OF THE FOREBODY DENSITY TO CHANGES IN FREE-STREAM VELOCITY
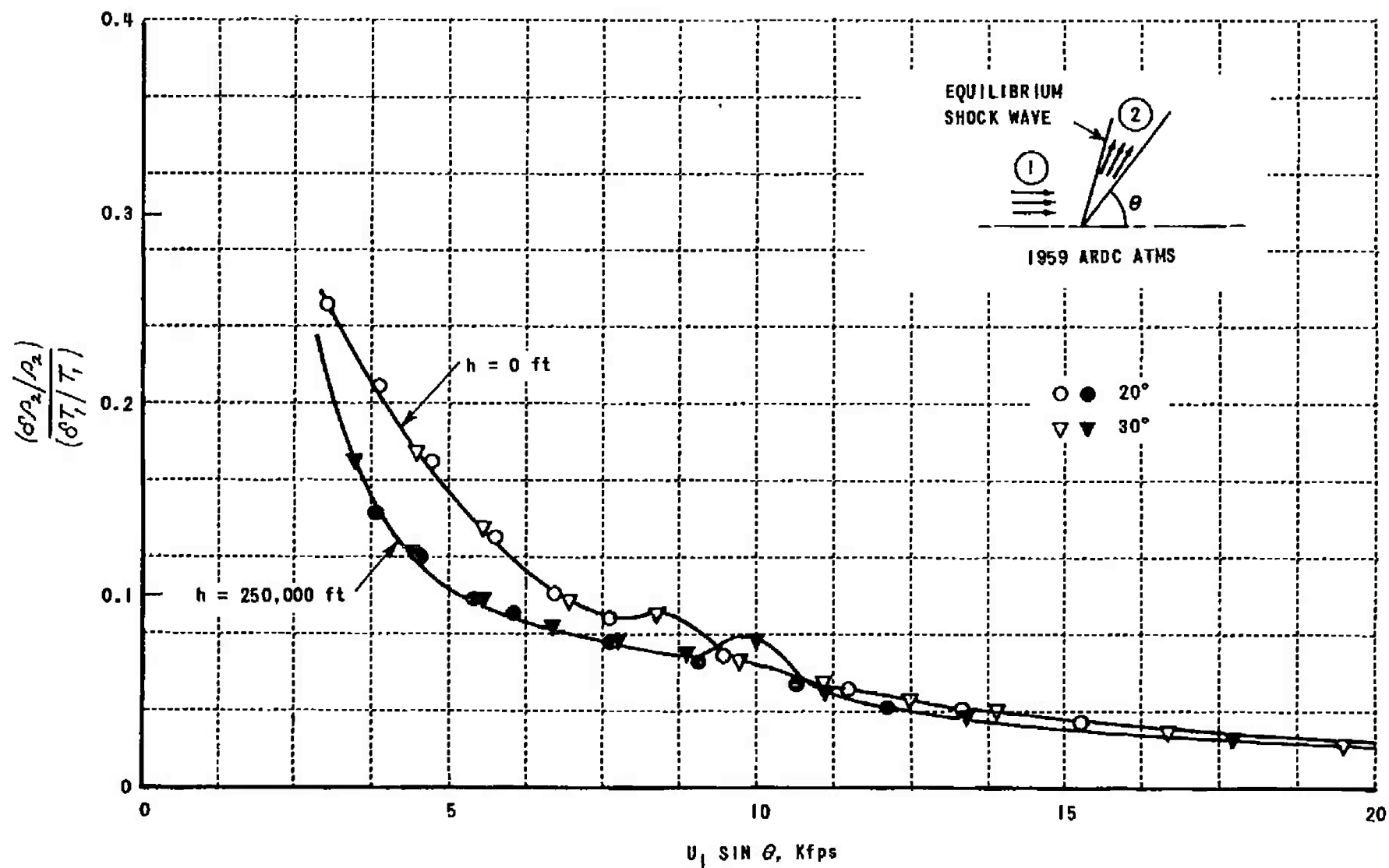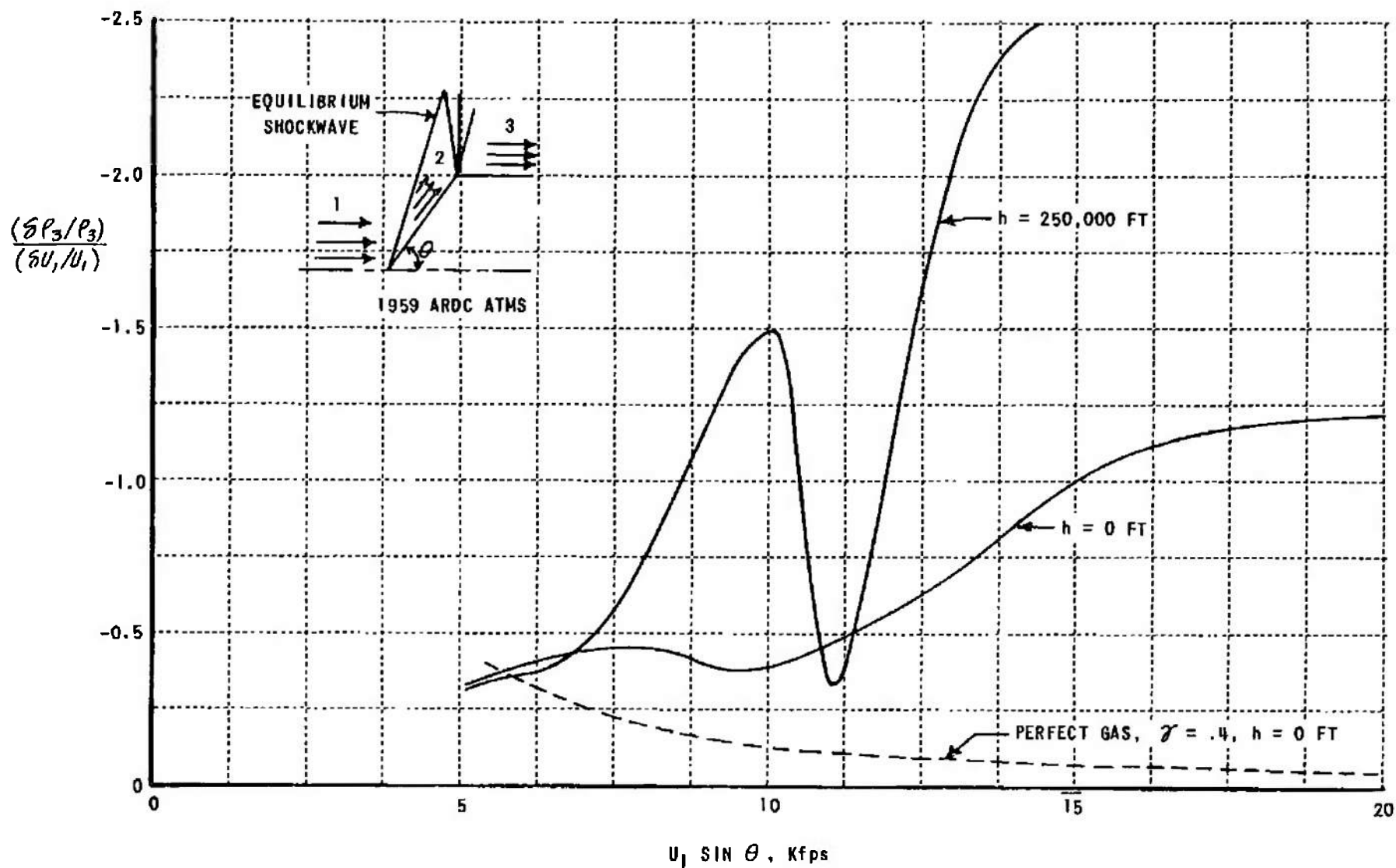
Figure 38b   SENSITIVITY OF FOREBODY DENSITY TO CHANGES IN FREE-STREAM TEMPERATURE
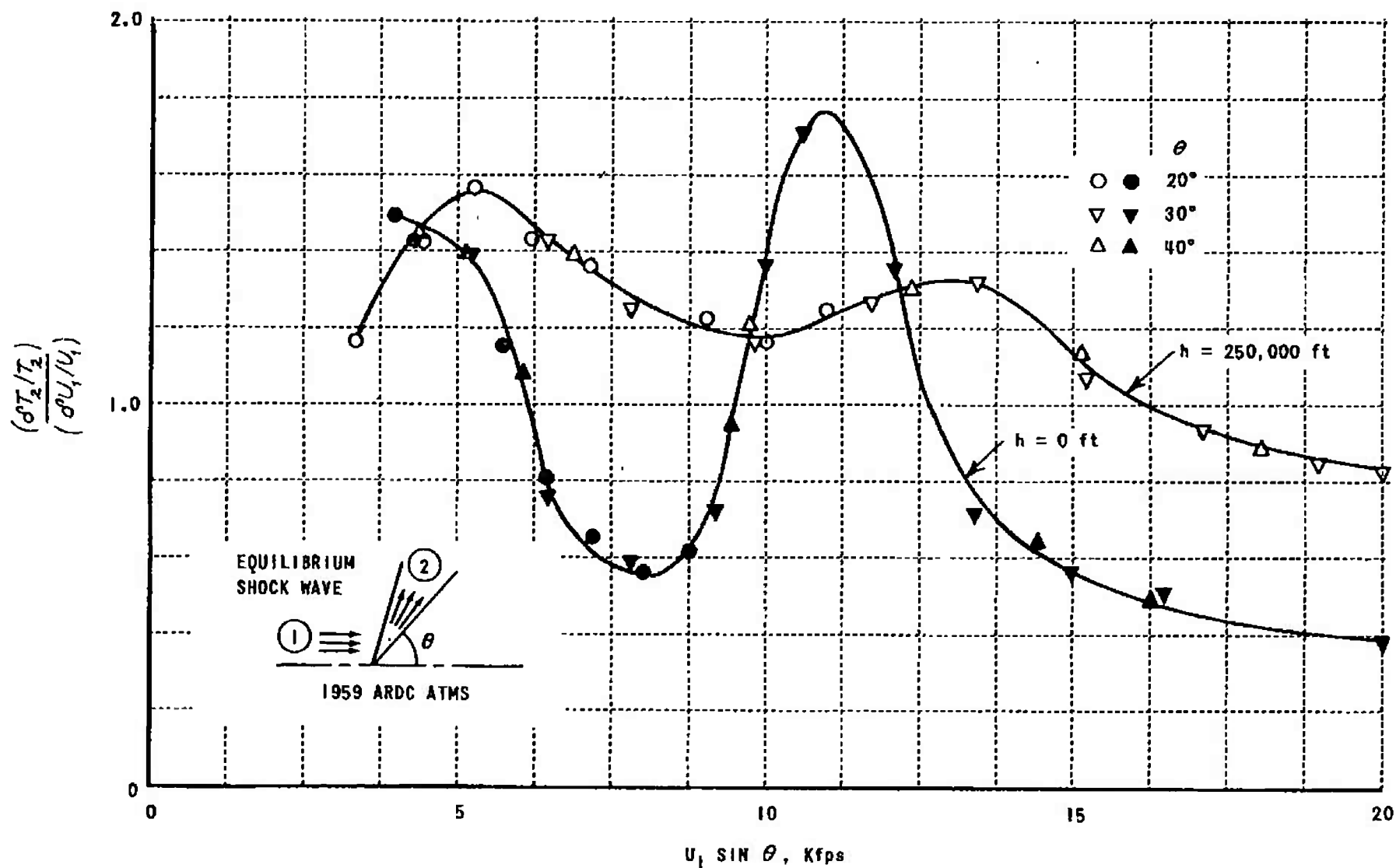
Figure 39a SENSITIVITY OF FOREBODY TEMPERATURE TO CHANGES IN FREE-STREAM VELOCITY
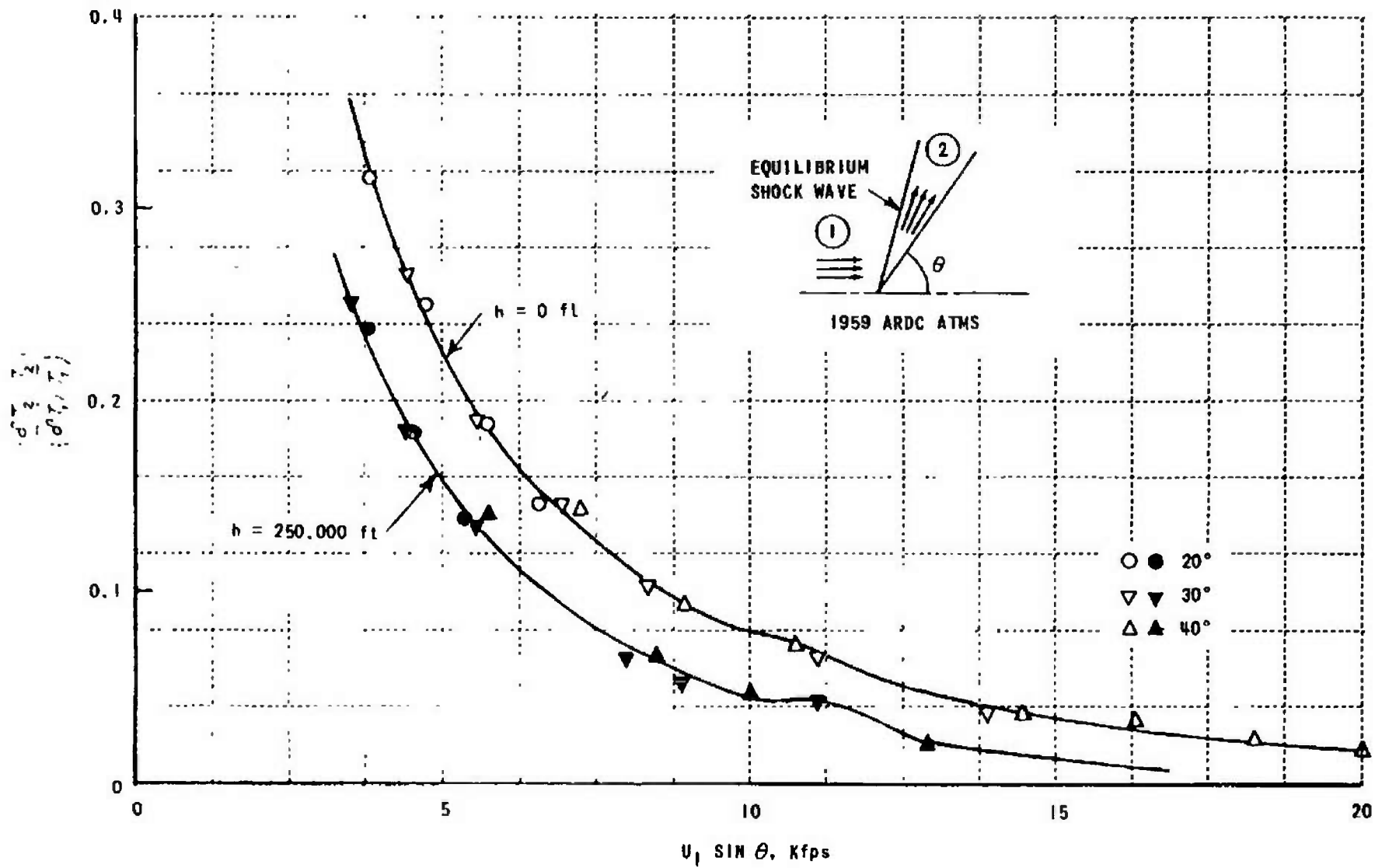
Figure 39b   SENSITIVITY OF FOREBODY TEMPERATURE TO CHANGES IN FREE-STREAM TEMPERATURE
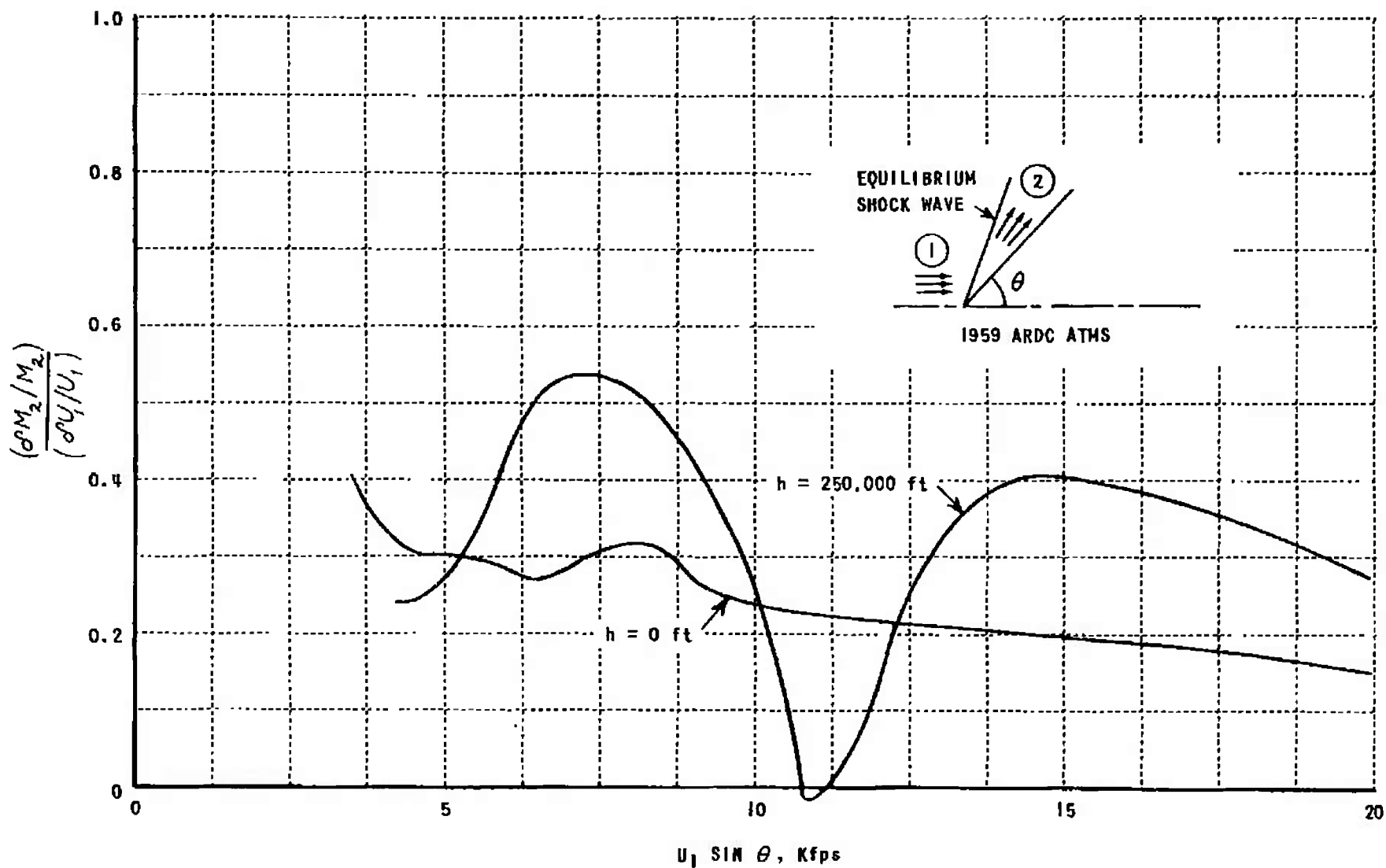
Figure 40a SENSITIVITY OF FOREBODY FROZEN MACH NUMBER TO CHANGES
IN FREE-STREAM VELOCITY
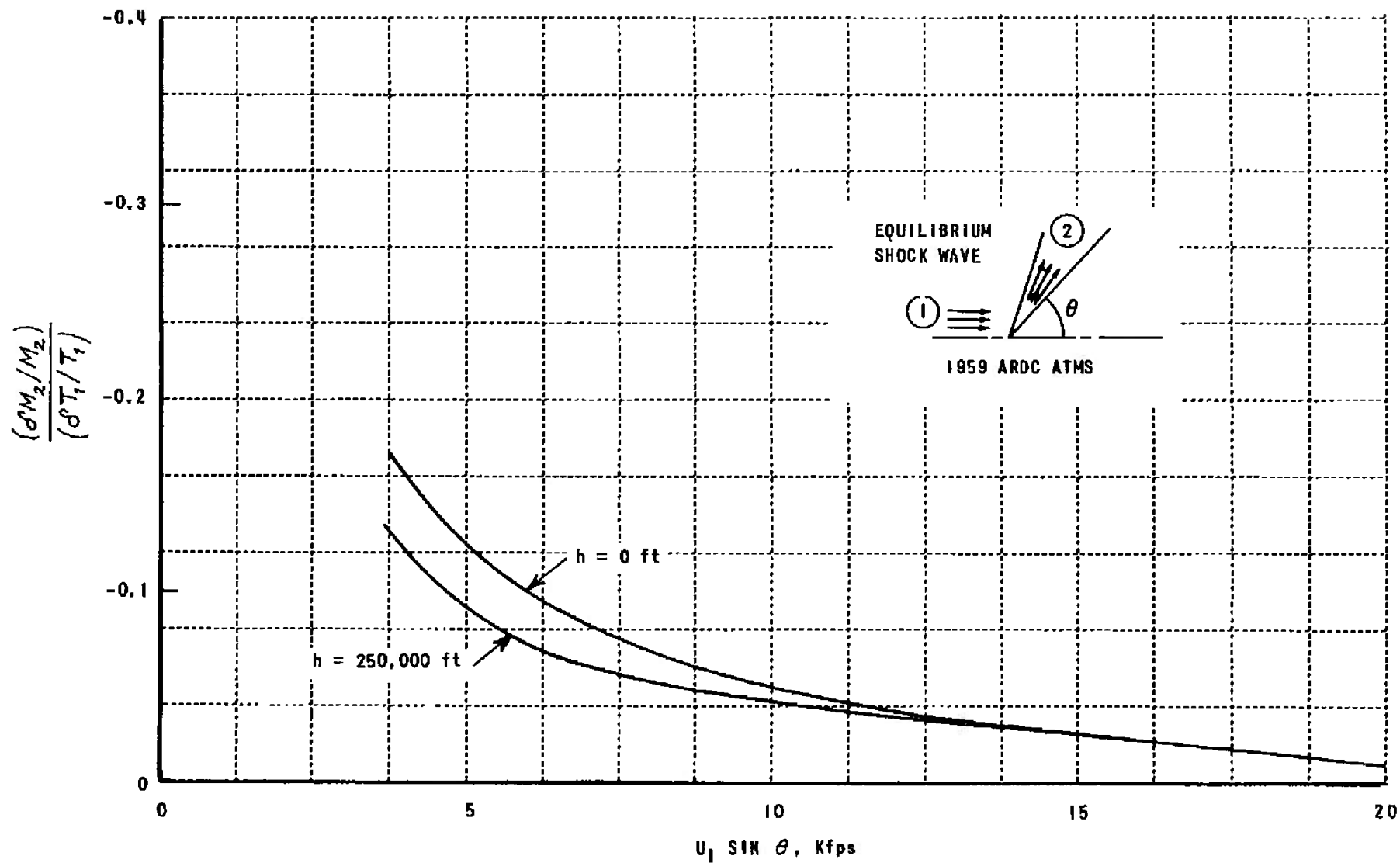
Figure 40 b   SENSITIVITY OF FOREBODY FROZEN MACH NUMBER TO CHANGES IN FREE-STREAM TEMPERATURE
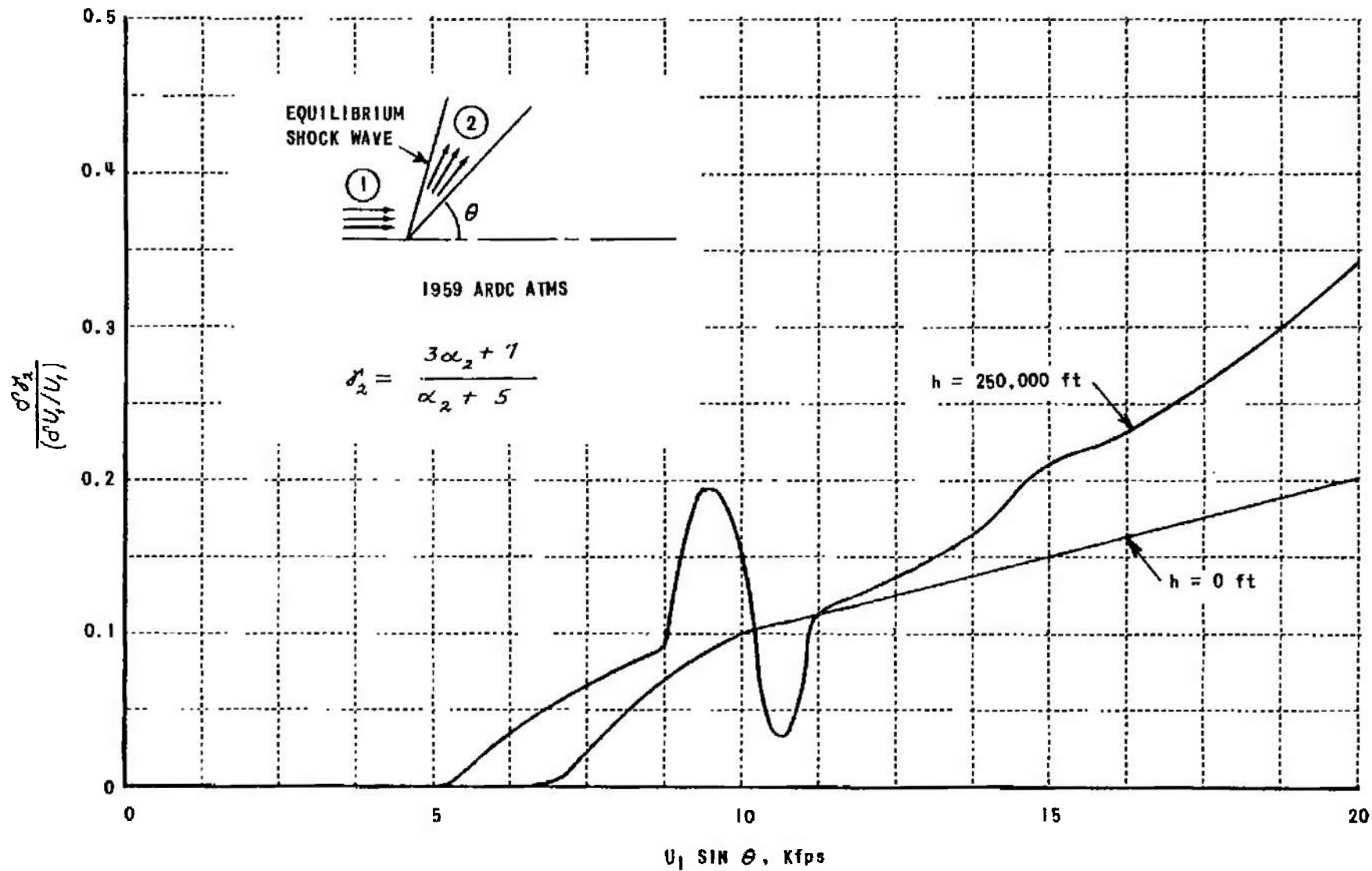
Figure 41a   SENSITIVITY OF FOREBODY FROZEN FLOW SPECIFIC HEAT RATIO
TO CHANGES IN FREE-STREAM VELOCITY
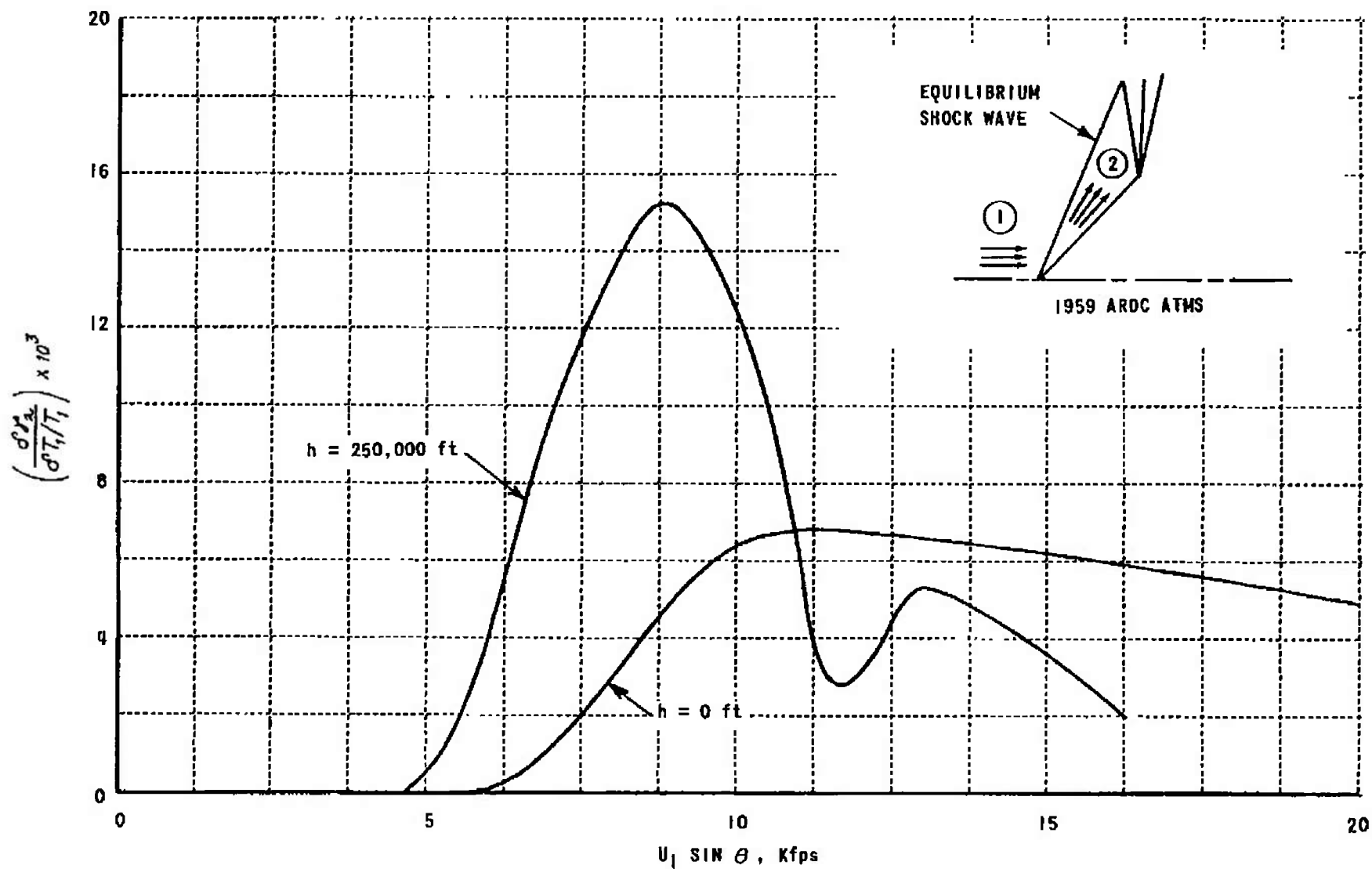
Figure 41b SENSITIVITY OF FOREBODY FROZEN SPECIFIC HEAT RATIO TO CHANGES IN
FREE-STREAM TEMPERATURE
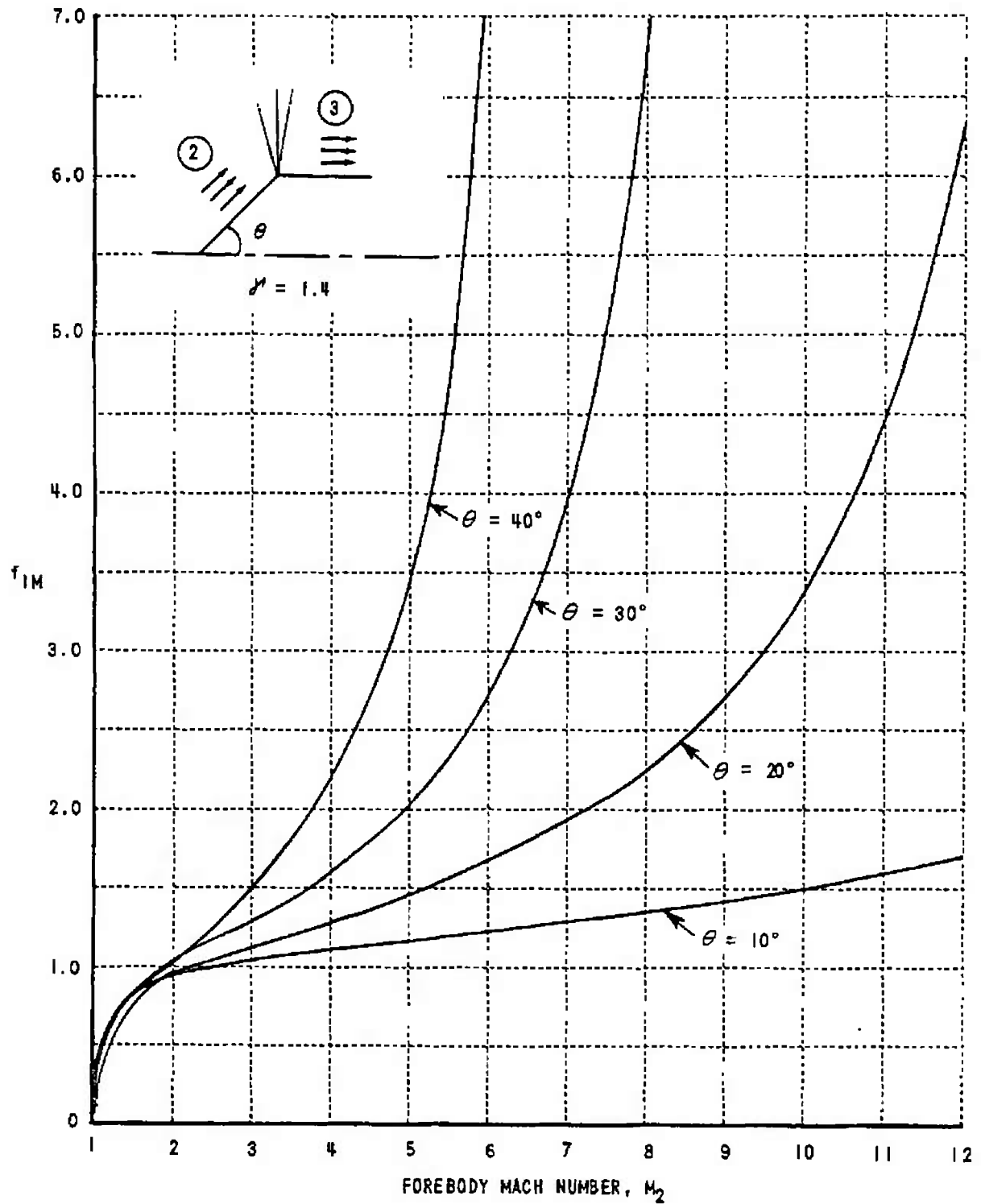
Figure 42a INFLUENCE COEFFICIENT FOR AFTERBODY MACH NUMBER WITH RESPECT TO CHANGES IN FOREBODY MACH NUMBER; $\gamma = 1.4$

261
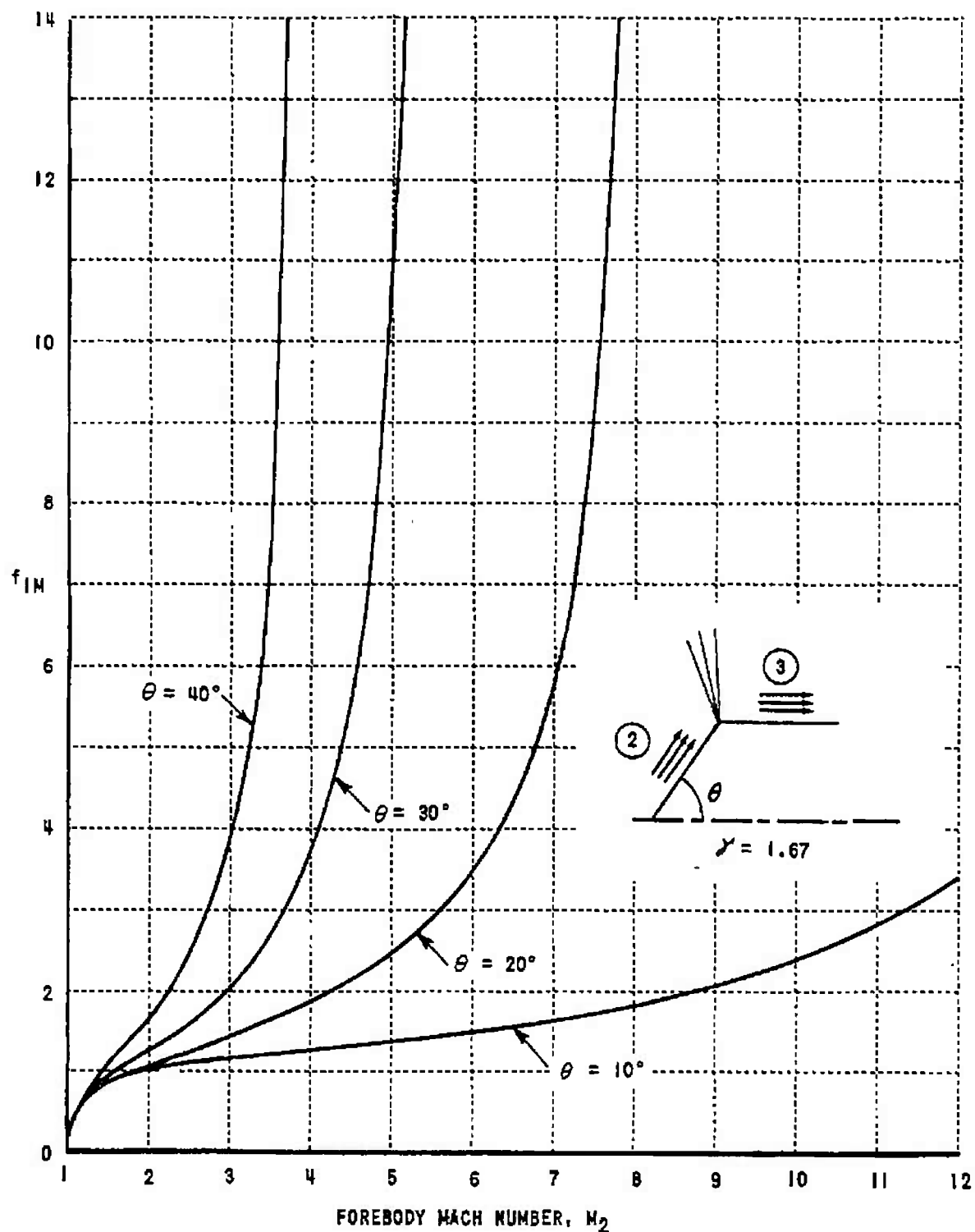
Figure 42b INFLUENCE COEFFICIENT FOR AFTERBODY MACH NUMBER WITH RESPECT TO CHANGES IN FOREBODY MACH NUMBER, $\gamma = 1.67$
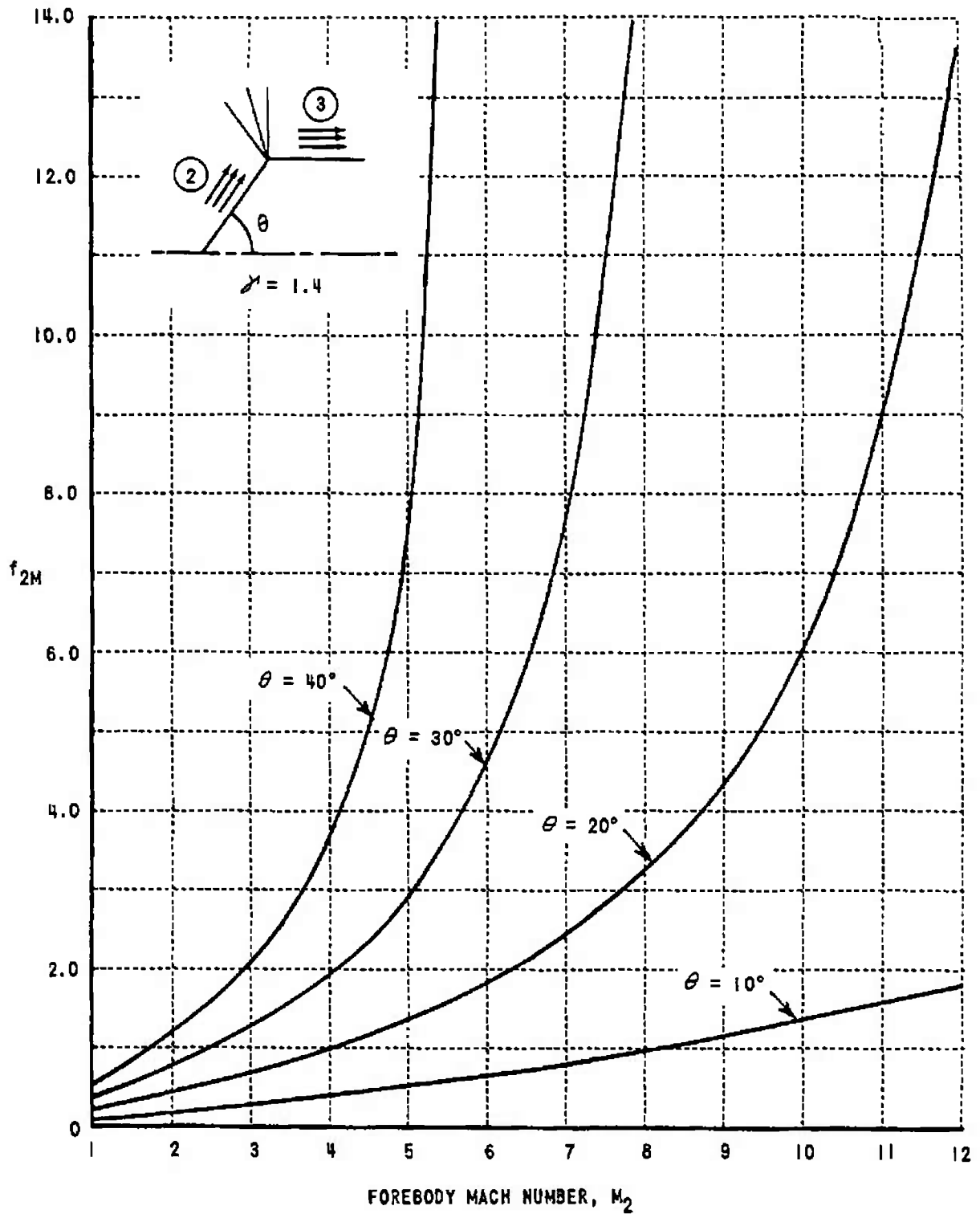
Figure 43a   INFLUENCE COEFFICIENT FOR AFTERBODY MACH NUMBER WITH RESPECT
TO CHANGES IN FOREBODY SPECIFIC HEAT RATIO, γ = 1.4
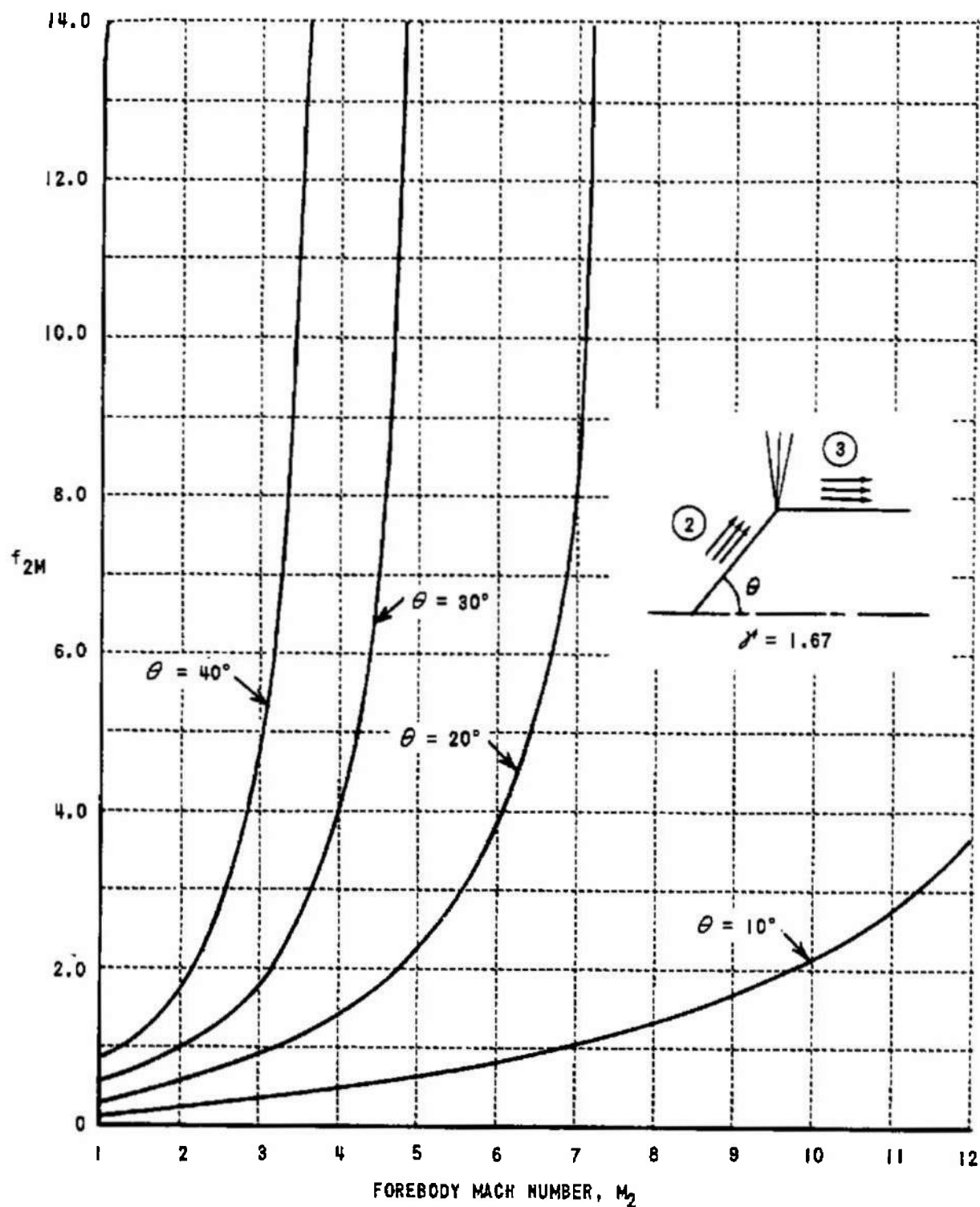
Figure 43b INFLUENCE COEFFICIENT FOR AFTERBODY MACH NUMBER WITH RESPECT
TO CHANGES IN FOREBODY SPECIFIC HEAT RATIO, γ = 1.67

Figure 44   INFLUENCE COEFFICIENTS FOR AFTERBODY PRESSURE   AND TEMPERATURE
WITH RESPECT TO CHANGES IN FOREBODY MACH NUMBER; $\gamma = 1.4$
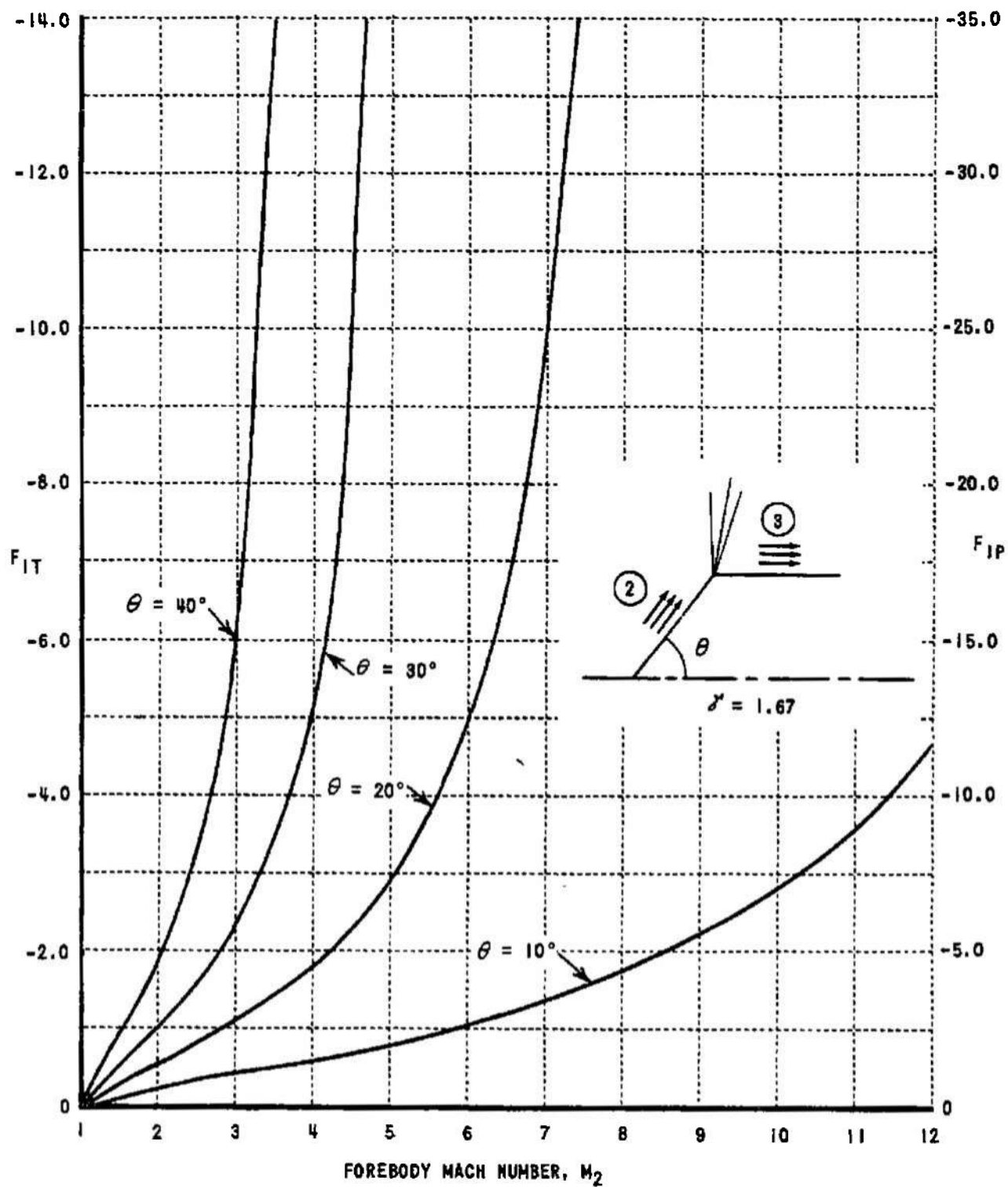
Figure 45 INFLUENCE COEFFICIENTS FOR AFTERBODY TEMPERATURE AND PRESSURE
WITH RESPECT TO CHANGES IN FOREBODY MACH NUMBER, γ = 1.67
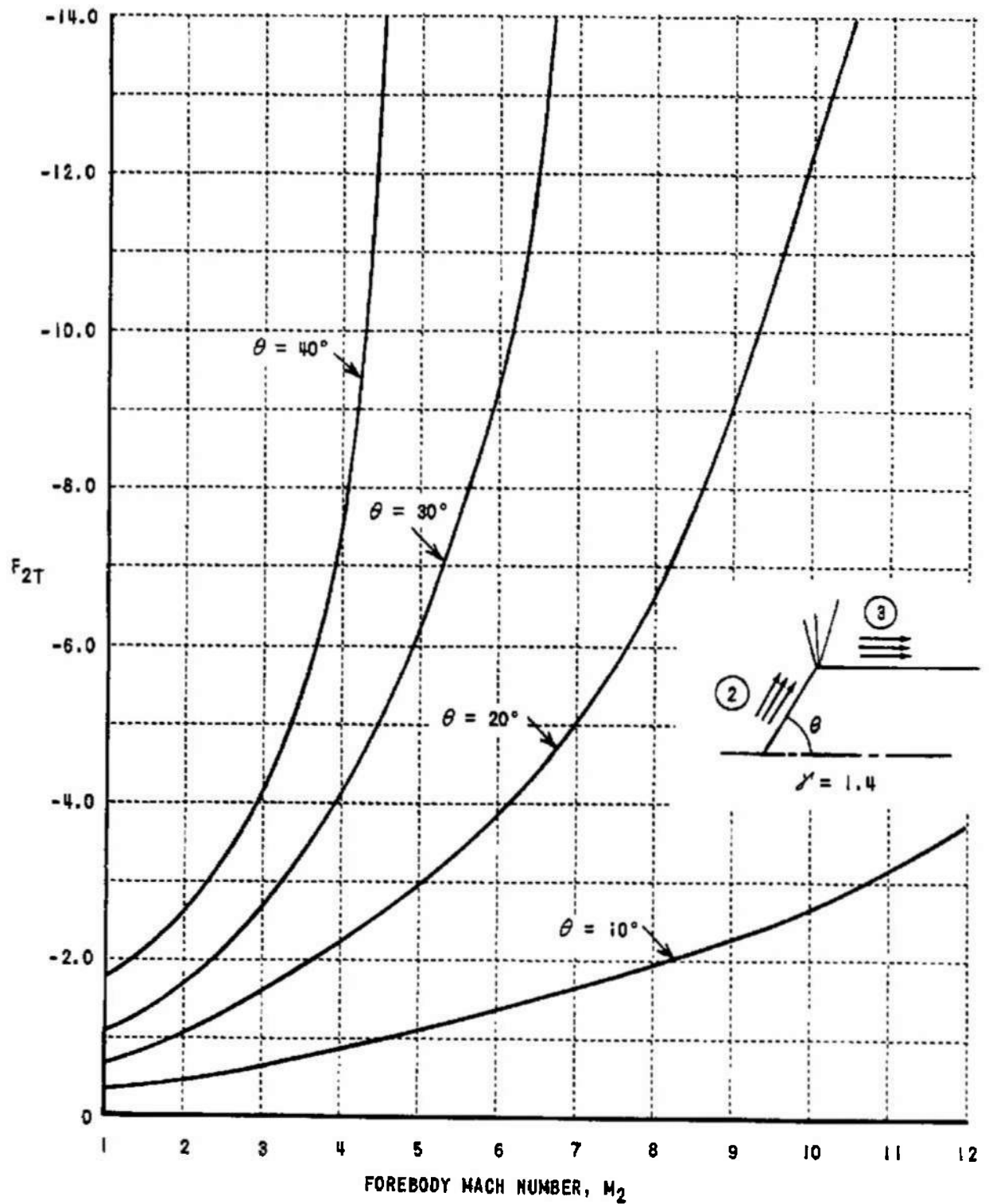
Figure 46a INFLUENCE COEFFICIENT FOR AFTERBODY TEMPERATURE WITH RESPECT
TO CHANGES IN FOREBODY SPECIFIC HEAT RATIO, $\gamma = 1.4$
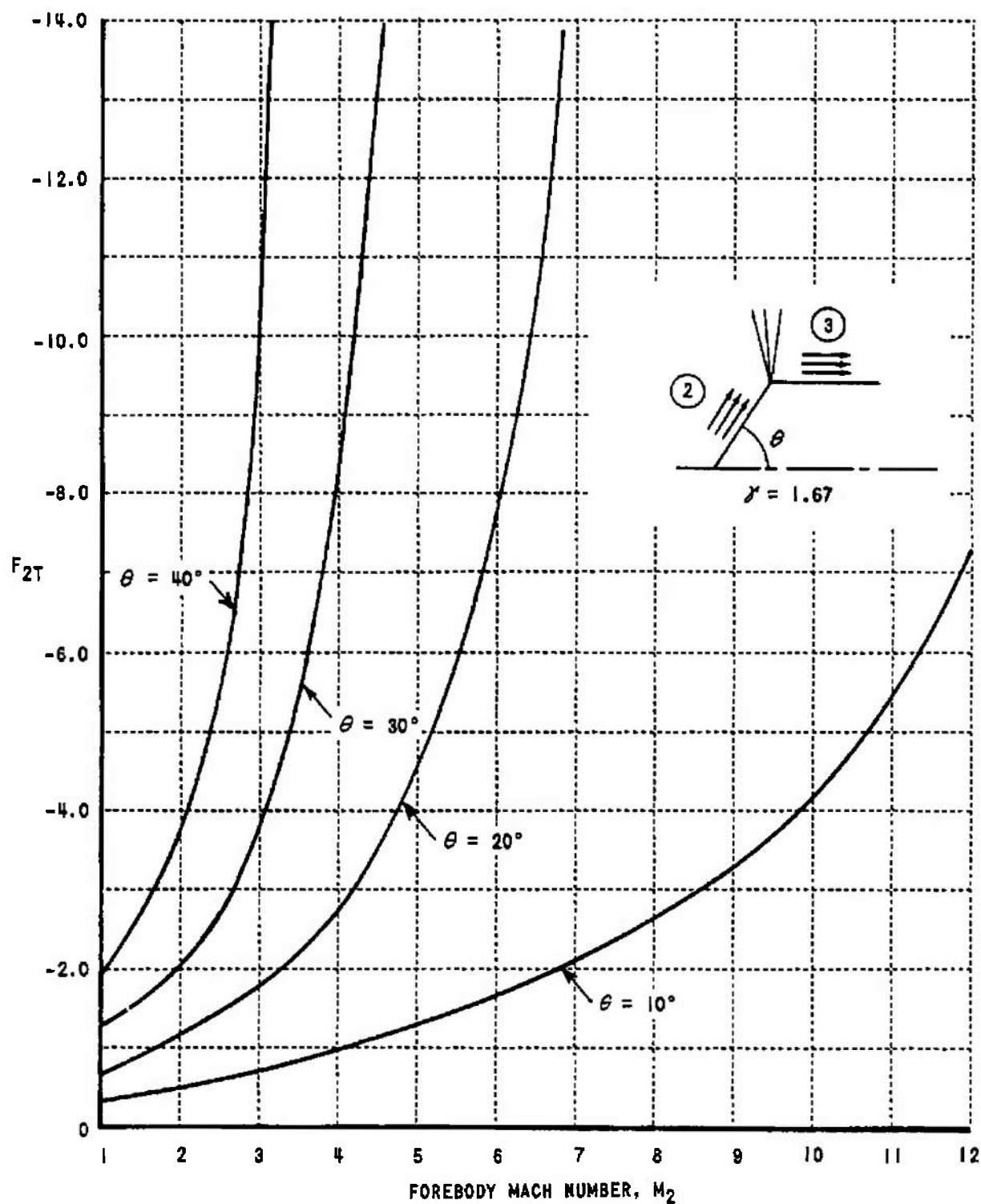
Figure 46b   INFLUENCE COEFFICIENT FOR AFTERBODY TEMPERATURE WITH RESPECT
TO CHANGES IN FOREBODY SPECIFIC HEAT RATIO, $\gamma = 1.67$
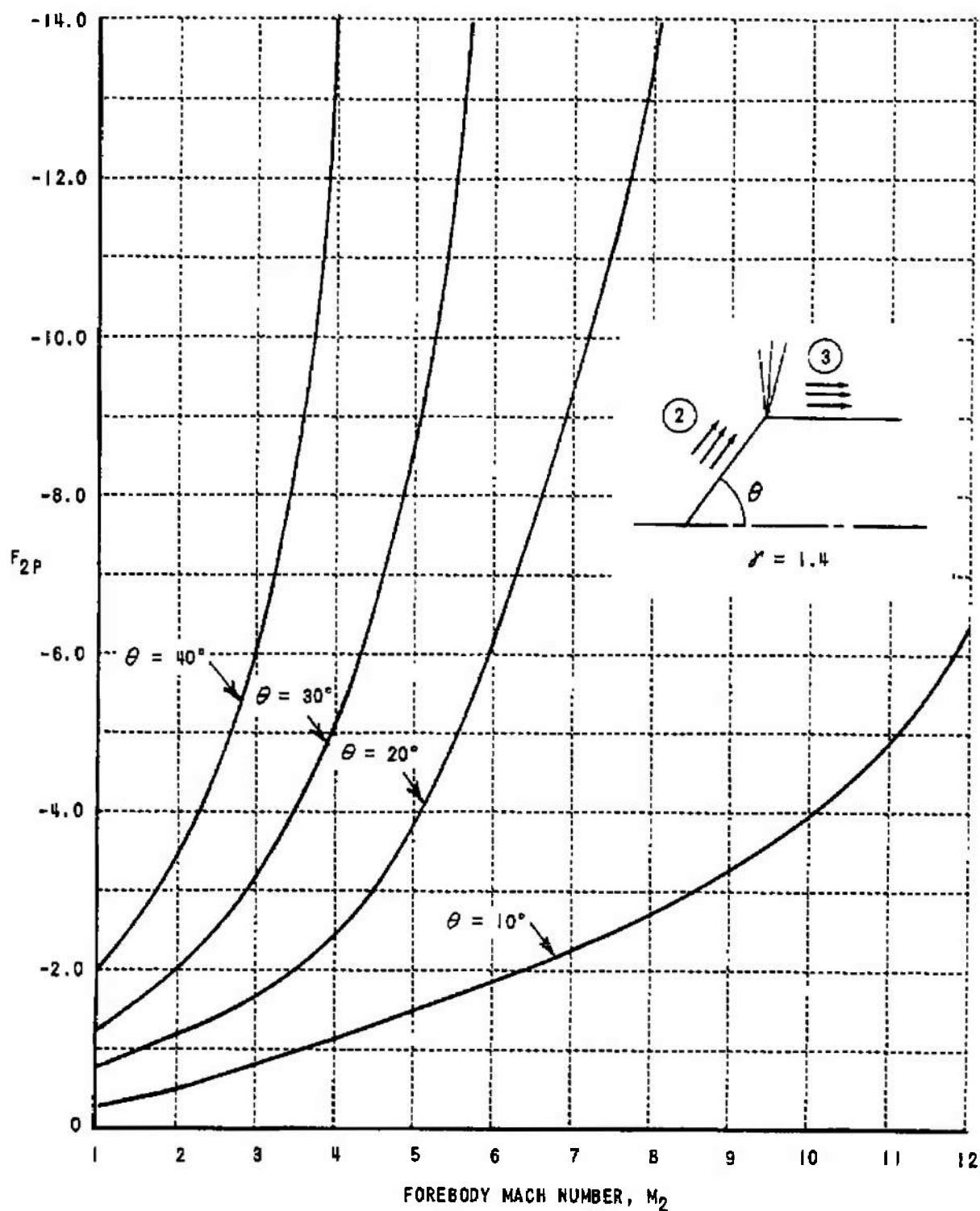
Figure 47a   INFLUENCE COEFFICIENT FOR AFTERBODY PRESSURE WITH RESPECT TO
CHANGES IN FOREBODY SPECIFIC HEAT RATIO, $\gamma = 1.4$
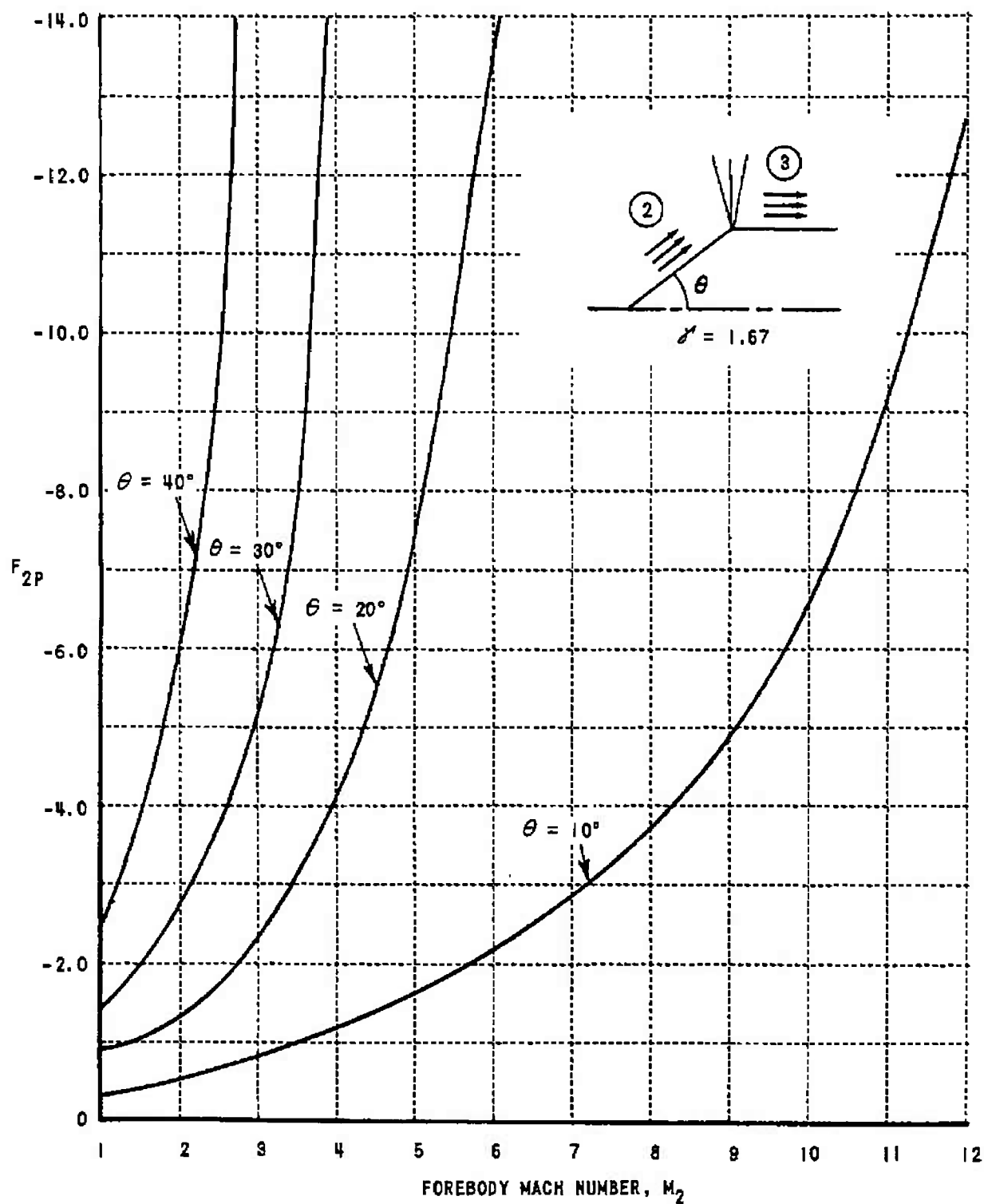
Figure 47b   INFLUENCE COEFFICIENT FOR AFTERBODY PRESSURE WITH RESPECT TO
CHANGES IN FOREBODY SPECIFIC HEAT RATIO, γ = 1.67

270

Figure 48a SENSITIVITY OF AFTERBODY DENSITY TO CHANGES IN FREE-STREAM VELOCITY
(e-f MODEL)
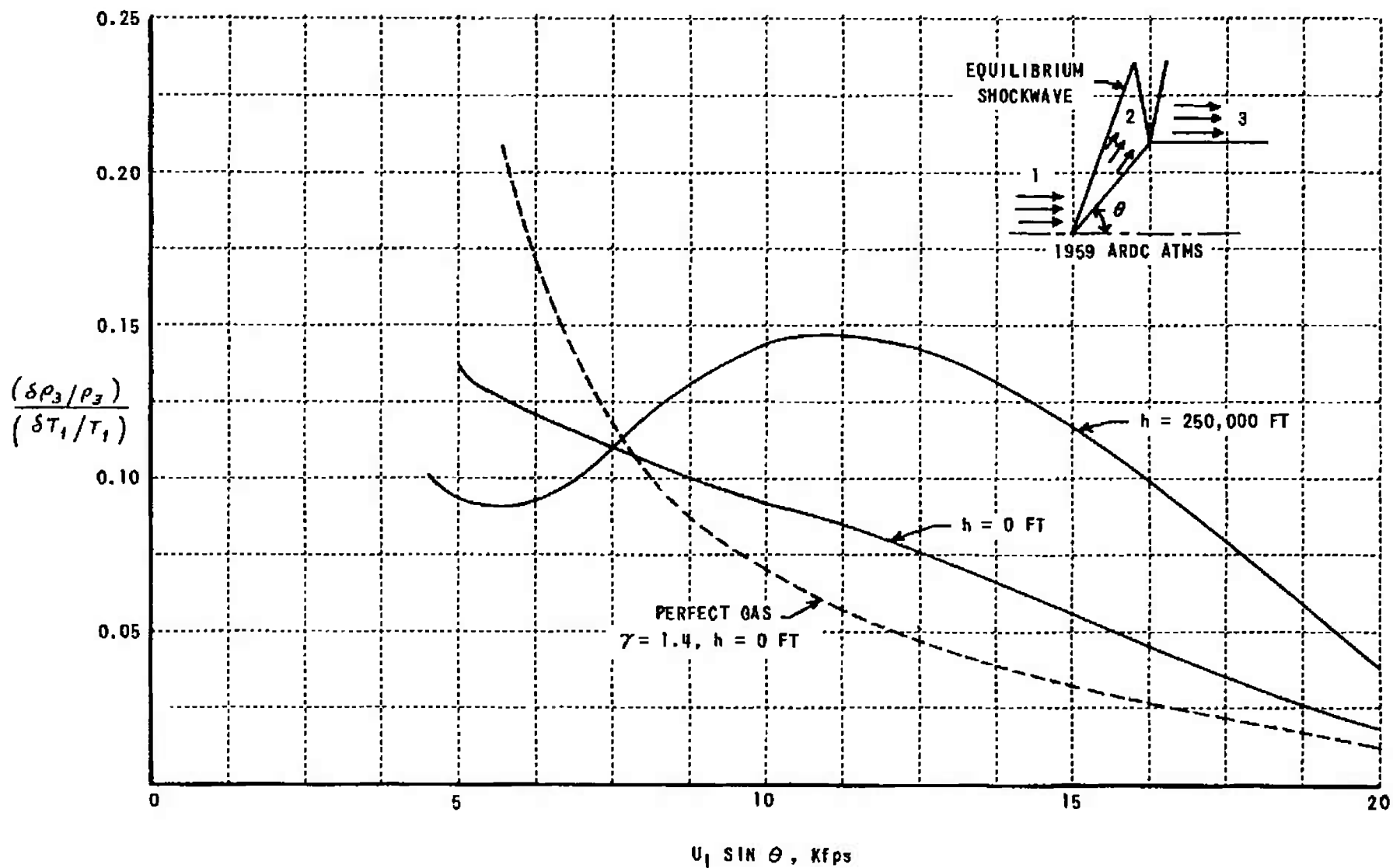
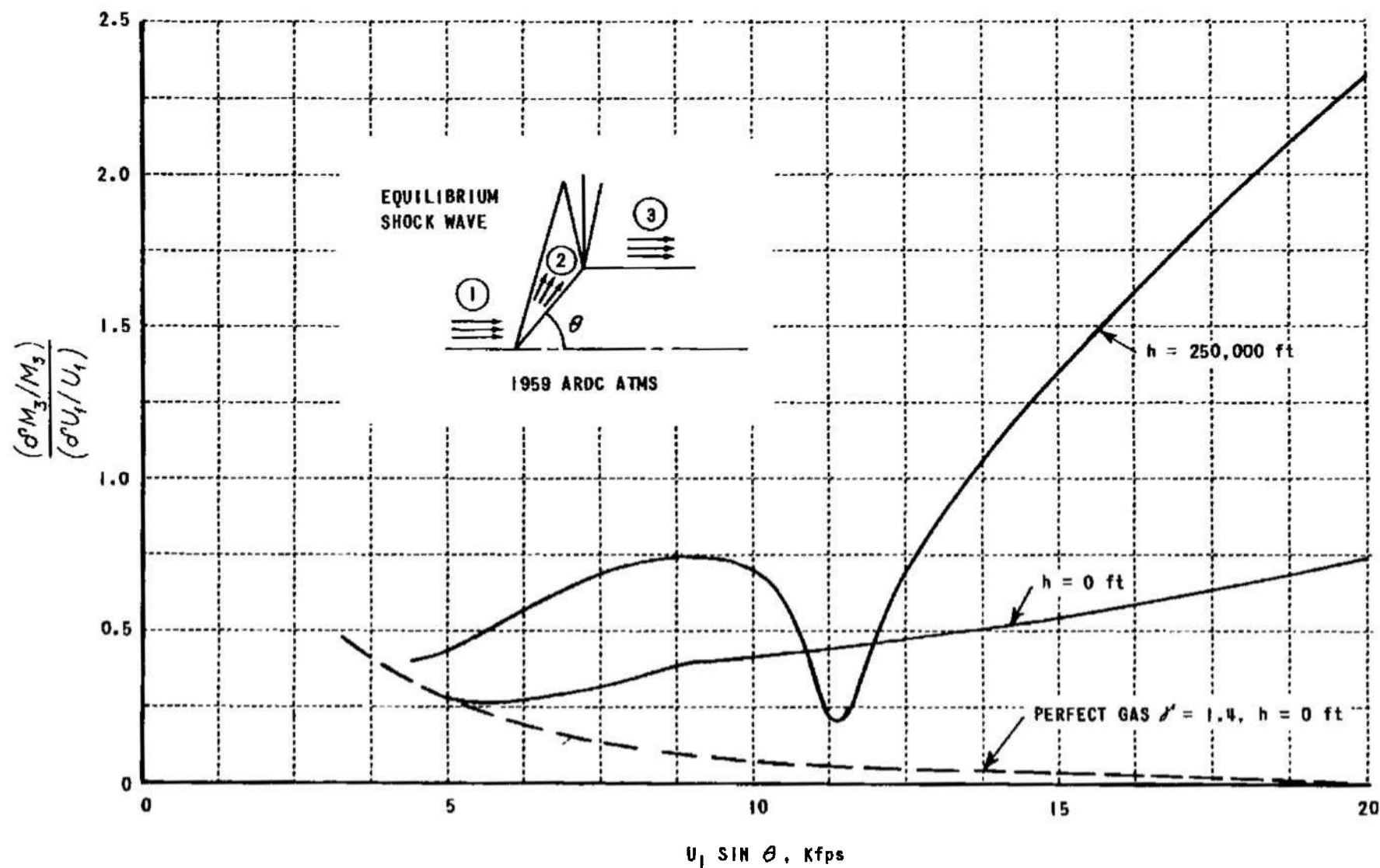Figure 48b   SENSITIVITY OF AFTERBODY DENSITY TO CHANGES IN FREE-STREAM TEMPERATURE
(e-f MODEL)
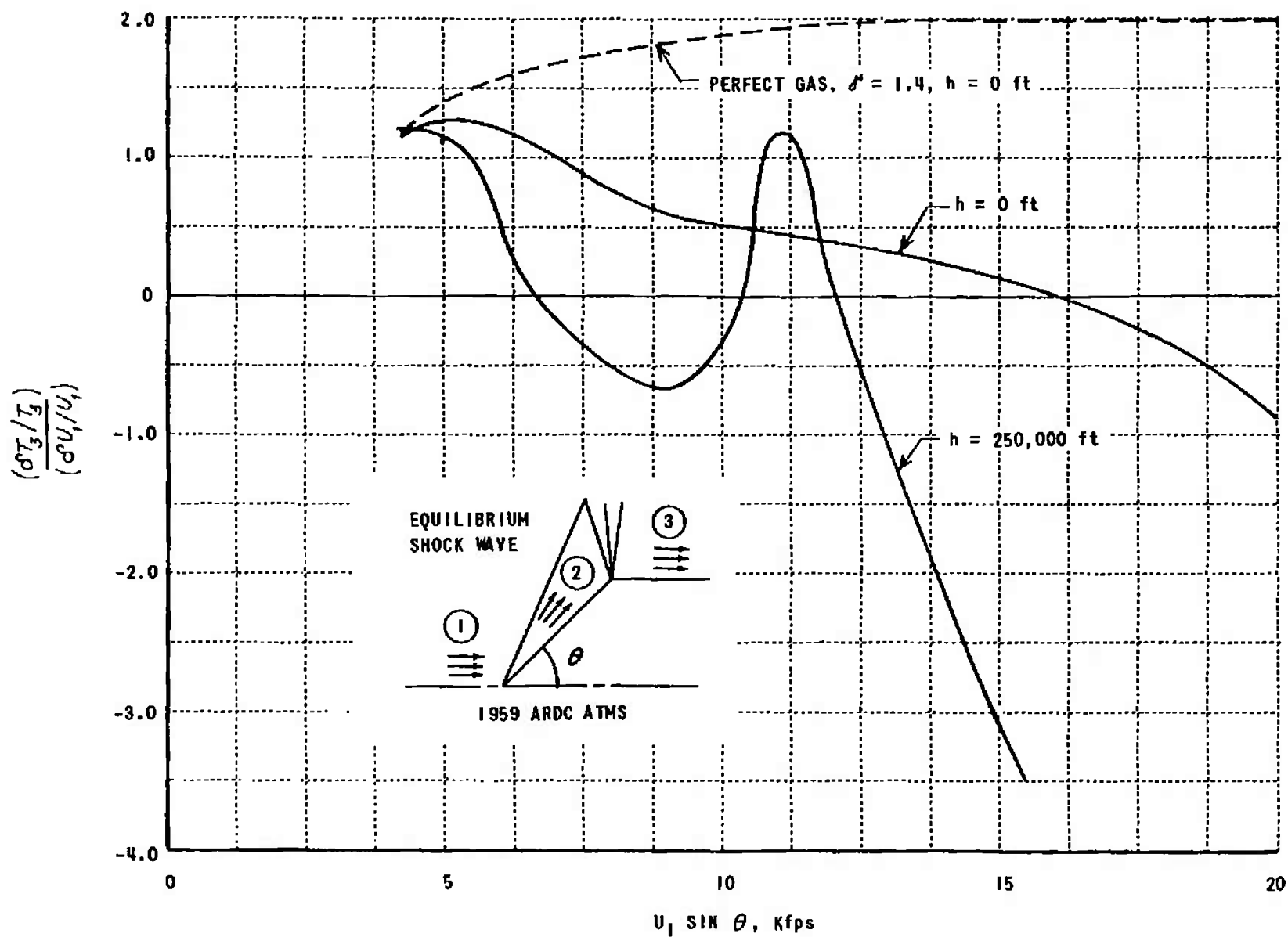
Figure 49a   SENSITIVITY OF AFTERBODY TEMPERATURE TO CHANGES IN FREE-STREAM VELOCITY (e-f MODEL)
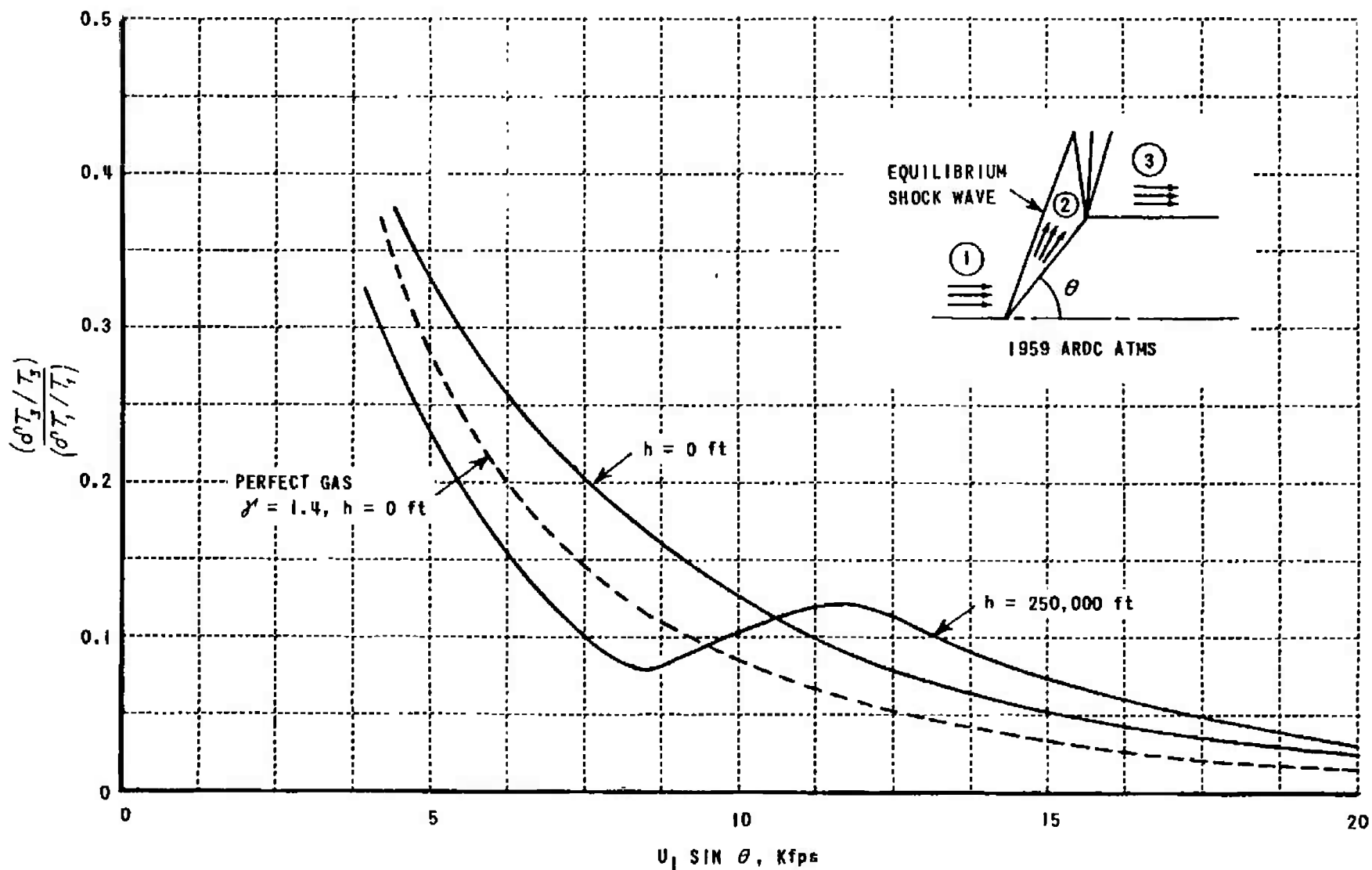
Figure 49b SENSITIVITY OF AFTERBODY TEMPERATURE TO CHANGES IN FREE-STREAM TEMPERATURE (e-f MODEL)
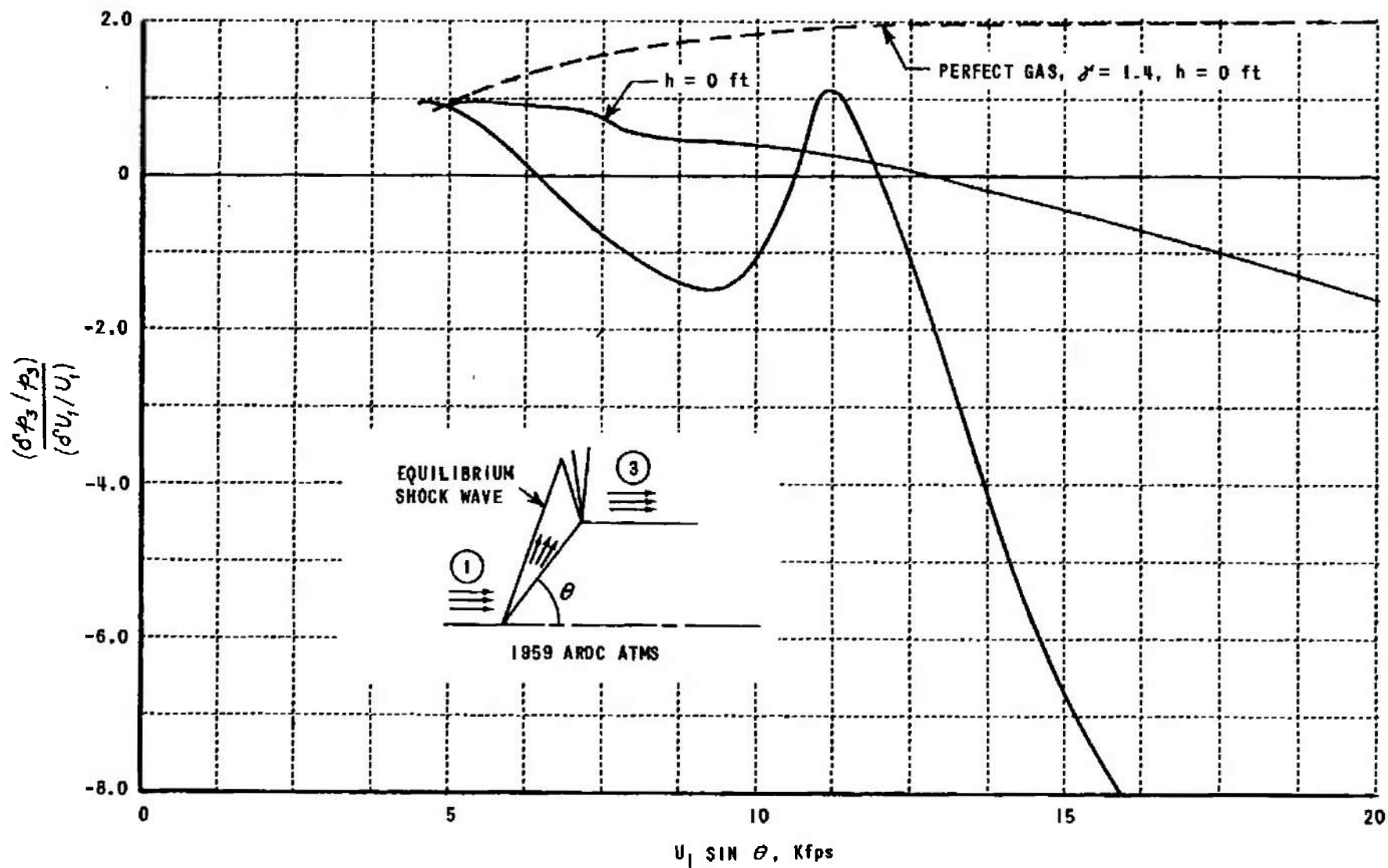
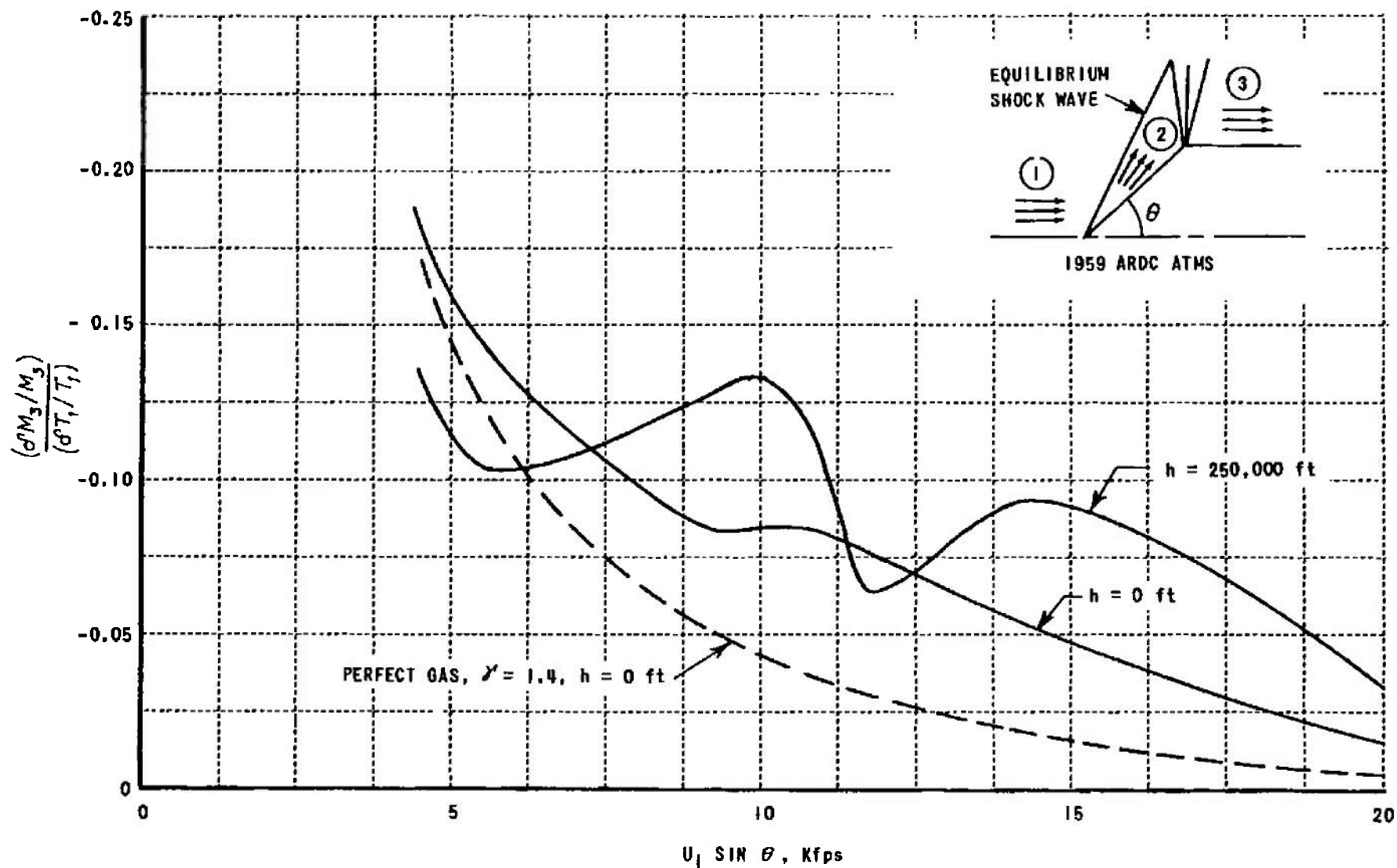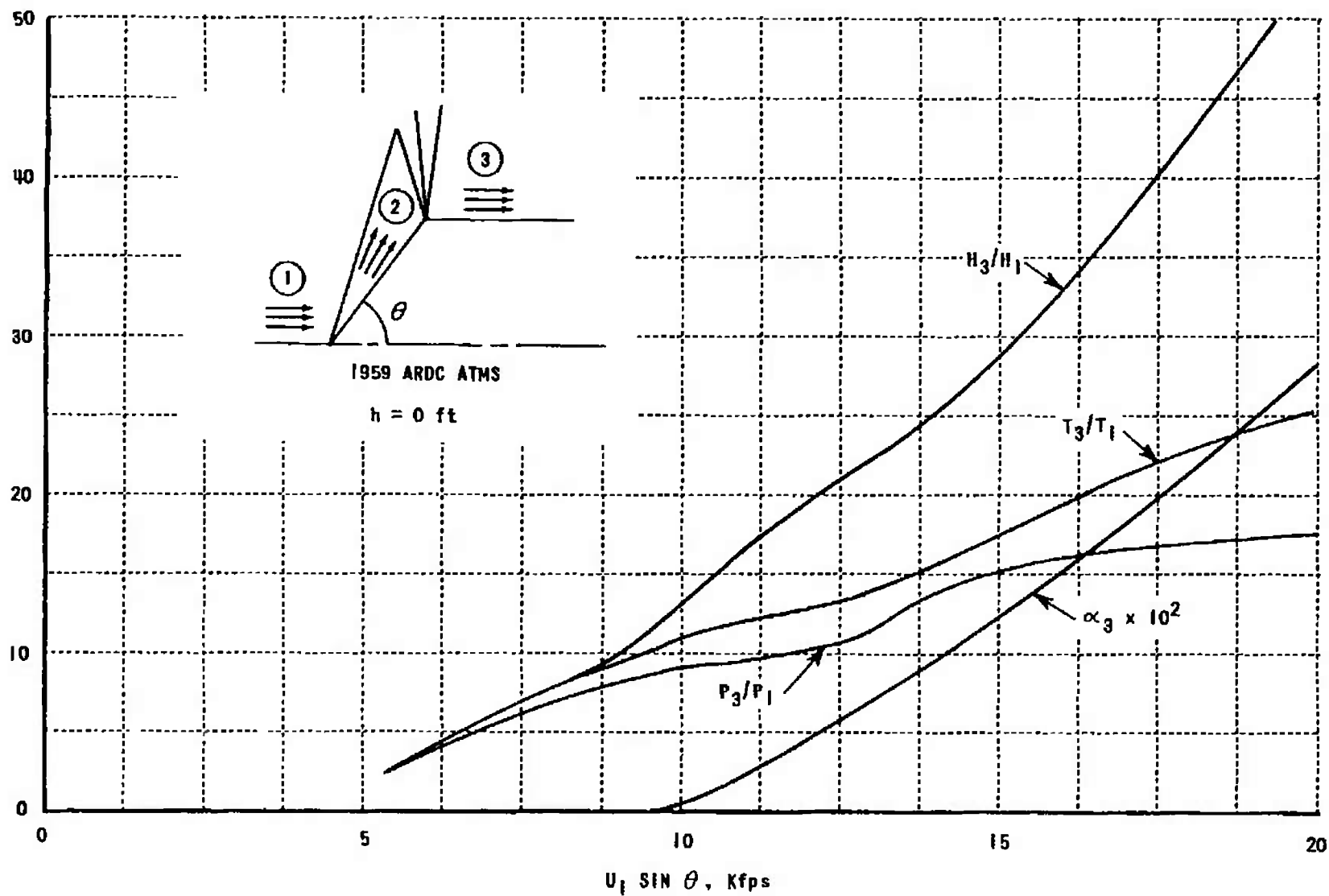Figure 50a SENSITIVITY OF AFTERBODY PRESSURE TO CHANGES IN FREE-STREAM VELOCITY (e -f MODEL)
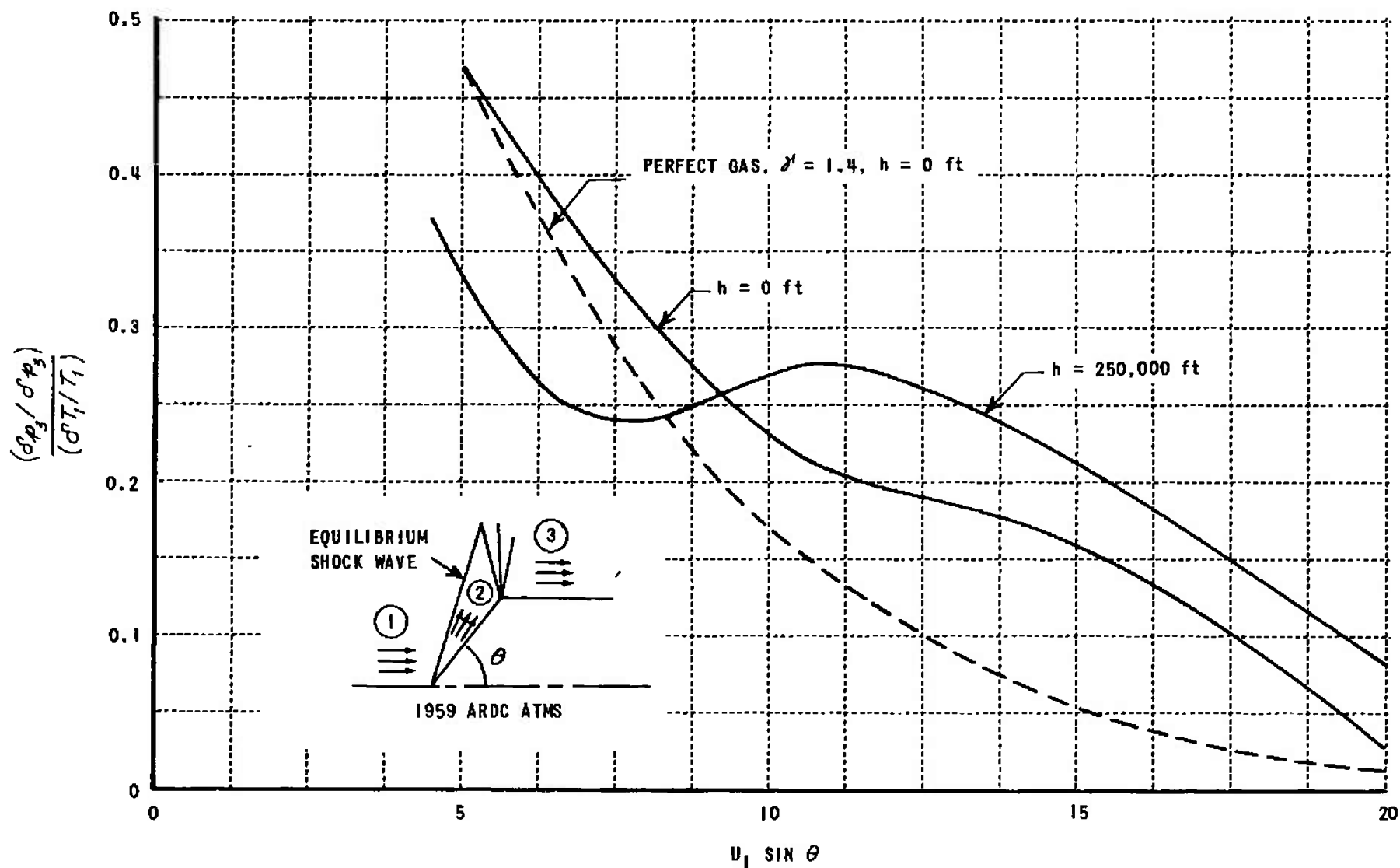
Figure 50b SENSITIVITY OF AFTERBODY PRESSURE TO CHANGES IN FREE-STREAM TEMPERATURE
(e-f MODEL)

Figure 51a SENSITIVITY OF AFTERBODY MACH NUMBER TO CHANGES IN FREE-STREAM VELOCITY
(e-f MODEL)

Figure 51b SENSITIVITY OF AFTERBODY FROZEN MACH NUMBER TO CHANGES IN FREE-STREAM TEMPERATURE
(e-f MODEL)

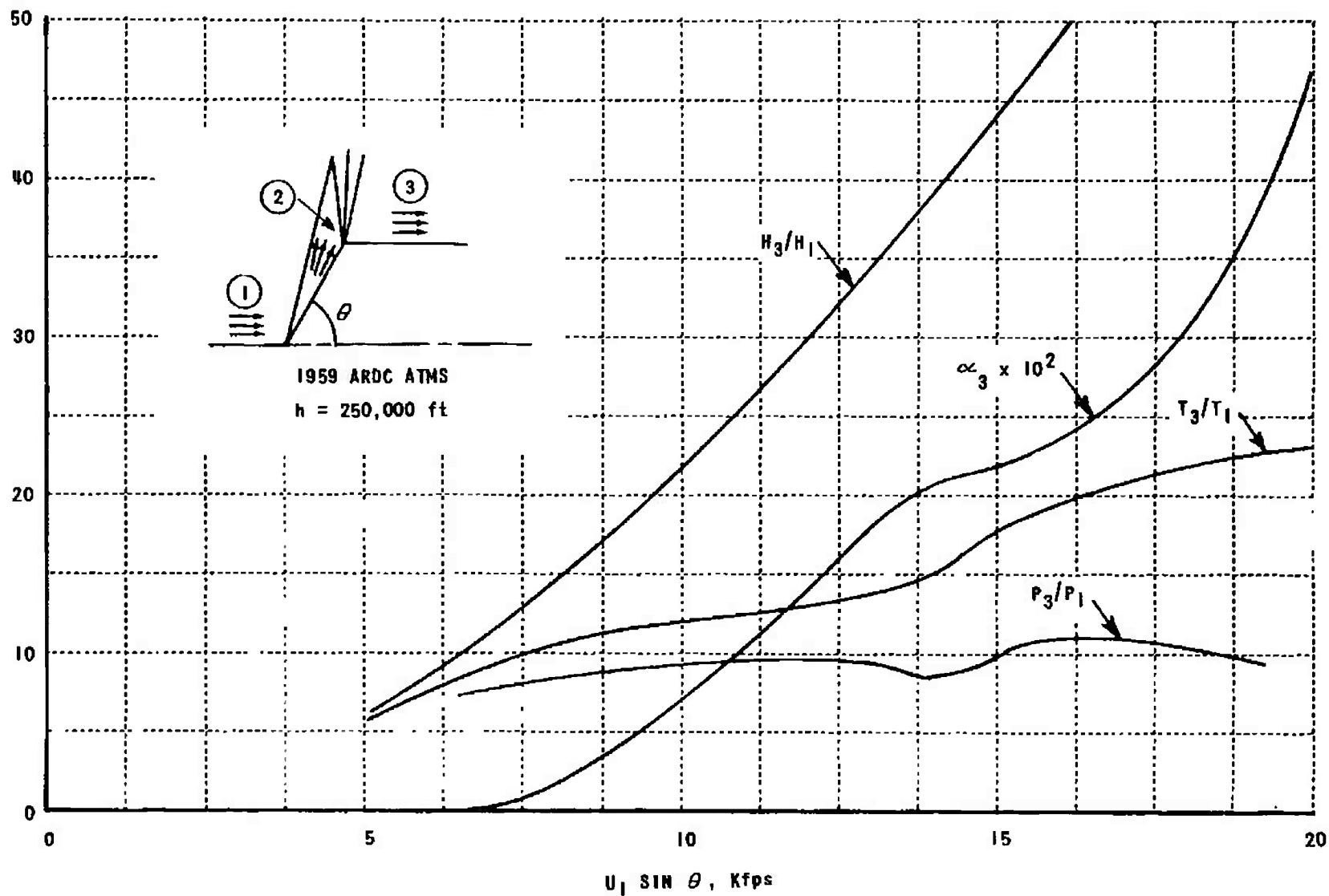Figure 52a   VARIATION OF AFTERBODY FLOW QUANTITIES FOR h = 0 FT
(e–e MODEL)

Figure 52b   VARIATION OF AFTERBODY FLOW QUANTITIES FOR   h = 250,000 ft (e-e MODEL)
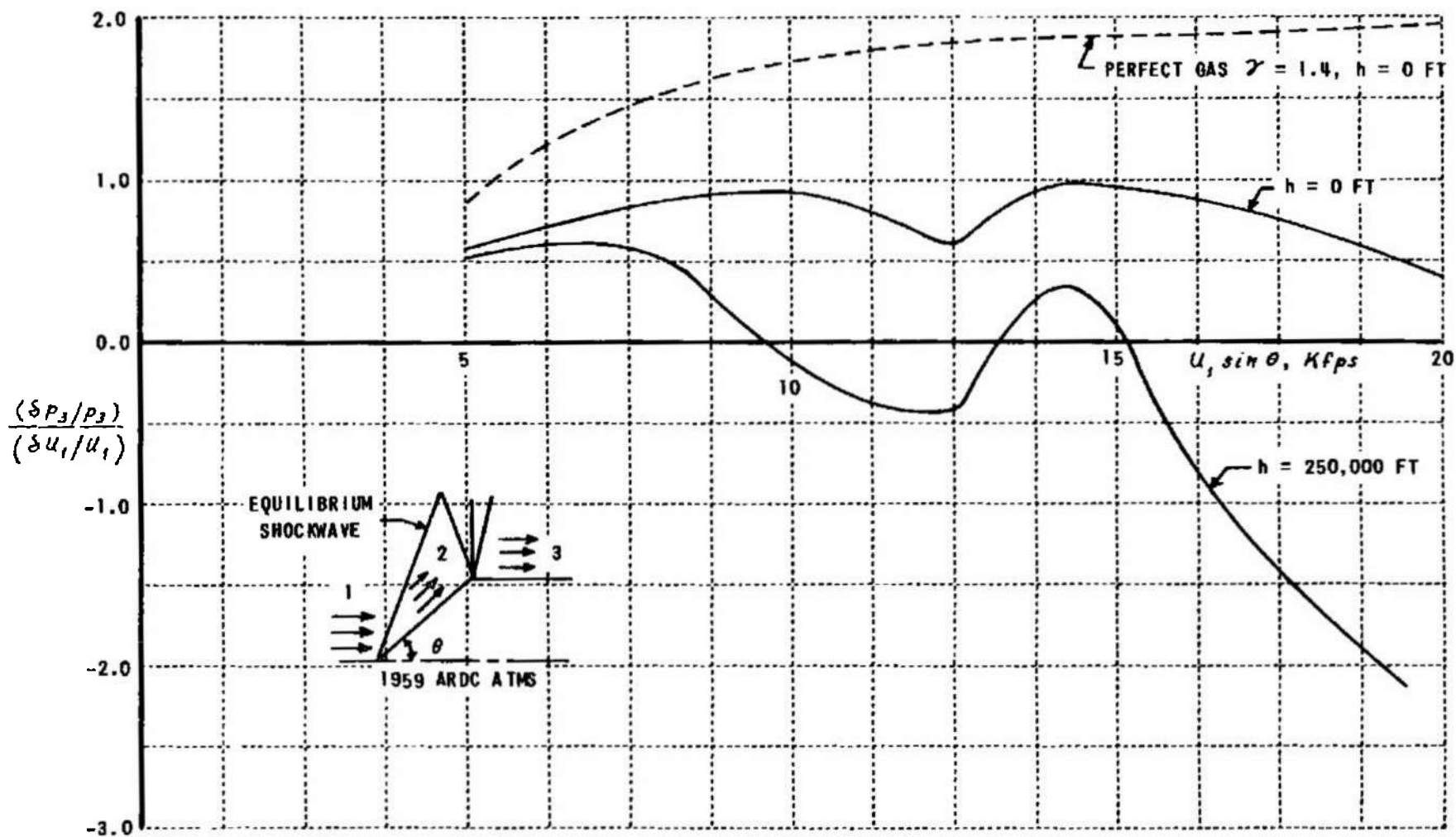
Figure 53a   SENSITIVITY OF AFTERBODY PRESSURE TO CHANGES IN FREE-STREAM VELOCITY
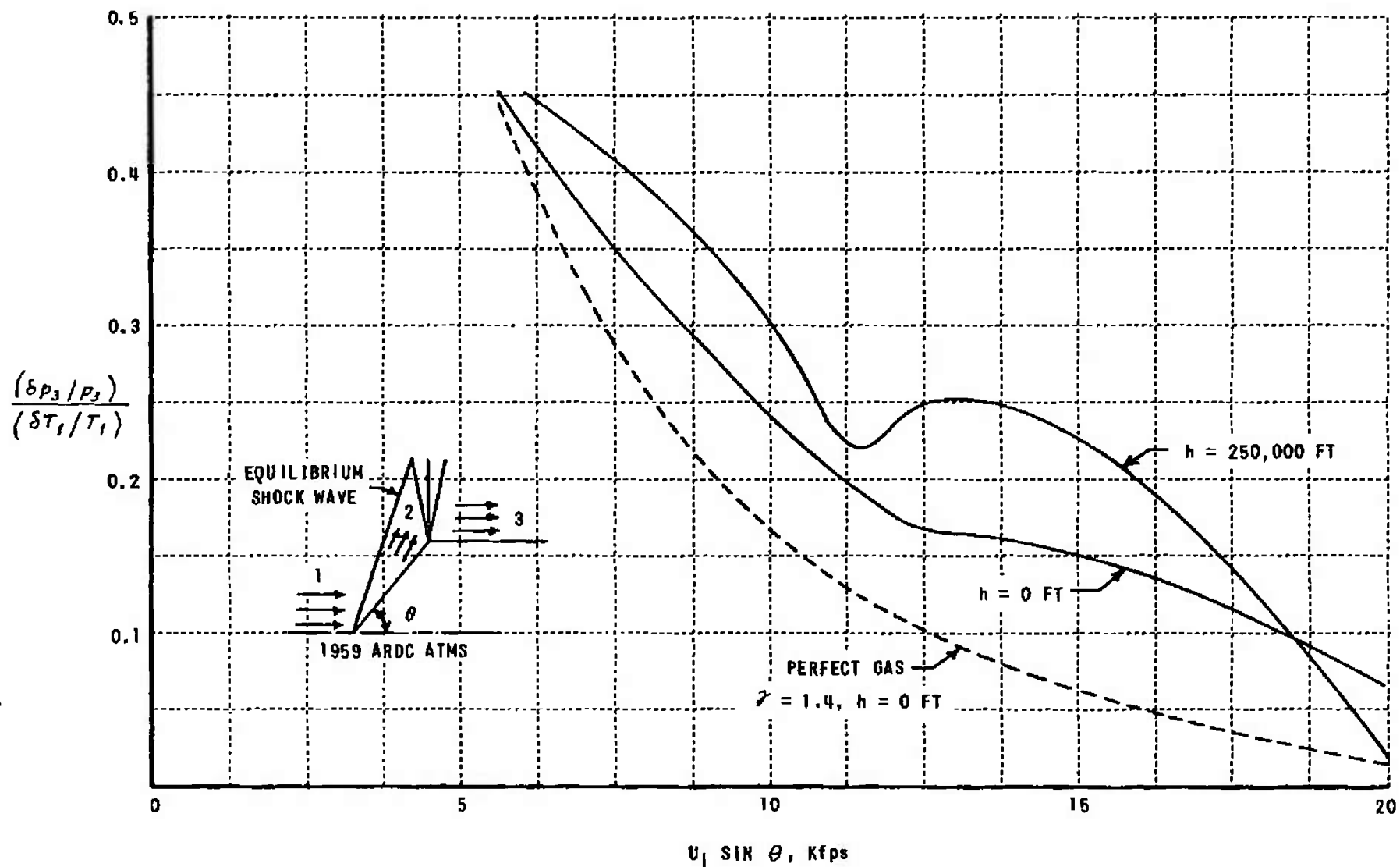(e-e MODEL)

Figure 53b   SENSITIVITY OF AFTERBODY PRESSURE TO CHANGES IN FREE-STREAM TEMPERATURE
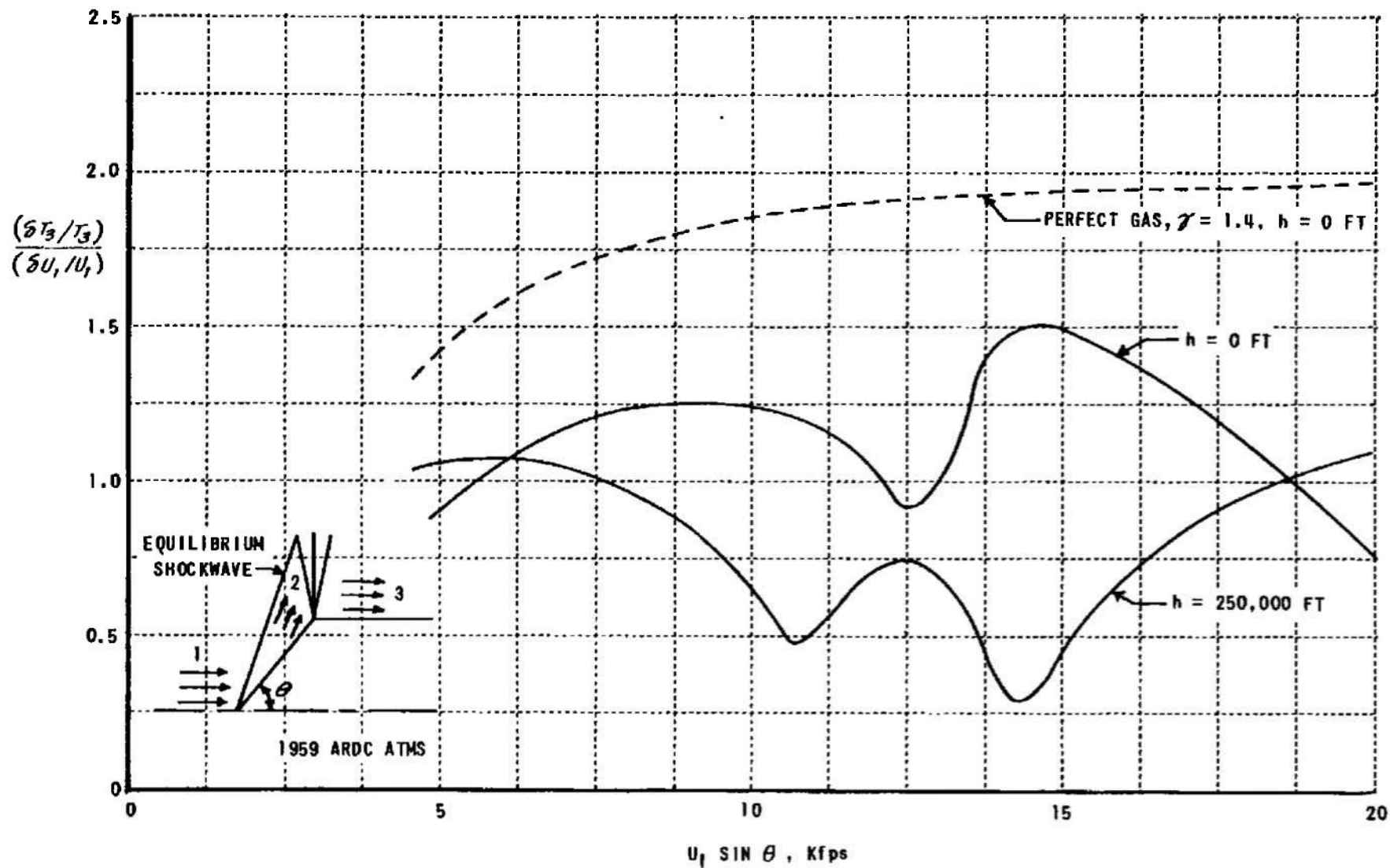(e-e MODEL)

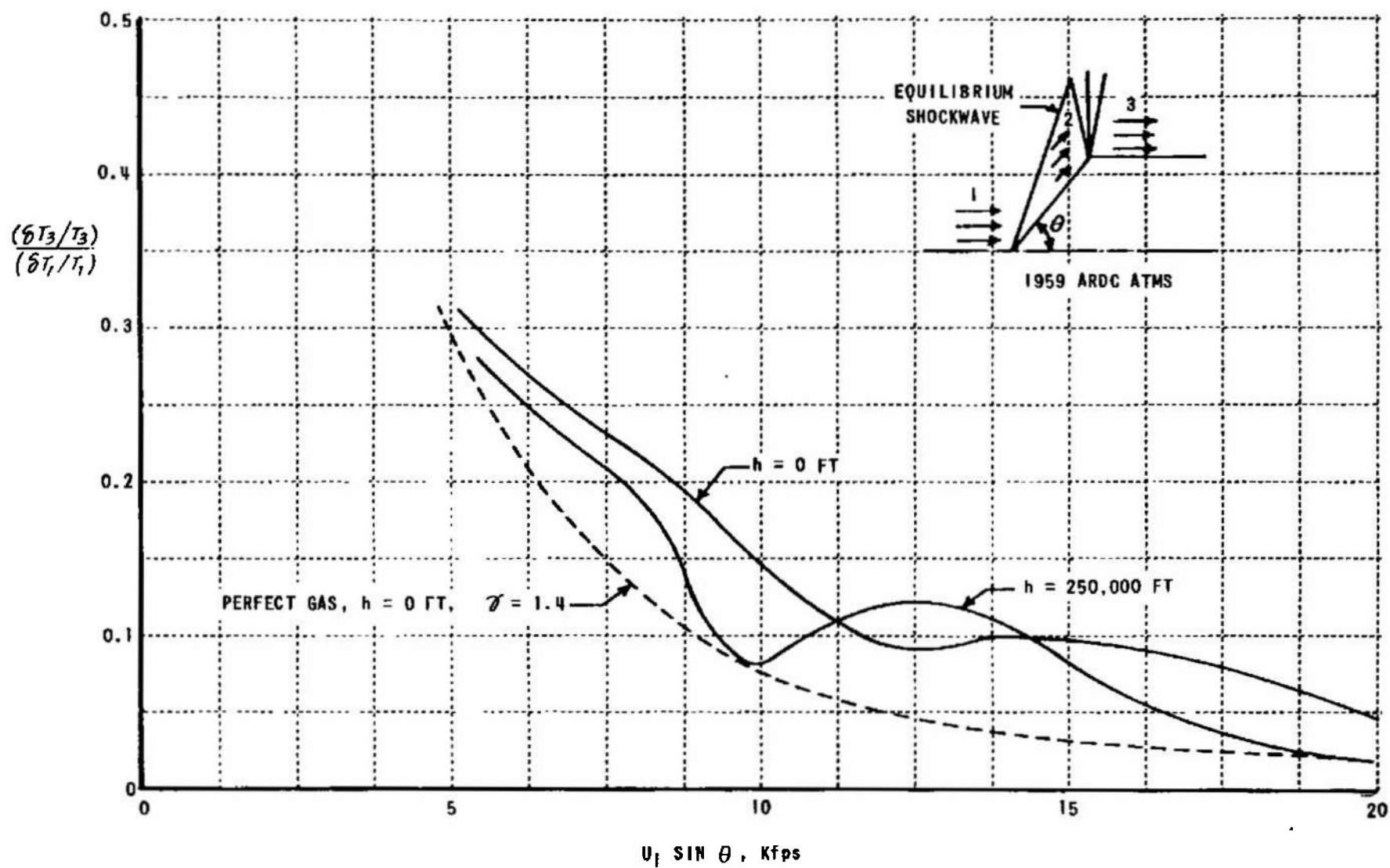Figure 54a   SENSITIVITY OF AFTERBODY TEMPERATURE TO CHANGES IN FREE-STREAM VELOCITY (e-e MODEL)

Figure 54b SENSITIVITY OF AFTERBODY TEMPERATURE TO CHANGES IN FREE-STREAM TEMPERATURE
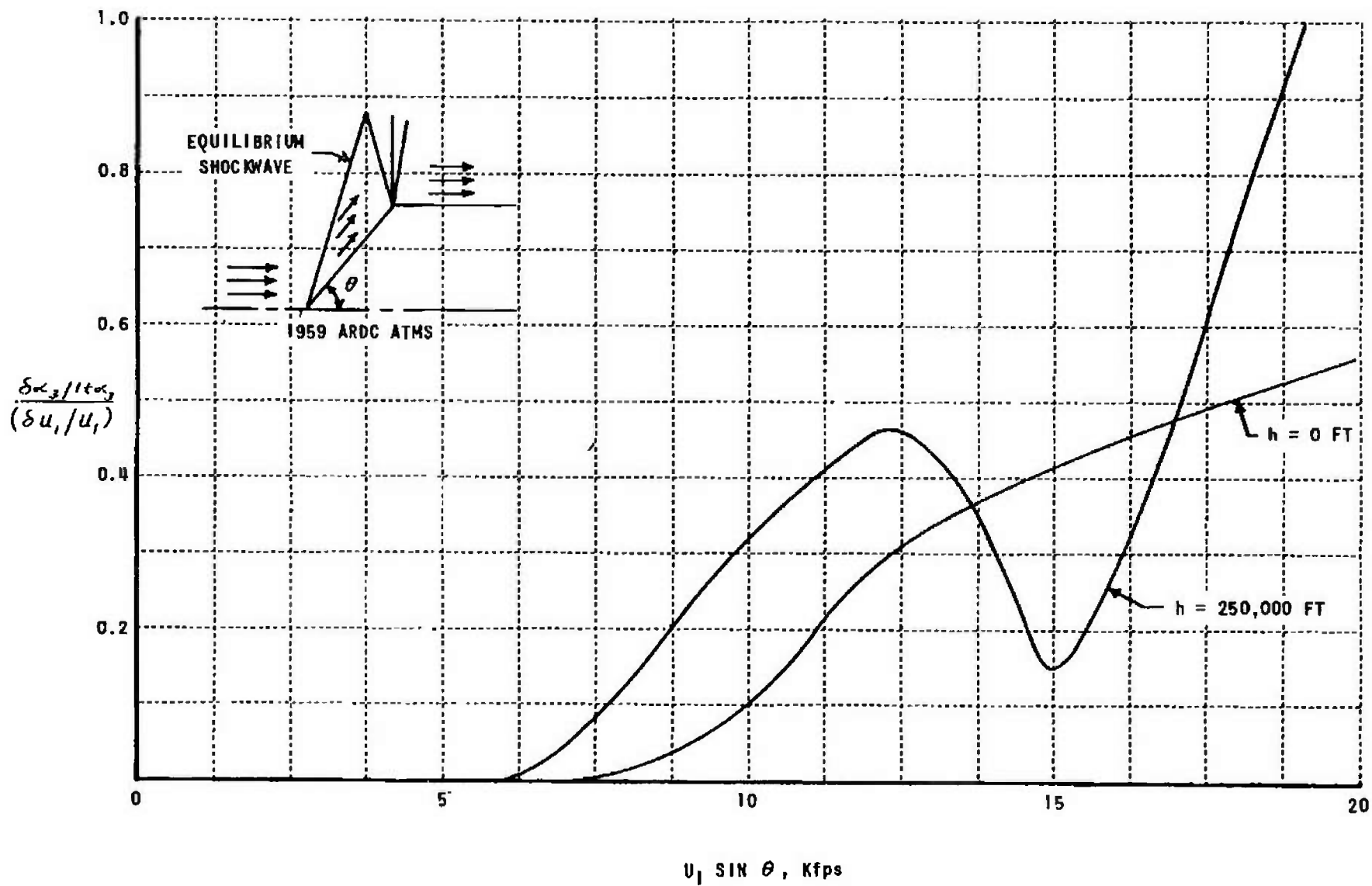(e-e MODEL)

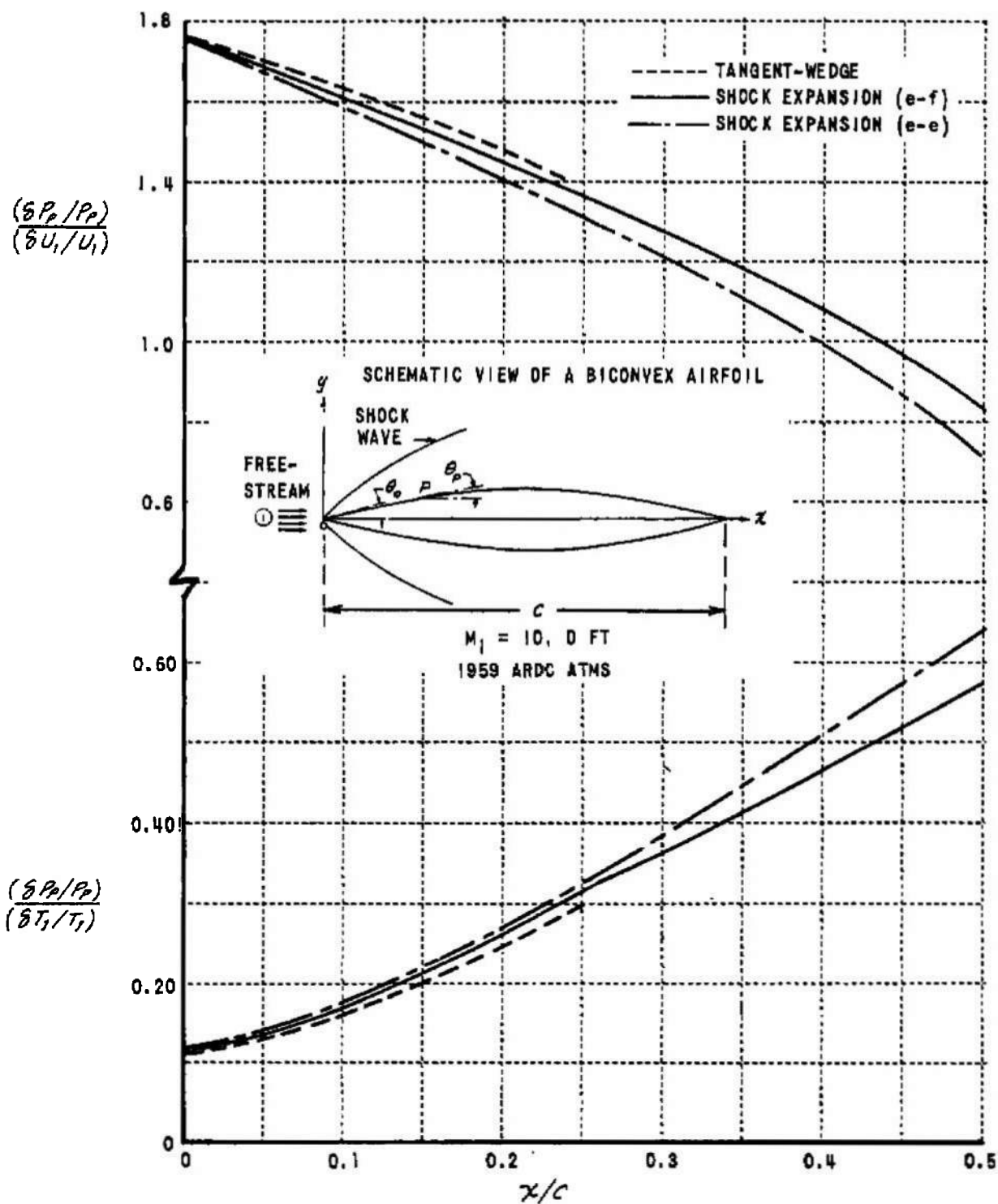Figure 55 SENSITIVITY OF THE AFTERBODY DISSOCIATION FRACTION TO CHANGES IN FREE-STREAM VELOCITY

Figure 56 SENSITIVITY OF PRESSURE ON A BICONVEX AIRFOIL TO CHANGES IN FREE-STREAM VELOCITY AND TEMPERATURE

DOCUMENT CONTROL DATA - R&D
(Security classification of title, body of abstract and indexing annotation must be entered when the overall report is classified)

1 ORIGINATING ACTIVITY *(Corporate author)*	2a REPORT SECURITY CLASSIFICATION
Cornell Aeronautical Laboratory, Inc. Buffalo, New York	UNCLASSIFIED
	2b GROUP N/A

3 REPORT TITLE

STUDY OF HIGH-DENSITY HYPERVELOCITY FLOWS AND SIMILITUDES

4 DESCRIPTIVE NOTES *(Type of report and inclusive dates)*
Interim Technical Report

5 AUTHOR(S) *(Last name, first name, initial)*

Wittliff, C. E., Sundaram, T. R., Rae, W. J., and Lordi, J. A.

6 REPORT DATE	7a TOTAL NO OF PAGES	7b NO OF REFS
April 1967	299	275

8a CONTRACT OR GRANT NO	9a ORIGINATOR'S REPORT NUMBER(S)
AF 40(600)-1131	
b PROJECT NO. 5950	AEDC-TR-67-72
c. Program Element 62410034	9b. OTHER REPORT NO(S) *(Any other numbers that may be assigned this report)*
d	CAL Rept. No. AF-2081-A-1

10. AVAILABILITY/LIMITATION NOTICES
This document is subject to special export controls and each transmittal to foreign governments or foreign nationals may be made only with prior approval of Arnold Engineering Development Center (AETS), Arnold AF Station, Tenn.

11 SUPPLEMENTARY NOTES	12. SPONSORING MILITARY ACTIVITY
Available in DDC	Arnold Engineering Development Center Air Force Systems Command Arnold Air Force Station, Tennessee

13 ABSTRACT

This report presents the results of a study of hypervelocity flows, with particular emphasis on the similitude requirements. A primary objective has been to delineate the similitude parameters for certain typical flows and, where possible, to evaluate the effects of not duplicating all of the similitude parameters in wind-tunnel tests. As a part of this study, a comprehensive review of inviscid and viscous similitude is given, as well as a state-of-the-art survey of flow solutions. It is shown that in many instances there do not exist, at present, sufficient experimental data or theoretical solutions to evaluate the sensitivity of various flow quantities to variations in the similitude parameters nor to determine whether some similitude parameters are less important than others. Such an evaluation has been accomplished for certain simple flows, such as wedges, cones, blunt-nosed flat plates and stagnation-region flows. For these flows it is found that in the flight regime of interest (velocities from 10,000 to 36,000 fps and altitudes from 50,000 ft. to 250,000 ft.) duplication of density-altitude and free-stream velocity are more important than duplication of free-stream Mach number (i.e., temperature). However, lack of duplication of Mach number can introduce significant errors in the case of slender bodies. Other topics that have been investigated are the effects of alkali-metal seed on hypervelocity flows, the importance of simulating ablation phenomena in wind-tunnel tests, and the testing time requirements for hypervelocity wind tunnels.

DD FORM 1 JAN 64 **1473**

14 KEY WORDS	LINK A		LINK B		LINK C	
	ROLE	WT	ROLE	WT	ROLE	WT
aerodynamic similitude						
hypersonic flow						
hypersonic wind tunnels						
frozen, equilibrium flow						
nonequilibrium flow						
boundary layers						

1 - 2

INSTRUCTIONS

1. **ORIGINATING ACTIVITY:** Enter the name and address of the contractor, subcontractor, grantee, Department of Defense activity or other organization (*corporate author*) issuing the report.

2a. **REPORT SECURITY CLASSIFICATION:** Enter the overall security classification of the report. Indicate whether "Restricted Data" is included. Marking is to be in accordance with appropriate security regulations.

2b. **GROUP:** Automatic downgrading is specified in DoD Directive 5200.10 and Armed Forces Industrial Manual. Enter the group number. Also, when applicable, show that optional markings have been used for Group 3 and Group 4 as authorized.

3. **REPORT TITLE:** Enter the complete report title in all capital letters. Titles in all cases should be unclassified. If a meaningful title cannot be selected without classification, show title classification in all capitals in parenthesis immediately following the title.

4. **DESCRIPTIVE NOTES:** If appropriate, enter the type of report, e.g., interim, progress, summary, annual, or final. Give the inclusive dates when a specific reporting period is covered.

5. **AUTHOR(S):** Enter the name(s) of author(s) as shown on or in the report. Enter last name, first name, middle initial. If military, show rank and branch of service. The name of the principal author is an absolute minimum requirement.

6. **REPORT DATE:** Enter the date of the report as day, month, year; or month, year. If more than one date appears on the report, use date of publication.

7a. **TOTAL NUMBER OF PAGES:** The total page count should follow normal pagination procedures, i.e., enter the number of pages containing information.

7b. **NUMBER OF REFERENCES:** Enter the total number of references cited in the report.

8a. **CONTRACT OR GRANT NUMBER:** If appropriate, enter the applicable number of the contract or grant under which the report was written.

8b, 8c, & 8d. **PROJECT NUMBER:** Enter the appropriate military department identification, such as project number, subproject number, system numbers, task number, etc.

9a. **ORIGINATOR'S REPORT NUMBER(S):** Enter the official report number by which the document will be identified and controlled by the originating activity. This number must be unique to this report.

9b. **OTHER REPORT NUMBER(S):** If the report has been assigned any other report numbers (*either by the originator or by the sponsor*), also enter this number(s).

10. **AVAILABILITY/LIMITATION NOTICES:** Enter any limitations on further dissemination of the report, other than those imposed by security classification, using standard statements such as:

   (1) "Qualified requesters may obtain copies of this report from DDC."

   (2) "Foreign announcement and dissemination of this report by DDC is not authorized."

   (3) "U. S. Government agencies may obtain copies of this report directly from DDC. Other qualified DDC users shall request through

              _____."

   (4) "U. S. military agencies may obtain copies of this report directly from DDC. Other qualified users shall request through

              _____."

   (5) "All distribution of this report is controlled. Qualified DDC users shall request through

              _____."

If the report has been furnished to the Office of Technical Services, Department of Commerce, for sale to the public, indicate this fact and enter the price, if known.

11. **SUPPLEMENTARY NOTES:** Use for additional explanatory notes.

12. **SPONSORING MILITARY ACTIVITY:** Enter the name of the departmental project office or laboratory sponsoring (*paying for*) the research and development. Include address.

13. **ABSTRACT:** Enter an abstract giving a brief and factual summary of the document indicative of the report, even though it may also appear elsewhere in the body of the technical report. If additional space is required, a continuation sheet shall be attached.

It is highly desirable that the abstract of classified reports be unclassified. Each paragraph of the abstract shall end with an indication of the military security classification of the information in the paragraph, represented as (*TS*), (*S*), (*C*), or (*U*).

There is no limitation on the length of the abstract. However, the suggested length is from 150 to 225 words.

14. **KEY WORDS:** Key words are technically meaningful terms or short phrases that characterize a report and may be used as index entries for cataloging the report. Key words must be selected so that no security classification is required. Identifiers, such as equipment model designation, trade name, military project code name, geographic location, may be used as key words but will be followed by an indication of technical context. The assignment of links, rules, and weights is optional.